Head Office: Università degli Studi di Padova

Department Of Civil, Environmental and Architectural Engineering

Ph.D. COURSE IN SCIENCES OF CIVIL, ENVIRONMENTAL AND ARCHITECTURAL ENGINEERING

CURRICULUM: MATERIALS, STRUCTURES, COMPLEX SYSTEMS AND ARCHITECTURE

DOCTORAL CYCLE: XXXV

INTEGRATION OF PHASE CHANGE MATERIALS IN CONSTRUCTIONS: THERMAL AND STRUCTURAL ANALYSES

Coordinator:
Prof. Carmelo Maiorana

Supervisor:
Prof. Luca Doretti

Ph.D. Student:
Francesca Martelletto

"Never be too big to ask questions, never know too much to learn something new"

(Og Mandino)

Contents

List of Figures

List of Tables

Acronyms

During the discussion, the following acronyms were used:

Acronym	Meaning
ASHRAE	American Society of Heating, Refrigerating and Air-Conditioning Engineers
CFD	Computational Fluid Dynamics
CSP	Concentrated Solar Power
DSC	Differential Scanning Calorimetry
ENEA	Italian National Agency for New Technologies, Energy and Sustainable Economic Development
FEM	Finite Element Method
HTF	Heat Transfer Fluid
HVAC	Heating, Ventilation and Air Conditioning
LH	Latent Heat
LHTES	Latent Heat Thermal Energy Storage
PCM	Phase Change Materials
SH	Sensible Heat
SHTES	Sensible Heat Thermal Energy Storage
TES	Thermal Energy Storage
UNIPD	Università degli Studi di Padova

Nomenclature

During the discussion, the following symbols were used:

Latin symbols:

Symbol	Unit of measurement	Meaning
A	[m^2]	Area
a	[m^2/s]	Thermal diffusivity
C	[$J/(m^3K)$]	Volumic heat capacity
c	[J/(kgK)]	Specific heat capacity
H	[J]	Enthalpy
l	[m]	Lenght
m	[kg]	Mass
Q	[J]	Heat
$\dot{Q}$	[W]	Power, Energy flux
r	[m]	Radius
r_0	[J/kg]	Specific latent heat
s	[m]	Thickness
T	[K]/[°C]	Temperature

Greek symbols:

Symbol	Unit of measurement	Meaning
λ	[W/(mK)]	Thermal conductivity
ϱ	[kg/m^3]	Density
σ	[Pa]	Stress
τ	[τ]	Time

Abstract

Phase change materials are substances that absorb and release heat energy when they change phase, usually from a solid phase to a liquid phase and vice versa. During the phase transition, many materials are able to absorb or release a significant amount of heat energy. Different materials will melt and solidify at different temperatures and are able to absorb different amount of heat energy. In this way, the phase change materials can contribute to the efficient use and conservation of waste heat and solar energy. Their use provides increases in the efficiency of the storage and use of energy in many building and industrial sectors. For this reason, the application of phase change materials in different situations is gaining increasing and continuous attention. Phase change materials can be used purely as they are, or integrated into other supportive materials, like metals, plastics, wood or concrete. Concrete has already been demonstrated to give suitable and feasible energy storage solutions, so it has been selected for the current study, with the integration of the phase change materials.

The phase change materials, in fact, represent a real hope to overcome the arising problems related to climate change and the energy crisis. They can both ensure the storage of the energy produced by any kind of resource, first of all, the renewable ones, which greatly suffer from intermittency, but also reduce the energy consumption, particularly strong in this historical period, with all the advantages brought with it.

This work regarded various aspects of the symbiotic thermal behaviour of the analysed storage systems, starting from the deep study of the basic concrete, in different situations, then with the enormous enhancements that the integration of the phase change materials can bring to the thermal system.

A lumped capacitance-based computing model was developed for a concrete module supposed to store and release thermal energy to a thermal oil working as heat transfer fluid. The code permits the thermal and energetic analysis of concrete thermal energy storage during time. The code was validated against the experimental data, and two thermal efficiencies were implemented. This

model allows for a drastic reduction of the needed computational time. Then, the effect of the modules' arrangement on the performance of the thermal energy storage system was studied. Series and parallel arrangements were investigated, to determine the most performant one, which was determined by a thermal energy assessment. After that, the integration of the phase change materials in the concrete was analyzed. The experimental tests regarded two concrete mixtures, with 5% of phase change materials and without it. The module was simulated and the results were compared with the experimental tests. Further analyses were conducted to test higher phase change materials percentages, leading to an impressive improvement in thermal performance.

The following step regarded the numerical study of building walls with the integration of phase change materials. A perimetral wall has been studied, in three configurations. Concrete was used for the basic simulation, that was then mixed with 10% of phase change materials, creating a wall with a homogeneous dispersion. Also, another system with two layers of phase change materials on the outside was studied, both providing very good improvements.

The intent was to provide a study, articulated in several steps, with the final aim to identify the possibilities of real applications of the phase change materials to different situations, to fully exploit and take advantage of their thermal properties and performances. My personal hope is to have contributed to a proficient improvement in this field and to have provided feasible suggestions for enhanced thermal systems.

Sommario

I materiali a cambiamento di fase sono sostanze che assorbono e rilasciano energia termica quando cambiano fase, solitamente da fase solida a fase liquida e viceversa. Durante la transizione di fase, questi materiali sono in grado di assorbire o rilasciare una notevole quantità di energia termica. Inoltre, i diversi materiali si fondono e solidificano a diverse temperature e sono in grado di assorbire varie quantità di energia termica. In questo modo, i materiali a cambiamento di fase possono contribuire ad un utilizzo efficiente e consapevole dell'energia termica, riducendo le perdite di calore e sfruttando anche le fonti rinnovabili. L'utilizzo di questi materiali consente di aumentare l'efficienza dell'accumulo e dell'utilizzo dell'energia in molti settori, tra cui, in primis, l'edilizia e l'industria. Per questo motivo, la loro applicazione sta guadagnando una sempre maggiore attenzione e anche uno spiccato interesse da parte di enti di ricerca e aziende produttive. I materiali a cambiamento di fase si possono utilizzare puri oppure possono essere integrati in altri materiali che fungono da supporto, come i metalli, il legno o il calcestruzzo. Il calcestruzzo ha già dimostrato di essere un buon materiale di base per l'accumulo termico, con caratteristiche adeguate sia da un punto di vista pratico che teorico, quindi è stato selezionato per il presente studio, come base per l'integrazione dei materiali a cambiamento di fase.

I materiali a cambiamento di fase, infatti, rappresentano una concreta possibilità di superare e risolvere gli emergenti problemi legati al cambiamento climatico e alla crisi energetica. Possono sia garantire l'accumulo dell'energia prodotta da qualsiasi tipo di fonte, in primis quelle rinnovabili, che tipicamente risentono molto di intermittenza, ma anche ridurre i consumi energetici, con tutti i vantaggi ad essi legati, che sono particolarmente sentiti e importanti in questo periodo storico.

Il presente lavoro ha riguardato vari aspetti della simbiosi termica dei sistemi di accumulo analizzati, partendo da uno studio approfondito del calcestruzzo di base, in diverse condizioni e poi successivamente con gli enormi miglioramenti che l'integrazione dei materiali a cambiamento di fase può apportare al sistema

termico integrato.

È stato sviluppato un modello di calcolo a parametri concentrati, con un codice che consente l'analisi termica ed energetica dell'accumulo di calore nel calcestruzzo nel tempo, per un modulo progettato per immagazzinare e rilasciare energia termica ad un olio diatermico funzionante come fluido termovettore. Il codice è stato validato attraverso i dati sperimentali e sono anche state implementate due diverse efficienze termiche. Questo modello consente una drastica riduzione del tempo di calcolo necessario rispetto alle più tradizionali simulazioni numeriche di dettaglio. Successivamente, è stato studiato l'effetto che la disposizione dei moduli di accumulo possa avere sulle prestazioni complessive del sistema. Sono state studiate le disposizioni in serie e in parallelo, per determinare quella più performante, che è stata individuata attraverso una serie di parametri termici ed energetici. Dopo di ciò, è stata analizzata l'integrazione dei materiali a cambiamento di fase nella mescola calcestruzzo, con prove sperimentali che hanno riguardato due diverse mescole, con il 5% di materiali a cambiamento di fase e senza di essi. Il modulo di calcestruzzo è stato poi simulato e i risultati sono stati confrontati con le prove sperimentali, con un'ottima concordanza dei valori. Sono state condotte ulteriori analisi per testare percentuali più elevate di materiali a cambiamento, portando a un notevole miglioramento delle prestazioni termiche.

Il passo successivo ha riguardato lo studio delle murature edilizie con la successiva integrazione di materiali a cambiamento di fase. È stata analizzata una parete piana perimetrale, in tre configurazioni; per la simulazione di base, usata come riferimento, è stato utilizzato il calcestruzzo, che è stato poi miscelato con il 10% di materiali a cambiamento di fase, creando un muro con una dispersione omogenea. Inoltre, è stato studiato un altro sistema con due strati di materiali a cambiamento di fase all'esterno. Entrambe le soluzioni studiate forniscono ottimi risultati con notevoli miglioramenti rispetto alla parete base.

L'intento di questo lavoro era quello di realizzare uno studio, articolato in più fasi successive, con l'obiettivo finale di identificare le possibilità di reali applicazioni dei materiali a cambiamento di fase in diverse tipologie di sistema, per sfruttarne appieno e trarre vantaggio dalle loro caratteristiche e prestazioni termiche. La mia speranza, come autrice di questa tesi, è di essere riuscita a contribuire ad un miglioramento in questo campo e di aver fornito suggerimenti e spunti di riflessione per possibili nuovi lavori e sviluppi futuri, in un'ottica di miglioramento energetico, incremento dello sfruttamento delle risorse rinnovabili ed adattamento alle nuove esigenze che si stanno creando nella società attuale.

1. Introduction

One of the main factors that influence the increase in global energy consumption is the increase in the world population. Since 1974, there has been a large increase in energy consumption in the domestic, commercial and service sectors. The building requirements, over the next decade, predict that more than 20% of expected global building additions will be built. Recent projections predict also that primary energy consumption will increase by 50% in 2050.

It is estimated that, in most developed countries, between 20% to 40% of total energy consumption is attributed to commercial and residential buildings, whereas about 50% is associated with the thermal conditioning of interior spaces. The depletion of fossil resources, as well as their negative impact on the environment, has accelerated the shift to sustainable energy sources. In fact, the European Union's policy objective is to move towards a low-carbon economy, with at least a 40% reduction in greenhouse gas emissions by 2030.

Renewable energies such as solar radiation, wind and biogas have played an important role in reforming the natural balance and meeting the needs of growing demographic demand. However, the need of storing these types of renewable energy has become urgent. This has led to the need to develop efficient and sustainable methods of storing energy. This need for energy storage and its relevant technologies have attracted the attention of researchers to find solutions to meet the increased energy demand arising from the development worldwide. Energy storage has hence become an important part of renewable energy technology systems.

The needs and the habits of modern society are also changing, if in the past the thermal focus on building envelope was posed on insulating the external walls, to cope with the winter temperature, now this strategy is becoming less and less useful. The temperature peaks in the summer season are rising and becoming more frequent, with the direct consequence of higher employment of air conditioning systems, increasing energy consumption and polluting effects.

It is my personal opinion that something should be done to overcome the

arising thermal and energetic problems, and it is in this context that the work presented in this thesis was realised. The traditional steady insulating layers are not suitable anymore to guarantee adequate thermal comfort. Hence, I tried to find new solutions that are able to mitigate the dynamic thermal loads typical of the summer season, by using the phase change materials combined with the building envelopes.

Thermal energy storage system integration is a consistent way to improve energy performances and thermal management, it is a technology that stocks thermal energy by heating or cooling a storage medium so that the stored energy can be used at a later time for heating and cooling applications and power generation.

Phase change materials are substances that absorb and release heat energy when they change phase (known as latent heat). When a material melts, it changes from a solid phase to a liquid phase. During the phase transition, many materials are able to absorb a significant amount of heat energy. The opposite is true when the material freezes and solidifies: the material will give out the heat that it absorbed when it melted. Different materials will melt and solidify at different temperatures and are able to absorb different amount of heat energy. They are useful because they melt and solidify at specific, defined temperatures, making them suitable to control the temperature in range of diverse applications. Materials that melt to absorb heat are much more efficient at absorbing heat energy compared to sensible heat energy materials. This means that it takes a much smaller amount of a material to store heat energy phase change material than using a material that does not change phase.

Phase change materials, used for the storage of thermal energy as sensible and latent heat, are innovative materials that substantially contribute to the efficient use and conservation of waste heat and solar energy. Using phase change materials for energy storage provides an elegant and realistic solution to increase the efficiency of the storage and use of energy in many domestic and industrial sectors. The principles of latent heat storage can be applied to any appropriate storing materials. Using latent heat storage in buildings can meet the demand for thermal comfort and energy conservation. Thermal mass materials can absorb and store heat before releasing it later on, when necessary. They typically act as heat sinks during the daytime and as heat sources during the nighttime. Regarding industrial applications, the integration of thermal energy storage systems within concentrated solar power plants is considered to be one of the key factors for providing low-cost electricity from solar power. The thermal energy storage integration would permit to overcome the peak demand through an optimization

of the energy production by the concentrated solar power plants, especially during nighttime or cloudy weather.

Concrete is a thermal mass material mainly composed of cement, water and aggregates. Compared to other expensive ceramic materials, concrete has already been demonstrated to give suitable and economically feasible energy storage solutions. However, there is still insufficient knowledge about the application of phase change materials-concrete in operative situations. More experimental studies and simulations are required to consider the efficiency of concrete based on its thermal properties in different weather conditions and different types of applications. Designing a concrete module and determining its operating conditions is not an easy task, due to the fluid dynamics and heat transfer phenomena involved in the storage process between heat transfer fluid, piping and storage material.

An experimental campaign, in collaboration with ENEA Researchers, took place. The aim was to evaluate the performance of concrete storage elements, realized with an appropriate mixing, and to examine the geometric characteristics of the storage elements and the applied measurements equipment. The experimental data have been used to compare the conducted numerical simulations. The experimental setup was able to operate between 215 and 280 °C, which can be an average temperature range for an industrial application. The numerical simulations, which were based on the tests, follow the same temperature range. The first part of the work consisted in realizing a simple lumped capacitance based computing model, using Fortran language. The code permits the thermal and energetic analysis of concrete thermal energy storage during time. The simulated system consists of a parallelepiped concrete module that can be heated and cooled by a single-phase working fluid flowing in a tube embedded in the concrete. The modules can be piled up in different configurations to build any desired thermal energy storage. The new simulation code was validated against the experimental data carried out by ENEA with two different concrete mixtures, during both the heating and cooling processes using mineral oil as working fluid. Furthermore, two different thermal energy storage thermal efficiencies were implemented in the study to evaluate the charge or discharge progresses over time. This easy-to-use model allows for a drastic reduction of the computational time needed to simulate the thermal energy storage and it can be easily integrated, in various arrangements, to any concentrated solar power plants and associated energy conversion plant simulation models to have a quick evaluation of the whole system performance.

Then, the following main step consisted in focusing on the effect of the modules' arrangement on the overall performance of the thermal energy storage sys-

tem. Series and parallel arrangements were investigated, to determine the most performant solutions in terms of exchanged thermal energy as a function of the main operating conditions: oil mass flow rate and pressure drop, both in the heating and cooling phase. This study, as a direct consequence of the previous work, expanded the temperature range of the numerical simulations, using 150-300 °C. Two different boundary conditions were considered: adiabatic and diabatic external walls. The simulations were carried out using an extended version of the model previously proposed for a single concrete block. The exchanged thermal energy, the oil mass flow rate, the pressure drops, and the duration of the process were changed to evaluate the storage under different operating conditions. The best thermal energy storage configuration was determined by a thermal energy assessment: it coincided with the first one that reached the asymptotic values with the minimum number of elements. Furthermore, in the diabatic case, the loss heat flux toward the environment had a significant role and highlighted the differences between charging and discharging phases, its presence contributed to a more aware choice of the most suitable and performant modularized system.

After that, the integration of the phase change materials in the concrete matrix could take place. The geometry of the thermal energy storage system slightly changed, because the ENEA's Researchers preferred to focus on a smaller cylindric concrete model. A stainless-steel pipe was inserted in the centre of the concrete cylinder and the whole system was insulated. The experimental tests regarded two concrete mixtures, with 5% phase change materials and without it. At this stage, the temperature range was even more expanded, working between 30 and 300 °C, in order to consider also the initial transient stage needed to heap up the block. The charging stage was obtained by heating the pipe's surfaces by Joule effect and the module was then cooled with compressed air through the pipe. The two mixtures were tested in the same conditions. A binary mixture of salts was used as phase change materials, composed of KNO_3 and 60% of $NaNO_3$, and they were absorbed by diatomite, a porous fossil flour. The module was numerically simulated, with the computational fluid dynamics software ANSYS Fluent, and the results were compared with previous experimental tests to calibrate the model. Further numerical simulations were conducted to test other phase change materials percentages, 20% and 40%, in the same conditions of the experimental tests and with thermal oil as heat transfer fluid, to have a representation more similar to an operative condition. The phase change materials integration into the storage system led to an impressive improvement in thermal performance.

The following step regarded the numerical study of building walls with the integration of phase change materials technologies. A perimetral wall has been

studied, in three configurations. Concrete was used for the basic simulation. It was then mixed with 10% of phase change materials (microcapsules of paraffin waxes), creating a wall with a homogeneous dispersion. Also, another system with two layers of phase change materials (microencapsulated paraffin within a copolymer) added to the outside of the wall was studied. The three configurations were analyzed and compared, using ANSYS Fluent. A sinusoidal temperature profile was applied to the wall, following the profile that occurred in Padua. These analyses were conducted considering a typical summer temperature range, between 15 and 40 °C. The system with 10% of phase change materials presents a lower temperature compared with the basic one. Considering the wall with two layers, the temperature values are the lowest of the three. A focus was placed on the transmitted heat flux in the room, which gives thermal comfort information. Both solutions brought a reduction in the loss of thermal power, but the wall with the two layers assured better comfort. The best solution is the wall with the integration of two layers of phase change materials in the considered terms. The system with the mixed phase change materials is however well performant and allows for a better thermal behaviour than the basic wall, but its improvements are less relevant.

The comparison regarded the wall with the integration of 10% of phase change materials and with the two layers of phase change materials. In this way, the phase change materials amount was almost the same and the results were comparable. Anyhow, the designer can select a different percentage of phase change materials or number of applied layers, according to the needing. Regarding the impact that the two technologies may have on the building structure, the direct integration of the phase change materials could compromise the concrete compressive resistance. On the other side, with the application of layers, significant changes to the building would ruin the thermal systems.

I think that, even if in a small way, the results reported in this work could stimulate and provides some interesting food for thought, or at least this is what I hope to have done in this thesis. Changes are always difficult and could take much time to be done, but the phase change materials could have a little advantage in this since they are made to change.

2. Thermal energy storage concept

Recent and developing research has focused on increasing energy efficiency through the share of renewable energy, managing energy demand and reducing both heating and cooling. This has originated from the dramatic increase in global energy demand as a result of rapid growth in the world's population and economy, which is leading to a severe environmental impact, according to Faraj et al. (2021). Acheampong (2018) stated that the total carbon emissions leading to global warming are influenced by economic growth, the intensity of energy consumption, population growth and the intensity of carbon emissions.

However, researchers and policymakers have attributed the high intensity of carbon emissions to energy consumption resulting from rapid economic growth and the amplified use of fossil fuels, according to Sohag et al. (2015). The construction sector, being the most energy-intensive sector, accounts for around 25-30% of final energy consumption on a global basis , according to Rabani and Rabani (2019), and Putra et al. (2019). It is also considered an equally important source of CO_2 emissions (Devaux et al. (2017)).

Furthermore, according to the IEA, if no energy efficiency improvements are made in the construction sector, a 50% increase in energy consumption could be triggered by 2050 (Vanaga et al. (2018)). Globally, the construction sector is the main source of energy consumption and accounts for about 40% of total energy consumption (Sun et al. (2018, and Landi et al. (2020)). The results of the IEA's solar heating and cooling program highlighted that more than 75% of the energy consumed in single- and multi-family homes is attributed to the demand for space heating and cooling, according to Patel et al. (2018). However, the environmental crisis has just begun, when expectations show that energy demand in the construction sector will have increased by 50% by 2050, with the demand for space cooling tripling over the projected period (Souyoufane et al. (2016)).

Thermal Energy Storage (TES) is being explored as a method to reduce the environmental impact of heating and cooling, as a way to address the mismatch

between supply and demand between renewable resources and energy demand, as stated by Mahon et al. (2022)

The storage of thermal energy is possible by changing the temperature of the storage medium by heating or cooling it. This allows the stored energy to be used at a later stage for various purposes (heating and cooling, waste heat recovery or power generation) in both buildings and industrial processes (Jouhara et al. (2020)). The use of TES in the energy system allows energy savings, increases the overall efficiency of the systems by eliminating the differences between energy supply and demand, as reported by Fallahi et al. (2017), and reduces investment and operating costs as well as carbon dioxide emissions (CO_2) and other environmental pollutants (Sarbu and Sebarchievici (2018)). In addition, the use of low-carbon renewable energy sources can be improved, in particular with solar technologies and Power-to-Heat concepts.

This statement is valid if the storage is carried out in favor of very low cost energy (e.g. solar) compared to the production of energy with traditional methods in periods of absence of the previous one. However, sometimes storage is not advantageous in terms of energy, for example if it is used to smooth out absorption peaks that would be covered using the same energy source. In this case, the irreversibility linked to the exchanges in the charge and discharge phases almost always lead to a decline in the overall efficiency of the system compared to the direct supply of energy in times of need. The type of TES studied in the thesis is designed for applications in which this option is not feasible or in any case not of primary interest. The production of electricity from solar sources is limited to predominantly sunny days, excluding cloudy days and nights. The TES in question is designed to be charged, for example, in the central hours of the day, when there is an excess of solar energy compared to the demand, and then be discharged at night, when it is impossible to produce electricity directly from the solar source, since he is absent at such moments.

2.1 Typologies

It is possible to consider thermal storage on the hot and/or cold side of the plant. The former allows the storage of hot water from the collectors (and from the auxiliary heater) to be supplied to the generator of the absorption chiller (in cooling mode) or directly to the users (in heating mode), as reported by Sarbu and Sebarchievici (2018). The latter allows the storage of cold water produced by the absorption chiller to be supplied to the cooling terminals inside the building.

It is usual to identify three situations as "hot", "warm", and "cold" storage based on the different temperature ranges. Typically, a hot tank may work at 80–90 °C, a warm tank at 40–50 °C, and a cold tank at 7–15 °C, as stated by Noro et al. (2014).

Due to the intermittence in availability and the constant variation of the weather, TES has found its place in thermodynamic systems. TES not only reduces the mismatch between supply and demand by saving thermal energy but also improves the performance and thermal reliability of the system. The main types of TES are presented in Fig. 2.1. An energy storage system can be described in terms of the following characteristics:

- Capacity, which defines the energy stored in the system and depends on the storage process, the medium, and the size of the system
- Power, which defines how fast the stored energy can be charged and discharged
- Efficiency, which is the ratio of the energy provided to the user to the energy needed to charge the storage system. It accounts for the energy loss during the storage period and the charging/discharging cycle
- Storage period, which defines how long the energy is stored and lasts hours to months
- Charge and discharge time, which defines how much time is needed to charge or discharge the system
- Cost, which refers to either capacity or power of the storage system and depends on the capital and operation costs of the storage equipment and its lifetime (i.e., the number of cycles)

Capacity, power, and discharge time are interdependent variables. In some storage systems, capacity and power can also depend on each other. High-energy storage density and high power capacity for charging and discharging are desirable properties of any storage system.

The basic parameter determining the dynamics of change in the TES system is thermal conductivity. The low thermal conductivity can reduce the storage of thermal energy. An additional criterion to be considered for the selection of TES material is operating temperature, peak load, duty cycle, ease of control and wider system integration. Table 2.1 classifies the different requirements of TES

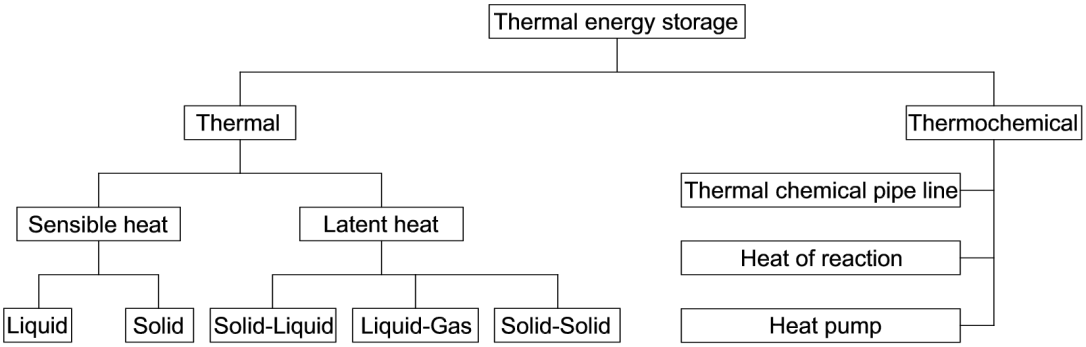

Figure 2.1: Types of thermal energy storage systems

materials and systems in terms of optimum chemical, kinetic, physical, thermal, economic, environmental and technological, performance.

As reported by de Gracia and Cabeza (2015), it is well known that there are three methods for TES at temperatures from -40 °C to more than 400 °C: sensible heat, latent heat associated with Phase Change Materials (PCM), and thermo-chemical heat storage associated with chemical reactions, as can be seen in Fig. 2.2.

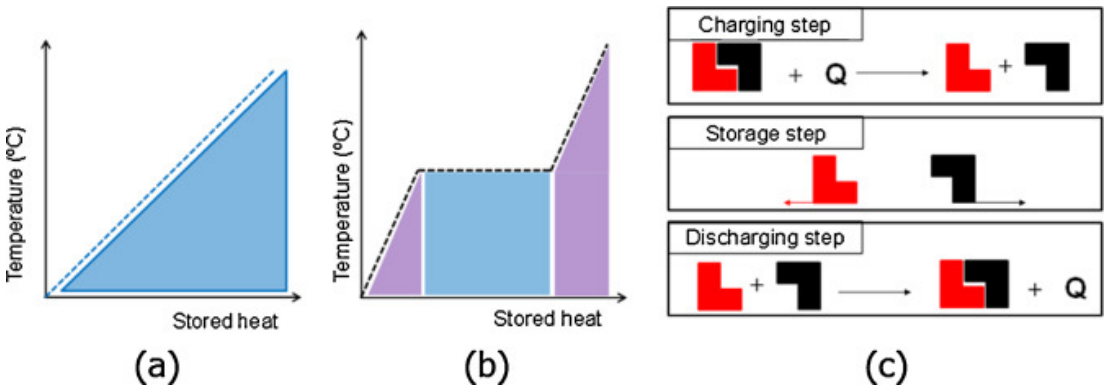

Figure 2.2: Methods of thermal energy storage. (a) Sensible heat, (b) latent heat, (c) thermochemical reaction, by de Gracia and Cabeza (2015)

2.1.1 Sensible thermal energy storage

Sensible heat storage is the simplest and most used method based on storing thermal energy by heating or cooling a liquid or solid storage medium. Sensible heat is the heat exchanged by a system that does not change its phase but changes the temperature of a storage medium. The temperature changes almost linearly with the stored heat. The amount of heat stored depends on the specific heat of the medium, the temperature change, and the amount of storage material through radiation, convection and conduction and is described by the formula below:

Table 2.1: Different requirements of TES materials and systems

Typology	**Requirements**
Chemical	Long-term chemical stability No fire and explosion hazard No toxicity No phase separation / incongruent melting Compatibility with storage materials
Kinetic	Small or no sub cooling Sufficient crystallisation rate
Physical	High density Low vapour pressure Small volume changes
Thermal	Favourable phase equilibrium High specific heat High thermal conductivity in both solid and liquid states Melting / solidification temperature range High latent heat of transition per volume unit Congruent melting
Economic	Abundant and available Large lifetime Cost effective
Environmental	Low manufacturing energy Easy recycling
Technological	Operational strategy Integration into the facility Efficiency improvement suitable heat transfer

$$Q_s = \int_{T_1}^{T_2} m_s \cdot c \cdot dt = m_s \cdot c \cdot (T_2 - T_1) \tag{2.1}$$

Where Q_s is the sensible heat storage, T_1 is the initial temperature, T_2 is the final temperature, m_s is the mass of the heat storing material and c is the specific heat capacity. For the current study, the specific heat capacity has been assumed constant because it was a reliable assumption, but in general, it could be temperature dependent, so this simplification can not be done.

Ceramics, such as concrete, are the most commonly used storage material, as well as water and oil. They can be applied in both industries and buildings. Commonly applicable systems include solutions using underground energy storage

such as: borehole, aquifer, cavern, ducts in soil, pit hot water storage (hydro accumulation), and rock-filled storage (rock, pebble, gravel).

2.1.2 Latent thermal energy storage

Latent heat storage consists in storing (or releasing) thermal energy through the phase change that occurs over a specific temperature range in the material in question. The most used materials for this purpose are molten salt, paraffin wax and water/ice materials, as reported by Elias et al. (2019).

Two latent heat storage systems differ in terms of heat transfer: direct and indirect. The direct system takes place when the heat transfer occurs through direct contact between the Heat Transfer Fluid (HTF) and the material. The indirect one occurs when there is a solid heat transfer boundary between HTF and the latent storage material.

Phase changes include the processes that lead to a change in the state of aggregation: evaporation and condensation, crystallization and melting and which occur without a change in the state of aggregation, in the solid or liquid phase. In this process, it is possible to store a large amount of heat depending on the properties of the selected material. With increasing temperature, the phase change from solid to liquid occurs with a small volume change, usually, less than 10%, as reported by Mehling and Cabeza (2008), and the pressure does not change significantly. All this causes the melting and solidification of the stored material to occur at a constant temperature, if the substance is pure, known as the phase change temperature. When the fusion is completed, further heat transfer causes sensible heat to be stored again. The energy storage density in latent systems usually provides a higher storing capacity than in sensible systems because they use the transformation of chemical bonds in the mass structure of the material.

The stored heat in this case is equal to:

$$Q_s = \int_{T_i}^{T_m} m_s \cdot c_s \cdot dt + m \cdot r + \int_{T_m}^{T_f} m_s \cdot c_l \cdot dt \tag{2.2}$$

$$Q_s = m_s \left[c_s \cdot (T_m - T_i) + r + c_l \cdot (T_f - T_m) \right] \tag{2.3}$$

where T_m is the melting temperature, T_i is the initial temperature, T_f is the final temperature, m_s is the mass of the heat storing material, c_s is the average specific heat of the solid phase between, c_l is the average specific heat of the liquid

phase, r is the latent heat of fusion. The specific heat capacity during the solid and the liquid stage usually assume different values, in fact, the two terms are reported as different parameters in the equation. However, in the present thesis, the specific heat capacity values before and after the transition stage are assumed as equal, since the change is negligible.

Latent heat storage materials are known as phase change materials due to their property of releasing or absorbing energy with a change in physical state. The heat is mainly stored in the phase-change process and it is directly connected to the latent heat of the substance. The use of a latent system using PCMs is an effective way of storing thermal energy and has the advantages of high-energy storage density and the isothermal nature of the storage process. Typical phase change materials are based on paraffin waxes, fatty acids, and hydrated salts, but more details will be provided later in the following sections.

2.1.3 Thermo-chemical thermal energy storage

Thermochemical energy storage is quite a new method and is under research and development phase at various levels (Prieto et al. (2016)). In this technique, the energy is stored and released in the form of a chemical reaction and is generally classified under the heat storage process. The thermochemical material, used to store thermochemical energy storage, undergoes either a physical reversible process involving two substances or a reversible chemical reaction as given below:

$$\mathrm{AB} + \mathrm{Q} \leftrightarrow \mathrm{A} + \mathrm{B} \tag{2.4}$$

Where Q is the amount of heat required to dissociate A and B. The dissociation of AB, which results in the formation of A and B is an endothermic reaction, while the reversible of this chemical reaction is an exothermic reaction (Krese et al. (2018)). Hence, during the forward reaction, the energy is stored and during the backward, the energy is released which can be used for various applications. This technique of energy storage has gained popularity because of higher energy density and lower heat losses. However, there are various bottlenecks which limit the application of this technology in buildings like, unsuitable operating condition (i.e. too high charging conditions), corrosiveness, environmentally-unfriendly production, chemical instability, and high cost.

2.2 Phase Change Materials

2.2.1 Overview

Phase change materials used for the storage of thermal energy as sensible and latent heat are an important class of modern materials which substantially contribute to the efficient use and conservation of waste heat and solar energy. The storage of latent heat provides a greater density of energy storage with a smaller temperature difference between storing and releasing heat than the sensible heat storage method. Many different groups of materials have been investigated during the technical evolution of PCMs, including inorganic systems, organic compounds such as paraffins or fatty acids and polymeric materials. Historically, the relationships between the structure and the energy storage properties of a material have been studied to provide an understanding of the heat accumulation/emission mechanism governing the material's imparted energy storage characteristics.

Using PCM for TES systems that can be released as sensible heat and latent heat became an important aspect for energy management following the 1973–1974 energy crisis. Today, the limited reserves of fossil fuels and concerns over greenhouse gas emissions make the effective utilization of energy a key issue. Using PCM for TES provides an innovative and realistic solution to increase the efficiency of the storage and use of energy in many domestic and industrial sectors. The application of PCMs for energy storage reduces the mismatch between supply and demand, improves the performance and reliability of energy distribution networks and plays an important general role in conserving energy. PCMs exhibit a high enthalpy of fusion with the ability, in a relatively small volume, to store or release large amounts of energy as latent heat during melting and solidification. Additionally, practical PCMs require their upper and lower phase transition temperatures to be within the operational temperature range for a given application and possess high thermal conductivity for efficient heat transfer with congruent phase-change behaviour to avoid irreversible separation of their constituents.

In the last three years, the following articles have been published:

- 1909 regarding phase change materials in general
- 1545 regarding phase change materials in general for building applications
- 832 regarding the different types of requirements of phase change materials
- 369 regarding the integration methods of phase change materials

Showing an increasing trend through the years, confirming the rising interest in this field. Scopus has been used to conduct this research on the publication trends. In the following sections, more details about the topic beforehand mentioned will be given.

2.2.2 Classification of PCMs

Over the last 40 years different classes of materials, including hydrated salts, paraffin waxes, fatty acids, the eutectics of organic and non-organic compounds and polymers have been considered as potential PCMs. PCMs can be divided into three main groups, based on the temperature ranges over which the TES phase transition occurs:

- low temperature PCMs, with phase transition temperatures below 15 °C, usually used in air conditioning applications and the food industry;
- mid temperature PCMs, the most popular, with phase transition temperatures in the range $15 \div 90$ °C with solar, medical, textile, electronic and energy-saving applications in building design;
- high temperature PCMs, with a phase transition above 90 °C developed mainly for industrial and aerospace applications.

PCMs can be classified by their mode of phase transition: gas–liquid, solid–gas (which is quite unusual, so it would not be explored in this thesis,), solid–liquid and solid–solid systems, as in Fig. 2.3. Because the two most important criteria, the melting temperature and the melting enthalpy, depend on molecular effects, it is not surprising that materials within a material class can behave in a similar way. Fig.2.4 shows the typical range of melting enthalpy and melting temperature of common material classes used as PCM, as reported by Mehling and Cabeza (2008). Fig.2.4 indicates, also, that the energy density is roughly proportional to the melting temperature. This can be understood from thermodynamics according to the theory of Richards, which shows that the melting enthalpy per volume is proportional to the melting temperature, the number of bonds per molecule, and the density divided by the molar mass that relates to the packing density of the molecules or atoms (Lindner 1984).

Phase change materials that undergo phase change between liquid and solid are classified into three main categories: Organic, Inorganic, and Eutectics. These categories are subdivided into further categories based on the chemical components forming the PCM. Organic compounds are subdivided into these categories:

paraffin, fatty acids and organic mixtures. With their remarkable temperature range that covers most applications, paraffins seem to have great properties and wide advantages, since their latent heat is mass-based, they have no phase separation after solid-liquid transition frequent cycles. They also have low vapour pressure, however, they have low thermal conductivity and are flammable. The enhancement in thermal conductivity acquired great attention recently.

Inorganic PCMs are salt hydrates (most used), or metals and are of higher densities and energy efficiency than organics with the merits of wider transition temperature range, high latent heat and high thermal conductivity, besides, they are non-toxic, non-flammable and of low cost, compared to organic PCMs [96]. On the other hand, supercooling, phase segregation, lack of thermal stability, corrosion and decomposition, are drawbacks which dominate their benefits.

Eutectics are prepared combinations of two or more low melting temperature components of organics, inorganics, or both, each of which undergo congruent melting and freezing to produce components' crystals mixture upon crystallization. Their best features are not having concern about super-cooling and phase segregation. The main advantage of eutectics over other types of PCMs is that their melting points can be adjusted by combining different weight percentages of components.

2.2.3 Integration methods

It is notified that PCMs struggle to work effectively if they are added without any supportive process. Directly adding PCM may cause an unexpected chemical reaction or microstructure changes, leading to decreasing working performance of both PCM and matrix materials. Researchers have tried various methods to enhance or maintain the performance of PCMs; anyway, incorporation is an indispensable part as presented by near all PCM applications. The positive incorporation maintains the thermal properties of PCM and allows them to keep away from potentially unstable changes. There are two popular incorporation methods called encapsulation and shape stabilization.

Encapsulation

The encapsulation method means some compacted materials are coating the core PCM as capsules, which is an easy solution. The coated PCMs have certain independent spaces that physically shield themselves from matrix materials and the capability of energy regulation is maintained as much as possible. The encapsulation method is further classified into microencapsulation and macroen-

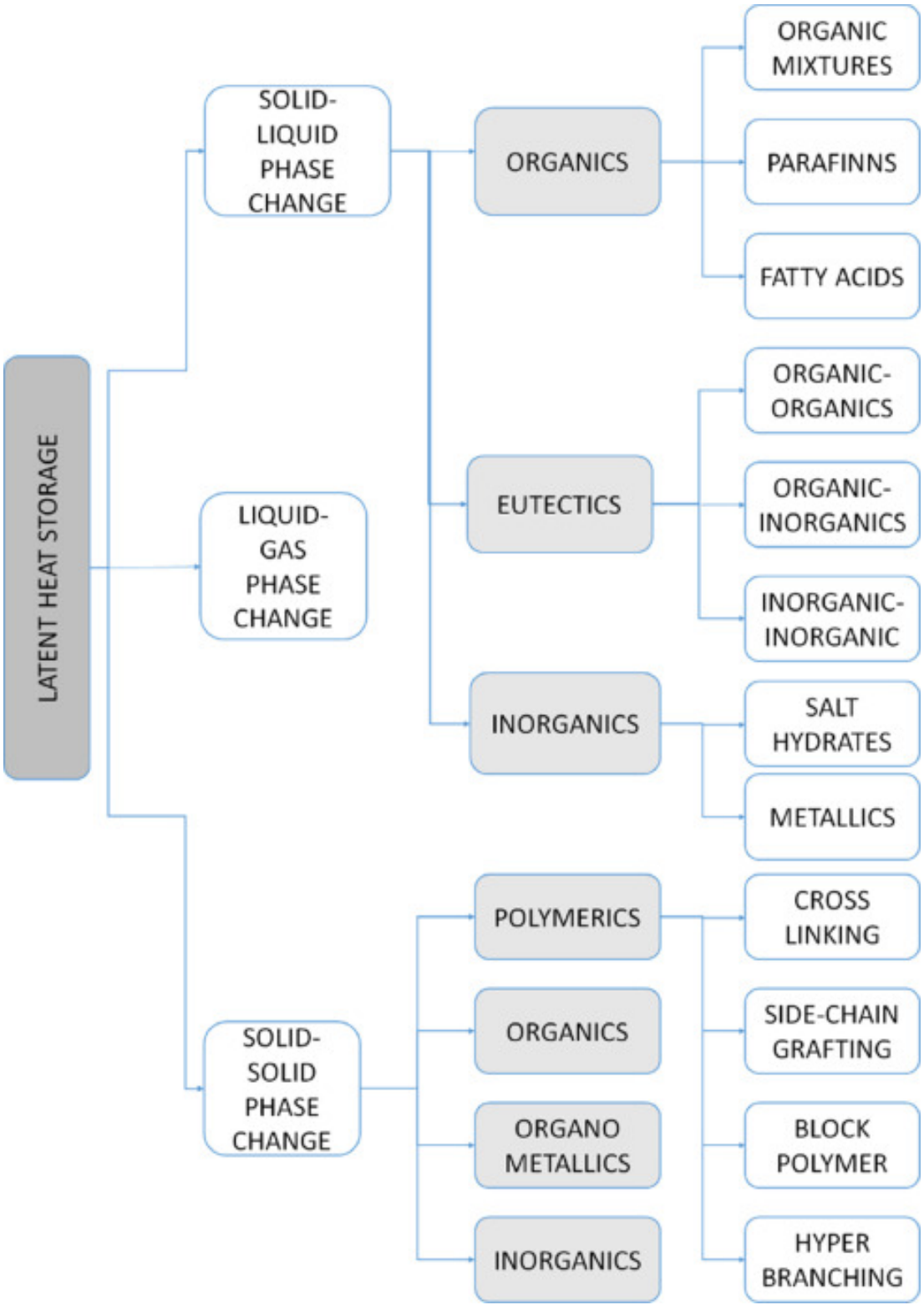

Figure 2.3: Classification of energy storage materials, from Jouhara et al. (2020)

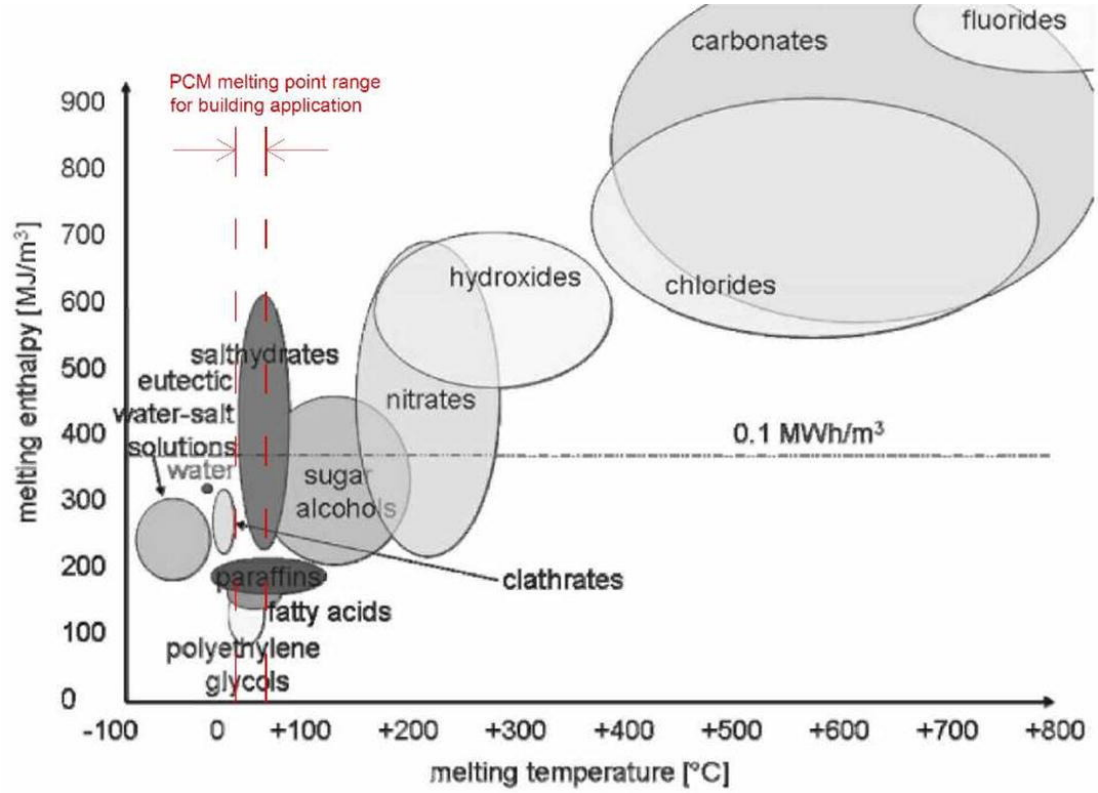

Figure 2.4: Classification of PCMs according to temperature range of phase change, from Mehling and Cabeza (2008)

capsulation but the difference does not involve just the size. The former showed that numerous capsules filled with PCM can be randomly and uniformly introduced into matrix materials. The latter usually was made as a part of structures like a layer embedded in a wall or a panel bonded at the surface.

In microencapsulation mode, the PCM is enclosed in a small capsule (from 1 μm to 1000 μm) made from natural and synthetic polymers. In the literature, two main microencapsulation methods have been reported, which are classified as physical and chemical methods. In the first technique, the PCM can be microencapsulated through spray drying, pan coating, centrifugal extrusion, pan coating or air-suspension coating. In the second method, the PCM is microencapsulated through the matrix, interfacial or in situ polymerization. Organic PCMs are the most suitable PCM type for this technique and, in particular, paraffin and fatty acid PCMs. In the direct incorporation technique, the PCM is leaked during the phase change process while using microcapsules prior to the mixing process with the construction elements, which on one hand, successfully overcomes this problem and, on the other hand, improves the heat transfer processes through increasing the heat transfer area, reducing the PCM volume change and improving the thermal reliability.

PCM macroencapsulation is defined as the process of packing PCMs into containers shell with sizes greater than 5 mm. Several forms of containers can be used, such as spheres, tubes, panels and pouches. The main advantages of this encapsulation technique are improving the heat transfer rate, increasing the amount of used PCM, reducing the PCM volume change, and avoiding the leakage problem. However, the disadvantages of macroencapsulation include corrosion, the macrocapsules should be protected in the case of drilling holes in building walls, and it equires more work during the integration into the building envelope.

Shape stabilization PCM

Shape stabilization is another welcomed incorporation technique. It impregnates PCMs into the supporting material rather than coated by a shell. This application method is similar to that of MicroPCM. For leakage prevention and high absorbing rate, the supporting material has a porous structure in most cases. Hence, PCMs are absorbed into porous supporting materials and become shape stabilized PCM composites.

The most prevailing processing methods are vacuum impregnation and melting (direct) impregnation, also others like the self-acting combination. Many factors determined the incorporation of shape stabilized PCM. For example, a high temperature of liquid PCM could accelerate the absorbing rate but may affect the maximum absorption proportion, and vacuum impregnation did not always work better than direct impregnation. Using these supporting materials, up to 80% of the PCM mass proportion can be used.

2.2.4 Physical, technical, and economic requirements

A suitable phase change temperature and a large melting enthalpy are two of the main requirements of a PCM. They have to be fulfilled in order to store and release heat at all. However, there are more requirements for most, but not all, applications. These requirements can be grouped into physical, technical, and economic requirements.

- Physical requirements, regarding the storage and release of heat:
  - Suitable phase change temperature T_{pc}, to assure storage and release of heat in an application with given temperatures for heat source and heat sink.
  - Large phase change enthalpy ΔH, to achieve high storage density compared to sensible heat storage.

  - Reproducible phase change, also called cycling stability, to use the storage material as many times as required by an application. The number of cycles varies from only one, when the PCM is used for heat protection in the case of a fire, to several thousand cycles when used for heating or cooling of buildings. One of the main problems of cycling stability is phase separation, which is the effect that phases with different composition are separated from each other macroscopically. When a PCM consists of several components, phases with different compositions can form upon cycling. The phases with a composition different from the correct initial composition optimized for heat storage then show a significantly lower capacity to store heat.
  - Little subcooling, to assure that melting and solidification can proceed in a narrow temperature range. Subcooling (also called supercooling) is the effect that a temperature significantly below the melting temperature has to be reached, until a material begins to solidify and release heat, please see Fig.2.5. If that temperature is not reached, the PCM will not solidify at all and thus only store sensible heat.
  - Limited thermal hysteresis, which is defined as the separation between the actual melting point and the crystallization temperature of a PCM. The magnitude of the thermal hysteresis is proportional to the energy loss of a system. In addition, the latent heat of the PCMs cannot be exploited if the thermal hysteresis is beyond the operating temperature range of a system.
  - Good thermal conductivity, to be able to store or release the latent heat in a given volume of the storage material in a short time, that is with enough heating or cooling power. The required thermal conductivity, however, depends on the application and the design of the storage.

- Technical requirements, regarding the construction of a storage:

  - Low vapor pressure, to reduce requirements of mechanical stability and tightness of the casing containing the PCM.
  - Small volume change, to reduce requirements of mechanical stability of the casing containing the PCM.
  - Chemical stability of the PCM, to assure long lifetime of the PCM.
  - Compatibility of the PCM with other materials, to assure long lifetime of the casing that contains the PCM, and of the surrounding materials in the case of leakage of the PCM.

  - Safety constraints the construction of a storage can be restricted by laws that require the use of non-toxic, non-flammable materials. Other environmental and safety consideration can apply additionally.

- Economic requirements, regarding the development of a marketable product:

  - Low price, to be competitive with other options for heat and cold storage, and to be competitive with methods of heat and cold supply without storage at all.
  - Good recyclability, for environmental and economic reasons.

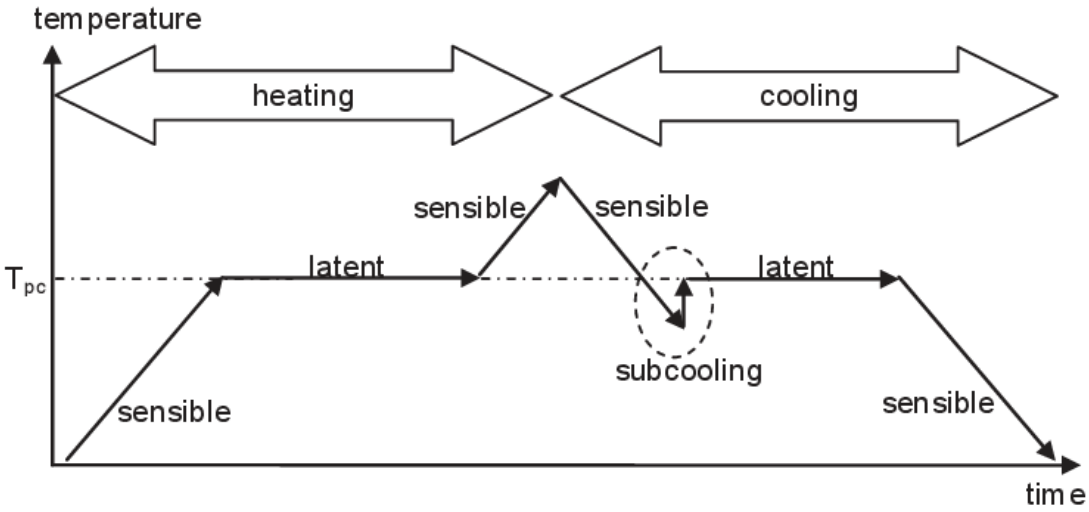

Figure 2.5: Schematic temperature change during heating (melting) and cooling (solidification) of PCM with subcooling

Lane et al. (1983) gives a detailed discussion of these selection criteria and examples of how to select candidate materials. A first selection of a material is usually done with respect to the physical requirements phase change temperature, enthalpy, cycling stability, and subcooling. The classes of the materials to choose from, as well as lists of examples for different classes with data on phase change temperature and enthalpy, are discussed in the following section.

Usually, a material is not able to fulfill all the requirements mentioned above. For example, the thermal conductivity of a PCM is usually small, inorganic PCM often show subcooling, and compatibility with the container material is not always given. Therefore, different strategies have been developed to cope with these problems.

2.2.5 Measurement of thermal properties of PCMs

The process of selecting a suitable PCM is very complicated but crucial for thermal energy storage. The potential PCM should have a suitable melting temperature, desirable heat of fusion and thermal conductivity specified by the practical application. Thus, the methods of measuring the thermal properties of PCMs are very important.

There are many existing measurement techniques, among which Differential Scanning Calorimetry (DSC) and Differential Thermal Analysis (DTA) are most commonly used, but there are also other suitable options.

Differential scanning calorimetry

In DSC test, the sample and the reference, with known thermal properties, are maintained at the almost same temperature throughout measurement process, and by measuring the difference of heat added between the sample and the reference, many thermal properties of the sample can be obtained, such as heat of fusion, heat capacity and melting/solidification temperature.

The DSC method can also be used for analysing the thermal properties of PCM-wallboards. Through DSC test, not only can the melting temperature and heat of fusion of PCM be obtained, but also the distribution of PCM in wallboard, the heat storage capacity of PCM-wallboard and the effect of multiple thermal cycling on thermal properties of PCMs can be tested.

Differential thermal analysis

In DTA test, the heat applied to the sample and the reference remains the same (rather than the temperature in DSC test). The phase change and other thermal properties can then be tested through the temperature difference between the sample and the reference.

T-history method

Some Authors analysed the limitations of conventional methods including conventional calorimetry, DSC and DTA, and then put forward a new method called T-history method to determine the melting temperature, degree of supercooling, heat of fusion, specific heat and thermal conductivity of PCMs.

The T-history method is based on recording the temperature as a function of time for a PCM sample and a sample of reference material. Initially, both samples are in equilibrium with the environment at constant temperature that is

significantly higher or lower than the PCM phase transition temperature. The test starts when the PCM and reference samples are suddenly immersed in the environment with a temperature different from the equilibrium temperature of the samples. Thus, if the temperature of the PCM and the reference is below the phase change temperature, they should be placed in an environment with a temperature significantly higher than the phase change temperature to realize the phase transition during the heating process. In the other case, when the temperature of the samples is higher than the phase change temperature, they should be placed in an environment of sufficiently low temperature to realize the phase transition during a cooling process. For this purpose, the test samples are, for example, immersed in a water bath or put into a thermal chamber at a suitable temperature.

In the experiment, thermocouples are placed in the center of the samples with PCM and reference material, and another thermocouple is positioned at some distance from the samples. Registration of measurement data provides two temperature vs time curves, one for the PCM and the other for the reference, and a third for the environmental temperature. The areas under the PCM and reference temperature curves are compared with each other to determine the thermo-physical properties of the PCM. A new modified T-history method was then developed by improving some improper assumptions in the original one.

2.2.6 Thermal stability of PCMs

The long-term stability of the PCMs is required by the practical applications of latent heat storage, and therefore there should not be major changes in the thermal properties of PCMs after undergoing a great number of thermal cycles. Thermal cycling tests to check the stability of PCMs in latent heat storage systems were carried out for organics, salt hydrates and salt hydrates mixtures by many researchers. Some potential PCMs were identified to have good stability and thermo-physical properties.

Shukla et al. (2008) carried out the thermal cycling tests for some organic and inorganic PCMs selected based on thermal, chemical and kinetic criteria and their results showed that organic PCMs tend to have better thermal stabilities than inorganic PCMs. Other Authors conducted the thermal cycling test for calcium chloride hexahydrate and found minor changes in the melting temperature and heat of fusion, only about $1 \div 1.5$ °C and 4% average variation respectively during the 1000 thermal cycles. They recommend the calcium chloride hexahydrate be a promising PCM for applications.

Inorganic materials cover a wide temperature range. Compared to organic materials, inorganic materials usually have similar melting enthalpies per mass, but higher ones per volume due to their high density. Their main disadvantage is material compatibility with metals since severe corrosion can be developed in some PCM-metal combinations.

2.2.7 Heat transfer enhancement

Bugaje (1997) reported that the phase change time is one of the most important design parameters in latent heat storage systems and found adding aluminium additives to paraffin wax can significantly reduce the phase change time in heating and cooling processes. However, this method results in weight increasing and high cost of the system. Metal foams manufactured by sintering method, have many desirable characteristics such as low density, large specific surface area, high specific strength-to-density ratio as well as high thermal conductivity. All these desirable properties offered by metal foams make them promising in heat transfer enhancement for PCMs.

Boomsma et al. (2003) found using open-cell metal foams in compact heat exchangers generated thermal resistances twice and three times lower than the best commercially available heat exchanger tested. Thermal transport in high porosity open-cell metal foams was experimentally and numerically investigated in more studies, in which it is found that the effective thermal conductivity increases rapidly as temperature increases and porosity decreases.

Tian and Zhao (2010) conducted a numerical and experimental investigation of heat transfer in PCMs enhanced by metal foams, and their experiment showed a significant increase in heat transfer rate. Their numerical simulations employed a two-equation non-thermal equilibrium model to account for coupled heat conduction and natural convection, and a good agreement with experimental data was achieved. They reported that metal foams suppress natural convection whilst promoting heat conduction significantly, with the overall heat transfer rate still being higher than the pure PCMs. Py et al. (2001) impregnated paraffin wax in a graphite matrix by employing capillary forces, and high thermal conductivity and stable power output were observed. Fukai et al. (2003) found carbon fibres improved the heat exchange rate during the charge and discharge processes even when the volume fractions of carbon fibres were only about 1%. Zhou et al. (2011) carried out relevant experiments to compare the effects of metal foams and graphite materials on heat transfer enhancement, and the results indicate that both metal foams and expanded graphite can enhance heat transfer rate in the

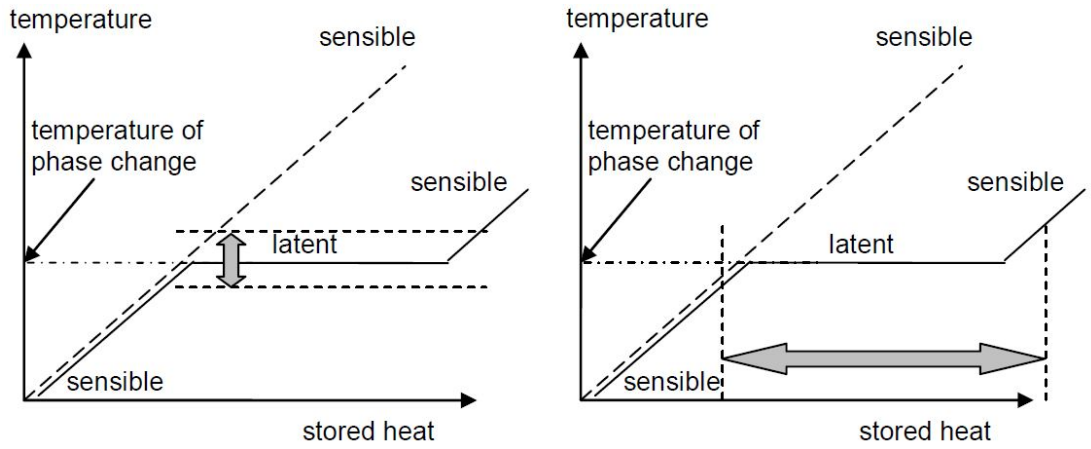

Figure 2.6: Potential fields of application of PCM: temperature control (left) and storage and supply of heat or cold with small temperature change (right)

thermal storage system, with metal foams showing a much better performance than expanded graphite. Opolot et al. (2020) analysed the melting/solidification rate of the PCM and found out that the cascading of the graphite porous foams results in an efficient design that enhances heat transfer compared to when one graphite foam is used and that having a lower porous foam closer to the heating/-cooling wall accelerates the charge-discharge cycle. Righetti et al. (2022) showed that the addition of a foam can drastically shorten the phase change materials charging and discharging times up to 10 and 5 times, respectively.

2.2.8 Applications of PCMs

PCMs find applications in the building industry, textiles, the automotive sector and solar energy installations. In recent years an increasing number of applications, including those in electronics and medicine, has emerged. The traditional sectors, such as the construction industry, are being advanced by novel, more sophisticated TES materials for smart textiles and thermoregulated biomaterials, etc. Potential fields of application of PCM can be found directly from the basic difference between sensible and latent heat storage, shown in Fig 2.6 and a complete overview can be seen in Fig. 2.7. They can be divided as a simplification into temperature control and storage and supply of heat or cold with small temperature changes.

Thermal storage in buildings

TES for space heating and cooling of buildings is becoming increasingly important because of the increasing cost of fossil fuels and environmental concerns.

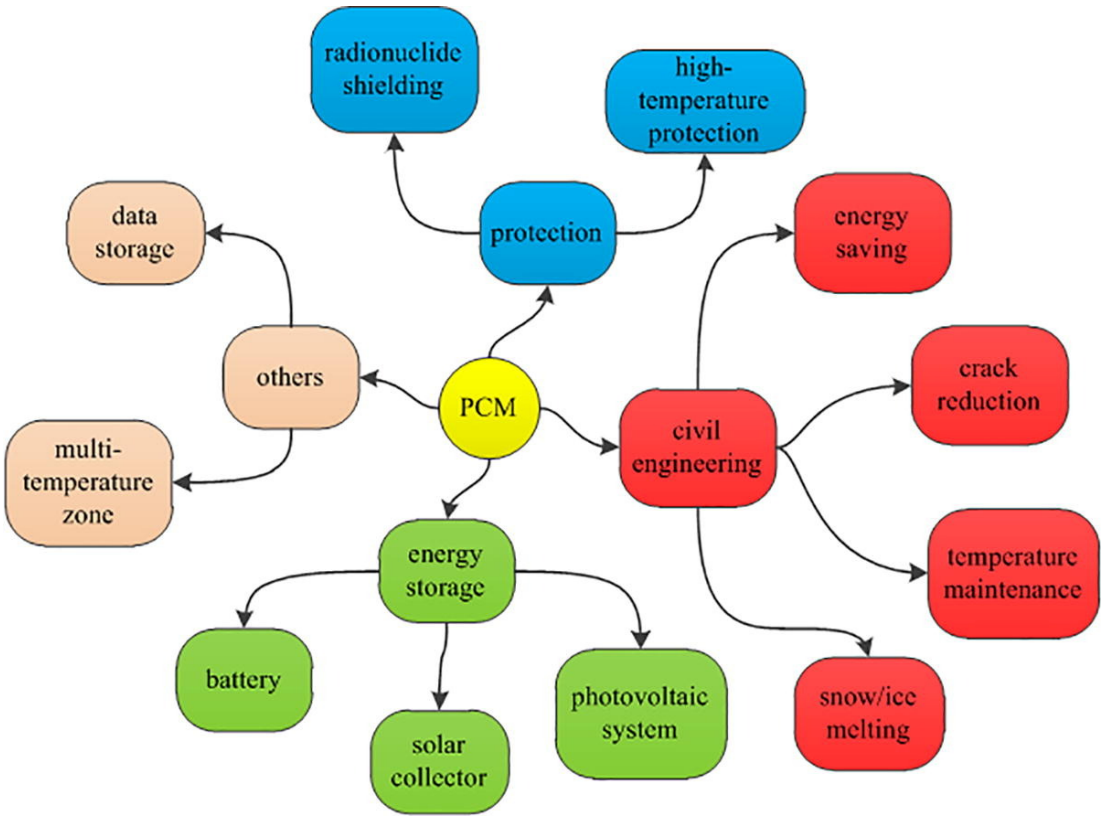

Figure 2.7: Specimens of PCM application in various areas, from Wang et al. (2022)

In extremely cold or hot areas, electrical energy consumption varies greatly during the day and the night due partly to the varying demand for domestic heating or cooling. PCMs in passive or active storage systems are able to minimize these variations. Passive heating or cooling systems refer to the technologies or design features for heating or cooling buildings without active mechanical devices using a system which uses little or no external energy. Active storage systems are used mainly for off-peak storage of thermal energy in buildings. Thus, the peak loads may be reduced and shifted to nighttime when electricity costs are generally lower. PCMs are continuously being investigated for active storage systems, including floor heating systems and photovoltaic devices.

Heating/cooling of water

The behaviour of encapsulated salt hydrates, used for LHS in a heat transfer system with a domestic hot water tank, was analyzed and it was found that the shortest time for complete solidification occurred with small spherical capsules, with high thermal conductivity. Cabeza et al. (2006) studied a hot-water storage tank with stratification containing a PCM module consisting of several cylinders. A granular PCM–graphite composite was selected as the PCM for the experiments, which showed that immersing a PCM module in a water tank for domestic hot-water supply provided hot water for a longer period even without an external supply of energy.

The latent functional thermal fluids

In recent years, research on latent functional thermal fluids, or two-phase heat transfer fluids, has increased because they exhibit greater apparent specific heat in the phase change temperature range than conventional single-phase heat transfer fluids. These latent functional thermal fluids are composed of PCM particles and a heat transfer fluid and may exist as a phase change microcapsule slurry or a phase change emulsion.

Since the PCM will absorb or dissipate latent heat in its phase change temperature range, it will show a much greater apparent specific heat. In addition, it may significantly enhance the heat transfer rate between the fluid and the tube wall, reduce the mass flow rate and energy consumption of the pump being used. Therefore, latent functional thermal fluids have many potentially important applications for heating, ventilating, air-conditioning, refrigeration and heat exchange.

Solar energy storage

Extensive efforts have been made in recent years to use the latent heat storage materials in thermosolar energy systems, where it is required to store heat during the day for use at night. The studies focused on an examination of the key aspects of heat transfer in PCMs and their behaviour in full size heat storage units.

The current revival of solar thermal electricity generating systems shows that economic TES for the temperature range from 250 °C to 500 °C are still needed. The TES-benchmark for parabolic trough power plants is direct two tank storage, as installed at the solar thermal electricity generating plant at Barstow (USA). Cascaded latent heat storages are marked by a minimum of necessary storage material. One of the early studies favoured cascaded latent heat storages and concrete regenerators.

Other applications

The previously cited applications were the nearest to the object of this thesis, however, PCMs are used in a lot of other contexts. The most important are smart textiles, biomaterials and biomedical applications, electronics, automotive industry, space applications, and food industry.

2.2.9 Benefits and drawbacks

PCM can effectively regulate the indoor temperature of the building. However, there are also some limitations regarding integration of the PCM in TES systems. Below are some limitations/demerits:

- there is a need to investigate mechanical, environmental and economic aspects along with experimental study of the proposed material to evaluate the feasibility of the technology, as reported by Elias et al. (2019)
- effect of heat transfer on total energy savings and a detailed comparison between all the systems is needed, as reported by Bastani et al. (2014)
- there is still no international standard for PCM testing and analysis, as reported by Fallahi et al. (2017)
- the materials with the best thermal properties, such as paraffin wax or fatty acids, are highly flammable, as reported by Faraj et al. (2021)
- to maintain stable performance of the storage systems, future work must avoid phase separation and supercooling of PCMs

- the latent heat activation of unsuitable selection of the PCM based on phase transition temperature can cause higher cooling energy demand in the summer season, as reported by Farid et al. (2004)
- if the temperature change range of the PCM occurs only during summer, the PCM does not show any effect during the winter season, as reported by Gil et al. (2010)
- microencapsulated PCM can show a demerit of PCM damage during mixing with concrete; thus, there is a need to understand the loss of PCM on its long-term effect on energy efficiency, as reported by Huang et al. (2019)
- the compressive strength of the concrete reduces when it is incorporated with thermal energy storage material like PCM, as reported by Cabeza et al. (2007)
- most of the studies in the literature use a small amount of PCM for conducting experiments, so the results will deviate when the quantity of the PCM increases and the experiment was done on real size building, as reported by Du et al. (2021)

In the following chapters, some preliminary studies regard pure concrete TES systems, with a single block and with multiple elements arranged in series, parallel and combined configurations.

Then, the focus will be on investigating higher PCM percentages, trying to limit the concrete compressive resistance reduction, and comparing the heat transfer and the total energy savings, with different PCM types and solutions.

3. Simplified model for concrete TES simulation

3.1 Introduction

Electrical power generation by using concentrated solar thermal energy is one of the most promising renewable energy technologies. It is widely accepted that a great improvement in CSP plants can be accomplished by adding a thermal storage system. It would permit to meet the peak demand through a rational optimization of the energy production by the CSP plant, especially during night time or cloudy weather. During energy storage process, commonly called charging or heating stage, the heat transfer fluid, heated by the solar field, warms up the TES, flowing through the modules and stores a certain amount of energy by increasing the TES temperature. Conversely, during energy discharge process, commonly called discharging or cooling stage, the cold fluid is pumped through the TES to extract heat to be released to the power plant. The HTF flows in pipes that are commonly embedded in the thermal storage materials, which can be molten salts, concrete, soil, sand, or rocks, etc.

The technology for Sensible Thermal Energy Storage (STES) for CSP plants is well known and it has been widely investigated; in the last decades, various solar plants with different fluids and storage systems, have been built in USA, Spain, Germany, and Italy, as reported in Gil et al. (2010), Medrano et al. (2010), and Kuravi et al. (2013). Concrete is widely used for the construction of TES because it offers low cost, good, and stable thermal properties, appropriate structural conditions, long durability and simple industrial production, as clearly reported in Salomoni et al. (2015) and Laing et al. (2006 and 2009). In particular, the proper selection of the concrete mixture allows for obtaining a good resistance and stability at temperature values even greater than 300 °C. At high temperature, the humidity contained in the concrete can become a severe problem, inducing pressure gradients, matrix damage and performance reductions; for this reason,

the concrete has to undergo to a degassing process, (i.e. a very slow first heating cycle), to remove the excess of humidity and preserve the integrity of the module.

Besides, the HTF is basically an energy-carrying medium, so the heat transfer process between TES material and the HTF is of crucial importance in order to properly study the charge and discharge processes.

In the open literature, many different models to simulate various types of TES systems have been proposed and published. The literature regarding STES models is very large; for this reason, only the main models for concrete STES are here reported and briefly reviewed. For the sake of clarity, in what follows, the models are subdivided in three main categories: analytical, Finite Element Method (FEM), and simplified models. This classification could be debatable because various analytical models due to their assumptions could also be considered simplified models, but it allows for a clear and schematic overview.

3.1.1 Analytical models

One of the most desirable ways to analyze a system is trough analytical models, so various studies have been accomplished to get this result. However, only a few recent works present a full analytical solution. Among others, Tu and Lee (2015) presented a solution for the hollow cylinder with time-dependent boundary conditions and diabatic external boundary based on shifting functions, while Zhou (1995) presented a Laplace transform methodology for the same geometrical configuration with well stirred fluid and adiabatic boundary. They can achieve an exact solution, which is very appreciable, but, because of the complexity of the methodology, none of them can be easily implemented and practically used for simulation codes.

More over, in Salomoni et al. (2014), an analytical-type relation was derived from an exact physical model to calculate the charging time in concrete modules. Then, verification via FEM models was conducted. The implementation of two mathematical models for solving the balance equation within CAST3M^{TM} and simulating charge and discharge processes for a TES element was described. Both models were validated referring to Bai et al. (2009), in which the Authors found a semi-analytical relation by solving the heat transfer process in the solid heat storage medium using an integral approximate method.

In Xu et al. (2012) a corrective coefficient was found to extend the validity of lumped capacitance method for large Biot numbers in thermocline heat storage tank. However, the Authors considered an adiabatic outer boundary surface, which is not always applicable.

3.1.2 FEM models

A closed-form solution of the analytical models cannot usually be found; hence, one of the most used approaches is the numerical one. Simulations based on FEM are very accurate, even though quite rigid, so they are commonly used to discretize simple or complex objects, in each field, also in the case of STES systems.

In Laing et al. (2008), a model was developed to conduct an energetic and exergetic analysis of modular storage operation concepts to achieve an optimized configuration and a related cost reduction of the heat exchanger in concrete storage system.

Bai et al. (2011) proposed a numerical simulation model for a two-stage concrete thermal storage system; the model was based on the conservation principle of mass and energy. In Laing et al. (2012), a study concerning concrete thermal energy storage was conducted. A FEM transient thermal simulation was run to calculate the temperature inside the concrete module.

In Ferone et al. (2014), the focus was STES systems using solid media and numerical simulation of their transient behavior.

High performance TES materials from the literatures were also tested and used as reference benchmarks. In Giannuzzi et al. (2017), experimental tests were analyzed by means of suitable numerical models using a commercial code. The agreement between experimental and numerical results confirmed the predictive capabilities of the adopted tools. In Mazzucco et al. (2014), a 3D FEM model have been developed by University of Padova to simulate the TES behavior during plant's transient cycles and it was compared with a previously 1D model developed by ENEA. The new model achieved a better agreement as compared to the 1D solution.

The presented FEM models are always very accurate and allow precise analyses, but they have been specifically implemented for the object of the studies; thus, due to their intrinsic nature, they cannot be easily extended to different cases or geometries. Another implicit limitation is related to the computational time, which is not compatible for quick simulation.

3.1.3 Simplified models

In some cases, depending on the requirements, a simplified model could be a more suitable solution, instead of the more accurate, though more complex and rigid, FEM simulations, since there is the particular need in an operative situation for results on the overall performance of the whole systems, considered

as a macro element, instead of the more precise, but also more computational time-consuming, simulations on the micro elements. For this purpose in the last decades, a few methods and models have been developed; here, a brief overview.

Sragovic (1989) proposed a practical method for designing and predicting operational performance of a high temperature STES system. Two computer codes for the design of TES were developed, based on steady state and transient analyses, and they allowed to predict the performance of the TES and to optimize its design.

In Wu et al. (2009), a simplified numerical model was proposed. The aim was to determine the dynamic characteristics of the composite sorbents and to evaluate the specific capacity and the coefficient of performance of an open-type thermal energy storage system. The governing equations were solved by using the Finite Volume Method.

In Bruch et al. (2014), a 1D numerical model, based on two energy balances, was developed and validated for dual-media thermocline storage. The model consisted of a finite difference representation of the energy balance equations.

Simulation environments for modeling can also be used. The most common environment is Dymola, in Modelica platform. For example, in Tamme et al. (2004), a simulation tool for the analysis of the transient performance of solid media STES was implemented.

In Laing et al. (2006), two different storage materials were investigated: a castable ceramic and a high temperature concrete, which seemed to be the more favorable material. This model was previously developed and described in detail by Tamme et al. (2004). In Laing et al. (2009), a concrete STES was developed and tested. The simulated oil temperature at the outlet of the module and the oil temperature measured were in fair agreement. For the heat flow rate between oil and storage unit, the difference was more pronounced. A simplified power block, the collector field, and the concrete storage, were modeled using Modelica. For the validation of the model, a comparison of simulation data and experimental data was performed, showing a good agreement.

In Stuckle et al. (2014), an overview of coupled systems was given. A transient model with a short calculation time was required allowing for a fast simulation of the system during a period of days or months. To run fast simulation, an approach to simplify the two dimensional transient heat conduction problem, inside the hollow cylindrical heat storage mass, was sought. Schmidt and Willmott (1981) proposed a method, originally developed by Hausen (1931), in which the heat transfer coefficient between fluid and storage was adapted to account for the radial heat conduction inside the hollow cylinder. With this approach, the hollow

cylinder was treated as a lumped system.

Other modelling solutions can be found in Gil et al. (2010) and Medrano et al. (2010). The Authors stated that the development of an efficient and cost-effective TES is crucial for the future development of CSP plants; however, the number of papers addressing this issue was considered relatively scarce.

Even if the concrete TES systems have already been studied, their application is still a matter of research; in particular, there is a strong need of practical prediction tools to enable simple and fast simulations of TES embedded in power plants.

From this standpoint, this work aimed at developing a new computational tool able to predict the behavior of the concrete storage modules. In particular, the attention was focused on a modular and flexible tool that, under the necessary assumptions, allows for the real-time simulation of the general TES module's parameters during the operation of the entire system.

As it clearly appears from this brief overview, the models reviewed have many limitations, which can be summarized as:

- high computational efforts and low flexibility (Computational Fluid Dynamics (CFD)/FEM models)
- high complexity (analytical models)
- adiabatic external boundary conditions (CFD/FEM and analytical models)
- no models consider the presence of insulating layers on the external surface of the TES system
- necessity of semi-empirical constants or parameters derived from FEM simulations

Hence, those models are not suitable for on-field analysis, because in that situation it is essential to know the results in real time, in order to safely and efficiently manage the system at any time and conditions.

The main parameter describing the TES is the ability of each element (or module) to store (during heating stage) or to release (during cooling stage) the thermal energy from or to the HTF; in the case of concrete TESs and in general for STESs, this parameter is the mean temperature of the concrete TES.

The developed model was meant to compute the stored or the transferable energy over time, related to the ideal maximum value (thermal efficiency or effectiveness) and the related HTF temperature at the outlet of the module.

3.2 Model description

As previously described, the first and main aim of this work is to provide a simplified model that could resolve or at least mitigate the described limitations of the proposed approaches without introducing any additional one. With this in mind, the first problem to face up was to reduce the complexity of the geometry of the TES module, in which cylindrical tubes were embedded in a concrete parallelepiped, which then was covered by multiple insulating layers.

It is well-known that axial symmetric geometries can lead to interesting simplifications and thus, as depicted in Fig. 3.7, the entire concrete module was schematized to be a cylinder with an equivalent diameter based on volume (i.e. keeping constant the mass) defined as:

$$D_{eq,TES} = \sqrt{\frac{4L_{side,TES}^2}{\pi}} \tag{3.1}$$

Similarly, the two external insulating layers were approximated with two equivalent annular volumes with diameters calculated keeping constant their actual heat transfer areas, as:

$$D_{eq,ins1} = \frac{A_{ins1,ext}}{\pi L_{TES}} \tag{3.2}$$

$$D_{eq,ins2} = \frac{A_{ins2,ext}}{\pi L_{TES}} \tag{3.3}$$

As showed in Figs. 3.4 and 3.7, the embedded steel tube presented a 4-passage configuration; thus, by neglecting the three curves that have no effect on the global system performance, the storage module can be considered of being constituted by 4 sub-units, called basic elements, arranged in series. A similar schematization was also used by different Authors such as Sragovich (1989), Bai et al. (2009), and Salomoni et al. (2014). In this way, the basic element assumes the well-known geometry, often described as "washer", in which the tube is placed in the cylinder center; in the specific case, as showed in Figure 3.7, each of 4 elements has 2 adiabatic sides (towards the adjacent elements), and 2 diabatic sides (towards the external insulating layers).

Also, in the case of the concrete sub-system, an equivalent diameter based on

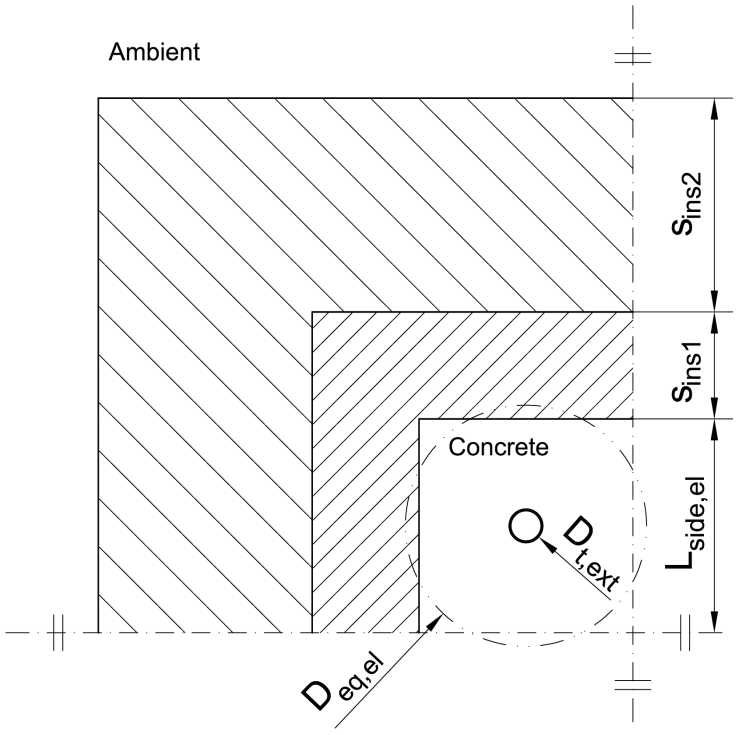

Figure 3.1: Concrete sub-element and insulating layers scheme

volume (to keep constant the mass) can be defined as:

$$D_{eq,cnc} = \sqrt{\frac{4L_{side,el}^2}{\pi}} \tag{3.4}$$

more details on geometrical parameters are reported in Tab. 3.3.

All the simplified simulation models are based on the well-known lumped capacitance method, a good review of this method can be found in Xu et al. (2012), in which the former analysis of Schumann (1929) is reported and commented. In the lumped capacitance method, which cannot be applied for high values of Biot numbers, the basic assumption is that the concrete temperature must be constant along the cylinder radius.

Li et al. (2014) and Jian et al. (2015) presented two interesting modified or "extended" lumped capacitance models for different TES systems: in the first case the model was only compared against a CFD analysis, while the second model was verified against both analytical and experimental results. In particular, Li et al. (2014) proposed an "extended" lumped capacitance model for Biot number up to 100. In the present study, the estimated Biot numbers are equal to 123 and 153 for the two different mixtures. The section has been divided into four square sub-elements and they have been studied as equivalent cylinders. Hence, the

characteristic length used to calculate them has been assumed as the equivalent diameter of the cylindric sub-element of the section, which is equal to 0.11284 m.

The model here proposed assumes the fundamental lumped capacitance hypotheses, but it also introduces a set of new assumptions:

- The heat exchange processes are described by means of suitable thermal resistances, in order to obtain a series/parallel overall scheme
- The entire module is assumed to be characterized by the mean concrete temperature, being constant on both radial and axial directions; this temperature is assumed to be the temperature of the two symmetry planes which divide the entire module in 4 sub-units, as described in the previous section
- The energy dissipation of the TES module towards the surroundings is estimated by the external surface temperature of the TES system
- In order to take into account the internal energy variation of the insulating layer mass, the time dependent mean temperature of each insulating layer is estimated and the internal energy variation is obtained at each time step
- The desired model calls for a non-steady solution, so the temperatures of concrete, oil and insulating layers are estimated by two energy balance equations (one for charging and one for discharging phase), by discretizing the time variable in time steps ($\Delta\tau$). The time step duration can be selected as a function of the total time length of the charging or discharging process. For 5-10 hours process a standard time step can be suggested to be around 10-30 seconds. Considering the available experimental data, in which the recording interval was exactly 5.56 s, the same value was also chosen in the simulations to exactly match numerical and experimental data. The balance equations of the heat fluxes and the consequent temperatures are solved with a simple numerical iterative procedure because heat fluxes and temperatures are coupled and an explicit solution cannot be implemented
- For the outlet oil temperature calculation during heating/charging process only, the exchanged latent heat due to the evaporation of the free water, present in the concrete mixture, was considered and evaluated

3.2.1 Governing equations

When combining the internal (A) and external (B) section calculations (Fig. 3.2, upper part), and taking into account the 4 basic elements arranged in series

that constitute the entire TES system, the heat flux balance for the entire TES element for the heating and cooling phase can be written. The balance equations for the charging/discharging processes are slightly different due to the different role of the heat flux dissipated by the TES towards the environment (convective and radiative).

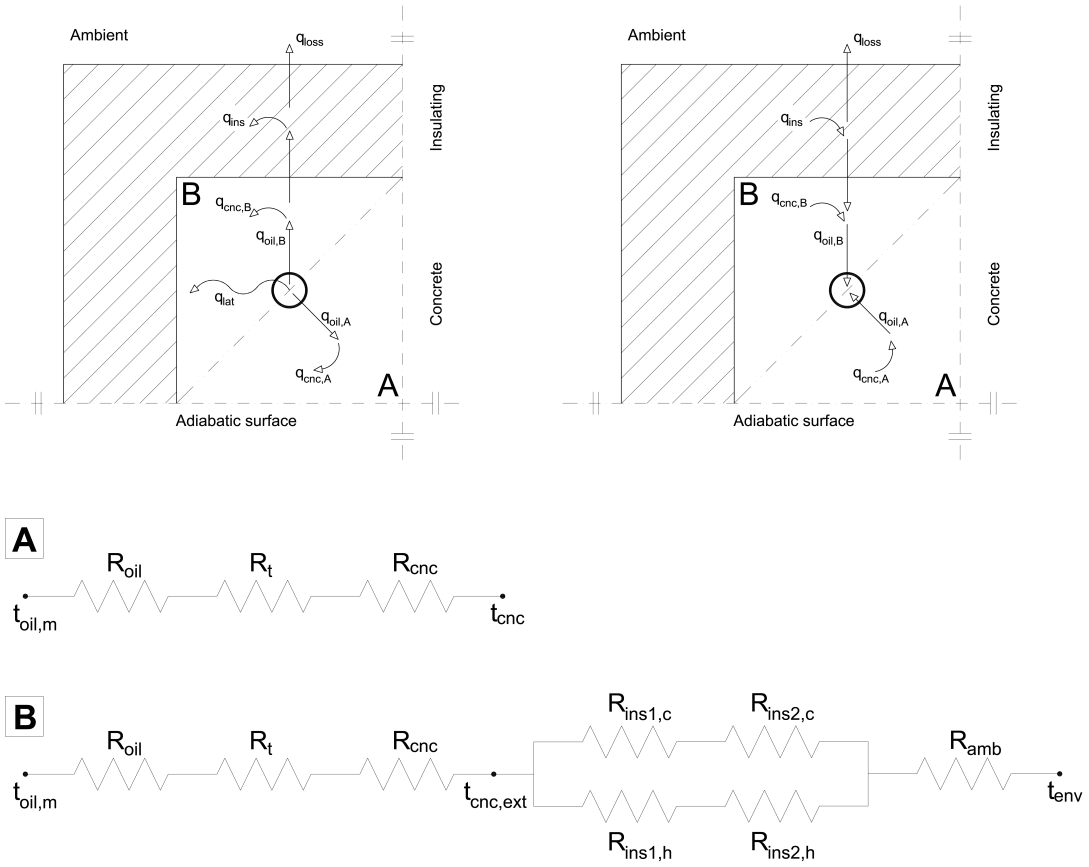

Figure 3.2: Heat fluxes scheme for heating (left) and cooling (right) test (up). Thermal resistances network (bottom)

Heating/charging phase energy balance (referring to Fig. 3.2, left-hand side schematic)

$$q_{cnc,A} = q_{oil,A} \tag{3.5}$$

$$q_{cnc,B} = q_{oil,B} - q_{ins} - q_{loss} \tag{3.6}$$

$$q_{cnc} = q_{cnc,A} + q_{cnc,B} = q_{oil,A} + q_{oil,B} - q_{ins} - q_{loss} \tag{3.7}$$

Cooling/discharging phase energy balance (referring to Fig. 3.2, right-hand side schematic)

$$q_{cnc,A} = q_{oil,A} \tag{3.8}$$

$$q_{cnc,B} = q_{oil,B} - q_{ins} + q_{loss} \tag{3.9}$$

$$q_{cnc} = q_{cnc,A} + q_{cnc,B} = q_{oil,A} + q_{oil,B} - q_{ins} + q_{loss} \tag{3.10}$$

In this way, after an iterative procedure on heat fluxes and temperatures, the internal energy variation of concrete TES and, consequently, the new value of TES element temperature can be obtained at each time-step:

$$\Delta t_{cnc} = \frac{q_{cnc}}{m_{cnc} c_{cnc}} \cdot \Delta\tau \tag{3.11}$$

$$\Delta t_{cnc} = |t_{cnc,\tau+\Delta\tau} - t_{cnc,t\tau}| \tag{3.12}$$

with sign (+) for heating (the concrete temperature is increasing) and sign (-) for cooling (the concrete temperature is decreasing). After the concrete and oil heat fluxes calculation, the outlet oil temperature can be estimated and compared against the experimental results. The entire model structure and the relative iteration scheme are summarized in the flow chart reported in Fig. 3.3.

The calculation of the heat fluxes in the governing equations is fully described in the following paragraphs. The detailed model description can be started from the definition of the thermal conductive resistances of the system and, in particular, from the insulating layer.

The total insulating cover area can be divided into the side surface of the equivalent hollow cylinder and the plane one of the two cylinder bases (the "heads"

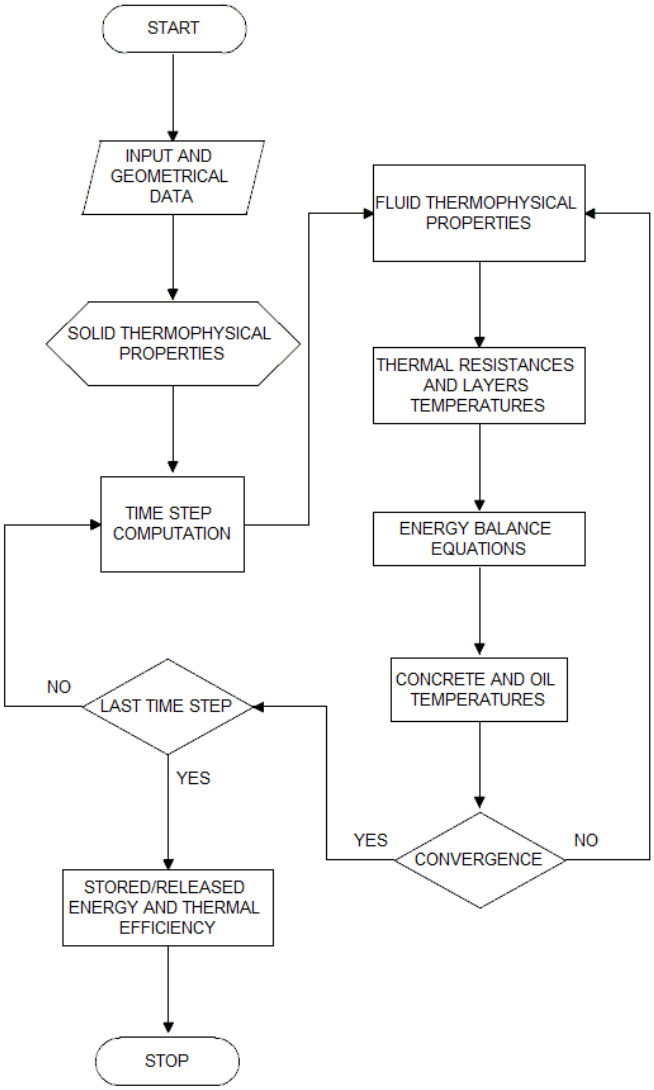

Figure 3.3: Model procedure flow chart

of the module) of the equivalent cylinder. The thermal resistances of side surfaces for each insulating layer can be evaluated as:

$$R_{ins1,c} = \frac{1}{2\pi\lambda_{ins1}L_{TES}} \ln\left(\frac{D_{eq,ins1}}{D_{eq,TES}}\right) \tag{3.13}$$

$$R_{ins2,c} = \frac{1}{2\pi\lambda_{ins2}L_{TES}} \ln\left(\frac{D_{eq,ins2}}{D_{eq,ins1}}\right) \tag{3.14}$$

Being in series, the total thermal resistance for the side surface can be calculated as:

$$R_{ins,c} = R_{ins1,c} + R_{ins2,c} \tag{3.15}$$

The thermal conductive resistances for each insulating layer, computing the "heads" surface as plane wall, can be calculated as:

$$R_{ins1,h} = \frac{s_{ins1}}{\lambda_{ins1} 2A_{ins1,h,m}} \tag{3.16}$$

$$R_{ins2,h} = \frac{s_{ins2}}{\lambda_{ins2} 2A_{ins2,h,m}} \tag{3.17}$$

Again, being in series, the total thermal resistance for the "heads" surface can be calculated as:

$$R_{ins,h} = R_{ins1,h} + R_{ins2,h} \tag{3.18}$$

The overall thermal resistance of the insulating layers which cover the TES can be calculated considering that the thermal resistances of the side cylinder and the heads are arranged in parallel and subjected to the same temperature difference:

$$R_{ins} = \left(\frac{1}{R_{ins,c}} + \frac{1}{R_{ins,h}} \right)^{-1} \tag{3.19}$$

The ambient thermal resistance, which combines convective and radiation effects, can be calculated as:

$$R_{amb} = \frac{1}{h_{amb} A_{ins2,ext}} \tag{3.20}$$

Thus, the overall thermal resistance between concrete and environment is given by:

$$R_{ext} = R_{ins} + R_{amb} \tag{3.21}$$

The forced convective heat transfer coefficient oil is estimated by means of the well-known Dittus-Boelter semi-empirical correlation, thus the associated oil convective thermal resistance can be computed as:

$$R_{oil} = \frac{1}{h_{oil} A_{t,int}} = \frac{1}{h_{oil} \pi D_{t,int} L_t} \tag{3.22}$$

The HTF Nusselt number is considered equal to 3.66 in the laminar zone, while it is estimated with the Dittus-Boelter semi-empirical correlation in the turbulent zone, and interpolated as reported by Gnielinski (2013) in the transition zone:

$$Nu = (1 - \gamma) \cdot Nu_{lam,2300} + \gamma \cdot Nu_{turb,4000} \tag{3.23}$$

with:

$$\gamma = \frac{Re - 2300}{4000 - 2300} \tag{3.24}$$

where $Nu_{lam,2300}$ is the Nusselt number at the end of the laminar zone ($Re = 2300$) and $Nu_{turb,4000}$ is the Nusselt number at the beginning of the turbulent zone ($Re = 4000$).

The steel tube conductive thermal resistance is given by (see Tab. 3.3 for tube parameters):

$$R_t = \frac{1}{2\pi \lambda_t L_t} \ln\left(\frac{D_{t,ext}}{D_{t,int}}\right) \tag{3.25}$$

The concrete elementary system conductive thermal resistance, between external tube surface and elementary sub-system external boundary can be calculated as:

$$R_{cnc} = \frac{1}{2\pi \lambda_{cnc} (4L_{el})} \ln\left(\frac{D_{eq,cnc}}{D_{t,ext}}\right) \tag{3.26}$$

Finally, the overall thermal resistance between oil and concrete is given by:

$$R_{int} = R_{oil} + R_t + R_{cnc} \tag{3.27}$$

A summary scheme of the thermal resistances network, both for A and B sections, is reported in Figure 3.3 (bottom part).

It has to be pointed out that the heat flux equations (with the exception of loss heat flux) are here reported for the two different processes: thus, referring to heating/charging process in which the oil heats the concrete TES (Figure 3.3, left-hand side), and in the case of cooling/discharging (in which the concrete heats the oil mass flux) in which the absolute value has to be used (Figure 3.3, right-hand side).

As described in Figures 3.3, once the thermal resistances are defined, it is possible to present the heat flux between oil and concrete for the internal section (called "A", from the oil to the TES core), considering the complete TES system (the sum of the 4 sub-units), as:

$$q_{oil,A} = \left| \frac{t_{oil,m} - t_{cnc}}{2R_{int}} \right| \tag{3.28}$$

the section A is geometrically equal to the B one, each section has the half of the entire area, so the overall thermal resistance is multiplied for the factor 2.

The heat flux between oil and concrete for the external section (called "B", from the oil to the TES boundaries), considering the complete TES system (the sum of the 4 sub-units), is given by:

$$q_{oil,B} = \left| \frac{t_{oil,m} - t_{cnc,ext}}{2R_{int}} \right| \tag{3.29}$$

While the heat flux between concrete and environment is:

$$q_{loss} = \frac{t_{cnc,ext} - t_{env}}{R_{ext}} \tag{3.30}$$

The concrete external temperature can be estimated as:

$$t_{cnc,ext} = t_{oil,m} \pm \frac{q_{oil}}{R_{int}} = t_{oil,m} \pm \frac{q_{oil,A} + q_{oil,B}}{R_{int}} \tag{3.31}$$

with sign (-) for heating, and sign (+) for cooling processes. Thus,

$$t_{ins1,int} = t_{cnc,ext} \tag{3.32}$$

$$t_{ins1,ext} = t_{ins1,int} - \frac{q_{loss}}{R_{ins1}} \tag{3.33}$$

$$t_{ins2,int} = t_{ins1,ext} \tag{3.34}$$

$$t_{ins2,ext} = t_{ins1,int} - \frac{q_{loss}}{R_{ins}} \tag{3.35}$$

The temperature along the radius in the insulating layer is supposed to follow a logarithmic profile, and a mean temperature by volume for each insulating layer can be calculated as:

$$t_{ins,m} = \frac{\int_{int}^{ext} t(r) 2\pi r \; dr}{\pi(r_{ext}^2 - r_{int}^2)} \tag{3.36}$$

$$t(r) = t_{ins,int} + \frac{t_{ins,ext} - t_{ins,int}}{\ln\left(\frac{r_{ext}}{r_{int}}\right)} \cdot \ln\left(\frac{r}{r_{int}}\right) \tag{3.37}$$

$$\begin{aligned} t_{ins,m} = t_{ins,int} &- \frac{t_{ins,ext} - t_{ins,int}}{\ln\left(\frac{r_{ext}}{r_{int}}\right)} \cdot \ln\left(r_{int}\right) \\ &+ \frac{t_{ins,ext} - t_{ins,int}}{\ln\left(\frac{r_{ext}}{r_{int}}\right)} \cdot \frac{r_{ext}^2\left(\ln\left(r_{ext}\right) - \frac{1}{2}\right) - r_{int}^2\left(\ln\left(r_{int}\right) - \frac{1}{2}\right)}{(r_{ext}^2 - r_{int}^2)} \end{aligned} \tag{3.38}$$

Finally, the temperature variations of insulating layers to take into account the internal energy variation can be calculated as:

$$\Delta t_{ins,1} = |t_{iso1,m,\tau+\Delta\tau} - t_{iso1,m,\tau}| \tag{3.39}$$

$$\Delta t_{ins,2} = |t_{iso2,m,\tau+\Delta\tau} - t_{iso2,m,\tau}| \tag{3.40}$$

where $\Delta\tau$ is the defined time step.

The internal energy stored in insulating layers due to their mean temperature variations is given by:

$$q_{ins1} = \frac{m_{ins1} c_{ins1} \Delta t_{ins1}}{\Delta\tau} \tag{3.41}$$

$$q_{ins2} = \frac{m_{ins2} c_{ins1} \Delta t_{ins2}}{\Delta\tau} \tag{3.42}$$

$$q_{ins} = q_{ins1} + q_{ins2} \tag{3.43}$$

During the model validation, a constant offset between the calculated and experimental outlet temperatures, only during the heating processes, was observed, while the experimental cooling processes were perfectly matched. In particular, the calculated outlet oil temperature was always greater than the experimental one, meaning that, during the experimental heating tests, a certain amount of heat was exchanged, but not computed by the model. The Authors attributed this constant offset to a continuous humidity evaporation, which only occurs in the heating phase and disappears once the whole water is evaporated and drained from the concrete. This behavior is well known, even if not completely investigated because the water evaporation (often called "degassing" or "thermo-hydral" process) depends on many different parameters, such as concrete composition, dimension and shape of the concrete element, temperature slope, room temperature, concrete aging etc. Thus, when introducing, only for the heating phase, a latent heat flux due to the slow evaporation of the humidity trapped in the concrete mixture (often called "free water") the calculation perfectly matched the experimental results.

Referring to the recent and experimentally based works of Khalifa et al. (2000), Martins et al. (2015), and Laing et al. (2011), evaporated water mass flux was assumed to be 1 kg/h or 0.28 g/s for the entire TES concrete element. Laing et al. (2011) reported oven tests which showed that the concrete samples

reached a full stabilization only over 500 °C and after a long period of time and many thermal cycles, the mass loss could reach the 5.3% of the initial concrete mass. Khalifa et al. (2000) underlined that the loss of water started at 180 °C and it could be a very slow process because the water evaporates, migrates through the concrete and then condenses again as soon as the thermodynamic condition are satisfied. In fact, the saturation vapour pressure inside the concrete matrix could be very high so the condensation temperature could be consequently higher than apparent value. The overall mass loss for different concrete mixtures is normally between 4 and 5%. Martins et al. (2015) measured the concrete mass loss during thermal cycling from 220 to 420 °C for relatively short time (less than 10 hours) and it was evaluated around 2%, because the water tends to evaporate and re-condensate inside the concrete, if not drained.

The phase change of water is isothermal and for this reason it does not affect the heat flux balance based on concrete temperature variation. As described before, in the reference experimental campaign, TES modules were new and not fully degassed; a progressive decrease of water evaporation with the concrete aging has to be expected. For fully stabilized TES concrete, the latent heat flux can be neglected as well for cooling/discharging stage in which the partial pressure of the water vapour in the concrete reduces during the process and this fact stops the water evaporation.

Thus, the latent heat flux (for the charging phase) and the outlet oil temperature (for both dis/charging phases) can be calculated as:

$$q_{lat} = \dot{m}_w \cdot l_v \tag{3.44}$$

$$t_{oil,out} = t_{oil,in} \pm \frac{q_{oil} + q_{lat}}{\dot{m}_{oil} \cdot c_{oil}} \tag{3.45}$$

with (-) for charging (outlet oil temperature is lower than inlet one) and (+) for discharging phase (outlet oil temperature is higher than inlet one). For discharging process, the latent heat flux must be set equal to zero.

The evaporation effect is considered only in the first cycle, not in fully operative situations because it only reproduces the vaporization effect of the interstitial water contained in the concrete, which is not completely degassed. The insulation is made of rock wool, but there is no vapour barrier and during the experimental tests, in the first heating cycle, the water evaporates, moves to the outside and

then comes out of the concrete block, not recondensing inside the element, so it is not necessary to consider the latent heat of condensation. The latent heat of evaporation was considered only in the model validation stage, but in the fully developed state simulations, it is eliminated from the model, as it is not present.

3.3 Experimental setup and data reduction

In order to validate the developed model, a suitable set of experimental tests was selected. The experimental campaign investigated the effects of concrete composition by testing two different mixtures during both heating and cooling phases. For the sake of clarity, in what follows, a brief description of the concrete prototypes and of the experimental procedure is given; more details can be found in Giannuzzi et al. (2014).

Two concrete modules were built, using two different concrete mixtures, by two Italian manufactures: Cestaro srl (called type A) and Italcementi Spa (called type B). The thermal-mechanics characteristics of the two concrete mixtures are described in Girardi et al. (2014) and Mazzucco et al. (2014) and summarized in Tab. 3.1. The two modules presented the same sizes and piping layout; the stainless steel AISI 316 tube was embedded into the concrete matrix in a 4-passages configuration (Fig. 3.4). The module is 3 m long while the tube has an inner diameter equal to 14 mm and an outer diameter of 16 mm, the total tube length is 12 m. The concrete TES modules were tested in a dedicated experimental setup, developed and built by ENEA. ParathermTM NF mineral oil was chosen as HTF. The main thermo-physical properties of the heat transfer oil are reported in Tab. 3.2. In Fig 3.5 the sample preparation is represented, while in Fig. 3.6 there is a picture of the experimental setup.

Table 3.1: Concrete mixtures properties

Properties	**Unit of measurement**	**Type A concrete**	**Type B concrete**
Specific heat capacity	[J/(kgK)]	820	930
Density	[kg/m^3]	2483	1837
Thermal conductivity	[W/(mK)]	2.21	1.80
Thermal diffusivity	[m^2/s]	$1.123 \cdot 10^{-6}$	$1.054 \cdot 10^{-6}$

Each concrete module was a square cross-section parallelepiped (0.2×0.2 m), with a total weight of around 290 kg. The modules were covered with two insulating layers, one made of ceramic wool and the other by Rockwool, to reduce the

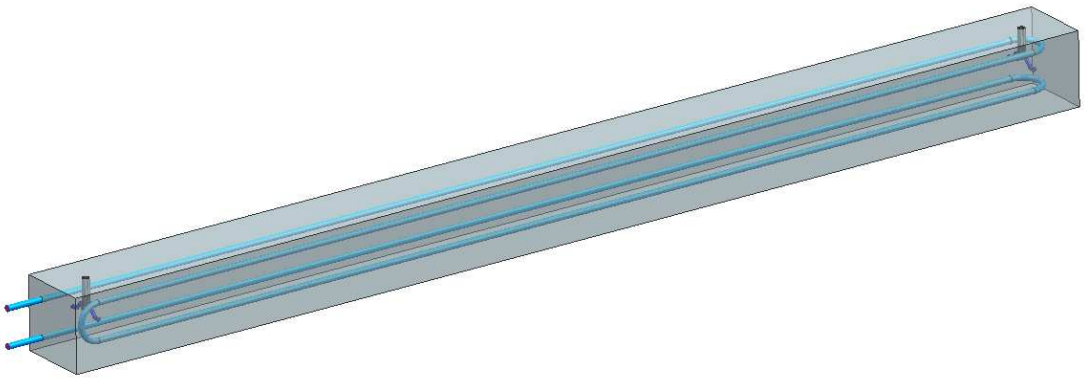

Figure 3.4: Concrete module and piping 3D sketch

Figure 3.5: Sample preparation

convective heat losses to the surroundings. The main thermo-physical properties and geometrical parameters of the TES are reported in Tab. 3.3.

The concrete module was instrumented with many thermocouples which were installed during the manufacturing; in particular, 5 thermocouples were embedded into the concrete in the central section, 9 thermocouples were placed along the outer surface of the module, and 4 thermocouples were soldered over the outer surface of the tube (Fig. 3.7). The oil temperatures at the inlet and outlet of the module and the room temperature were also measured and recorded. The oil mass flow rate was set at around 0.13-0.15 kg/s, which assures the fully developed turbulent flow in the tube, with a mean Reynolds number of around 55000. The

Figure 3.6: Experimental setup

Table 3.2: Paratherm NF oil properties (temperatures in °C)

TES properties	**Best-fitting equations/Values**	**Unit of measurement**
Density	$\varrho = -0.651 \cdot t + 895.6$	[kg/m^3]
Specific heat capacity	$c = 5.284 \cdot t + 1720$	[J/(kgK)]
Thermal conductivity	$\lambda = -8 \cdot 10^{-5} \cdot t + 0.110$	[W/(mK)]
Dynamic viscosity	$\mu = (53238 \cdot t^{-2.138})/1000$	[kg/(ms)]
Max. film temperature	343	[°C]
Max. operating temperature	332	[°C]
Min. operating temperature	36	[°C]

inlet oil temperature should have been ideally kept constant. As showed in Fig. 3.8, which reports an example of a heating test, the realized control loop was able to set the inlet oil temperature at 250.4 °C ±2 °C, which is more than acceptable for this kind of application. From the analysis of the concrete temperatures profiles, it can be observed that the difference between the mean concrete temperature and the maximum/minimum values is relatively small and it is always less than 5 °C in heating test. Similar results were obtained during the cooling tests (not reported in a figure for the sake of brevity).

Table 3.3: Concrete mixtures properties

Parameter	**Symbol**	**Unit of measurement**	**Value**
TES length	L_{TES}	[m]	3
TES side length	$L_{side,TES}$	[m]	0.2
TES equivalent diameter	$D_{eq,TES}$	[m]	0.226
Basic element side length	$L_{side,el}$	[m]	0.1
Basic element equivalent diameter	$D_{eq,el}$	[m]	0.113
Total tube length	L_t	[m]	12
Tube inner diameter	$D_{t,int}$	[m]	0.014
Tube external diameter	$D_{t,ext}$	[m]	0.016
Tube thermal conductivity	λ_t	[W/(mK)]	16
Insulating layer 1 thickness	s_{ins1}	[m]	0.05
Insulating layer 2 thickness	s_{ins2}	[m]	0.1
Insulating layer 1 thermal conductivity	λ_{ins1}	[W/(mK)]	0.06
Insulating layer 2 thermal conductivity	λ_{ins2}	[W/(mK)]	0.035
Insulating material density	ϱ_{ins}	[kg/m^3]	80
Insulating material specific heat	c_{ins1}	[J/(kgK)]	1030
Environment coefficient	h_{env}	[W/(m^{2}K)]	15

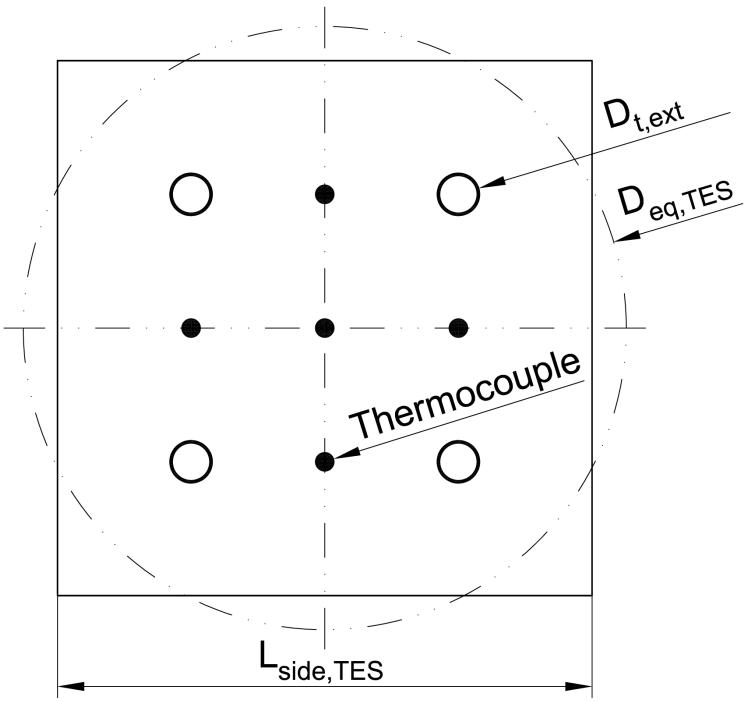

Figure 3.7: Entire TES module cross section and thermocouples position

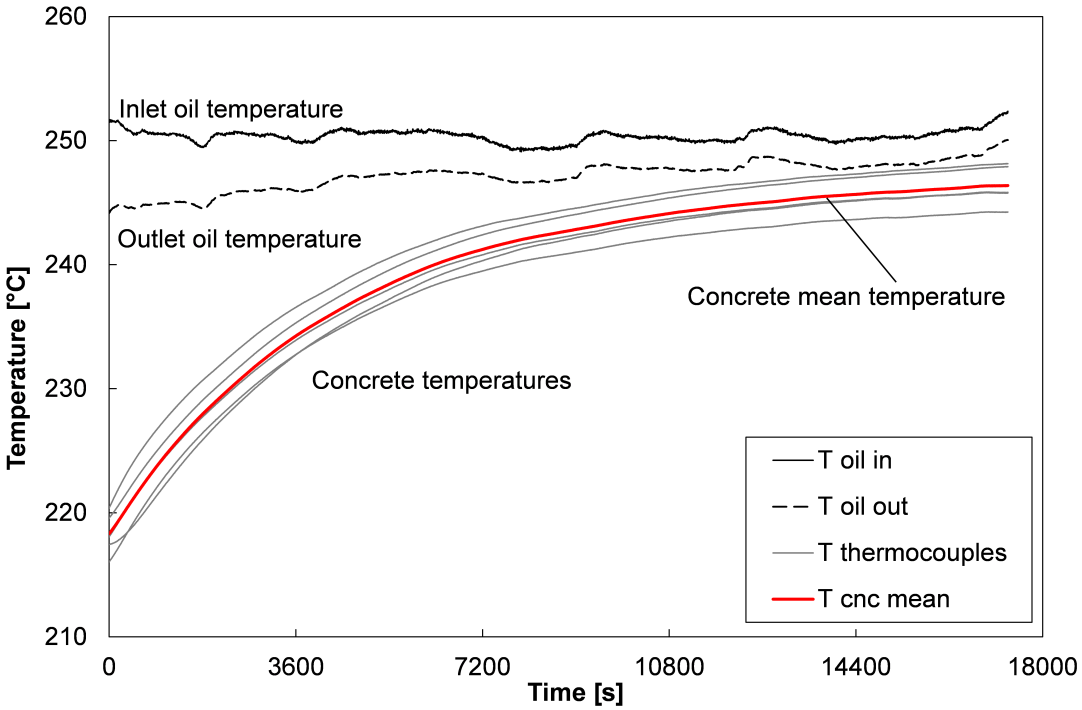

Figure 3.8: Example of concrete and oil temperatures trends during a heating test (type A mix, test 2)

Numerical simulation of the concrete TES allowed for the estimation of the volume weighted temperature over time on the entire TES where the experimental temperature was recorded. These results were then compared against the average value calculated from the temperature readings collected by the 5 thermocouples: the deviation was always less than 3 °C. Hence, the use of the mean concrete temperature obtained by averaging the measured values can be considered a fair estimation.

For these reasons, the mean concrete module temperature can be assumed as the main parameter which describes the entire module thermal behaviour. The profile of this mean concrete temperature is also presented in Fig. 3.8.

Furthermore, it is worth underlying that the concrete temperature profiles were always relative smooth even if the oil temperature presented the cited fluctuations; this can be explained considering the high thermal capacity of the TES and it is important for the choice of the right simulation model. Finally, as reported in Table 4 with the main tests parameters, the ambient temperature is relatively high (more than 30 °C), and this fact strongly reduced the heat dissipation of the TES towards the surroundings.

3.4 Comparison with experimental data

As previously described, the described model was compared and validated against experimental data by Giannuzzi et al. (2014). The comparisons between experimental and model calculated oil and concrete temperature profiles of the two concrete mixtures are reported in Figs. from 3.10 to 3.16, during both the charging and discharging processes.

In general, a good agreement between the calculated and the experimental results is found. However, the two concrete mixtures presented different behaviours. In the case of type A concrete, the numerical model slightly overestimates the heating profile while the final concrete temperature is correctly estimated (Fig. 3.9 and 3.10). Similarly, during the cooling phases (Fig. 3.13 and 3.14), the model slightly overestimates the heat released by the concrete and the calculated final concrete temperature are lower than that measured values. This means that, for type A mixture, the model predicts a higher stored or released thermal energy than the measured one, even if the difference is within the experimental uncertainty.

Differently, in the case of type B mixture, the code slightly underestimates the concrete's temperature compared to the experimental one, both during heating (Fig. 3.11 and 3.12) and cooling stages (Fig. 3.15 and 3.16). In fact, the calculated concrete temperature is lower than the real one during heating, but it is higher than the experimental one during cooling. Hence, with type B, the model slightly underestimates the stored or released thermal energy, again within the experimental uncertainty.

It is also worth underlying that the calculated outlet oil temperature follows faithfully the experimental one, also when the inlet oil temperature shows contrary peaks compared to the general increasing or reducing trend. This fact is clear in Figures 3.9, 3.12 and 3.14 and confirms the stability of the model and of the solution scheme, which are not affected by the input data.

However, the first aim of the model was to predict the concrete temperature during the two stages. The charts show that the calculated temperature is in fine agreement with the experimental one, both as instant values and global trend.

In order to evaluate the actual accuracy of the developed model in estimating the concrete TES performance, a deviation can be defined between the calculated and the experimental total TES energy stored or released during the charging or discharging processes, respectively. The deviations can be also calculated as a function of concrete temperatures, under the assumption of constant heat capacity and density of solid concrete, as:

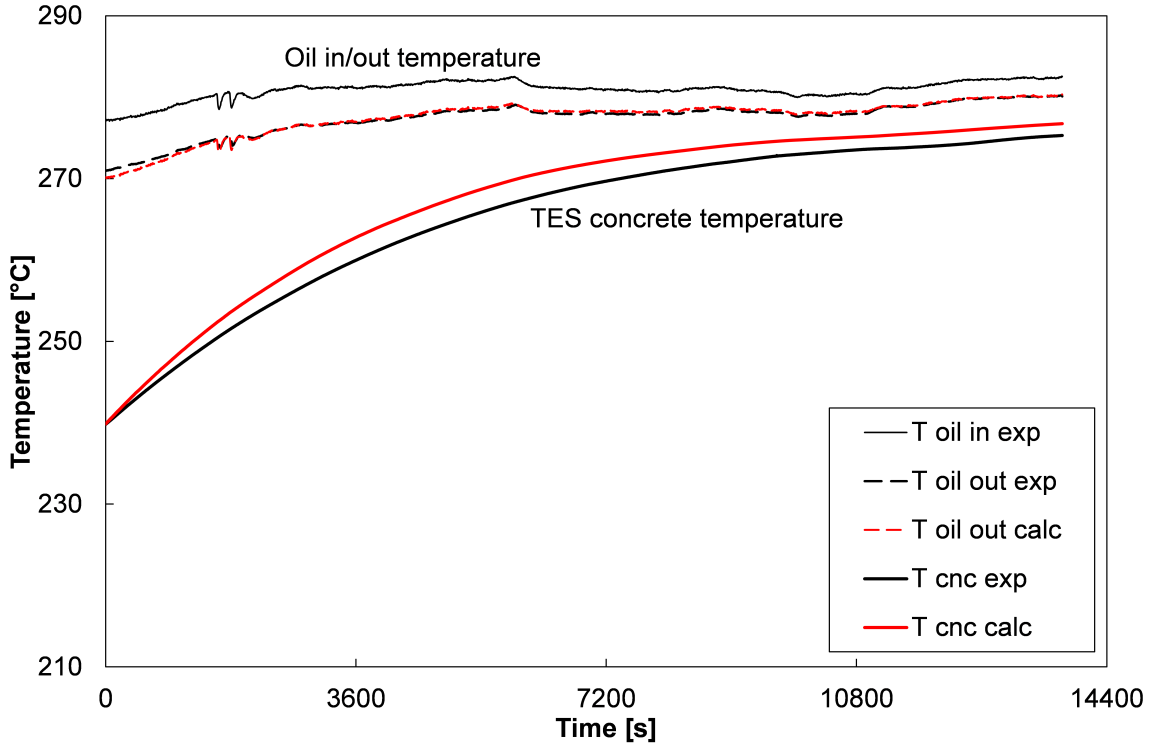

Figure 3.9: Experimental vs. calculated temperatures (type A concrete, heating test 1)

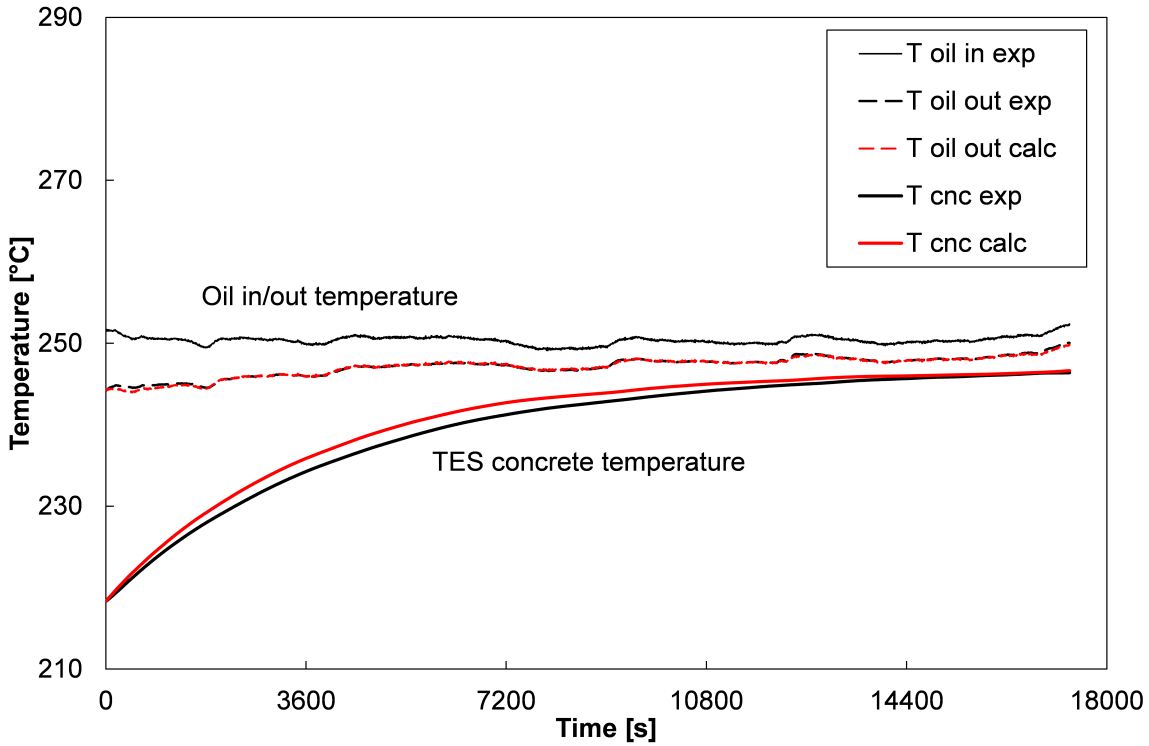

Figure 3.10: Experimental vs. calculated temperatures (type A concrete, heating test 2)

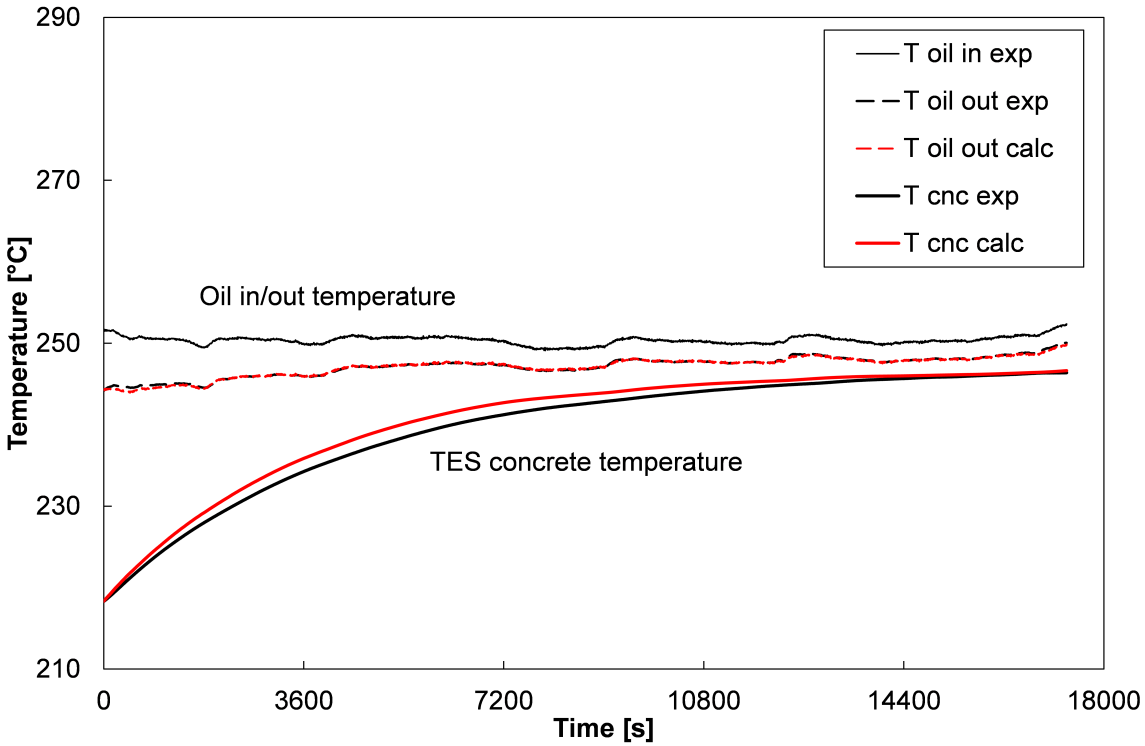

Figure 3.11: Experimental vs. calculated temperatures (type B concrete, heating test 1)

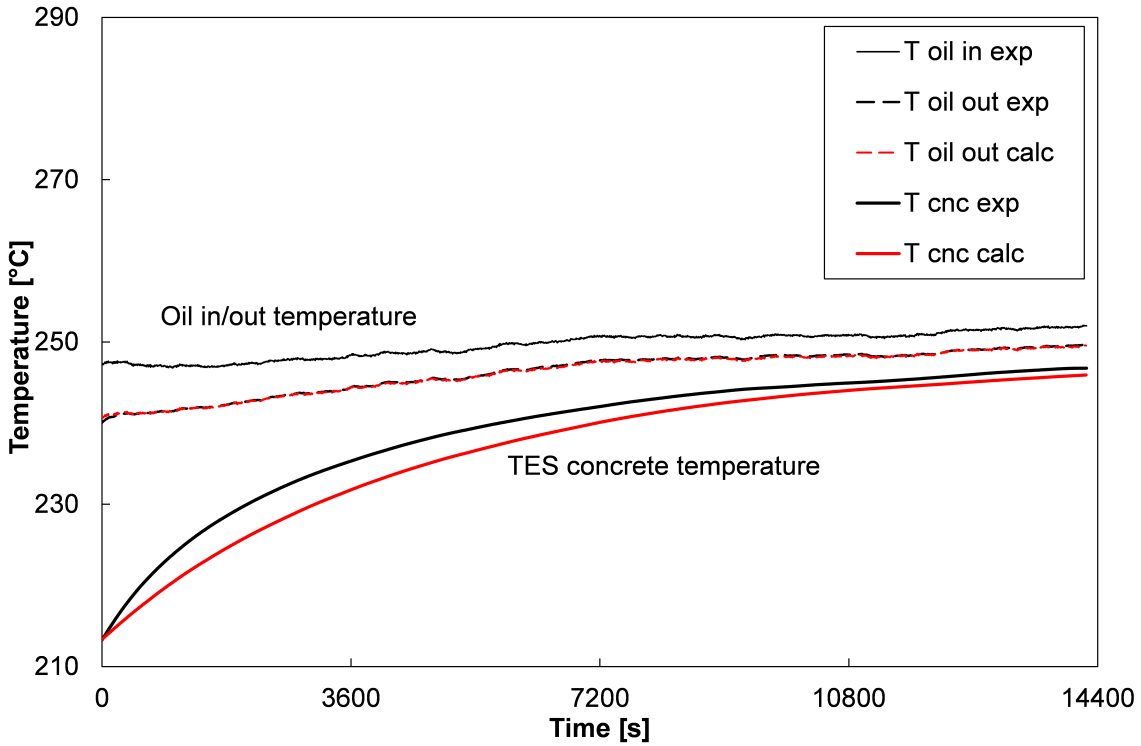

Figure 3.12: Experimental vs. calculated temperatures (type B concrete, heating test 2)

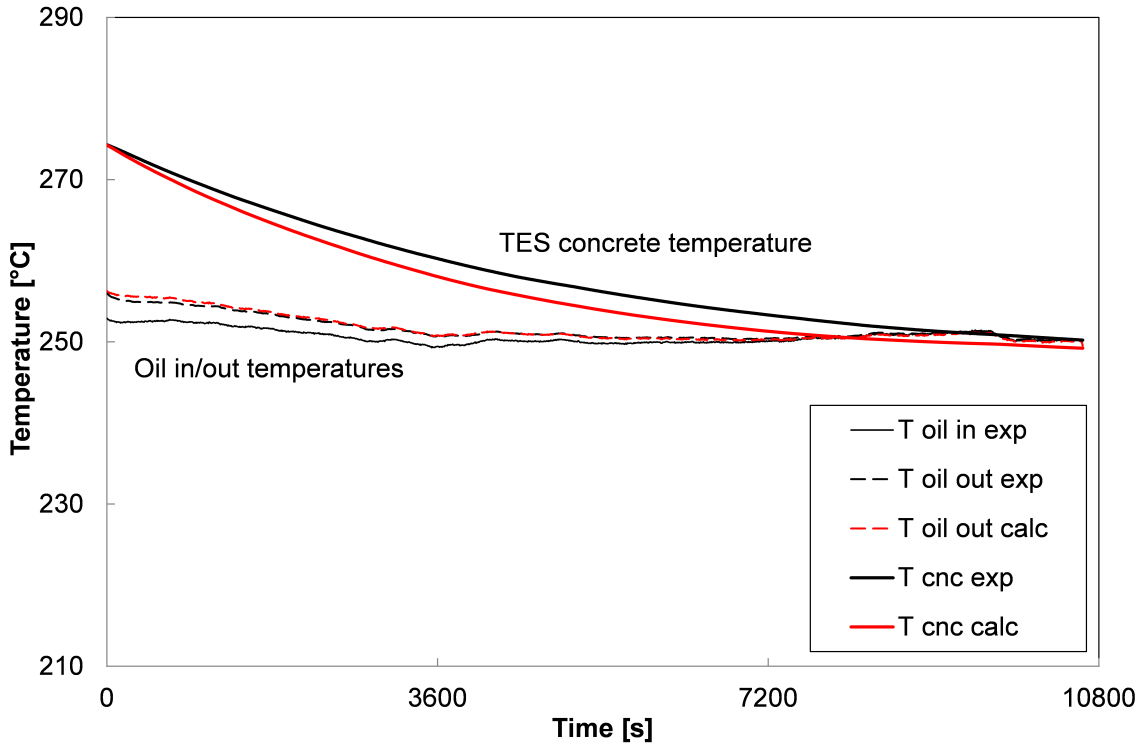

Figure 3.13: Experimental vs. calculated temperatures (type A concrete, cooling test 1)

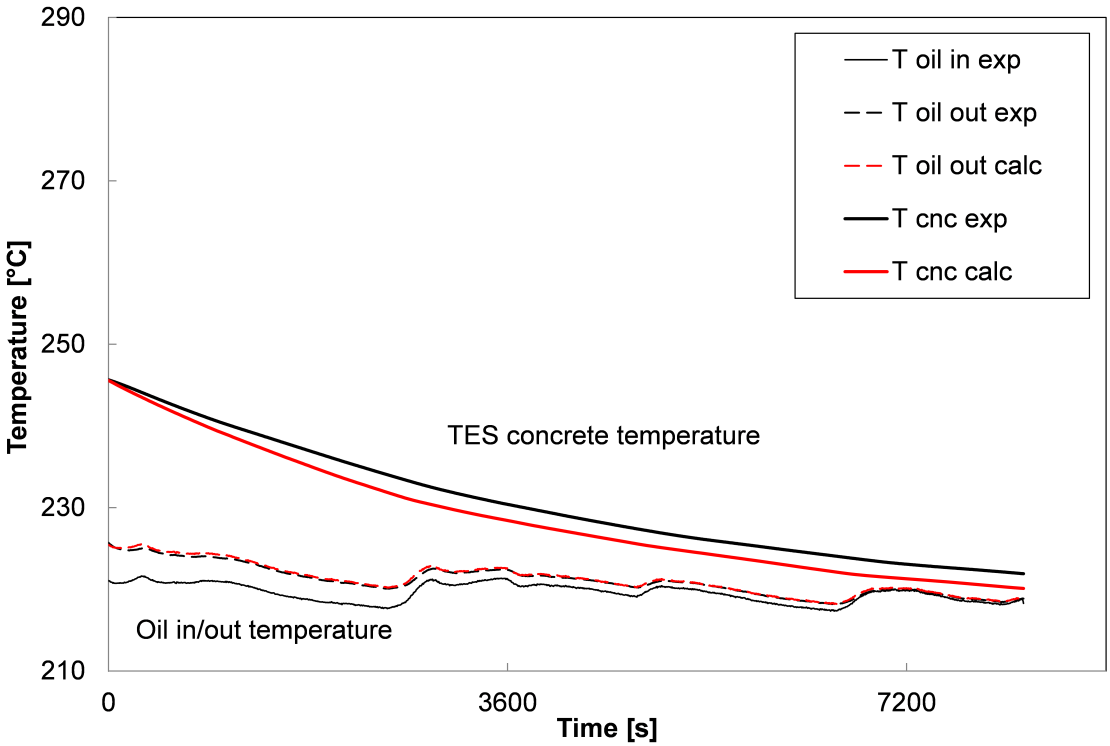

Figure 3.14: Experimental vs. calculated temperatures (type A concrete, cooling test 2)

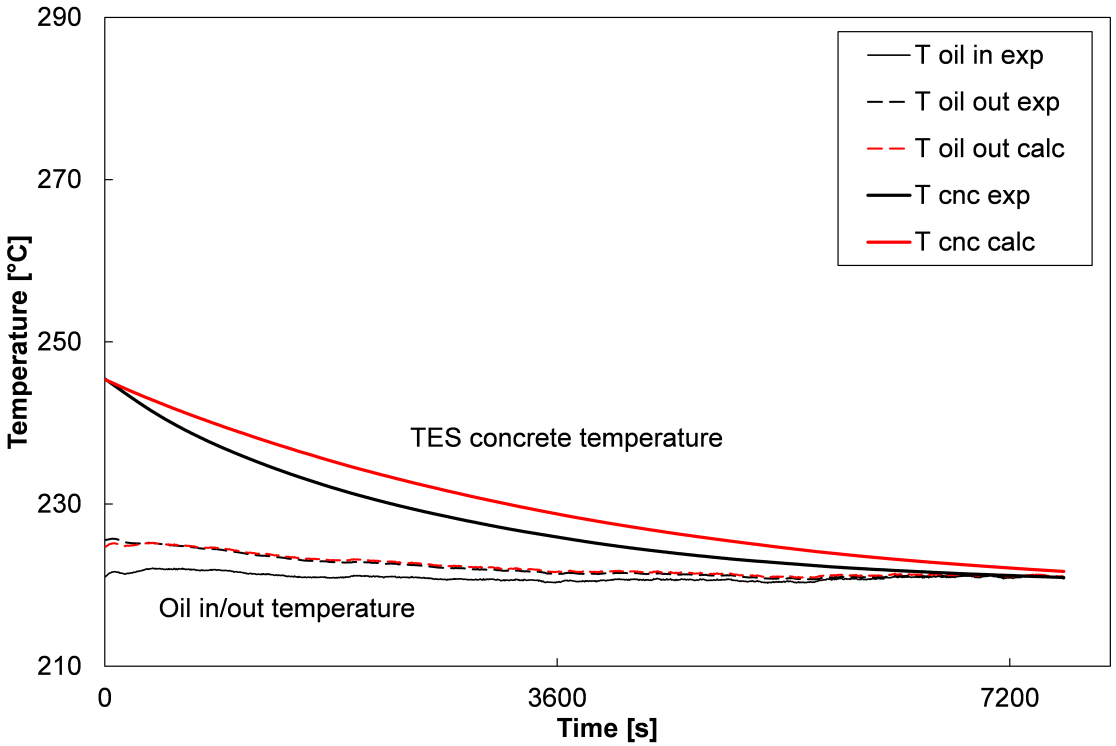

Figure 3.15: Experimental vs. calculated temperatures (type B concrete, cooling test 1)

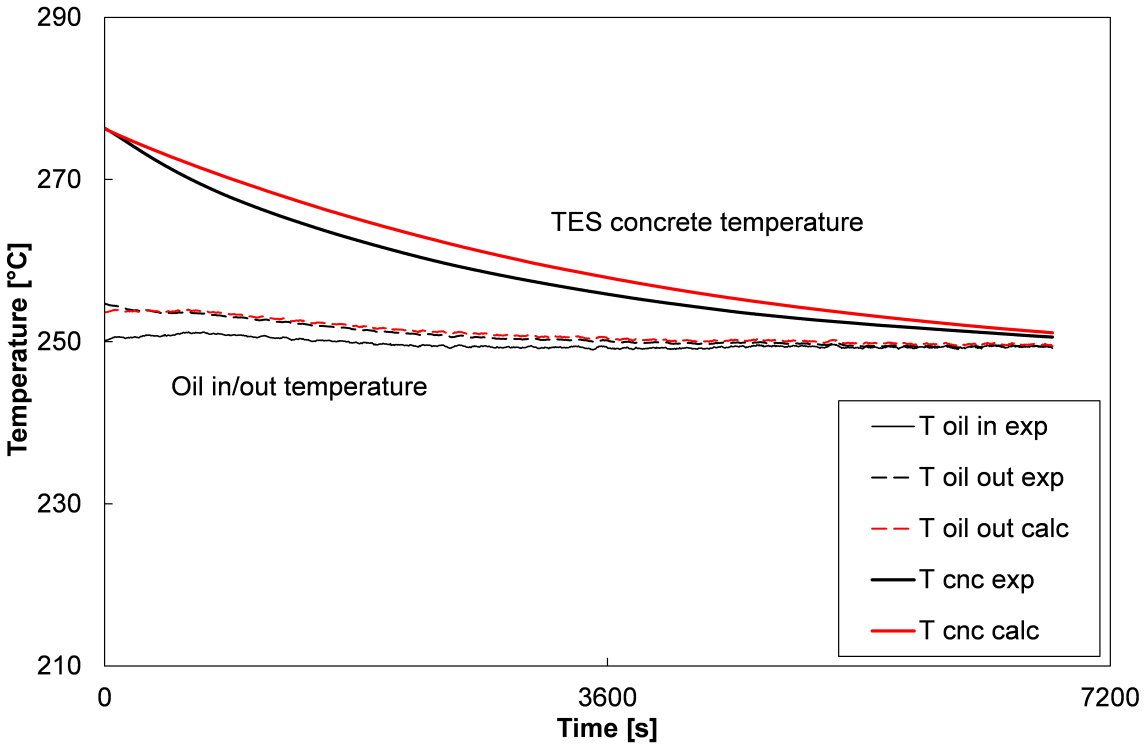

Figure 3.16: Experimental vs. calculated temperatures (type B concrete, cooling test 2)

$$Dev = \frac{\Delta Q_{calc-exp,e}}{Q_{exp,e-s}} = \frac{m_{cnc} \cdot c_{cnc} \cdot (T_{calc,e} - T_{exp,e})}{m_{cnc} \cdot c_{cnc} \cdot (T_{exp,e} - T_{exp,s})} = \frac{T_{calc,e} - T_{exp,e}}{T_{exp,e} - T_{exp,s}} \quad (3.46)$$

The percentage calculated values of the deviation are reported in Tab. 3.4 (last column). As already mentioned above, the deviation between calculated and experimental exchanged energy is very low and always within the experimental uncertainty. This confirms the suitability of the model to correctly describe the system behaviour. The deviation is always positive for type A concrete (with a maximum value of around +7%), instead it is always negative for type B concrete mixture (with a maximum value of around -3%); this can be due to the different thermo-physical properties of the two concrete mixtures, such as the thermal conductivity, the heat capacity or to the different operating test conditions (i.e. an oil mass flow rate not really stable during the test).

Table 3.4: Main parameters for experimental tests and results

		Experimental parameters					Calculated parameters			
Cnc	Test	$T_{cnc,s}$	$T_{oil,in,s}$	T_{env}	$\dot{m}_{oil}$	Time	Q_{cnc}	ε	ε_{mod}	Dev
		[°C]	[°C]	[°C]	[kg/s]	[s]	[MJ]	[%]	[%]	[%]
A	1 Charge	239.8	280.9	34.0	0.145	13760	8.73	88.7%	94.8%	+4.08%
	1 Disch.	274.3	250.6	34.0	0.145	10625	6.75	105.3%	96.1%	+4.15%
A	2 Charge	218.3	250.4	32.5	0.131	17330	6.33	87.8%	94.7%	+0.91%
	2 Disch.	245.6	219.6	32.5	0.131	8254	6.75	96.9%	90.0%	+7.60%
B	1 Charge	213.3	249.7	30.3	0.131	14237	5.98	86.5%	93.9%	-2.49%
	1 Disch.	245.4	220.9	31.4	0.131	7630	6.03	96.7%	88.0%	-3.07%
B	2 Charge	241.3	279.7	31.3	0.145	16391	4.76	87.5%	95.5%	-2.29%
	2 Disch.	276.3	249.7	32.4	0.145	6786	5.03	94.2%	85.1%	-2.05%

The model also allows for the calculation of the heat fluxes exchanged during the simulated process. Two examples are reported in Figs. 3.17 and 3.18. The two main heat fluxes are those related to oil and concrete, which are higher at the beginning of the test and then progressively decrease with time, because the temperature difference between oil and concrete becomes accordingly lower. In Fig. 3.18, which shows a cooling stage, the oil heat flux becomes even negative near to the end of the test, it means that the experiment has lasted enough time to allow the concrete to achieve a temperature lower to the oil one, so the oil heat flux becomes negative due to that temperature crossing. The insulating layer and loss heat fluxes are also plotted.

The insulating material heat flux is very low and becomes approximately negligible at the end of the test, because the temperatures of the two insulating layers reached almost constant values. The loss heat flux, instead, is nearly constant during the whole test. The oil and concrete heat fluxes have almost the same trends and peaks, according with the inlet oil temperature.

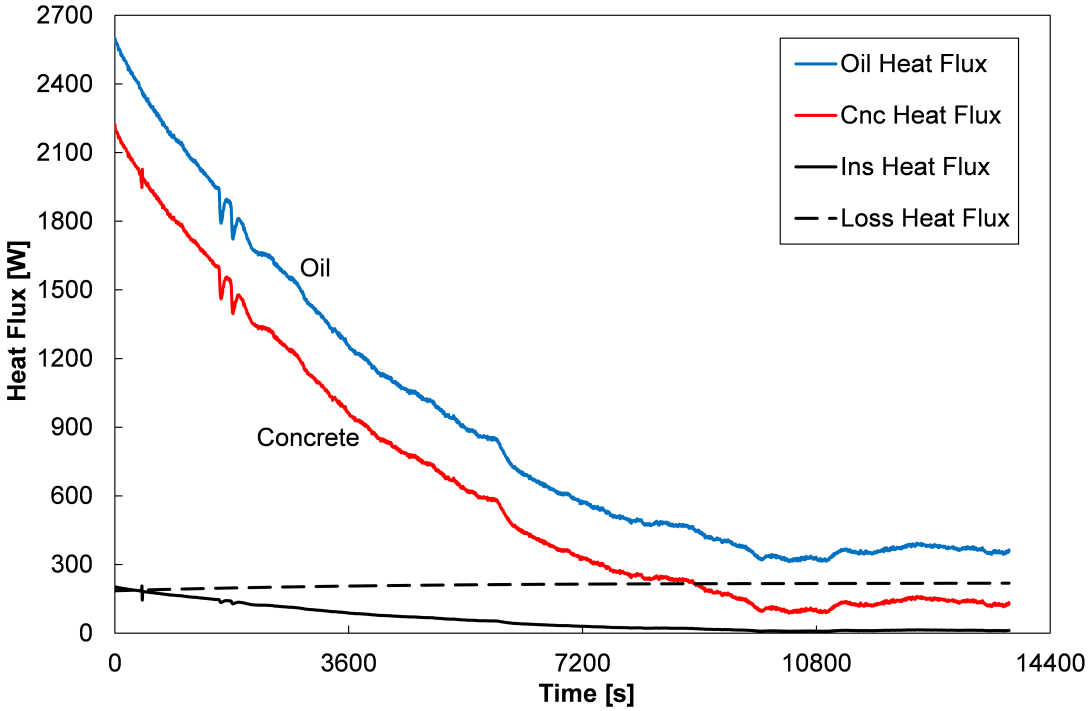

Figure 3.17: Calculated heat fluxes (type A concrete, heating test 1)

3.5 Thermal efficiency

One important parameter, useful to describe the system's behavior, is the thermal efficiency; Li et al. (2012) recently made a detailed review on thermal efficiencies and effectiveness for different TES systems depending on four main dimensionless parameters. Generally, the thermal process efficiency can be defined as the ratio between the value of the thermal energy stored in the TES and the maximum theoretical value, referred to inlet oil temperature (assumed constant), as:

$$\varepsilon = \frac{Q_{cnc}}{Q_{cnc,max}} = \frac{m_{cnc} \cdot c_{cnc} \cdot |T_{cnc,s} - T_{cnc,e}|}{m_{cnc} \cdot c_{cnc} \cdot |T_{cnc,s} - T_{oil,in}|} = \frac{|T_{cnc,s} - T_{cnc,e}|}{|T_{cnc,s} - T_{oil,in}|} \tag{3.47}$$

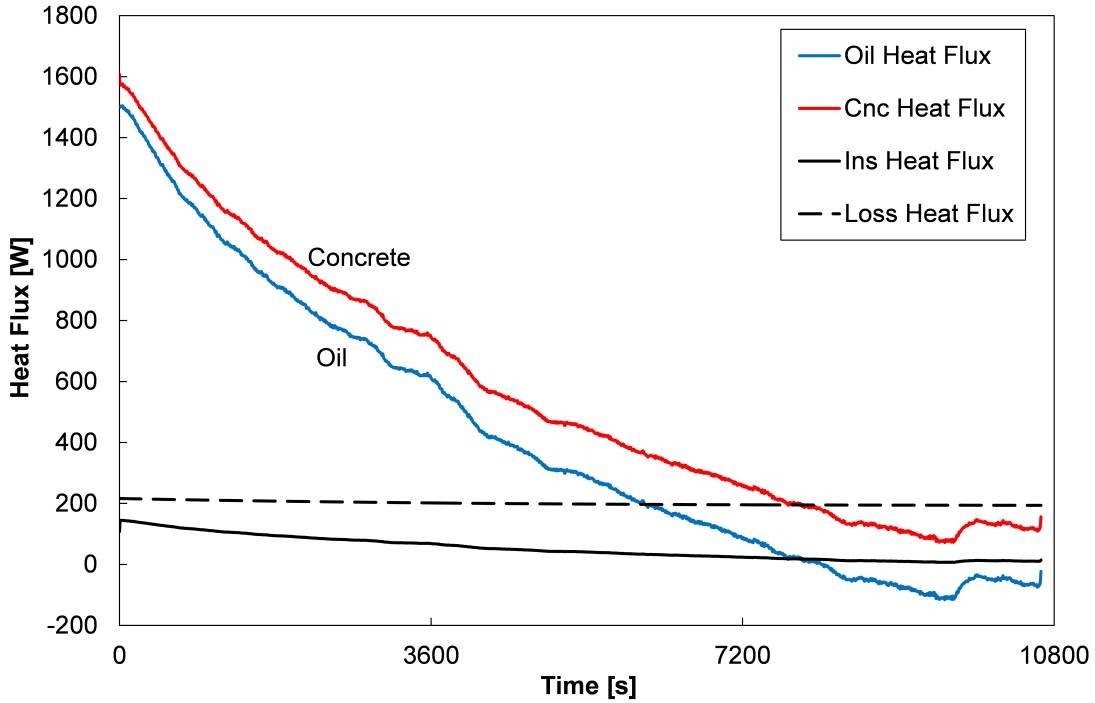

Figure 3.18: Calculated heat fluxes (type A concrete, cooling test 1)

The model simulations show that the efficiency enhances with the increase of oil mass flux and test duration, and it achieves an asymptotic value. During heating processes, the efficiency variations are lower than those during cooling ones. This occurs because, during discharging process, a low mass flux struggles to counteract the loss heat flux, so lower oil mass fluxes influence more significantly the efficiency value. The differences between the two mixtures are instead less significant: type A concrete achieves in general a higher stored thermal energy.

A problem related to such definition of the efficiency is that the reference value is the theoretical maximum energy, but it will not ever be achieved by the TES concrete module in real conditions. Hence, a new "modified efficiency" is here proposed, as:

$$\varepsilon_{mod} = \frac{Q_{cnc}}{Q_{cnc,ac}} = \frac{m_{cnc} \cdot c_{cnc} \cdot |T_{cnc,s} - T_{cnc,e}|}{m_{cnc} \cdot c_{cnc} \cdot |T_{cnc,s} - T_{cnc,th}|} = \frac{|T_{cnc,s} - T_{cnc,e}|}{|T_{cnc,s} - T_{cnc,th}|} \tag{3.48}$$

The reference value ($Q_{cnc,ac}$) is the maximum achievable energy, calculated with the same temperatures previously indicated, and with ideally infinite values for both oil mass flux and test duration. Regarding the heat exchange between oil and concrete, an infinite value for the oil mass flux equals to define a constant value for the inner temperature of the steel tube along the entire length of the pipe

and that temperature is equal to the oil inlet temperature. In other words, an infinite value for the oil mass flux leads to a convective inner thermal resistance equal to zero. For the numerical simulation, a very high test duration equal to 100000 s (≈28 h) and an oil mass flux of around 28 kg/s (100000 kg/h) are assumed; the resulted energies for the different operative conditions are very close to the theoretical ones, but they have the peculiarity to be achievable, even if the process could not be so easy, short, and cheap.

The comparison between the values of the standard and the modified efficiency is presented in Tab 3.4, Q_{cnc} is calculated with a constant inlet oil temperature, assumed equal to the mean value of the experimental one during the test duration. Anyhow, the difference between the entire concrete heats calculated with constant or variable oil temperature is less than 3.5%. It's important to note that the model simulations with variable experimental oil temperature as input are fundamental to verify the simulation code and his capability to reproduce outlet oil and concrete temperatures profiles, but the efficiency calculation has to be done with a constant inlet oil temperature, in order to have a stable reference point.

Some considerations can be made about the modified efficiency: during heating tests, its value is higher than the standard one; instead, in cooling simulations, its value is slightly lower. That behavior is due to the amount of energy used as denominator in the modified efficiency formulation. In heating tests, the maximum achievable thermal energy is lower than the theoretical one that appeared in the first efficiency formulation. In those stages, in fact, the concrete temperature continuously increases, but it will not ever achieve the oil's temperature, so the stored energy will always be lower than the ideal storable one.

In cooling simulations, the modified efficiency is lower than the one calculated with the first formulation. The heat used in the new formulation is higher than the theoretical one, because, for long time simulations with a room temperature lower than the inlet oil one, the concrete and oil temperatures cross and the concrete temperature becomes lower than the oil one (see Fig. 3.13). After this point, concrete and oil continuously exchange heat each other, but the TES becomes colder by exchanging with the environment and not with the oil. This fact does not have any practical utility because the discharge process scope is the energy transfer from the concrete TES to the oil, but this is what actually happens, so the stored energy apparently increases and the modified efficiency assumes lower values. As demonstration of that, for type A test 1, during discharge process (referred to Fig. 3.13), the standard efficiency reaches the unrealistic, wrong, value of 105.3% (greater than 100%), while the modified efficiency assumes the

proper value of 96.1%.

3.6 Conclusions

A simplified lumped capacitance model, useful to predict the behavior of a concrete thermal storage module, was developed, validated, and proposed. These characteristics makes this model suitable for the implementation in more complex solar thermal simulation tools and software, allowing for a fair estimation of the energy storable in concrete TES as well as its transient behavior during charging and discharging processes as a function of the main operating conditions.

The model permits the thermal and energetic analyses of the concrete storage module during time, both for charging and discharging phases. The developed calculation procedure can be considered a modular, flexible and quick tool that allows the computation of the module's parameters almost immediately. A unique reference concrete temperature was considered to describe the whole system; obviously it involves a few simplified assumptions, but the model computed accurate values with a computational effort drastically less than that of a CFD/FEM model.

The model was compared against the data of experimental campaign on two concrete mixtures, during heating and cooling stages, for a total of eight tests. The exchanged concrete energy deviation is very low for each test and always less than the experimental uncertainty. The experimental and calculated results achieve a very fine agreement, both as actual values and global trend. The comparison shows that the model is stable, because the solution scheme is not affected by the input parameters. The model allows also for calculating the actual heat fluxes for a constant monitoring of the TES performance.

Finally, two thermal efficiencies were also proposed. A standard efficiency was defined as the ratio between the thermal energy really achieved by the TES and the maximum theoretical value referred to inlet oil temperature. A new modified efficiency, in which the reference value is the maximum achievable energy, was calculated with ideally infinite values for both oil mass flux and test duration. The simulations show that the efficiency enhances with the increase of oil mass flux and time, and it achieves an asymptotic value.

4. Modules' arrangement

4.1 Introduction

This chapter is focused on modularized concrete sensible TES systems and the most efficient modules' arrangement is investigated, both in the heating and cooling phase. Different series, parallel and mixed configurations are considered, and their performances are evaluated, combining the exchanged thermal energy, the mass flow rate and the pressure drops along with the system. Many studies about TES modularization have been conducted but a specific comparison of the stored energy amount and a focus on the series or parallel connection are still missing in the open literature.

Many types of TES modularization have been studied. Haller et al. (2009) reviewed different methods to characterize thermal stratification in energy storage, focusing on the methods that can be used to determine the ability to promote and maintain stratification. The thermal response of a multi-tank TES was studied by Cruickshank et al. (2011). The storage was assembled from three standard hot-water storage tanks which were connected in series or parallel configuration. The series ones reached high levels of temperature stratification during periods of rising temperatures and limited destratification during periods of falling temperature. This effect was not observed in the parallel one. Then, Dickinson et al. (2013) investigated the thermal behavior of a stratified tank when subjected to constant temperature charging and constant volume hourly draws. Charging in the series configuration was the most effective option, when combined with parallel draws, led to the mixing of unequal delivery temperatures from the tanks. Macias et al. (2018) examined soda lime silicate glass-graphite composites for use as a storage medium in a TES unit. A simple one-dimensional model for thermal conductivity was developed based on equivalent thermal circuits for series-parallel composite walls but without an optimization analysis. Venegas-Reyes et al. (2019) presented a parametric methodology to size stationary solar collector fields. The costs of the collector loop piping and the pumping power

of different series-parallel arrays are considered. The optimal series-parallel array was determined by the assessment of the payback time. Vigneshwaran et al. (2019) developed a cost-effective concrete based TES system by performing experimental studies and numerical simulations. For evaluating the temperature variation along the length of the module, an object-oriented framework is adopted by implementing the theory of continuous stirred tank in series. Yongtai et al. (2019) designed a heat storage vacuum tube solar collector. The parallel and series-parallel solar air collector system prototype was designed and tested but without a focus on the best disposition.

Cimmino (2019) presented a semi-analytical method for the calculation of g-functions of bore fields with mixed arrangements of series and parallel connected boreholes. However, it was not possible to account for changes in flow direction within the bore field, which is expectable in seasonal storage systems. Rosato et al. (2019) investigated the performance of an Italian district heating network. The plant was based on the operation of solar thermal collectors connected to a double U-pipe vertical borehole TES. They analyzed also the connection type (series, parallel or mixed) and found out that for a given number of borehole TES, the series one was the most performant. Anyhow, they considered just a few elements in the simulation.

The TES systems that are based on phase change materials are also gaining attention because of their potential improvements. Keshavarz et al. (2010) studied a TES system, consisting of different PCMs arranged in series, from the irreversibility point of view, with charging and discharging processes occurring periodically. The number of PCMs and their arrangement influenced the irreversibility of the system. Amirifard et al. (2018) studied the integration of a solar pond with latent heat storage for performance stability. Two parallel and one series layouts were studied. The average efficiency of discharging time for the series layout showed a higher increase compared with the parallel one. A hybrid concentrator photovoltaic PCM system was developed by Emam et al. (2018). The developed system included four different configurations of PCM heat sinks and nine different pattern arrangements of PCM. Increasing the number of parallel cavities led to a reduction in solar cell temperature. However, increasing series cavities had an unfavorable effect on the solar cell temperature. Shang et al. (2018) proposed modularized TES fabricated by encapsulating paraffin, thermally enhanced via copper or nickel foams, with epoxy resin. Theoretical and experimental validations revealed that the effective thermal conductivity was increased, and they also developed a series-parallel model to predict it. Besagni and Croci (2019) proposed a pilot-scale PCM storage, to be coupled with solar-

assisted heat pumps. The storage system was operated considering series and parallel heat exchanger configurations and implementing a broad set of boundary conditions, to test the storage unit under relevant operating conditions. Rezaei et al. (2020) presented a design methodology for a high-temperature latent heat TES unit, employing metal PCM. They assessed that the in-series or in-parallel arrangement of multiple units into a complete system provides higher performances, but they did not study which layout gave the best result. Huang et al. (2020) proposed a system using a PCM as a TES unit combined with a water tank for solar heating systems. The series system showed an enhancement of the solar fraction compared with a single water tank system and with a water tank-PCM unit parallel system.

Concrete TES systems were studied mainly for CSP integrations. A new type of TES for CSP plants was presented by Bergan and Greiner (2014). The energy storage medium was concrete with high thermal conductivity. Heat is transported by the HTF which flows through the steel pipe. The flow through the modular system is arranged in parallel and series but without a specific investigation of the best configuration. Concrete was also studied for TES integration in CSP plants by Wu et al. (2014). The discharging performance of four concrete structures is studied. The packed-bed gives the best discharging performance, followed by the rod-bundle structure, the parallel-plate structure, and the channel-embedded structure. Hoivik et al. (2019) studied a TES based on concrete modular system design with steel pipe heat exchangers. A heat exchanger design using thermal elements arranged in series and parallel was developed. Multiple thermal elements were stacked inside a steel frame, and the elements were connected through pipes. The pipes in each element were configured so that the HTF flows in and out of one element through two parallel U-shaped pipes. However, the authors did not focus on finding the most efficient series/parallel configuration. Suarez et al. (2020) developed a simplified zero-dimensional model of a passive sensible TES system for application in CSP plants, using concrete as a storage medium and thermal oil as HTF. The authors used a correction function determined through a set of CFD numerical simulations and they did not investigate the effect of series/parallel disposition of the elements. Roy et al. (2020) studied a sensible TES made of concrete and water as HTF. The computational work was carried out using Comsol Multiphysics software, with a specific focus on the exergy factor, but without consideration of the possible modularized arrangements.

As an overall consideration of what was found in the open literature review, I would assess that the study of series and parallel dispositions of energy storing modules is a gaining interesting topic since there were several works related to it.

However, there are some lacks, that can be here reassumed.

- Most of the considerations are limited to a theoretical point of view, without focusing on practical issues, like the possibility to build too long elements.
- When considering the comparison between the overall performances of series and parallel arrangements, the pressure drops are fundamentals and it is important to take them into account because without them, the results might be trivial.
- Often, also the mixed combination of series and parallel dispositions is missed since many Authors just considered pure series or parallel arrangements .
- Also, both charging and discharging stages should be considered, because the all cycle is important in this type of system, but the majority of the studies regarded just the heating/charging stage.
- Finally, an overall assessment should consider an adequate element number, but many Researchers just considered a few modules.

The present work follows the model presented in chapter 3 and cover the lacks found in the open literature review. In particular, the integration of the series and parallel option is addedd, in order to study the possibility to arrange several blocks in different combinations, finding a way to determine the best disposition, considering all the involved parameters, for a real operative situation.

4.2 Model description

The previous model aimed at developing a computational tool to predict the behavior of a single concrete storage module. It allowed for the real-time simulation of the general TES module's parameters during the operation of the entire system. The main parameter describing the TES is the stored or released thermal energy from or to the HTF. So, the model was meant to compute the transferred energy over time, and the related HTF temperature at the outlet of the module.

As described before, the model was developed for a single concrete module, but the present work aims to analyze the performance of a modular system composed of several elements arranged in series and parallel arrays. The elements arranged in parallel have all the same behaviour, so these subdivisions are simply obtained by dividing the total oil mass flow rate by the number of parallel elements. All

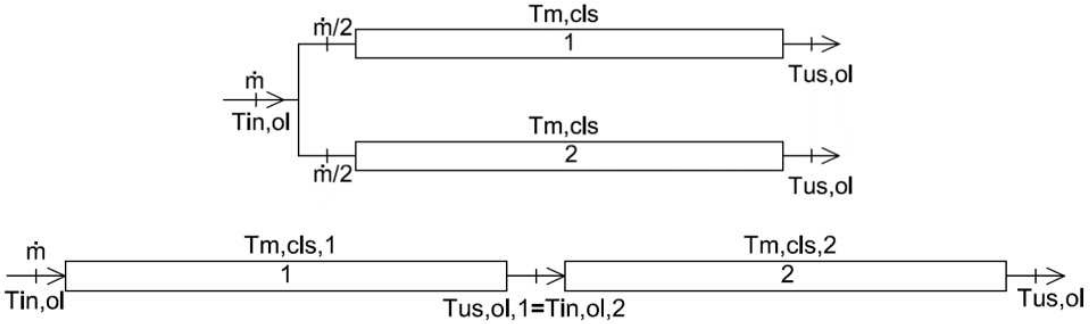

Figure 4.1: Parallel (top) and series (bottom) disposition of two representative elements

.

the calculations are then performed for a single element, then the total amount of energy is calculated by multiplying the resulted heat fluxes by the number of parallel elements.

Differently, the elements arranged in series present different working performances one from each other, the outlet oil of an element becomes the inlet of the following one. So, the oil temperature changes along with the series array and the code needed to be adapted to this configuration.

Mixed arrangements (with a variable number of branches and a different number of series elements) consider both the described procedure for series and parallel, in order to estimate their performance. The parallel and series disposition of the elements is reported in Fig. 4.1 for two elements, as an explanation.

4.3 Pressure drops calculation

In order to identify the best option between series, parallel and mixed configurations in terms of overall performance, the thermal energy is not enough, and the analysis needs to consider also the related pressure drops, since they increase the energy consumption needed to make the HTF flow through the pipe. Hence, a comparison of two systems with completely different pressure drops would not be representative or reliable. . As expected, for the same amount of inlet oil mass flow rate, their value remarkably varies when passing from a pure parallel configuration to a pure series.

The pressure drops are a function of the friction factor, which depends on the laminar or turbulent flow. The HTF flows inside circular pipes, so the following equations are used:

- in laminar flow

$$f = \frac{64}{Re} \tag{4.1}$$

- in turbulent flow, the well-known implicit Colebrook–White equation is implemented:

$$\frac{1}{\sqrt{f}} = -2\log\left(\frac{e}{3.7 \cdot D_{int}} + \frac{2.51}{Re\sqrt{f}}\right) \tag{4.2}$$

The pressure drops are calculated by:

$$\Delta p = f\frac{L}{D}\varrho\frac{v^2}{2} \tag{4.3}$$

4.4 Numerical simulations

All the numerical simulations presented in the following paragraphs are performed with the described code which in addition includes the possibility to estimate the performance of any different multiple module arrangements. The first part of the analyses considers the concrete blocks with adiabatic external surfaces. Then, the heat loss is introduced and a comparison with the adiabatic results is finally presented.

4.4.1 Adiabatic external boundaries

The first simulations consider adiabatic concrete surfaces. This condition is obtained by inserting a nearly-zero ambient heat transfer coefficient. In this way, the heat loss is equal to zero, so the exchanged heat fluxes are the ones related to concrete, oil and insulating material.

Single element simulations

A preliminary simulation with just one concrete block is conducted, both in the charging and discharging phase. The input parameters are chosen by referring to a compatible TES system in a CSP plant. So, in the charging phase the initial concrete temperature is set at 150 °C, the inlet oil temperature at 300 °C, the oil mass flow rate at 500 kg/h and the simulation time at 18000 s (5 hours). The number of hours in which the solar energy overcomes the production request coincides with the loading time of the TES system. It varies concerning the

latitude, the season and the industrialization level of the country in which the CSP plant is settled, so a simulation time of 5 hours could be a reasonable value, as reported by Herrmann et al. (2002), Kuravi et al. (2013), Zhang et al. (2013), Rodat et al. (2015), and Achkari et al. (2020).

During the discharging phase, instead, the inlet oil temperature is set at 150 °C and the concrete one at 300 °C, while all the other parameters (e.g. oil mass flow rate and simulation time) keep the same values, as reported by Cocco et al. (2016), and Rodríguez et al. (2016).

In this configuration, the thermal energy exchanged by oil and concrete is about 44 MJ, with a pressure drop of 0.2 bar, as reported in Figs. 4.2 and 4.3. During the simulation, the outlet oil and concrete temperature progressively get closer to the inlet oil temperature, with an asymptotic trend. This means that the energy exchanged by the two materials is very high at the beginning of the simulation, because of a high-temperature difference between oil and concrete and then decreases as the concrete temperature approaches the oil one.

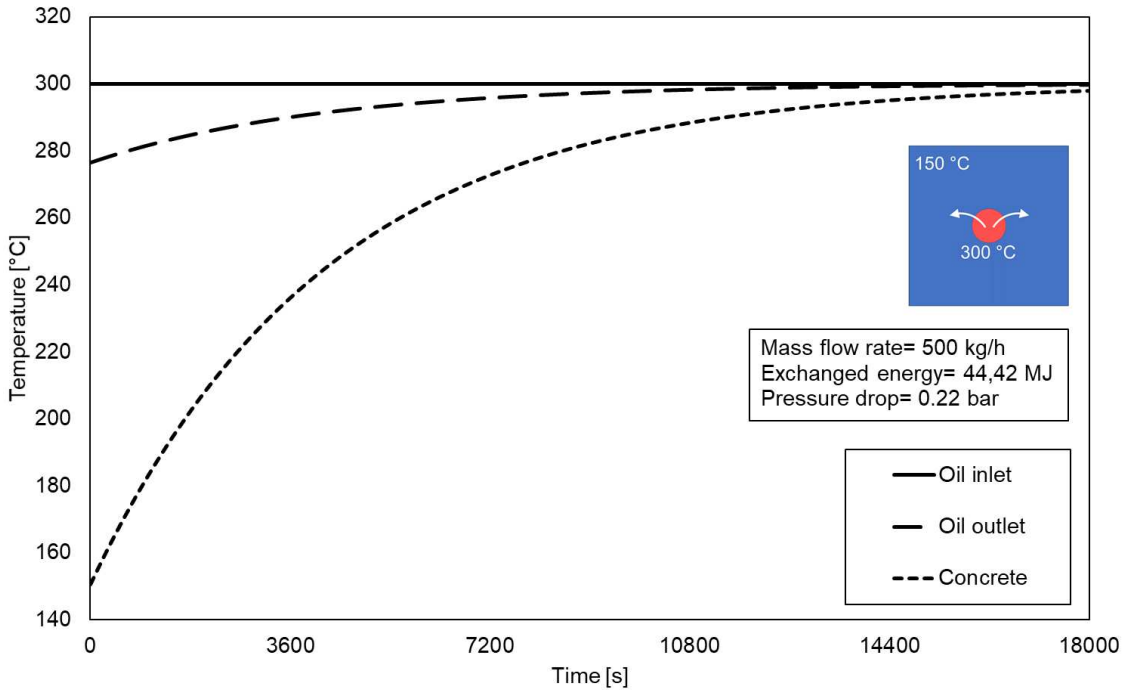

Figure 4.2: Mean concrete and oil inlet and outlet temperature of a single element in charging

When more elements are put in series or parallel, with the same total oil mass flow rate, the exchanged thermal energy increases, but the increase is not proportional to the number of elements. In Tables 4.1 and 4.2 the comparisons between two elements in series and parallel, in charging and discharging phase

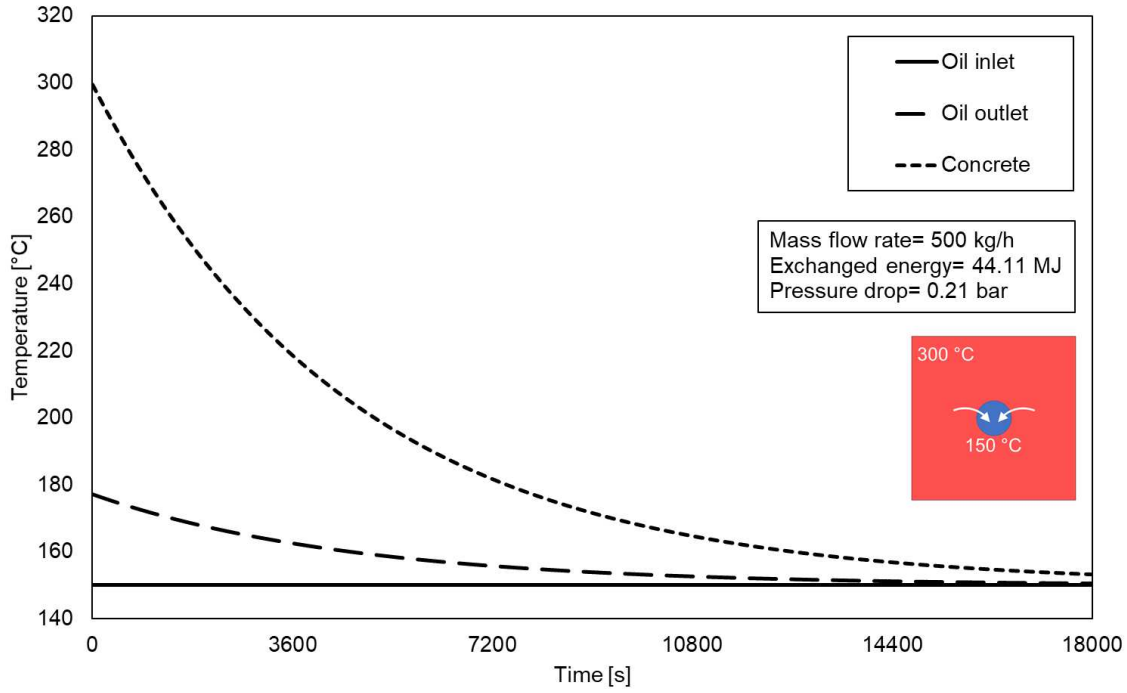

Figure 4.3: Mean concrete and oil inlet and outlet temperature of a single element in discharging

respectively, are reported. If a second element is put in series to a previous one, the thermal energy increases, but that exchanged in the second block is lower than the one in the first block. This is due to the lower inlet oil temperature. Besides, pressure drops also increase. If the two blocks are arranged in parallel, the total energy also increases, but it is lower than the one estimated for the series. Each block exchanges less because of the lower oil mass flow rate which leads to lower pressure drops. Looking at the Tables, it is evident that the pattern shows that the theoretical better configuration would be a pure series of elements, but it is not feasible in an operative situation. The pure series presents two main practical problems: the pressure drops are much higher than in the parallel case, also it would not be possible to build a unique pipe with the needed length for a pure series configuration. These considerations highlight the need of a more comprehensive analysis, in order to investigate the performances of more complex configurations, trying to identify a rationale best configuration for given operating conditions.

Please, note that for the specific single block configuration, the mass flow rate can be reduced, also reducing the pressure drops, since it has already stored nearly the maximum possible heat value well in advance of the total duration and by increasing the flow rate it is not possible to go beyond the inherent limitations

that each block can store. For the set duration, in fact, the single block reaches the asymptote already after 3 hours, while the total time is 5 hours. However, it was chosen to use the mass flow rate of 500 kg/h as a reference precisely because, even when it is subdivided in parallel, the two modules still managed to reach an asymptotic condition. If a lower mass flow rate had been chosen, once distributed, it would not have been sufficient to allow the blocks to accumulate enough heat and the comparison shown in the table would have been of little significance. In an operational situation, it is important to be able to identify the minimum mass flow rate that allows to exploit the maximum possible accumulation in the time required.

Table 4.1: Energy and efficiency comparison between 2 blocks in series and parallel in charging phase

Conf.	**En. I block**	**En. II block**	**Tot. energy**	**Eff.**	**Press. drop**
[–]	[MJ]	[MJ]	[MJ]	[%]	[bar]
1 module	44.42	-	44.42	98.58	0.22
2 in series	44.42	43.99	88.41	98.11	0.44
2 in parallel	43.98	43.98	87.96	97.61	0.11

Table 4.2: Energy and efficiency comparison between 2 blocks in series and parallel in discharging phase

Conf.	**En. I block**	**En. II block**	**Tot. energy**	**Eff.**	**Press. drop**
[–]	[MJ]	[MJ]	[MJ]	[%]	[bar]
1 module	44.11	-	44.11	97.92	0.21
2 in series	44.11	43.49	87.60	97.20	0.42
2 in parallel	43.31	43.31	86.62	96.12	0.11

Thermal energy at a variable number of elements

The performance of different configurations was assessed at different operating conditions. The simulations started by keeping constant the initial concrete and oil temperatures, the total time and the total oil mass flow rate and then, for each number of branches (from 1 to 8), the number of elements arranged in series that lead to a target pressure drop was calculated. Finally, for each combination, the exchanged thermal energy was estimated. The results are listed in Tables from 4.3 to 4.7.

For an oil mass flow rate of 500 kg/h and a target pressure drop of 2.5 bar, the combinations Series*Parallel (S*P) 11*1, 22*2, 32*3, etc. were obtained (Tab. 4.3). It means that with a mass flow rate of 500 kg/h and 3 branches, each branch needs 32 elements in series to get an overall pressure drop of 2.5 bar, with a total number of 96 elements. With a lower number of branches, the mass flow rate for each branch is higher, so the number of elements in series to reach the target pressure drop is lower (i.e. 22*2). The thermal energy during both charging and discharging phase was hence calculated. Table 3 also demonstrates that the total energy increases with the number of branches, because the total number of elements also increases (the elements numbers are valid both for adiabatic and diabatic boundary), but then it reaches an asymptotic value (for 3 branches), when the number of branches is increased, even if a higher number of elements is involved, the thermal energy remains almost the same, meaning that these configurations are not optimized.

When increasing the target pressure drop to 5 bar (Tab. 4.4), the resulted combinations, for a given number of branches, exhibit more modules arranged in series because of the greater amount of available pressure drop. The firsts were (S*P) 23*1, 44*2, 63*3 and so on. As already stated, by increasing the number of branches, the thermal energy also rises until the same asymptotic value of the previous simulations. However, in this case, the maximum value is obtained for lower parallel subdivisions (in particular, for 2 branches) because the number elements in series for each branch is higher. If the target pressure drop is brought to 10 bar (Tab. 4.5), the number of series elements for each branch increases accordingly, and the asymptotic thermal energy value is reached for 2 branches again.

Further considerations can be made by varying the oil mass flow rate, considering 250, 500 and 1000 kg/h, in Tabs. 4.6, 4.4, 4.7, respectively, while keeping constant the value of the pressure drop at 5 bar. The asymptotic value is reached at lower number of branches for lower mass flow rate; in fact, at 250 kg/h it is achieved with the first combination yet, while with 1000 kg/h at 6 branches. In any case, the asymptotic thermal energy value is different for the three simulations, because it increases with the inlet oil mass flow rate.

This preliminary analysis allowed to understand the effect of the oil mass flow rate and pressure drop on the performance of different arrangements of concrete modules in complex TES systems. Besides, in order to understand the specific underlining heat transfer behavior of these systems in their charging and discharging phases, a more detailed analysis must be done. However, it is unfeasible to study in detail all the operating conditions presented before, thus a typical set

Table 4.3: Thermal energy with 500 kg/h of mass flow rate and 2.5 bar of pressure drop for adiabatic (A) and diabatic (D) boundary

Total blocks	Series	Parallel	Discharging		Charging	
			[MJ]		[MJ]	
			A	D	A	D
11	11	1	470	403	453	431
44	22	2	1001	917	1037	1045
96	32	3	1090	1019	1091	1118
176	44	4	1091	1022	1091	1119
375	75	5	1091	1022	1091	1119
480	80	6	1091	1022	1091	1119
595	85	7	1091	1022	1091	1119
688	86	8	1091	1022	1091	1119

Table 4.4: Thermal energy with 500 kg/h of mass flow rate and 5 bar of pressure drop for adiabatic (A) and diabatic (D) boundary

Total blocks	Series	Parallel	Discharging		Charging	
			[MJ]		[MJ]	
			A	D	A	D
23	23	1	778	689	801	780
88	44	2	1089	1018	1091	1117
189	63	3	1091	1022	1091	1119
380	95	4	1091	1022	1091	1119
775	155	5	1091	1022	1091	1119
960	160	6	1091	1022	1091	1119
1155	165	7	1091	1022	1091	1119
1360	170	8	1091	1022	1091	1119

of parameters for the HTF was considered, as reported by Rodat et al. (2015), Achkari et al. (2020), Cocco et al. (2016), and Rodríguez et al. (2016).

In particular, in the next paragraphs, the analysis was carried out by keeping constant the oil mass flow rate at 500 kg/h, as also reported by Rodat et al. (2015), and Rodríguez et al. (2016), while the maximum allowable oil pressure drops were limited to 5 bar, that can be considered a consistent value for a centrifugal pump available in the market.

Oil and concrete temperatures along the series

The detailed analysis can start from one of the most meaningful parameters, the oil temperature profiles through the series of the concrete modules for the

Table 4.5: Thermal energy with 500 kg/h mass flow rate and 10 bar pressure drop for adiabatic (A) and diabatic (D) boundary

Total blocks	Series	Parallel	Discharging		Charging	
			[MJ]		[MJ]	
			A	D	A	D
47	47	1	938	938	1057	1069
176	88	2	1022	1022	1091	1119
369	123	3	1022	1022	1091	1119
800	200	4	1022	1022	1091	1119
1550	310	5	1022	1022	1091	1119
1920	320	6	1022	1022	1091	1119
2289	327	7	1022	1022	1091	1119
2640	330	8	1022	1022	1091	1119

Table 4.6: Thermal energy with 250 kg/h of mass flow rate and 5 bar of pressure drop for adiabatic (A) and diabatic (D) boundary

Total blocks	Series	Parallel	Discharging		Charging	
			[MJ]		[MJ]	
			A	D	A	D
88	88	1	546	511	546	559
400	200	2	546	511	546	559
960	320	3	546	511	546	559
1320	330	4	546	511	546	559
1700	340	5	546	511	546	559
2082	347	6	546	511	546	559
2450	350	7	546	511	546	559
2816	352	8	546	511	546	559

different parallel configurations, in the case of adiabatic boundary conditions. The profiles relative to the first four modules arrangements (23*1, 44*2, 63*3 and 95*4), at the end of the process (5 hours) at a mass flow rate of 500 kg/h and imposing the pressure drop at 5 bar, were plotted, both during charging (Fig. 4.4) and discharging (Fig. 4.5) phases. The profiles start at the inlet oil temperature and progressively approach the concrete one module by module, with a clear asymptotic trend. It is interesting to point out that the first configuration (23*1, pure series) does not reach the asymptote because the number of elements is limited by the allowable pressure drop. The second one (44*2) reaches the asymptotic value both for temperature and thermal energy (see Tab. 4.4): it is the first configuration that exchanges the maximum amount of thermal energy.

Table 4.7: Thermal energy with 1000 kg/h of mass flow rate and 5 bar of pressure drop for adiabatic (A) and diabatic (D) boundary

Total blocks	Series	Parallel	Discharging		Charging	
			[MJ]		[MJ]	
			A	D	A	D
6	6	1	262	219	265	250
24	12	2	941	807	977	931
51	17	3	1599	1422	1691	1656
88	22	4	2003	1834	2107	2090
135	27	5	2149	2000	2170	2216
192	32	6	2179	2039	2182	2235
252	36	7	2183	2044	2183	2237
360	45	8	2183	2044	2183	2237

All the other combinations also reach the asymptotic values, both for temperature and thermal energy , but they employ a larger number of elements, becoming more expensive solutions without storing a greater amount of energy, which remains almost the same.

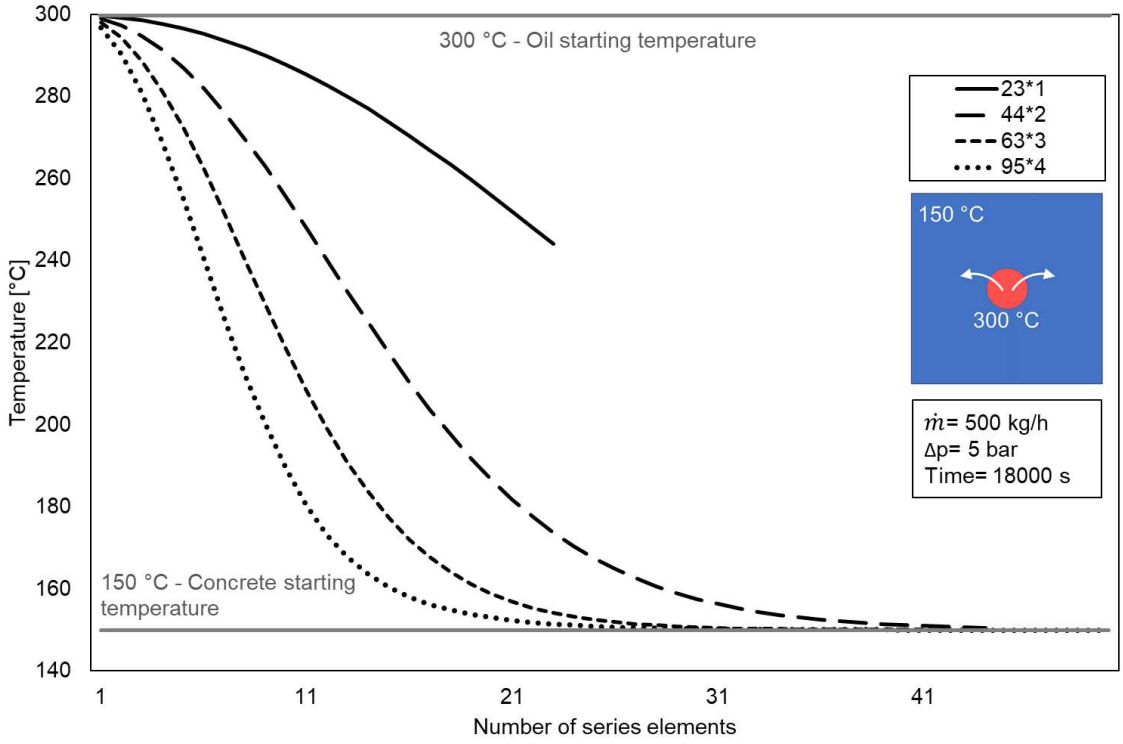

Figure 4.4: Adiabatic analysis: oil temperature at the end of the simulation in charging for different configurations

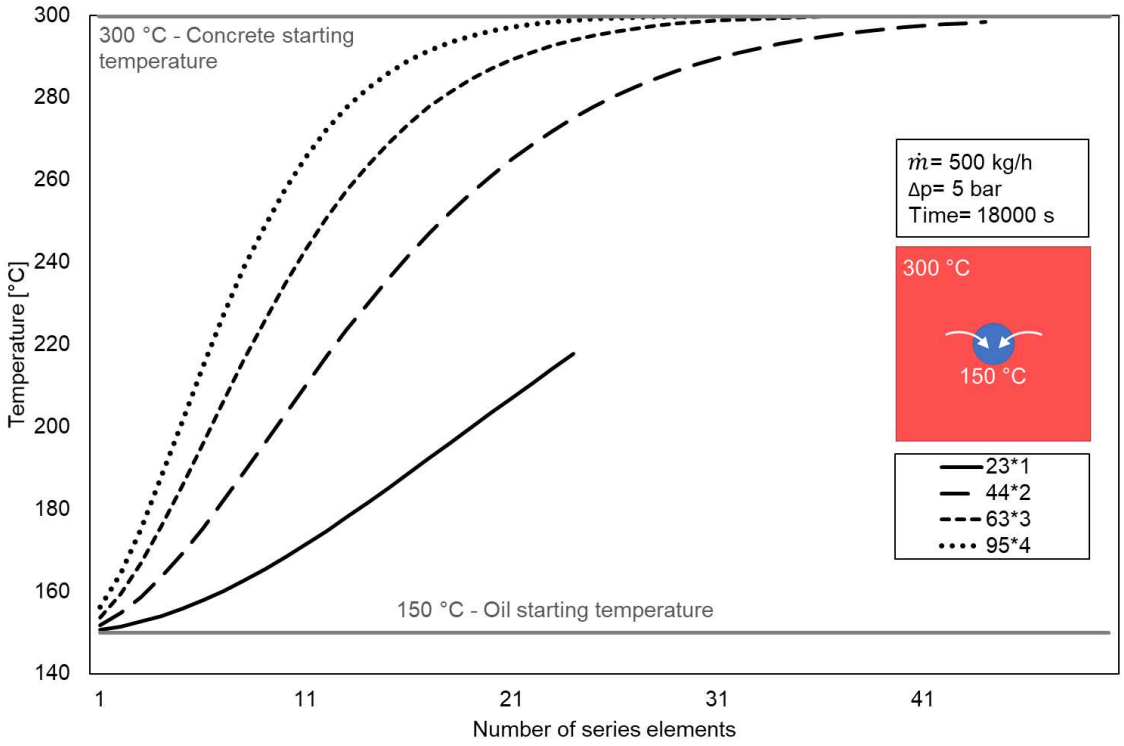

Figure 4.5: Adiabatic analysis: oil temperature at the end of the simulation in discharging for different configurations

Thermal energy over time

The stored thermal energy over time allows for a more comprehensive understanding of the behavior of the different modules' configurations. In the previous analyses, the simulation time was always set to 5 hours, which recalls a value of working hours for a typical CSP, that hardly can be extended to 6-8 hours (at relatively high solar radiation). When the working time is increased, the selected configurations show interesting results, all the charging and discharging curves (Fig. 4.6 and 4.7) present similar behavior because the temperature difference between oil and concrete and the other variables are set to equal values. In fact, the thermal energy profile of all the different combinations, at first linearly increases with time, then it approaches its specific asymptotic value, which depends upon the total number of elements and it is reached in a relative high time.

Considering a typical daily cycle for a CSP plant, the charging and discharging phases last in 6-8 hours, thus, the first configuration 23*1 has almost achieved its asymptotic value yet; differently, all the other configurations are still in the linear zone, storing higher values of thermal energy. This is further proof that the second combination (44*2) is the optimal one (for the set simulation time) because it gets the same thermal energy of 63*3 and 95*4, but with fewer concrete blocks.

With different simulation time, different optimal combination will be obtained.

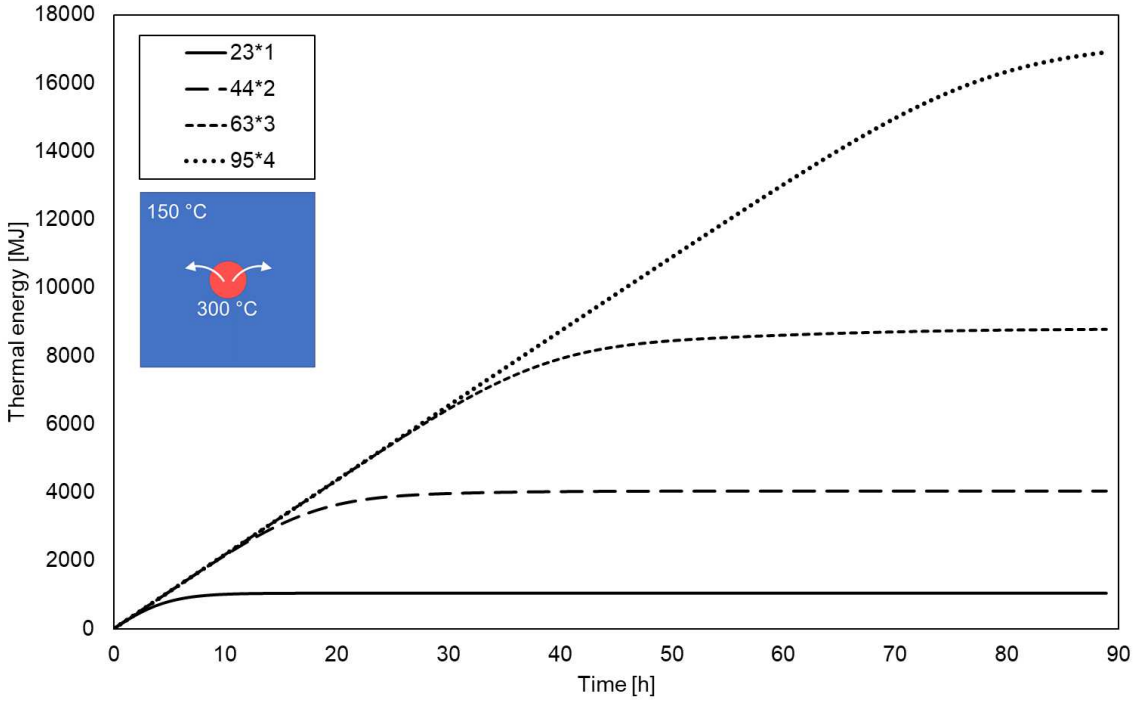

Figure 4.6: Adiabatic analysis: energy for different configurations at constant mass flow rate (500 kg/h) and pressure drop (5 bar) in charging

Oil heat fluxes over time

As already stated, the second configuration (44*2) has demonstrated the best overall performance in term of stored energy in reasonable time (5 h); for this reason, the oil heat flux at different time steps is plotted along the series, as shown for the charging phase in Fig. 4.8 and for the discharging one in Fig. 4.9.

At the beginning of the simulation (i.e. 1 h), all the concrete blocks present the same temperature, thus the first one exchanges the maximum oil heat flux, as it can be seen from Fig. 4.8. In charging phase, the oil cools down by flowing through the cold elements, and, consequently, the heat flux decreases through the series. Then, as the charging phase proceeds (i.e. 1.5, 2, 3 h, etc.), the first blocks asymptotically approaches the oil temperature and the heat flux sharply decreases to almost zero. The hot oil, which can be considered as a thermal wave, progressively reaches the following elements and the relative maximum heat flux moves to the central blocks and finally monotonically decreases as the oil temperature diminishes. The maximum value of heat flux moves gradually to the central blocks and reaches lower values. During the discharging phase (Fig

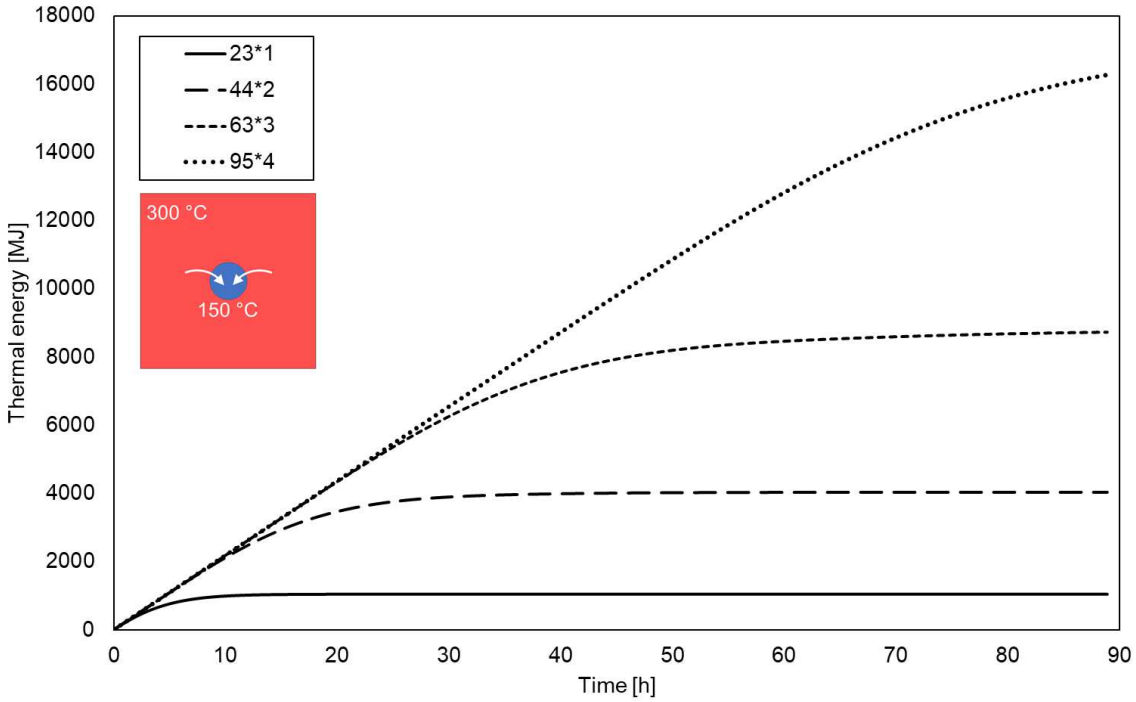

Figure 4.7: Adiabatic analysis: energy for different configurations at constant mass flow rate (500 kg/h) and pressure drop (5 bar) in discharging

4.9), the profiles are similar, but the oil and concrete temperatures are obviously switched. Hence, the oil becomes progressively hotter by flowing through the concrete blocks and this reduces the heat flux. Also, in this case, the curves present a maximum, but the profiles are smoother.

Heat fluxes along with the series

It is worth showing the profiles of the oil, concrete, insulating heat fluxes through the 44 elements of the 44*2 configuration after 5 h (i.e. at the end of the simulation) of both charging (Fig. 4.10) and discharging (Fig. 4.11).

Only three curves are shown because the reported simulation is carried out considering adiabatic conditions, so the loss heat flux is null and the difference between oil and concrete heat flux is equal to the insulating heat flux. They all have a maximum in the central blocks and then decreases progressively through the last element of the series. This means that the first blocks, have already exchanged heat with the oil mass flow rate in the previous hours, so the oil can reach the central block being still hot and charge the storage. This also means that even this configuration has not reached the maximum amount of storable energy.

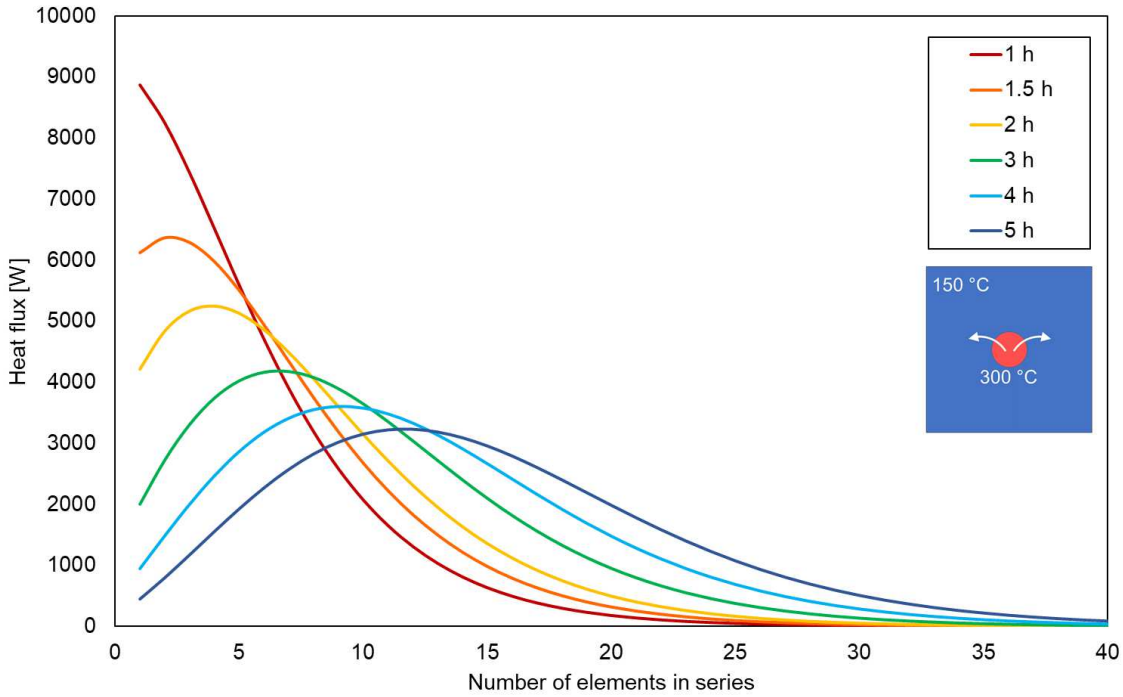

Figure 4.8: Adiabatic analysis: oil heat fluxes at different hours for 44*2 configuration (500 kg/h, 5 bar) in charging

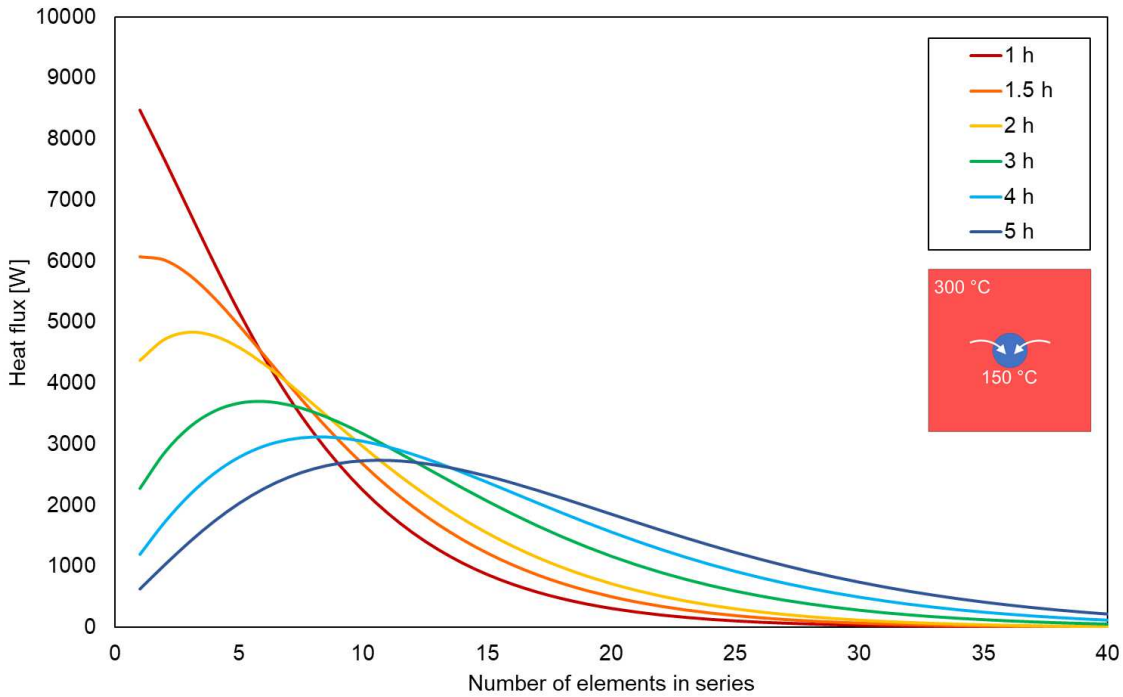

Figure 4.9: Adiabatic analysis: oil heat fluxes at different hours for 44*2 configuration (500 kg/h, 5 bar) in discharging

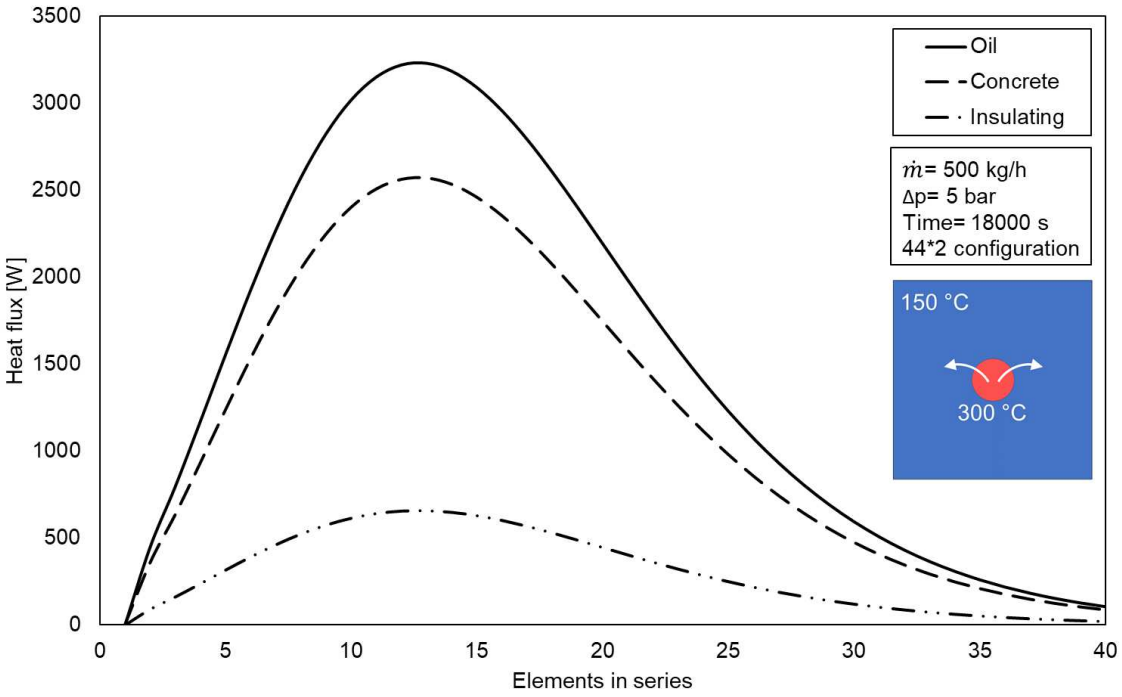

Figure 4.10: Adiabatic analysis: heat fluxes at the end of the simulation for 44*2 configuration in charging

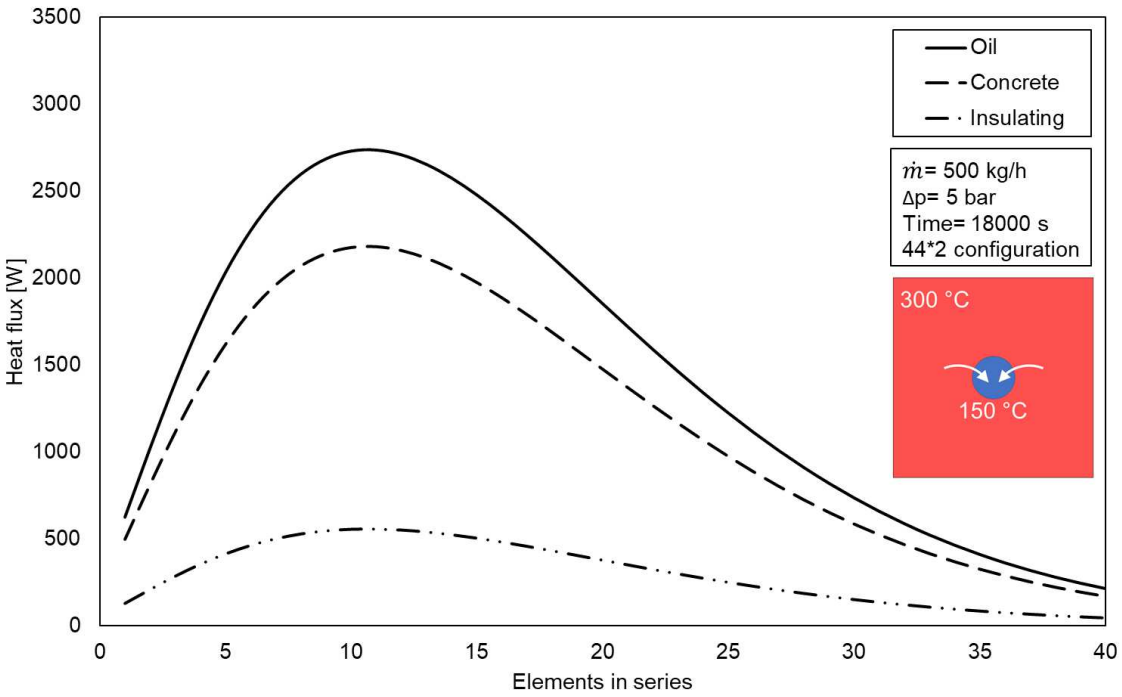

Figure 4.11: Adiabatic analysis: heat fluxes at the end of the simulation for 44*2 configuration in discharging

4.5 Diabatic external boundaries

Further investigations can be made by introducing the heat flux between concrete blocks and the environment. The insulating materials exchange heat with the surrounding ambient, set at 20 °C. This new boundary condition remarkably affects the results of the simulations and the differences between the charging and discharging phases emerge, in terms of both temperature and exchanged heat. It is important to assess this condition because it seems closer to a real operating situation.

The exchanged thermal energy both in charging and discharging phases is reported in Tables from 4.3 to 4.7 for the same combinations used for the previous analyses. In general, the results are similar to those obtained for adiabatic conditions, but there is important evidence: the asymptotic thermal energy related to charging and discharging set at different values and this is due to the loss of energy towards the environment. In fact, in charging phase, the concrete blocks are set at 150 °C and heated up by oil mass flow rate, which enters at 300 °C. Conversely, in discharging phase, the elements have 300 °C starting temperature, while the inlet oil one is equal to 150 °C. The environment temperature is always set at 20 °C, so the temperature difference between concrete and the surroundings changes during the simulation and it is different for the two phases. The diabatic boundary influences the heat flux and the thermal energy too, specifically in the charging phase more amount of thermal energy is exchanged than in discharging.

Oil and concrete temperatures along with the series

The temperature curves at the end of the simulations, for different configurations, are reported even for the diabatic analyses in Figs. 4.12 and 4.13. As before, they are related to 500 kg/h oil mass flow rate and pressure drop of 5 bar. The general trend is similar to the adiabatic one and the second combination (44*2) is even in this condition the first that reaches the asymptotic value, both in the charging (Fig. 4.12) and discharging phase (Fig. 4.13).

Nevertheless, the two (44*2) asymptotes are set on different values compared with the adiabatic case. In the charging phase, the temperature profiles do not stop at 150 °C, which is the initial concrete one, but they reach 140 °C and this is due to the heat loss to the environment by the hot concrete modules. In fact, the blocks are cooled by the heat loss to the external ambient, so the oil is brought to that temperature, too. In the same way, in the discharging phase, the blocks initially are set at 300 °C and progressively decrease their temperature. The oil mass flow rate temperature cannot arise until 300 °C and stops at 287 °C. The

temperature difference between the oil inlet and outlet is greater in charging than in the discharging phase. This causes a difference also in the related heat fluxes and thermal energy.

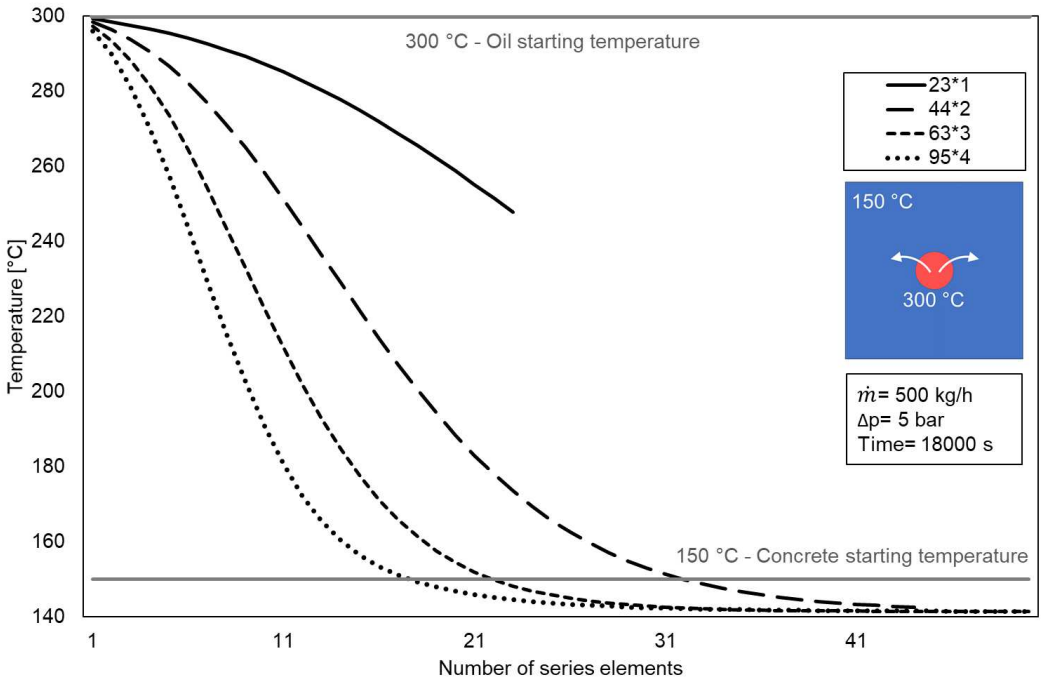

Figure 4.12: Oil temperature at the end of the simulation in charging (diabatic)

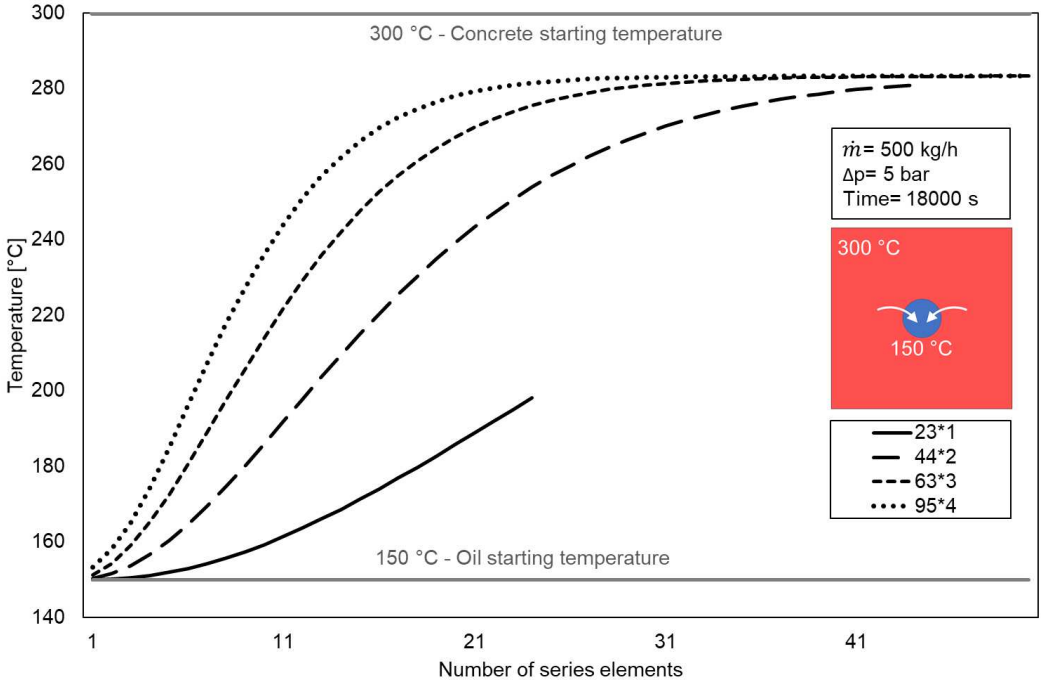

Figure 4.13: Oil temperature at the end of the simulation in discharging (diabatic)

Thermal energy during time

The major differences can be highlighted considering the thermal energy during time, in Figs. 4.14 and 4.15. After the initial linear trend, the curves do not set on an asymptotic value, but there is an increase in charging and a decrease in the discharging phase.

In the charging phase, the thermal energy keeps increasing, even if with a lower slope. In the discharging phase, instead, the thermal energy achieves a maximum, different for the various combinations, and then decreases progressively. It must be underlined that the two diagrams present different scales to improve the readability.

Even in diabatic conditions, the second combination (44*2) appears to be the optimum one in the range of operative time, usually of about from 8 to 10 hours, of a common CSP plant. It reaches the same thermal energy amount of the others, but with fewer concrete blocks.

Please, note that in the two figures the time axis arrives at 90 hours, which is a duration exclusively theoretical, used to see the pattern of the selected disposition. The most interesting part of the chart ends at around 10 hours because an operative plant does not work for more than this time and, considering the initial part of the graph, the curves are almost overlapped, storing the same energy amount. For this reason, since the thermal energy is almost the same, the most useful disposition is the one that reached almost the same thermal energy amount as the other, but with a considerable less amount of blocks, becoming cheaper and more feasible.

Heat fluxes along with the series

The different heat fluxes at the end of the simulations (5 hours) have been plotted along with the series even for this situation. There are some main changes compared to the adiabatic simulations; the results are reported in Figs. 4.16 and 4.17.

The loss heat flux has a relevant role in this situation, and it is more significant where the concrete block's temperature is higher. It happens for the first elements in charging phases, which have been already heated, and for the last ones in discharging phases, which still maintain a high temperature.

In the charging phase, the last elements encounter a negative concrete heat flux. This is due to the high loss heat flux, whose difference between the oil one brings the concrete heat flux below zero. For those elements, the insulating heat flux is null because it has already been balanced with the environment

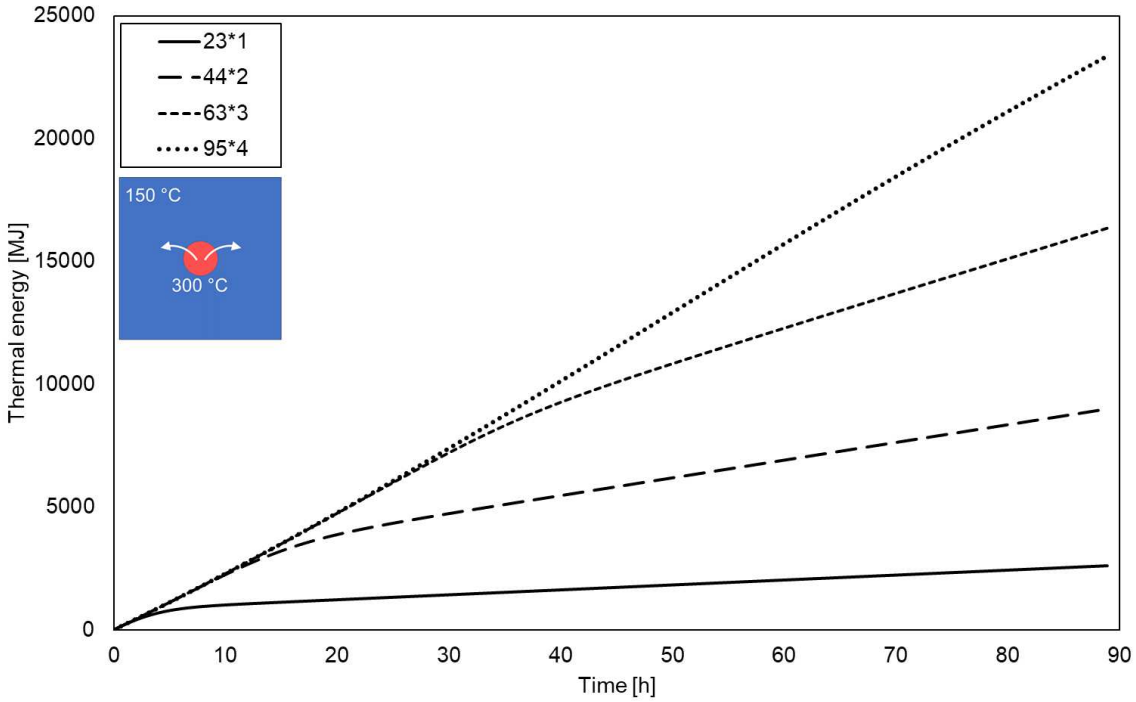

Figure 4.14: Diabatic analysis: energy for different configurations at constant mass flow rate (500 kg/h) and pressure drop (5 bar) in charging

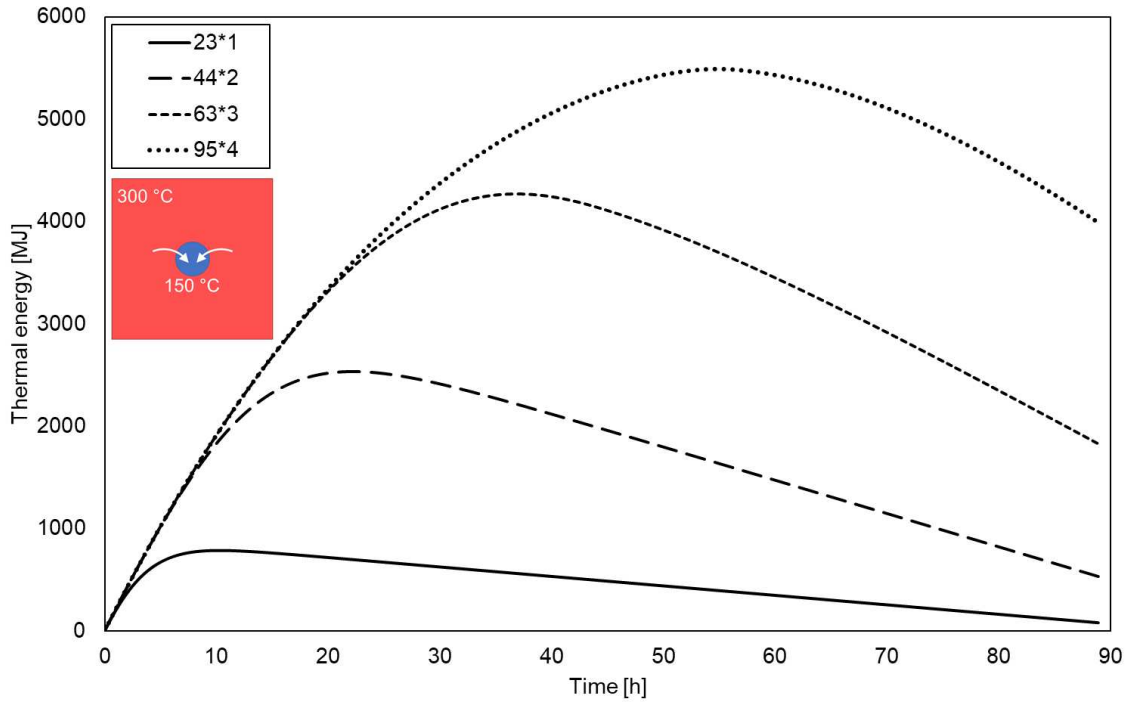

Figure 4.15: Diabatic analysis: energy for different configurations at constant mass flow rate (500 kg/h) and pressure drop (5 bar) in discharging

temperature, the central elements present the oil, concrete and insulating fluxes peaks.

In the discharging phase, the concrete heat flux has higher values that the oil one. Once again, this is due to the high loss heat flux, which enters in the balance and keeps the concrete heat flux higher than the oil one. The insulating heat flux has a peak in the middle, like the oil and concrete ones, while it is approximately negligible for the last blocks.

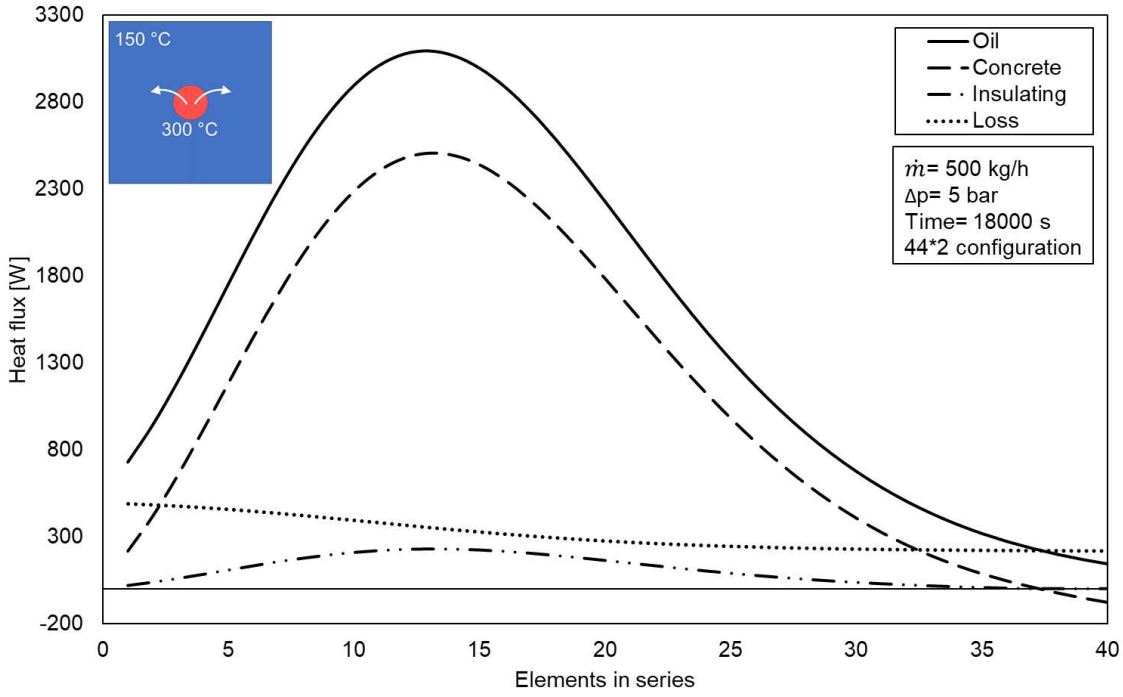

Figure 4.16: Diabatic analysis: heat fluxes at the end of the simulation for 44*2 configuration in charging

4.6 Conclusions

In this chapter, the numerical analysis for large-scale modularized concrete thermal energy storage systems was conducted. The simulations were carried out by means of a dedicated code, an improved version of the one presented, in the previous chapter, for single concrete TES block. Different arrangements of various elements in series, parallel and mixed configurations were investigated, and their performances were compared, to determine the best configuration as a function of the imposed operating conditions.

The exchanged thermal energy was assessed both during the charging and dis-

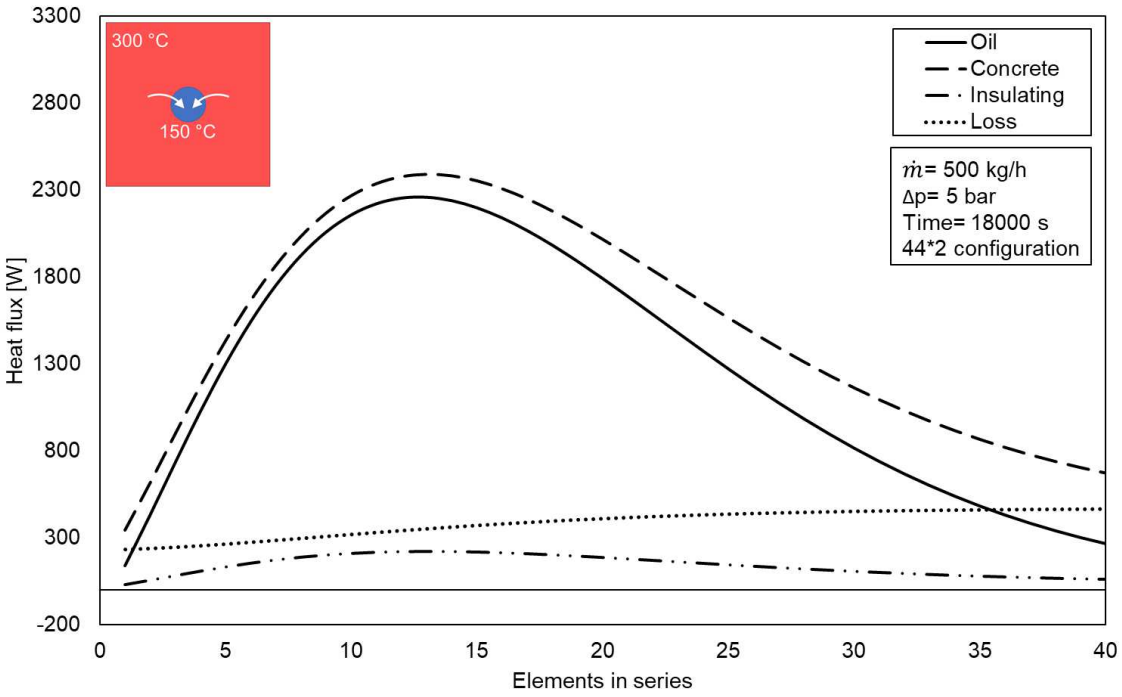

Figure 4.17: Diabatic analysis: heat fluxes at the end of the simulation for 44*2 configuration in discharging

charging phase, considering adiabatic and diabatic external surfaces. The initial concrete, oil and environment temperatures were set at fixed values, to achieve comparable results. The oil mass flow rate, the pressure drops, and the process duration were instead varied to evaluate the performance of the different configurations. All the parameters were set to be suitable values for a real CSP plant.

At fixed total mass flow rate and pressure drop, the number of parallel branches was progressively increased. The number of elements in series for each branch was consequently calculated. The thermal energy increased at each consecutive branch, until an asymptotic value. For mass flow rate (500 kg/h) and pressure drop (5 bar), the most performant configuration was (44*2) which exchanges the same amount of energy as the following ones, but with fewer blocks. Hence, for the given operating conditions, the best possible configuration was found, considering thermal energy, pressure drops and economic issues.

The oil temperature profiles were also predicted and there are relevant differences between the adiabatic and the diabatic situations. In the adiabatic case, the curves tended with an asymptotic way to the starting concrete temperature, while in the diabatic case the heat loss shifted down them. The exchanged heat with the surroundings led to a progressive increase in the thermal energy in the

charging phase while during the discharging phase a maximum value was observed. The best modules' configurations in diabatic conditions were the same for the adiabatic simulations but with different overall thermal energy, due to the heat loss to the surroundings.

Moreover, in the adiabatic case, after a few hours of operation, the exchanged heat fluxes presented a maximum in the central blocks of the series, the first elements had already been fully charged, so a peak appeared in the middle. In the diabatic case, the heat loss to the surroundings had a significant role and highlighted the differences between the charging and discharging phases. Its presence was not negligible and contributed to a more aware choice of the most suitable system.

The most interesting part, which is also the one on which the focus has been posed, is the thermal exchange between the HTF and the concrete matrix because the main heat transfer process occurs from the oil to the concrete, in the charging stage, and from concrete to the oil, in the discharging stage. The concrete needs to be heated in the heating stage to store thermal energy that will be then released to the colder oil in the cooling stage, that flow out heated and can be used in the CSP plant.

5. PCM integration

5.1 Introduction

The TES systems that are based on phase change materials are also gaining attention because of their potential improvements. Here reported below there are some of the most recent and interesting studies about this topic.

During the last 20 years, several forms of bulk encapsulated PCM were marketed for active and passive solar applications, including direct gain. However, the surface area of most encapsulated commercial products was inadequate to deliver heat to the building after the PCM was melted by direct solar radiation.

In contrast, the walls and ceilings of a building offer large areas for passive heat transfer within every zone of the building. Several workers have investigated methods for impregnating gypsum wallboard and other architectural materials with PCM.

However, the principles of latent heat storage can be applied to any appropriate building materials. Processes where this PCM could be incorporated into plasterboard, either by post manufacturing incorporating liquid PCM into the pore space of the plasterboard or by addition in the wet stage of plasterboard manufacture, were successfully demonstrated.

Latent heat storage with phase change materials provides a high heat storage density and has the capability of storing a large amount of heat during the phase change process with a small variation of PCM volume and temperature. Using latent heat storage in the buildings can meet the demand for thermal comfort and energy conservation purpose.

Phase change materials can be impregnated into construction materials in differetn ways. In almost all cases a PCM has to be encapsulated for technical use, as otherwise the liquid phase would be able to flow away from the location where it is applied. The main methods are here reported. They are divided in two sections: the incorporation methods and the containers.

5.2 Concrete as a thermal mass material for building applications

Identifying new energy saving methods in the building sector is essential due to limited natural energy sources and the rising population. Thermal mass materials have the ability to absorb and store heat before releasing it later on, when necessary. They act as heat sinks during the daytime and as heat sources during the night-time.

Thermal performance is evaluated according to the specific heat capacity and specific latent heat. Applying thermal mass materials such as concrete is deemed a suitable strategy to reduce the energy consumption of buildings. Concrete with low thermal conductivity and high specific heat capacity is desirable in building construction.

Thermal energy storage is based on sensible and/or latent thermal energy storage methods. With the sensible method, heat is released or stored by lowering or raising the thermal mass material's temperature. Whereas with the latent method, heat is released or stored as a material's phase change.

The amounts of sensible heat can be calculated with Eq.5.1.

$$Q_s = \int_{T_1}^{T_2} m_s \cdot c \cdot dt = m_s \cdot c \cdot (T_2 - T_1) \tag{5.1}$$

Where Q_s is the sensible heat storage, T_1 is the initial temperature, T_2 is the final temperature, m_s is the mass of the heat storing material and c is the specific heat. As reported before, for the current study, the specific heat capacity has been assumed constant because it was a reliable assumption, but in general, it could be temperature dependent, so this simplification can not be done.

The amounts of latent and heat can be intead calculated with Eq.5.2.

$$Q_l = m_l \cdot r_0 \tag{5.2}$$

Where Q_l is the latent heat storage, m_l is the mass of the phase change material and r_0 is the specific latent heat of the phase change material.

Various studies reveal that temperature, humidity, aggregate type, cementitious material type as well as phase change material used influence the thermal properties of concrete.

Thermal mass is defined as a material's ability to absorb, store and release

heat. Thermal mass materials, such as water, earth, bricks, wood, rocks, steel and concrete act as heat sinks in warm periods and as heat sources during cool periods, as schematized in Fig. 5.1. High thermal mass materials maintain indoor temperatures within desirable ranges without extreme energy consumption.

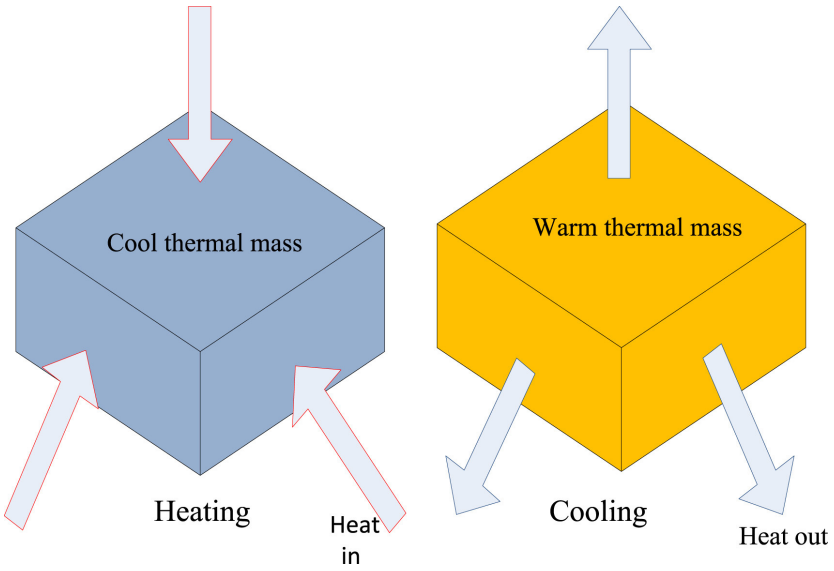

Figure 5.1: Thermal behavior of thermal mass materials

Concrete is a thermal mass material mainly composed of cement, water and aggregates. Concrete is used in building materials twice as much as all other building materials like plastic, wood and steel. Improving the thermal behavior of concrete reduces the energy consumption in buildings.

The heat capacity of a material indicates the heat storage capability per unit volume. Based on whether this process occurs at a constant volume or constant pressure, specific heat is categorized into specific heat volume (c_v) and specific heat pressure (c_p). For incompressible substances like concrete, the amounts of c_p and c_v are similar and can be denoted by a single symbol, c. The specific heat of solid materials depends on temperature.

Concrete with high specific heat is useful for boosting the temperature stability of buildings. Concrete with a low conductivity and high specific heat is desirable for building construction and insulation.

The thermal mass behavior of the materials, including concrete, is highly influenced by the thermal diffusivity, which is defined as:

$$a = \frac{\lambda}{\varrho c} \quad [\mathrm{m}^2/\mathrm{s}] \tag{5.3}$$

Where:

- λ is the thermal conductivity [w/(mK)]
- ϱ is the density [kg/m^3]
- c is the specific heat capacity [J/(kgK)]

Most researchers have investigated the thermal conductivity of cement-based materials, as reviewed by Asadi et al. (2018). In contrast, only a limited number of studies have investigated all thermal properties of cement-based materials.

According to Du and Ge (2021), three materials with thermal diffusivity of 0.22 mm^2/s are introduced as having the best cement paste heat insulation, compared to plain cement paste with thermal diffusivity of 0.37 mm^2/s. Among these three materials, silane treated with silica fume and containing cement, water, a water reducing agent, silica fume, methylcellulose and defoamer is the material most capable of absorbing heat without changes in temperature owing to its higher specific heat.

5.2.1 Thermal properties of hardening cement based materials

Cement hydration is a chemical reaction between cement and water. Heat is released during the hardening process of concrete due to the exothermic reaction of cement hydration. The properties of concrete are not constant during hardening due to the chemical reactions taking place. The value of already reacted cement is described as the degree of hydration.

Many Researchers found out that the conductivity of cement paste reduced by about 20% during hydration. However, reductions of 30% and 50% have also been reported. The following equation is suggested by Reinhardt et al. (1982) to estimate the conductivity of hardening concrete:

$$\lambda = \lambda_f(2 - r_h) \tag{5.4}$$

Where r_h is the degree of hydration and λ_f is the final value of hardened dry concrete.

Schutter and Taerwe (1995) reported a 13% reduction in the specific heat of concrete during hardening. They revealed a minor reduction in specific heat from 1.18 kJ/(kgK) at the age of 3 days to 1.16 kJ/(kgK) at the age of 10 days. Brown and Javaid (1970) reported a linear reduction of about 20% in the specific heat of hardening concrete. The specific heat of hardening concrete can be calculated

with the following equation, proposed by Reinhardt et al. (1982), which is similar to the previous one:

$$c = c_f(1.25 - 0.25r_h) \tag{5.5}$$

Some studies report reductions in the thermal diffusivity of concrete during hardening, but others found an increase in the thermal diffusivity of hardening cement paste. Schutter and Taerwe (1995), however, suggested the following equation to estimate the thermal diffusivity of hardening concrete:

$$a = 14.4 \cdot 10^{-3}(1.1 - 0.1r_h) \tag{5.6}$$

5.2.2 Methods of measuring the thermo-physical properties of concrete

Thermal conductivity

The steady state and transient methods are two main approaches of measuring the conductivity. Hotbox and hot plate are considered two principal techniques based on steady state, whereas transient plane source and hot wire are deemed the most common techniques used in transient condition. About 60% of studies reviewed in Shafigh et al. (2018) select the transient method to measure the conductivity of cement-based materials.

In measuring the steady state in which the sample's temperature remains constant over time, the specimen is placed between hot and cold plates. Heat is supplied to the sample and the temperature is measured with a thermocouple when the specimen is in steady-state condition. The conductivity is calculated using the following equation:

$$\lambda = \frac{Q \cdot \tau}{A \cdot \Delta T} \tag{5.7}$$

The conductivity of heterogeneous materials is usually measured with the transient method. The advantage of this method is the possibility to measure the conductivity of concrete moisture content.

Specific heat capacity

A calorimeter is an instrument used to determine the heat exchange rate and heat capacity. Isothermal, isoperibol, and adiabatic are three types of calorimeter classified based on the heat transfer conditions.

Generally, with calorimetry, a specimen with unknown specific heat capacity is mixed with a reference material that has known parameters. Heat transfer occurs between these materials and the heat emitted by one substance is equal to the heat taken up by another. The following equation, reported in Islam et al. (2014), is used to determine the specific heat of a specimen:

$$mc(T - T_f) = m_i c_i (T_f - T_i) \tag{5.8}$$

Where m, c and T are the mass, specific heat capacity and initial temperature of the reference material, m_i and T_i are the mass and initial temperature of the specimen and T_f is the final temperature of the mix.

Hansen et al. (1982) suggested a two-step temperature measurement to measure the specific heat capacity of hardening cement paste. The temperature rise was determined without and with the specimen inside the calorimeter. The specific heat of the cement paste was calculated with the following relation:

$$c = \frac{1}{m}\left(\frac{\dot{E}_2}{\Delta T_2} - \frac{\dot{E}_1}{\Delta T_1}\right) \tag{5.9}$$

Where c is the specific heat of the cement paste, m is the mass of the substance, $\dot{E}_2$ is the energy power in the configuration with the specimen, $\dot{E}_1$ is the energy power without the specimen, ΔT_2 is the difference of temperature with the cement paste specimen and ΔT_1 is the change in temperature without the specimen.

Howlader et al. (2012) used a semi-adiabatic calorimeter to measure the specific heat of concrete. After curing for 28 days, they drilled two holes with a 9.5 mm diameter drill bit in a cylindrical specimen. They immersed a thermometer into one hole, a 1000 W heater into the other hole and placed the specimen in the calorimeter. The specific heat of concrete was calculated using Eq.5.9.

Thermal diffusivity

The laser flash method is the most common transient mode for measuring the thermal diffusivity of concrete. This method is based on applying a very short,

but intense, laser energy pulse on one surface of a disc-shaped sample, while monitoring the temperature excursion of the opposite face. From the characteristic time dependence of the temperature rise, thermal diffusivity is calculated using the following equation:

$$a = \frac{138 s^2}{\tau_{1/2}} \tag{5.10}$$

Where a is the thermal diffusivity, s is the thickness and $\tau_{1/2}$ is the time necessary for the signal to reach 50% of its maximum value.

Xu and Chung (2000) prepared a disc specimen with 13 mm diameter and 2 mm thickness. They polished and coated both sides of the specimen with gold. The side that received the laser pulse was coated with carbon to avoid laser reflection. The temperature of the other specimen side, without carbon coating, was recorded and the thermal diffusivity was measured based on the temperature-time curve.

Howlader et al. (2012) used a cylindrical specimen to measure the thermal diffusivity. They made an axial hole with 9.5 mm diameter in which they inserted a thermocouple. The specimen was immersed in a boiling water bath, where it remained until the specimen's centre attained the desired temperature. The specimen was then suspended in a cold-water bath with constant temperature. After that, the temperature was changed at one-minute intervals. A semi-logarithmic graph of the time-temperature change was plotted and the following equation was employed to determine the thermal diffusivity:

$$a = \frac{60 \ln\left(\frac{T_1}{T_2}\right)}{(\tau_2 - \tau_1)\left(\frac{5.783}{r} + \frac{\pi^2}{l^2}\right)} \tag{5.11}$$

Where a is the thermal diffusivity, T_1 is the specimen's temperature at time τ_1, T_2 is the specimen's temperature at time τ_2, $(\tau_2 - \tau_1)$ is the time elapsed since the specimen's temperature changed from T_1 to T_2, r is the specimen's radius and l is the specimen length.

5.2.3 Sensible heat capacity of cement based materials

The sensible heat storage capability of concrete is affected by the moisture content, temperature, type of aggregate, type of cementitious materials and density of concrete.

The heat capacity of cement-based materials is higher than that of steel and lower than that of wood with specific heat values of 0.46 kJ/(kgK) and 1.6 kJ/(kgK), respectively. However, the specific of water is 4.186 kJ/(kgK), but this value for bound water in cement is about 2.2 kJ/(kgK).

The thermal conductivity and thermal diffusivity of concrete decrease with increasing temperature. However, the heat capacity increases at elevated temperatures. The specific heat of high-strength concrete is constant up to 400 °C, above which it increases. In particular, Shin et al. (2002) found that the specific heat increased from 1.10 kJ/(kgK)at 20 °C to 1.357 kJ/(kgK) at 700 °C and decreased to 1.119 kJ/(kgK) when the temperature was between 700 °C and 900 °C. They observed that the C-value enhanced again, when the temperature exceeded 900 °C. It should be noted that specific heat measurement at temperatures beyond 1100 °C is not applicable due to its decomposition at such elevated temperatures.

The specific heat of materials containing chemically bound water and free water can be estimated, as reported in Othuman et al. (2011), with the following equation:

$$c = c_{dry} + c_{add} \tag{5.12}$$

Where c is the overall specific heat capacity, c_{dry} is the specific heat capacity in dry condition and c_{add} is the amount of specific heat capacity to drive off water. c_{add} should be variable throughout the water evaporation temperature range. The start and completion of water evaporation are gradual processes. A triangular distribution of the C-value over the water evaporation temperature range is typically assumed.

The specific heat capacity in dry condition is related to the mass fraction and specific heat capacity of components in dry condition and can be calculated with:

$$c_{dry} = \sum_{i=1}^{n} f_i \cdot c_{pi} \tag{5.13}$$

Where c_{dry} is the specific heat capacity in dry condition, c_{pi} is the specific heat capacity of each component in dry condition and f_i is the weight fraction of each component.

The additional specific heat value is greater than the latent heat of water evaporation, so the Authors suggested the following equation for calculating the

average additional specific heat:

$$\Delta c = \frac{r_0}{\Delta T} \cdot e \cdot f \tag{5.14}$$

Where Δc is the average additional specific heat, r_0 is the latent heat of water evaporation, ΔT is the temperature interval during water evaporation, e is the dehydrated water content and f is a modification factor accounting for water movement.

About 60%–80% of the concrete volume comprises aggregate. The aggregate type is an important factor that affects the thermal properties of concrete. The specific heat is inversely proportional to the density of concrete and the it decreases with the rise in dry density.

5.2.4 Latent heat storage of cement-based materials

Brick, water, concrete, adobe and rammed earth, as high thermal mass materials in building applications, are the most commonly used materials to reduce energy consumption in buildings through a sensible heat storage approach. Combining building materials with PCMs is considered a proper means for enhancing the thermal energy storage capacity of buildings through latent heat. PCMs are preferred for improving the thermal comfort in buildings with phase changing temperatures in the range of $18 \div 30$ °C when the thermal comfort temperature varies between 23.5 and 25.5 °C in summer and between 21.0 and 23.0 °C in winter.

Inorganic PCMs are suitable for use in building applications due to their good conductivity, high heat storage capability, low cost and accessibility. Hydrated salts are the most common inorganic PCMs. The most used organic PCM are the paraffin waxes, which proved to be cost-effective, they are commercially available at a relatively low cost and are less detrimental for hardened state properties, allowing higher percentages of PCMs to be added.

5.2.5 PCM-concrete

Concrete slab, a thermal mass material, can absorb solar radiant heat in the daytime and release it at night time. The heat storage capacity of concrete increases when PCM is used. The extent of heat capacity enhancement is related to the PCM type and incorporation method applied during PCM-concrete production.

Different methods of incorporating PCM in concrete can be classified into immersion, immersing porous concrete in liquid PCM, impregnation, vacuum impregnation of PCM in permeable aggregates, and encapsulation, mixing an encapsulated PCM in the concrete mix. These methods were already discussed before for general building applications.

Encapsulation is a suitable way of incorporating concrete with PCMs. Micro encapsulation and macro encapsulation are two encapsulation approaches. The strength reduction and high cost of concrete are considered drawbacks of micro encapsulation. The various methods of incorporating PCMs and concrete are summarized in Fig. 5.2.

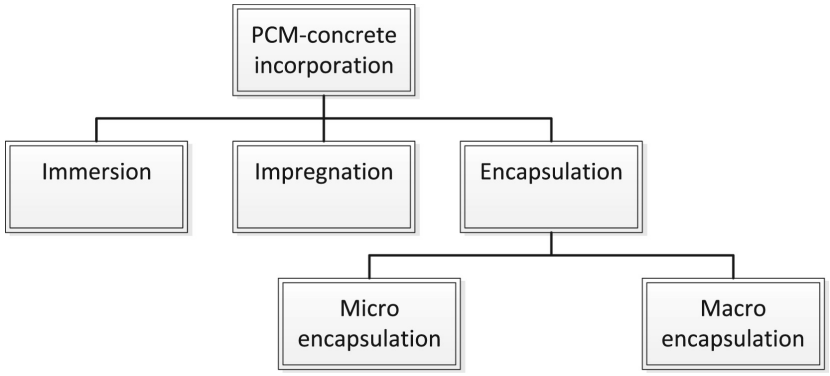

Figure 5.2: PCM-concrete incorporation methods

Many studies revealed that PCM-concrete can be considered as a proper heat storage based on latent heat storage approach. Though, still there is insufficient knowledge about the application of PCM-concrete in building sectors. More studies are required to evaluate the mechanical properties of these types of concrete as a building construction. More simulation and experimental studies are required to consider the efficiency of concrete based on its thermal properties in different weather conditions and different types of building.

Incorporation methods for building applications

The encapsulation of the PCM has developed interest in several researchers. Advantages and disadvantages of different geometries of PCM encapsulation with different materials and their compatibility were discussed in many papers. For the use of PCM in buildings applications, PCM is included in an unsaturated polyester matrix or integrated with the building materials without encapsulation (Shape-stabilised paraffin: 74% paraffin +26% high-density polyethylene). Different methods have considered the means of PCM incorporation: direct incorporation, immersion and encapsulation. The PCM must be encapsulated so

that it does not adversely affect the function of the construction material.

For many applications, PCM are microencapsulated, and this has been studied by several researchers and developed by companies. Nevertheless, the potential use of microencapsulated PCM in various thermal control applications is limited to some extent by their cost.

Hawes et al. (1993) reported that the three most promising methods of PCMs to be incorporated in the conventional construction materials were direct incorporation, immersion and encapsulation. They also found that the melting and freezing temperatures of PCMs varied slightly when being incorporated in building materials.

The direct incorporation is the simplest method in which liquid or powdered PCMs are directly added to building materials such as gypsum, concrete or plaster during production. No extra equipment is needed in this method but leakage and incompatible with construction materials may be the biggest problems.

The immersion is a technology in which the building structure components, such as gypsum, brick or concrete, are dipped into melted PCMs and then absorb PCMs into their internal pores with the help of capillary elevation. While some researchers pointed out this method may have a leakage problem which is not good for long-term use. Directly incorporation and immersion have different operation processes, but they both incorporate PCMs directly in conventional construction materials.

The technology with PCMs encapsulated in a container, for example, tubes, spheres or panels, is called macroencapsulation, with macroencapsulated PCMs, the leakage problem can be avoided and the function of the construction structure can be less affected. It has the disadvantages of poor thermal conductivity, tendency of solidification at the edges and complicated integration to the building materials.

It comprises the inclusion of PCM in some form of package such as tubes, pouches, spheres, panels or other receptacle. These containers can serve directly as heat exchangers or they can be incorporated in building products. It consists in encapsulation in containers usually larger than 1 cm in diameter, is the most common form of encapsulation. This solutions, also:

- Improves material compatibility with the surrounding, through building a barrier.
- Improves handling of the PCM in a production.
- Reduces external volume changes, which is usually also a positive effect for

an application.

Microencapsulated PCMs is commonly used in thermal energy storage of buildings. It is a technology in which PCM particles are enclosed in a thin, sealed and high molecular weight polymeric film maintaining the shape and preventing PCM from leakage during the phase change process. In particular, small, spherical or rod shaped particles are enclosed in a thin, high molecular weight polymeric film. The coated particles can then be incorporated in any matrix that is compatible with the encapsulating film. It follows that the film must be compatible with both the PCM and the matrix. It is much easier and more economic to incorporate the microencapsulated PCMs into construction materials.

This techonology regards the encapsulation in particles smaller than 1 mm in diameter, and it is a recently developed new form of encapsulation for PCM, that can currently only be applied to hydrophobic PCM. Micro encapsulation serves the same purpose as previously mentioned for macro encapsulation, but additionally:

- Improves heat transfer to the surrounding through its large surface to volume ratio.

- Improves cycling stability since phase separation is restricted to microscopic distances.

Hawlader et al. (2002) conducted thermal analyses and thermal cycle tests on microencapsulated paraffin and found that the microencapsulated paraffin still kept its geometrical profile and heat capacity after 1000 cycles. Some researchers think that the microencapsulated PCMs incorporated in the buildings structures may affect the mechanical strength of the structure.

Cabeza et al. (2007) designed two concrete cubicles with the same shape and size, one with microencapsulated PCMs called "Mopcon concrete" and the other one without PCMs respectively, in order to find the possibility of using microencapsulated PCMs in construction materials to achieve sizable energy conservation without significantly decreasing the mechanical strength of the concrete structures at the same time. They found Mopcon concrete reached a compressive strength over 25 MPa and a tensile splitting strength over 25 MPa which had already met the requirements in general structural purpose. However, the applications of microencapsulated PCMs still need further investigation in the aspect of safety, such as fire retardation capability.

Shape-stabilised PCMs, in which the PCM (like paraffin) is dispersed in another phase of supporting material to form a stable composite material, are attracting increasing attention due to their large apparent specific heat, suitable thermal conductivity, the ability to keep the shape of PCM stabilised in phase change process, as well as a good performance of multiple thermal cycles over a long period.

Zhang et al. (2006) considered the shape-stabilised PCM and found that it can make the thermal storage system simpler as it does not need special devices or containers to encapsulate the PCM. Based on the above benefits of this shape-stabilised PCM, they also proposed its potential application in efficient buildings used as inner linings, such as inner wall, ceiling and floor.

Zhou et al. (2008) simulated the thermal performance of a middle direct gain room with the shape-stabilised PCM plates as inner linings and examined several influencing factors to thermal performance such as melting temperature, heat of fusion, location and board thickness of the shape-stabilised PCM. Their results indicated the PCM plates were advantageous in direct-gain passive solar houses.

The conventional construction materials, such as gypsum board, concrete, brick and plaster, can be used to hold the PCMs. Some other panels, such as PVC panels, CSM panels, plastic and aluminium foils can also be used to encapsulated PCMs.

5.2.6 Mechanical properties

Compressive strength

The compressive strength results of PCM-concrete have been reported by several studies. The results indicate that the PCM content as well as the means of PCM incorporation in concrete noticeably affect the compressive strength of the PCM-concrete, as reported by Ling and Poon (2013). Investigations on using the immersion technique have found that there is no significant difference in the strength between the control and immersion PCM-concrete. Hawes (1991) reported that when paraffin wax is in the liquid state, the PCM-concrete exhibited a similar strength with that of the control concrete. However, when compared to the control concrete there was an approximately 50% increment in strength when paraffin wax was in the solid state. Cabeza et al. (2007) reported that the innovated PCM-concrete was found to achieve a compressive strength of over 25 MPa and a tensile splitting strength of over 6 MPa (after 28 days) which are appropriate levels for some structural application purposes. However, in the case of direct mixing, inclusion of PCM microcapsules in self-compacting concrete significantly

reduces the compressive strength, as reported by Hunger et al. (2009). The compressive strength of PCM– self-compacting concrete decreases by 13% for each additional percentage of microencapsulated PCM added by total concrete weight. The two mechanisms responsible for this decrease in strength are the significant disparity between the intrinsic strength of the microcapsules and other concrete constituents such as cement paste, and the damage of microencapsulated PCM resulting in paraffin wax leaking from the broken microcapsules and mixing with other concrete constituents.

Concrete porosity and intrinsic concrete density

Hunger et al. (2009) investigated the concrete porosity, as part of the void fraction which is open to the surface, of a control self-compacting concrete and PCM- self-compacting concrete mixtures prepared with 1%, 3% and 5% of microencapsulated PCM by total weight of concrete. They reported that the PCM–self-compacting concrete containing microencapsulated PCM had higher porosity values than the control one. This might be due to the structural change of the concrete packing density. The intrinsic concrete density of the PCM- self-compacting concrete decreased with an increase in the microencapsulated PCM content, probably due to the relatively low specific gravity of the microencapsulated PCM (0.915 kg/m^3) when compared to other constitutes in the concrete.

5.3 Models for concrete with PCM

In this chapter, the methods to analyse the behaviour of PCM reported in the scientific literature, divided by sections according to their type, are presented.

5.3.1 Analytical models

Meshgin and Xi (2013) presented the predictions of the effective thermal conductivity of PCM-concrete using different composite models, such as the parallel, the series models, Maxwell model and Generalized Self-Consistent model. Multiphase, multi-scale internal structural models were developed and combined with GSC model to predict the effective thermal conductivity of PCM-concrete. It was found that the configuration of the internal structure for the PCM phase is very important. The PCM phase needs to be considered as a matrix (a thin shell), which can effectively block the heat flow and thus reduce the thermal conductivity of PCM-concrete. The GSC model with the suggested internal structure model can predict the effective thermal conductivity of PCM-concrete. The prediction

agreed with test data quite well, and the prediction is within the upper and lower bounds. For the GSC model, it is required that the scale of the inhomogeneity is smaller than the characteristic dimension of the problem of interest. So, it was assumed the average size of aggregate particles is sufficiently smaller than that of the specimens. Considering this assumption would let a heterogeneous composite material be divided into many regions or elements that the volume fraction of each phase within each element is approximately a constant. These mean that the average size of inclusions is much smaller than the size of representative volume element of the composite, and the volume fractions of the constituents are constants. Fig. 5.3 shows how the volume fraction of the PCM affects the effective thermal conductivity of PCM-concrete. Increasing the amount of the PCM decreases the effective thermal conductivity of the PCM-concrete and this is due to the fact that the encapsulated PCM particles have a low thermal conductivity.

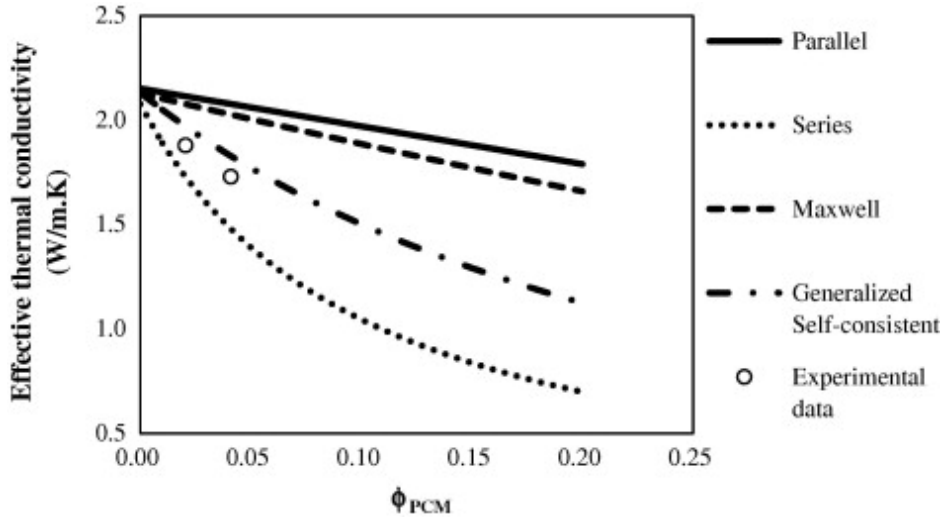

Figure 5.3: The effect of PCM volume fraction on the effective thermal conductivity, Meshgin and Xi (2013)

5.3.2 Numerical models

In recent years, numerical models are becoming increasingly popular, as they allow to solve problems, although in an approximate way, without an analytical solution in a closed form.

Finite difference approaches

Arora et al. (2017) employed a numerical simulation strategy to elucidate the influence of phase change materials on the thermal response of concrete pavements. The simulation methodology has been programmed using Matlab with

the capability to read climatic data from a national climate database, allowing the simulations of concrete pavements in any geographic location. Simulations of both the early and late age response of concrete pavements containing microencapsulated PCMs (of phase change temperatures in the range of 24 °C and 35 °C), replacing either a fraction of the cement paste or fine aggregate (1.25%÷5.5% of the total volume of concrete), with considerations of mixture proportions, PCM types, and structural and environmental boundary conditions, are carried out. Please, see Fig. 5.4 for a schematic model of a concrete pavement subjected to environmental effects at early ages. The latent-heat response of PCMs is explicitly integrated into the model. The early-age simulations show significant reductions in peak hydration temperature and the heating/cooling rates when PCMs, either as a partial replacement of the cement paste or fine aggregates, are incorporated in concrete, resulting in reduced cracking probabilities. Simulations on mature pavements also indicate temperature and curling stress reductions when appropriate PCMs are used. PCM type and dosage, depending on the imposed external temperature regimen, can be chosen based on the model to reduce the magnitude of critical stresses at both early- and late ages. The numerical model thus enables engineers and designers rationally design crack-resistant concrete pavements.

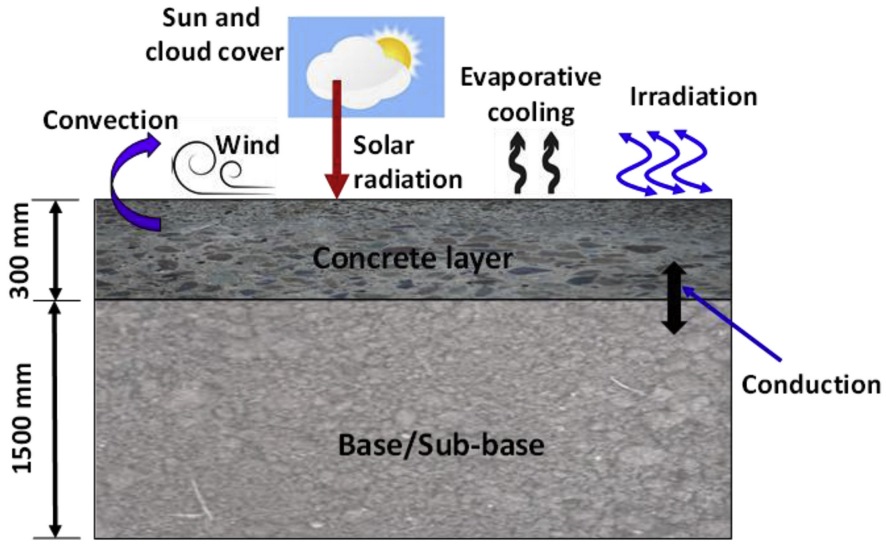

Figure 5.4: Schematic model of a concrete pavement subjected to environmental effects at early ages, Arora et al. (2017)

Athukorallage et al. (2018) studied the conditions for which PCMs mitigate extreme temperatures in a flexible pavement system. The temperature variation was obtained by solving the heat diffusion equation under transient conditions. The volume averaged energy equation with phase dependent thermal properties is used to analyse the heat transfer process in the integrated PCM pavement sys-

tem. The evolution of the latent heat of PCMs is assessed through an empirical formulation, through the enthalpy method, which uses a finite differences approximation, as reported by Voller et al. (1990), Srinivas Shastri et al. (1998) and Yifen et al. (2011). In that method, the enthalpy is expressed as a temperature function, as reported by Brousseau and Lacroix (1998) and Sharma et al. (2009). Different equations were used for the model, depending on the fraction of PCM volume present in the pavement layer. The effective thermal conductivity is calculated using the Maxwell-Eucken model, which assumes a distribution of small spherical particles within a continuous matrix. It can be used to calculate this parameter when the conductivity of the continuous phase is greater than that of the dispersed phase, as suggested by Wang et al. (2008) and Awad et al. (2008). As PCM, the commercial micro-encapsulated materials MPCM43D from Microtek Laboratories Inc. were used. They consist of a paraffin core encapsulated in a polymeric shell. The average diameter is about $15 - 20$ μm. Their results show that a pavement system consisting of a layer of PCM that is directly below the asphalt-concrete layer yields higher surface temperatures than a system without the PCM layer and a pavement system in which PCM is embedded in the layer with varying volume fraction has lower surface temperature values than that of the pavement without PCM when the PCM volume fraction is below a critical volume fraction, 60% for the conditions used; otherwise higher surface temperature values exist. Fig. 5.5 depicts the maximum surface temperature value and the corresponding time of occurrence with different PCM volume fractions. Firstly, it can be seen that the PCM volume fraction has a significant effect on the temperature and rate of change in temperature in the system. Secondly, a condition exists for which increased PCM results in increased maximum surface temperature; for the conditions studied a PCM volume fraction greater than 60% results in a higher maximum surface temperature. Thirdly, the time occurrence of maximum surface temperature decreases with the increase of the PCM volume fraction value. Finally, they showed the effective thermal conductivity has a strong effect on the temperature distribution throughout the surface layer of PCM embedded pavement system.

Bahrar et a. (2018) focused on the development of façade elements for improvement of energy efficiency in buildings. The proposed solution consists of new textile reinforced concrete panels including microencapsulated phase change materials in a variety of mix designs. A multiscale experimental characterization was performed to evaluate the thermal performance of different configurations. The results showed an increase in heat storage capacity and thermal inertia of the textile reinforced concrete with PCMs. Fig. 5.6 presents the evolution ver-

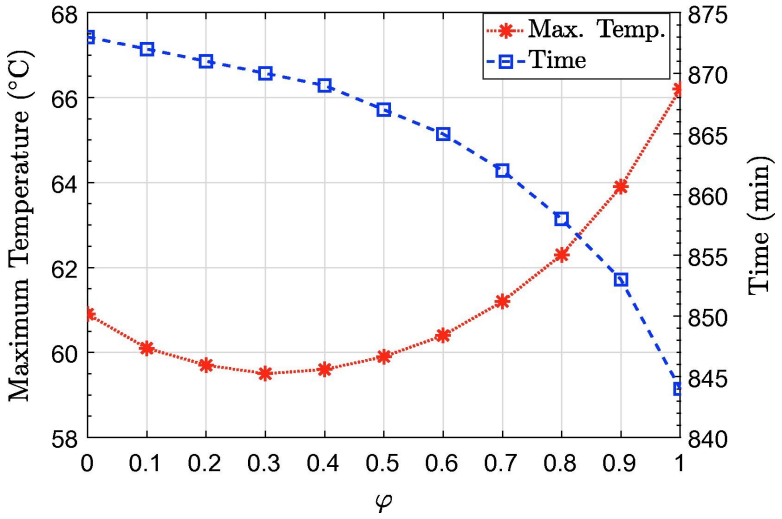

Figure 5.5: Maximum surface temperature value and the corresponding time of occurrence with different PCM volume fractions, Athukorallage et al. (2018)

sus temperature of the specific heat capacity measured by DSC for the PCM at the scanning rate 0.05 °C/min. In addition, A numerical model to study heat transmission through an opaque multilayer wall was developed and validated with experimental results. The equations of the model have been solved by an implicit finite difference method. The heat transfer is considered one-dimensional, since the flat slab has a relatively large width, compared to its thickness. The input data include the number of layers, the time step, the space step and the physical and thermal properties of each layer. The wall is discretized with a space step corresponding to the thickness of each layer. An energy balance is imposed at each node and the equations are solved so as to obtain the temperature at each node. The phase change, in this study, is modelled using the effective specific heat, temperature dependent, of PCM, as suggested by Richardson and Wood (2008). The evolution of specific heat as a function of temperature is obtained experimentally through differential scanning calorimetry. The results are introduced in the model to be then correlated to the temperature through a Matlab interpolation function. The accordance of the heating and cooling speed is maintained by comparing the temperature during three consecutive time steps. As phase change materials, microcapsules of the commercial Intertek 23 were used, available as dry powder. These materials are composed of vegetable wax encapsulated in polymer shells.

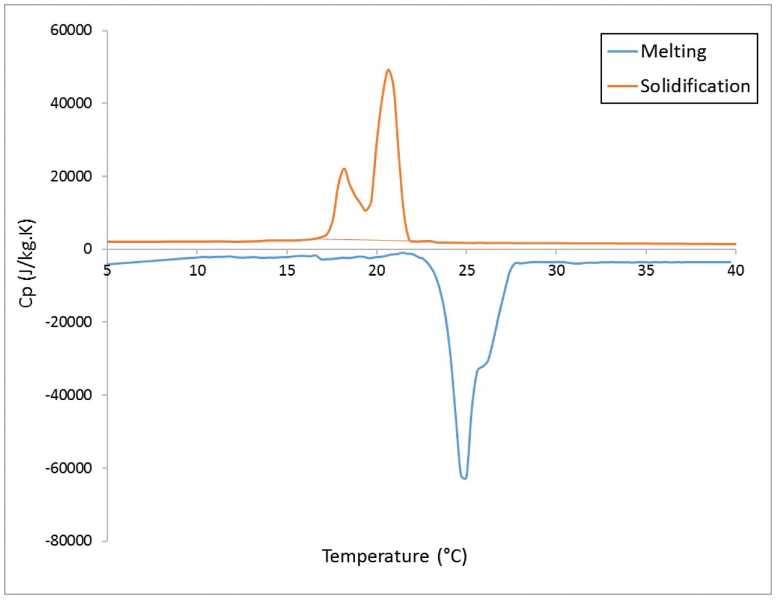

Figure 5.6: The specific heat capacity of microencapsulated PCMs at the scanning rate 0.05 °C/min, Bahrar et a. (2018)

Models with specific software

Mazzucco et al. (2017) analysed the coupled behaviour of concrete including PCM particles employed as solid energy storage media, even emphasizing the relevance of analyses at the mesoscale level. A study on the increased thermal capacity in thermal energy storage concrete solids with inclusions of PCM is developed within this paper. Particularly, the change in thermal behaviour of such composites by varying the inclusions percentage is assessed. Transient thermal analyses are conducted by considering a homogenized composite; a uniform distribution of PCM, obtained during mixing of fresh concrete, is assumed within the cementitious matrix. Additionally, the change in mechanical strength of such a material is analytically and numerically investigated, both at room temperature and during heating. 3D mechanical FE models are also developed at the meso-scale level to explicitly represent the main concrete components such as cement paste, coarse aggregates, and PCM to better describe the evolutionary process of thermal damage. Thermo-mechanical analyses at the meso level, to investigate the deterioration of the storage system occurring when PCM capsules are characterized by different filling degrees, are performed through the commercial software ABAQUS, suitably customized by user subroutines. A thermal damage process scheme is reported in Fig. 5.7: at room temperature the PCM cell is partly filled with salt in a solid state (Fig. 5.7a). When temperature exceeds the melting point, the salt changes phase and its thermal expansion accordingly increases. In this condition, if the filling percentage reaches 100% (Fig. 5.7b),

as temperature grows up the PCM cell accordingly expands, so increasing the stress level in the surrounding matrix (Fig.5.7c). Under higher temperatures, the elastic range for concrete is exceeded and damage occurs (Fig. 5.7d). The curve of specific heat capacity in function of temperature has been taken in agreement with Bazant and Kaplan (1996), please see Fig.5.8, left. An average value of the thermal conductivity between the two extremes provided by the Eurocode is determined, for each temperature step, obtaining the curve reported in Fig.5.8, right.

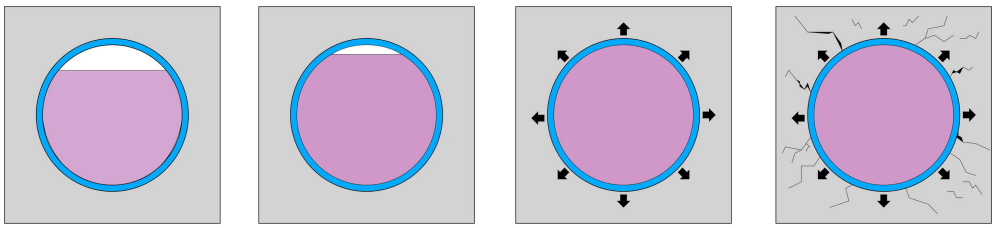

Figure 5.7: Volume variation of a PCM inclusion during phase change: solid state (a); solid-liquid phase change (b), Mazzucco et a. (2017)

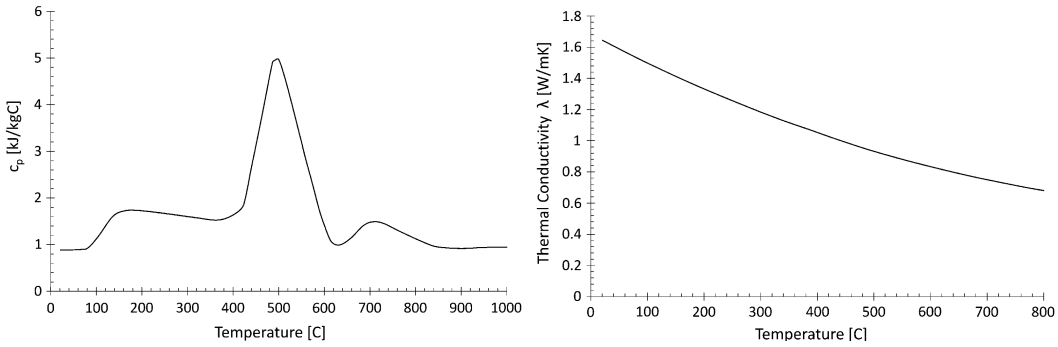

Figure 5.8: Concrete specific heat vs. temperature (left) and concrete thermal conductivity vs. temperature (right), Mazzucco et a. (2017)

Das et al. (2018) presented a microstructure-guided numerical homogenization technique to predict the effective thermal conductivity of a hierarchical cement-based material containing PCM-impregnated lightweight aggregates.

Porous inclusions embedded in a cementitious matrix are filled with multiple fluid phases including PCM to obtain desirable thermal properties for building and infrastructure applications. Simulations are carried out on realistic 3D microstructures generated using pore structure information. An inverse analysis procedure is used to extract the intrinsic thermal properties of those microstructural components for which data is not available. The homogenized heat flux is predicted for an imposed temperature gradient from which the effective composite thermal conductivity is computed. The simulated effective composite thermal

conductivities are found to correlate very well with experimental measurements. Finite element analysis, is employed in the inverse analysis procedure to predict the thermal conductivity of the solid phase of LWAs. The detailed two-step inverse analysis procedure is described schematically in Fig.5.9. The representative volume element is meshed and the heat flux response for the applied temperature gradient on the representative volume element is obtained using ABAQUS solver. A commercially available ordinary Portland cement, a paraffin-based PCM supplied by Entropy Solutions and four different light weight aggregates were used to proportion the mortars used in this study. The lightweight aggregates used were pumice, perlite, expanded shale/clay, and expanded slate. Coarse sand was used in the control mortar.

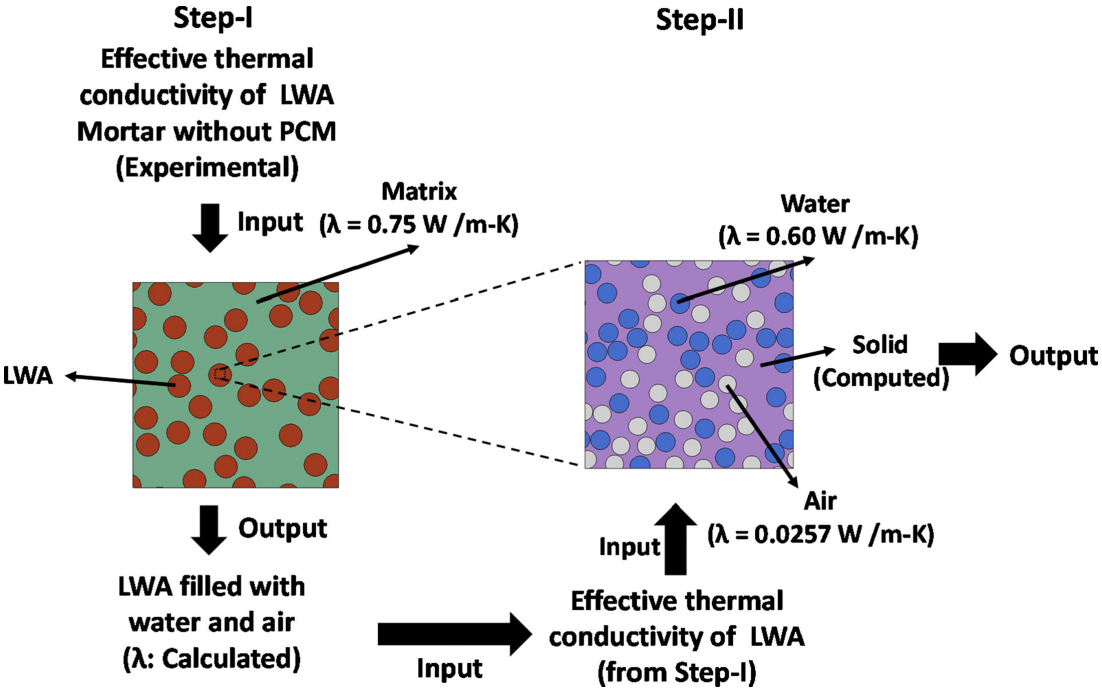

Figure 5.9: Inverse analysis procedure for the determination of thermal conductivity of the solid phase of LWAs, Das et a. (2018)

Faheem et al. (2016) presented a numerical procedure for predicting the thermal performance of ventilated hollow core slabs. The proposed approach is validated against experimental measurements available in the literature and then applied to study the effects of incorporating micro-encapsulated phase change materials in ventilated hollow core slabs for the cooling of office buildings. In particular, the impact of PCM content, PCM type and hollow core ventilation rates the slab's cooling potential is evaluated under two ideal room temperature cases. The Navier-Stokes equations for turbulent air flow and heat transfer are modelled numerically based on the Reynolds averaged Navier-Stokes approach,

for which the governing equations for mass, momentum and energy conservations, accounting for free convection effects (using Boussinesq approximation), are written in Cartesian tensor form. All the numerical simulations are carried out using the commercial CFD solver ANSYS Fluent 14. The governing equations are discretised by the second order upwind scheme for advection terms and central differencing scheme for diffusion terms.

Mohaine et al. (2016) developed a numerical multiscale approach to simulate the thermo-mechanical behaviour at high temperatures of concrete containing microencapsulated PCM, with a particular orientation to the fire behaviour. An investigation was also conducted on the effect of the thermo-mechanical properties of shell materials used to encapsulate the PCM. The finite element code Cast3m was used since the phase change model is already implemented in it. The problem considered is a general thermal transient analysis. The REV studied is governed by the heat equation and Fourier's law of thermal conduction, with an initial temperature and imposed temperature and heat flux as boundary conditions. PCM have been taken into account explicitly in modelling by considering their size distribution in a representative elementary volume. The effective thermo-mechanical parameters of the cement paste and the concrete have been calculated by a numerical homogenization method. Coupled thermal and mechanical loads have then been applied to the concrete with 10% and 15% of PCM at high temperatures. Two materials are considered as shell materials for the PCM: polymethyl methacrylate and melamine formaldehyde. The use of melamine formaldehyde, with a Young's modulus of 4.5 GPa, and a particular curve of thermal expansion coefficient instead of polymethyl methacrylate as shell material, showed a better thermo-mechanical behaviour at high temperatures. The thermal deformation and the damage of the resultant PCM concrete were found to be acceptable for building use. With high kinetics of heat flux, the phase change process is very fast and PCM cannot contribute to absorb the heat. So, in fire conditions, the phase change process can be neglected in simulations (Fig. 5.10).

5.3.3 Experimental models

Other Authors used experimental methods to evaluate the interaction between concrete and PCM. The most relevant are here reported.

Memon et al. (2015) revealed that incorporating normal weight aggregate concrete microencapsulated paraffin- lightweight aggregate reduced the energy consumption of buildings. They prepared a small test room containing five wooden panels and one panel at the top. The researchers placed a 500 W lamp as the heat

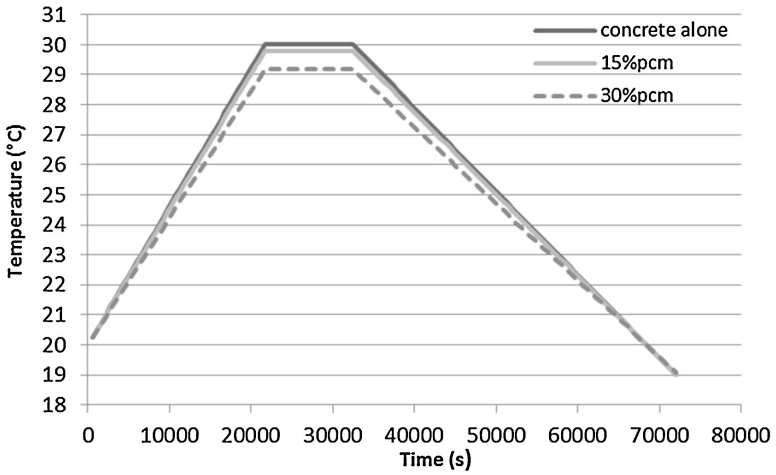

Figure 5.10: Temperature distribution at the centre of the representative elementary volume for the three concretes, Mohaine et al. (2016)

source 600 mm above the top panel. Thermocouples were located in the centre of the test room. The top panel was naturally cooled for 2 h after heating for 2 h. The indoor test room temperatures measured using normal weight aggregate concrete with and without PCM. The indoor test room temperatures measured of the two configurations are given in Fig.5.11

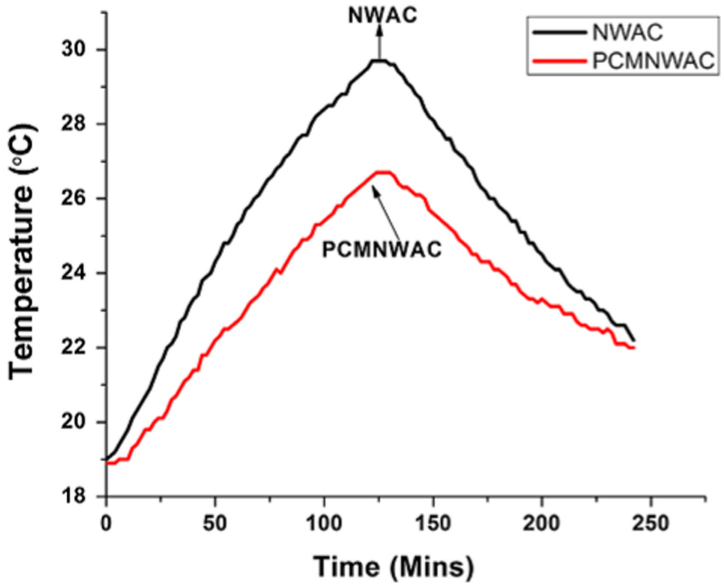

Figure 5.11: Indoor temperatures measured using different panels, Memon et al. (2015)

Cui et al. (2015) developed a macro encapsulated thermal energy storage concrete using lauryl alcohol–lightweight aggregate. They applied the vacuum impregnation technique to remove air from the porous lightweight aggregate areas and replace it with PCM. They revealed that the lauryl alcohol–lightweight

aggregate was in the occupant thermal comfort zone and its latent heat storage capacity was about 100.6 J/g. The general latent heat of building materials ranges from 15 to 150 J/g. Consequently, the Authors suggested their solutions as an adequate material for thermal energy storage applications to reduce the Heating, Ventilation and Air Conditioning (HVAC) load in buildings.

Zhang et al. (2004) proposed a two-step procedure for incorporating PCMs in building materials. First, they made a thermal energy storage aggregate using organic liquid PCM (Butyl stearate) and two porous aggregates of expanded shale and expanded clay. Second, they prepared thermal energy storage concrete by mixing raw materials of normal concrete, Portland cement and thermal energy storage aggregate. According to them, the two-step method is reasonable for producing PCM-concrete with suitable thermal energy storage capacity.

Jeong et al. (2013) evaluated the thermal performance of PCM- Silica fume applied in building materials like concrete. They combined silica fume with three different types of PCMs, namely hexadecane, octadecane and paraffin. They found that silica fume-hexadecane had the highest latent heat capacity compared to the other two. The latent heat of SF-hexadecane, SF-octadecane and SF-paraffin were reportedly 86.16, 90.72 and 56.19 J/g during melting and 86.32, 91.76 and 57.40 J/g during freezing.

Eddhahak-Ouni et al. (2014) measured the specific heat capacity, thermal conductivity and thermal diffusivity of PCM-concrete by using a differential scanning calorimeter (DSC), hot disc method and laser flash analysis. According to the Authors, the heat storage capacity of PCM-concrete is related to the proportion of PCM, but adding PCM does not affect the conductivity, please see Fig.5.12.

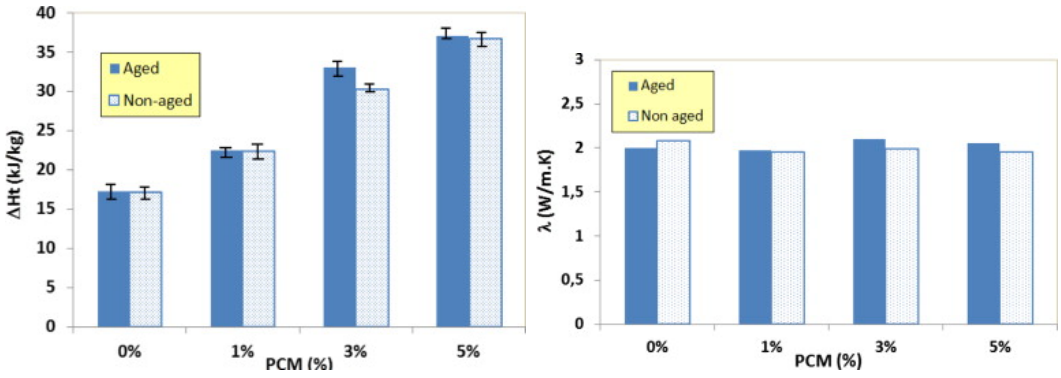

Figure 5.12: Specific heat capacity of PCM concrete mixes (left) and thermal conductivity of PCM concrete mixes before and after ageing (right), Eddhahak-Ouni et al. (2014)

Cui et al. (2017) evaluated the thermal performance of PCM-hollow steel ball concrete. They utilized octadecane as the PCM and a hollow steel ball as the

carrier for the PCM and coarse aggregate, Fig.5.13. An innovative method of macro-encapsulation of PCM using hollow steel balls (HSB) was developed and the thermal and mechanical performance of PCM-HSB concrete was examined. The microencapsulation system (PCM-HSB) was attached with a metal clamp (c) for better mechanical interlocking with the mortar matrix. They prepared a PCM-hollow steel ball panel to use at the top element of small test room. Furthermore, they prepared an environmental chamber using polystyrene foam panels. They applied a heater and an air conditioner to control the environmental chamber temperature. It was determined that PCM-hollow steel ball concrete is a proper heat storage material for building applications due to its high latent heat value. The latent heat of PCM-hollow steel ball concrete reported was about 153.1 J/g, which is more than the general latent heat of building materials (15–150 J/g). Consequently, using PCM-hollow steel ball concrete panels can reduce the heating and cooling loads in buildings. Furthermore, these panels can shift the thermal load away from the peak energy usage times.

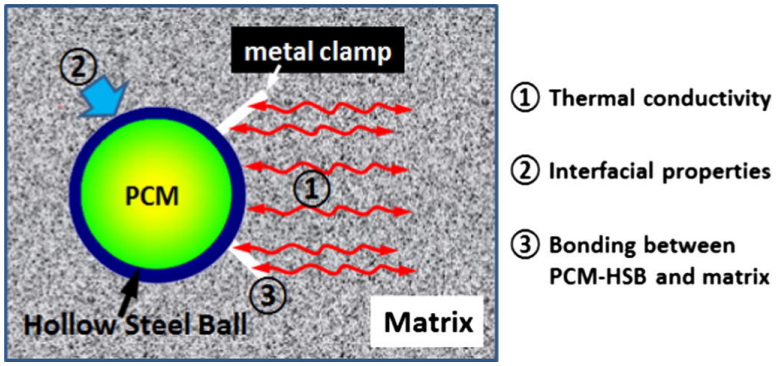

Figure 5.13: Schematic drawing of a PCM-HSB-c in concrete matrix. (1) metal clamp can improve thermal conductivity between PCM-HSB and matrix; (2) metal clamp improves interfacial transition zone between PCM-HSB and matrix; (3) metal clamp can improve bonding between PCM-HSB and matrix, Cui et al. (2017)

Zhang et al. (2013) evaluated the properties of thermal energy storage cement mortar and incorporated n-octadecane/expanded graphite composite PCM into ordinary cement mortar. They prepared a test room with five boards of ordinary cement mortar and four panels with different percentages of n-octadecane/EG PCM (0%, 0.5%, 1.2% and 2.5%) as the top panel. A 500 W halogen lamp was applied over the top panel to simulate sun heat. The researchers revealed that the different top panels in the test room caused varying indoor peak temperatures. They reported that the indoor peak temperatures for the top panels containing composite PCM with mass percentages of 0%, 0.5%, 1.2% and 2.5% were 39.0,

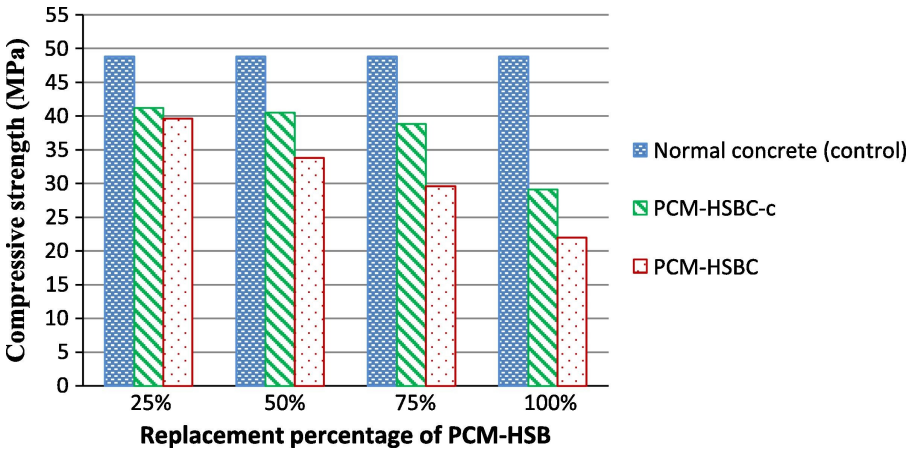

Figure 5.14: Comparison of compressive strength between PCM-HSBC concretes with and without metal clamps, Cui et al. (2017)

37.0, 35.0 and 30.3 °C respectively. Clearly, using composite PCM with mass percentage of 2.5% led to a 22% reduction in indoor peak temperature.

In Cao et al. (2018) microencapsulated phase change materials were added to geopolymer concrete for utilization as a thermal energy storage concrete for passive building applications. To investigate the effect of microcapsules on the thermal performance (energy saving aspect) of geopolymer concrete, a thermal system was set up as illustrated in Fig. 5.15. Three different PCM were compared to examine the influence of the hygroscopic nature of the PCM shell, the PCM core/polymer shell ratio, and the PCM size on the microstructure, thermal properties and compressive strength of geopolymer concrete. The combination of a hygroscopic nature of the polymer shell, a high core/shell ratio, and a small PCM size were found to improve the interface bonds between microcapsules and the concrete matrix, increase the energy storage capacity of concrete, and results in a good dispersion of PCM in the matrix. Adding PCM to geopolymer concrete induces a higher amount of air pockets, which weaken the compressive strength. Unfortunately, the same parameters that are advantageous for reducing the energy consumption also results in a greater decline of the compressive strength. The compressive strength is further reduced when the microcapsule core is in its liquid state. However, the compressive strength still satisfies the mechanical European regulation (EN 206-1, compressive strength class C20/25) for concrete applications.

D'Alessandro et al. (2018) presented a multiphysics thermomechanical investigation concerning innovative concretes incorporating paraffin-based PCM suitable for structural-thermal multifunctional applications in high-energy efficiency building envelopes. Both classic microPCM-capsules and the novel more pioneer-

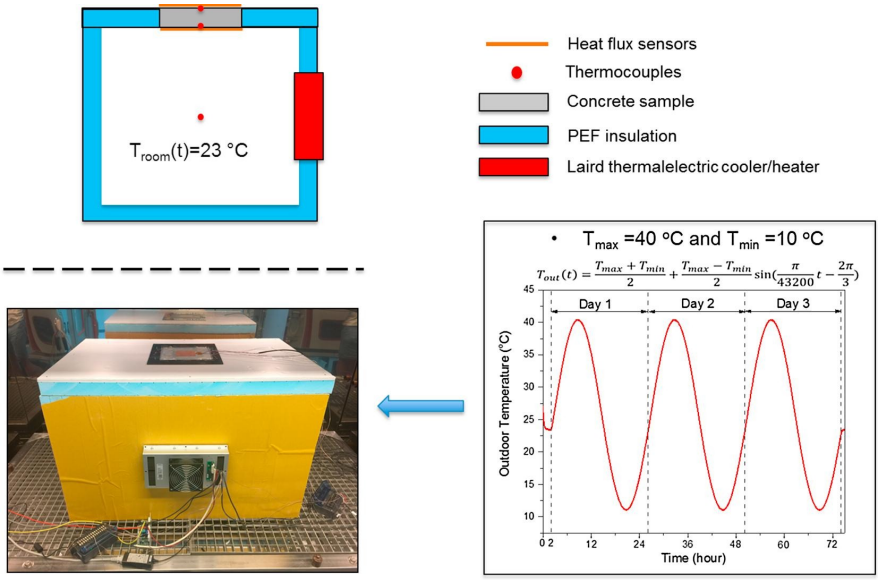

Figure 5.15: The thermal performance testing system with sketch of cross-section of the system and the simulated outdoor temperature profile, Cao et al. (2018)

ing macroPCM-capsules with 18 °C phase transition temperature are used for the new composite preparation. Fig.5.17 represents the structure of the PCM-filled concretes compared with the standard concrete. The figure illustrates the peculiar impact of the two different geometrical configurations, i.e. microPCM and macroPCM, in the resulting cementitious composite. Results confirm the thermal benefits of PCM and demonstrate that the addition of PCM reduces the mass density of concrete by almost twice PCMs weight. Average compressive strength decreases with increasing the amount of PCM, but its coefficient of variation is not as negatively affected, which is promising in terms of structural reliability.

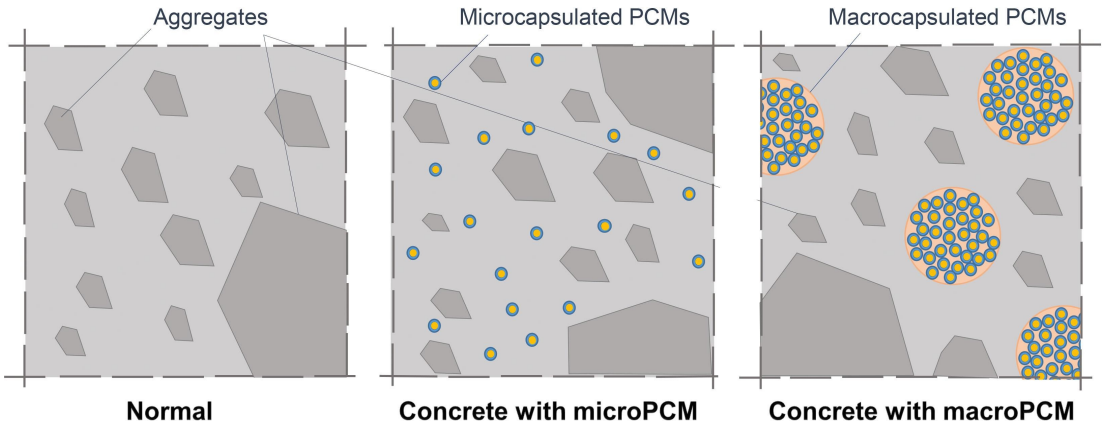

Figure 5.16: Sketch of the internal structure of normal, microPCM-filled and macroPCM-filled concrete, D'Alessandro et al. (2018)

Pomianowski et al. (2014) presented in this paper focuses on an experimen-

tal investigation of the specific heat capacity as a function of the temperature $c_p(T)$ of concrete mixed with various amounts of phase change material. They compared the theoretical method, the the simple method, the numerical simple method and the inverse method. The tested specimens are prepared by directly mixing concrete and microencapsulated PCM. This paper describes the development of the new material and the experimental set-up to determine the specific heat capacity of the PCM concrete material. The peak c_p obtained by the theoretical method is much higher than the peaks obtained from the methods utilizing experimental data. The peak obtained from the simple method is higher than the ones obtained from the simple numerical method and the inverse method, this method is expected to give overestimated results. The curves of the calculated $c_p(T)$ from the simple numerical method and inverse method lie very close to each other, but still the inverse method should give a more realistic representation of the $c_p(T)$ since this method is based on optimization algorithm.

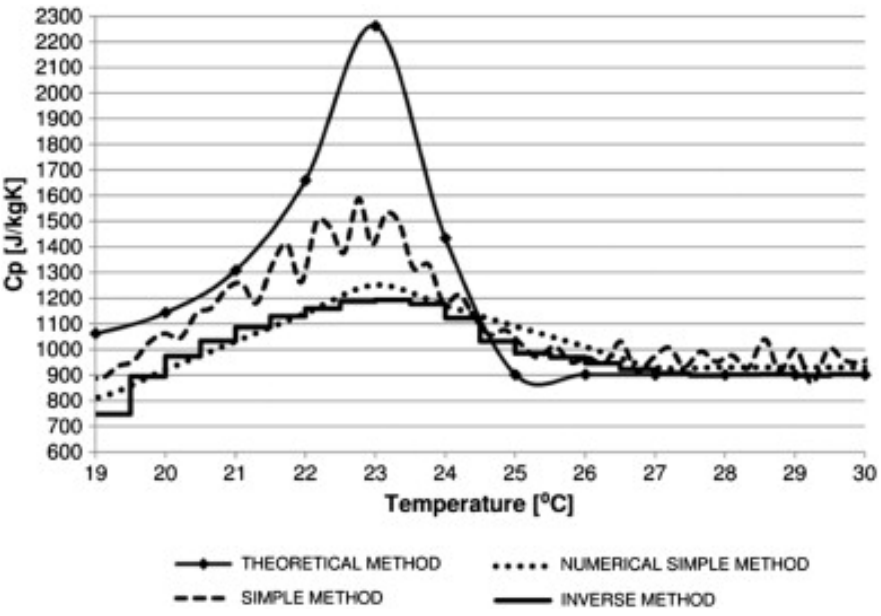

Figure 5.17: Comparison of results from various proposed calculation methods of $c_p(T)$, Pomianowski et al. (2014)

5.3.4 Final remarks

As final remarks of what was reported in the literature review, I can assess that concrete has been proved to be a good solid media to store sensible heat, due to its good thermal, mechanical and economic properties, but it could be also improved with the PCM integration because it, however, has some criticises.

- The thermal conductivity and the specific heat capacity decrease during the hydrating and hardening process.
- It has good values of density and specific heat capacity, which directly have a good effect on the thermal lag and temperature dumping of the transient thermal load typical of the summer season, but a too high thickness of the wall should be designed to adequately cope with it without the PCM integration.
- Various integration technologies of the PCM in the concrete elements have been developed and proposed, but there is a lack of analyses that compare the different integration methods with the same PCM amount.
- The different integration technologies might have impactant consequences on the systems, that should be carefully considered in the design process, depending on the needings.
- When the PCM is directly integrated into the concrete matrix, the compressive resistance would be reduced, which can be a non-negligible structural issue that should be taken into account.

However, there is a lack of studies regarding the integration of PCM in concrete, considered as the main storage material. For this reason, further improvements of the model presented in the previous chapters are here reported and include the integration of a chosen PCM quantity in the modules. The issue presented will be addressed in this and in the following chapters, to fill the lacks presented in the literature review and present the novelty of the actual work.

5.4 Model description and materials

The chosen PCM and quantity have been selected according to the request provided by the ENEA research group. The PCM was added as 5% or 10% in mass. It allows for the increase of the stored thermal energy, in the charging stage, and of the released energy, in discharging stage. The commonly called "solar salts" have been selected, which are composed of a mixture of sodium and potassium nitrate (composed of 40% of KNO_3 and 60% of $NaNO_3$). Its properties are reported in Tab. 5.1.

This material has been adsorbed by diatomite, which is a fossil sedimentary rock, with a highly porous microstructure, that originated from the siliceous fossilized skeletons of diatoms. It has been chosen as support media because of

its high porosity (almost 91%), which allows for the embedding of high PCM quantity and also allows the PCM to expand inside its cavity during the phase transitions. The diatomite properties are reported in Tab. 5.2.

Table 5.1: PCM "solar salts" properties

Properties	**Value**	**Unit of measurement**
Density	2290	[kg/m^3]
Specific heat capacity	820	[J/(kgK)]
Thermal conductivity	0.7	[W/(mK)]
Latent heat	110	[kJ/kg]
Initial melting temperature	493	[K]
Final melting temperature	517	[K]

Table 5.2: Diatomite properties

Properties	**Value**	**Unit of measurement**
Density	2000	[kg/m^3]
Specific heat capacity	900	[J/(kgK)]
Thermal conductivity	0.05	[W/(mK)]

The best ratio between PCM and diatomite has been identified, respectively, as 80/20% in weight. In order to take into account this proportion, each property has been conveniently weighted, through the following expression:

$$f = r_{PCM} \cdot f_{PCM} + (1 - r_{PCM}) \cdot f_{diatomite} \tag{5.15}$$

where f is the generic thermophysical property, and r_{PCM} is the PCM ratio in the diatomite, assumed equal to 0.8 in this specific case.

Due to the integration of the PCM in the diatomite, the latent heat of fusion has also been reduced to 88100 kJ/kg.

The integration of the PCM in the concrete mixture, through the diatomite, implies the need to consider the storage module as a unique element, constituted by a homogeneous material. For this reason, similarly to what was done for the PCM and the diatomite, all the properties have been again weighted with the concrete's ones, in order to obtain a unique material with homogeneous properties. The used equation takes the following form:

$$f = p_{PCM} \cdot f_{PCM} + (1 - p_{PCM}) \cdot f_{cnc} \tag{5.16}$$

Where f is the generic thermophysical property and p_{PCM} is the percentage of integrated PCM in the concrete mixture, which can be 0%, 5% or 10% in this study.

Particular attention should be paid to the specific heat capacity of the PCM, which was considered as reported by Lamberg et al. (2004):

$$c_{PCM} = \begin{cases} c_{PCM}, & T < T_{im} \\ c_{PCM} + \frac{r}{T_{fm} - T_{im}}, & T_{im} \leq T \leq T_{fm} \\ c_{PCM}, & T > T_{fm} \end{cases} \tag{5.17}$$

where r is the latent heat of fusion, T is the current cell temperature, T_{im} is the initial melting temperature, and T_{fm} is the final melting temperature.

5.5 Results

In this section, the results obtained by the simulations are reported, considering basic concrete and concrete with 5% and 10% of PCM integrated. As input parameters, the following data have been given to the code, for the charging stage:

- Concrete initial temperature = 50 °C
- Oil inlet temperature = 300 °C
- Oil mass flow rate = 500 kg/h
- Environment temperature = 20 °C
- Duration of the simulation = 14400 s (4 hours)

Similarly, for the discharging stage, we have:

- Concrete initial temperature = 300 °C
- Oil inlet temperature = 50 °C
- Oil mass flow rate = 500 kg/h
- Environment temperature = 20 °C
- Duration of the simulation = 14400 s (4 hours)

5.5.1 Exchanged thermal energy

The thermal energy absorbed in the heating phase and released in the cooling phase is shown respectively in Figs. 5.18 and 5.19. In both cases, it can be seen that the addition of PCM to the concrete basic mixture implies an increase in the exchanged energy, thus representing an interesting improvement. Also note that the curves tend to almost overlap during the initial phase of the simulation, and then separate. This behaviour is due to the fact that the concrete block's initial temperature is far from the phase change range of the PCM, and therefore requires time before being able to exploit the latent heat absorbed or released. Furthermore, after 4 hours of simulation, the heating curves begin to bring themselves to a condition of approaching the asymptote, while the cooling curves are still rising. This happens because, in cooling, the heat dissipated to the external environment takes on a more relevant role than in the case of heating, so the system takes longer to be able to reach an asymptotic condition.

However, the difference in thermal energy exchanged by the three concrete mixes, although present and clearly visible, is not relatively high. This is due to the low percentage of PCM integrated within the storage element. Quantities equal to 5% and 10%, in fact, are not sufficient to fully appreciate the potential and advantages that this technology allows. The increase in the percentage of PCM within the compound also implies a reduction in the mechanical properties of the material, a factor to be taken into due consideration if an element with structural functions is being designed. In this situation, nevertheless, the element has the sole role of having to support its own weight. For this reason, even the integration of a high amount of PCM would not be particularly detrimental to the mechanical performance that the block should perform, while it would greatly improve the results from the thermal storage point of view.

5.5.2 Temperature profiles

The curves of the average concrete temperature and oil outlet temperature are shown in Figs. 5.20 and 5.21 , respectively for heating and cooling. The average concrete temperature is influenced by the presence of PCM. In the curve corresponding to the 10% content, in particular, a discontinuity is also visible in correspondence with the phase change temperature range. The presence of PCM reduces the slope of the temperature curves and this represents a further advantage since it implies less probability of structural damage to the cement matrix.

In any case, the curves are still very close to each other, since the amount of

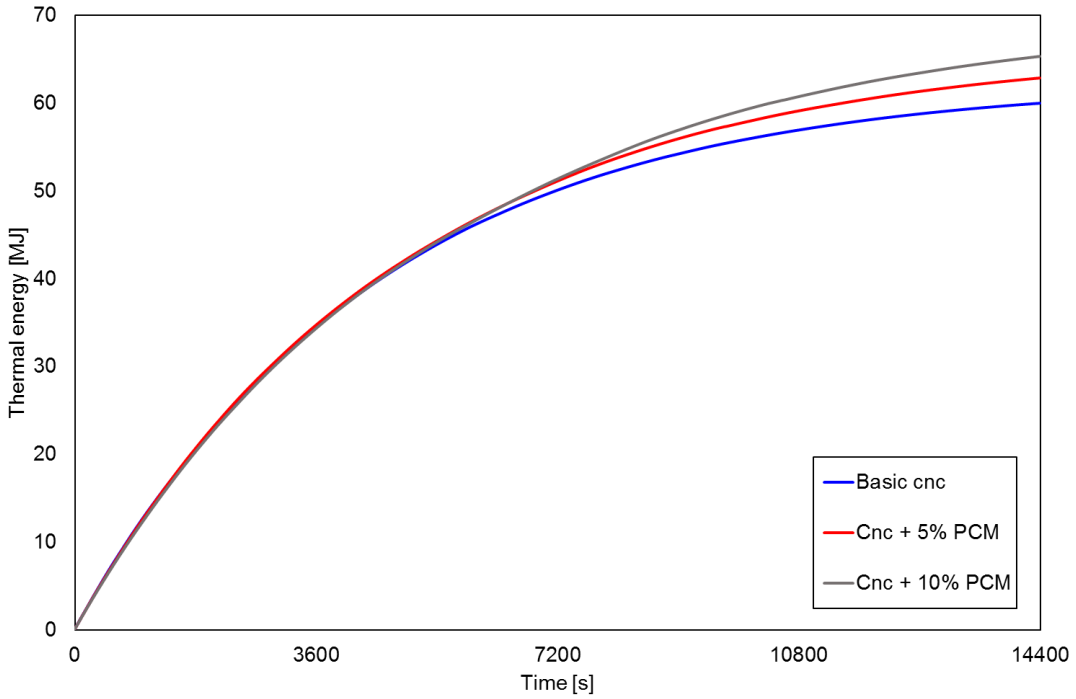

Figure 5.18: Stored energy during the charging stage

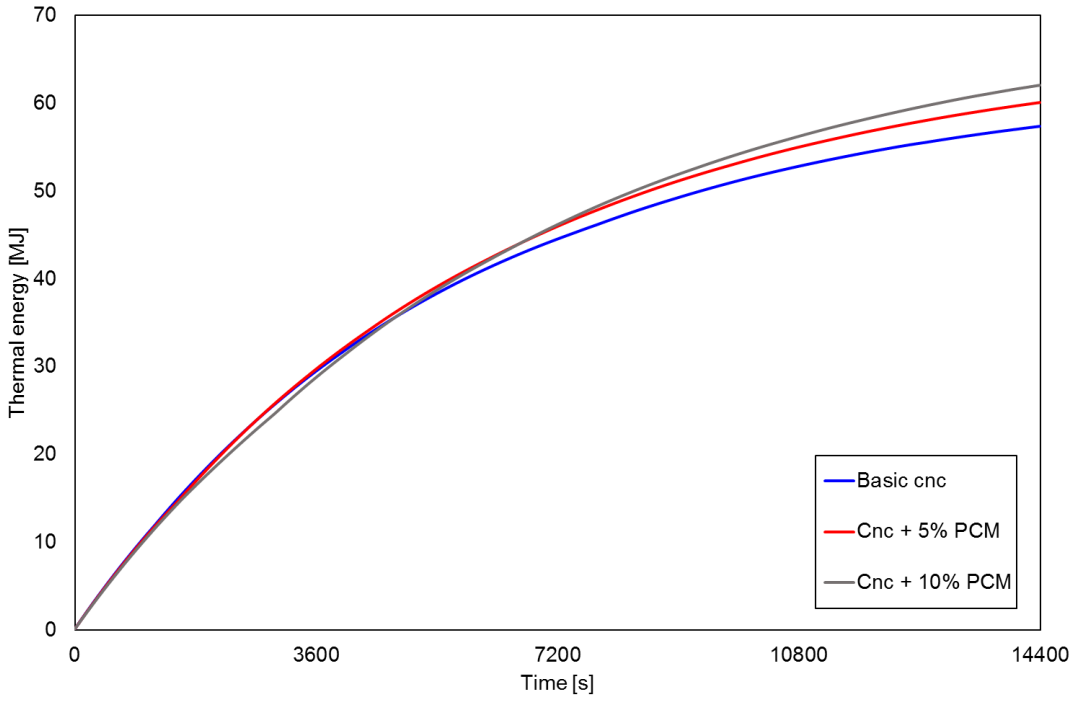

Figure 5.19: Released energy during the discharging stage

integrated PCM is not very high, this also affects the oil outlet temperature. In both cases, in fact, it can be seen that it is not particularly influenced by the presence of PCM in the concrete. This is due to the fact that the PCM does

not directly affect the oil, but the temperature of the concrete, which, in turn, is reflected in the oil outlet temperature. Since the percentage of PCM is low, there is a visible effect on the temperature of the concrete, which integrates the PCM, but the difference between the three temperature profiles is not high enough to make a significant difference that corresponds also to the outlet temperature oil. Note that the oil always enters the block at the same temperature, while the concrete evolves continuously, so a small difference in the concrete does not correspond to a variation in the oil.

As for the exchanged energy, also for the temperature profiles, it is possible to note that in charging the curves relating to the concrete are close to the asymptote, being very close to the oil curves. In discharging, however, the concrete is not yet close enough to the oil temperature to be able to establish an asymptotic profile.

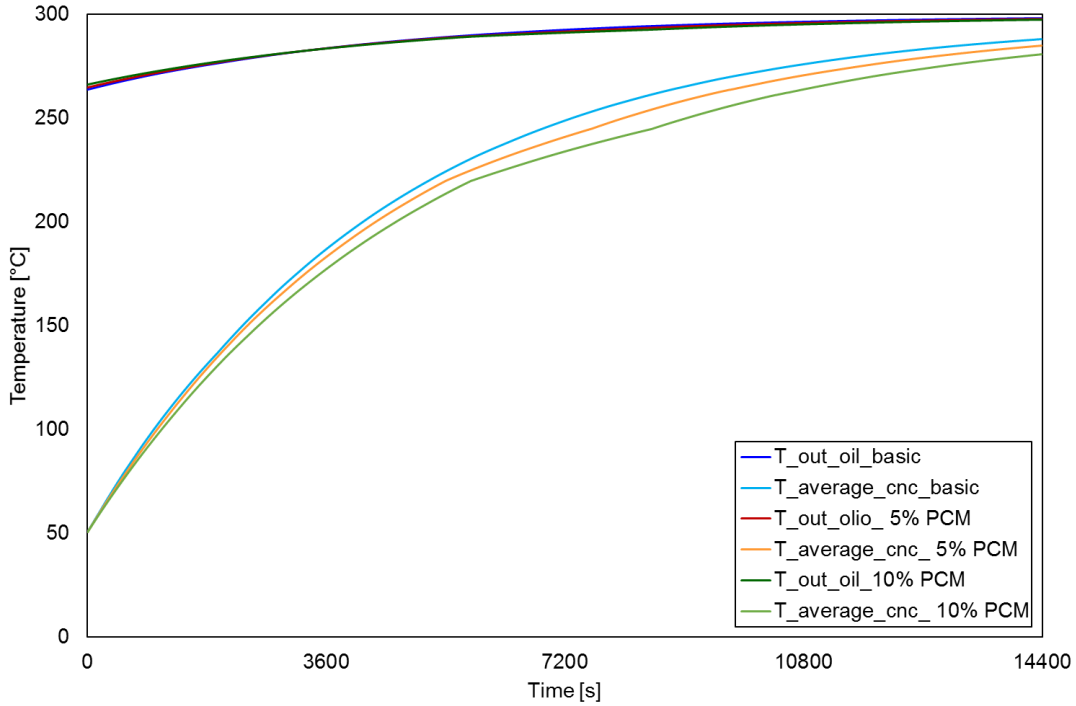

Figure 5.20: Oil outlet temperature and concrete average temperature in charging stage

5.5.3 Thermal efficiency

The theoretical thermal efficiency of the different concrete mixtures, subjected to the same analysis conditions, was also analyzed. The results were shown in Fig. 5.22, in a chart that combines the values of energy exchanged with efficiency. It can be seen that, as the percentage of PCM increases, the efficiency value

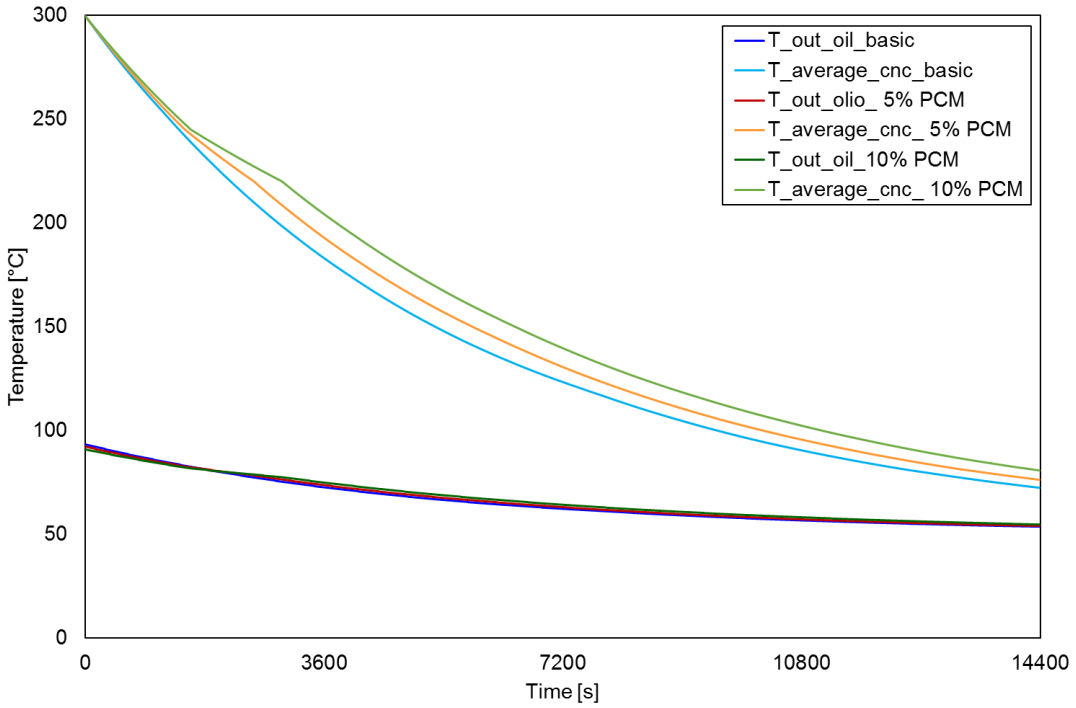

Figure 5.21: Oil outlet temperature and concrete average temperature in discharging stage

decreases. This phenomenon occurs both in heating and in cooling, but in the latter, it is particularly evident.

Thermal efficiency is defined as:

$$\varepsilon = \frac{Q_{tot}}{Q_{max}} \tag{5.18}$$

where Q_{tot} is the total energy really exchanged by the concrete block and PCM, while Q_{max} is the maximum energy that can theoretically be exchanged under ideal conditions (infinite time and mass flow rate, without heat loss to the external environment). The denominator takes into account the presence of PCM and, as its quantity increases in the concrete, the theoretical maximum energy value also increases significantly.

It is therefore correct that the thermal efficiency, for the type of simulation implemented, decreases with the increase in the percentage of the PCM: when the block is at high temperatures, in fact, the part of the exchanged heat flow that is dispersed into the external environment becomes high. Since the overall heat power exchanged is greater with the presence of the PCM, the part relating to the dissipated heat flow is also greater. This phenomenon is particularly evident in cooling for two reasons: the simulation begins with the block at a high tem-

perature, which is never reached in heating so that the flow dissipated towards the environment is greater. With the integration of the PCM, moreover, the temperature profiles have a lower slope, so the blocks are warmer as the percentage added increases, further increasing the dissipation with the outside.

In any case, again in Fig. 5.22, the energy exchanged was also reported. As explained previously, it can be seen that this parameter increases with a higher percentage of PCM and it represents the most interesting quantity on which to focus the attention for an element whose purpose is to accumulate thermal energy. Efficiency, therefore, is another useful parameter to be analyzed in order to have a more complete understanding of the physical phenomenon that is occurring, but it is not the only value on which to pause to verify which solution is more convenient from a more generic point of view and therefore also economic.

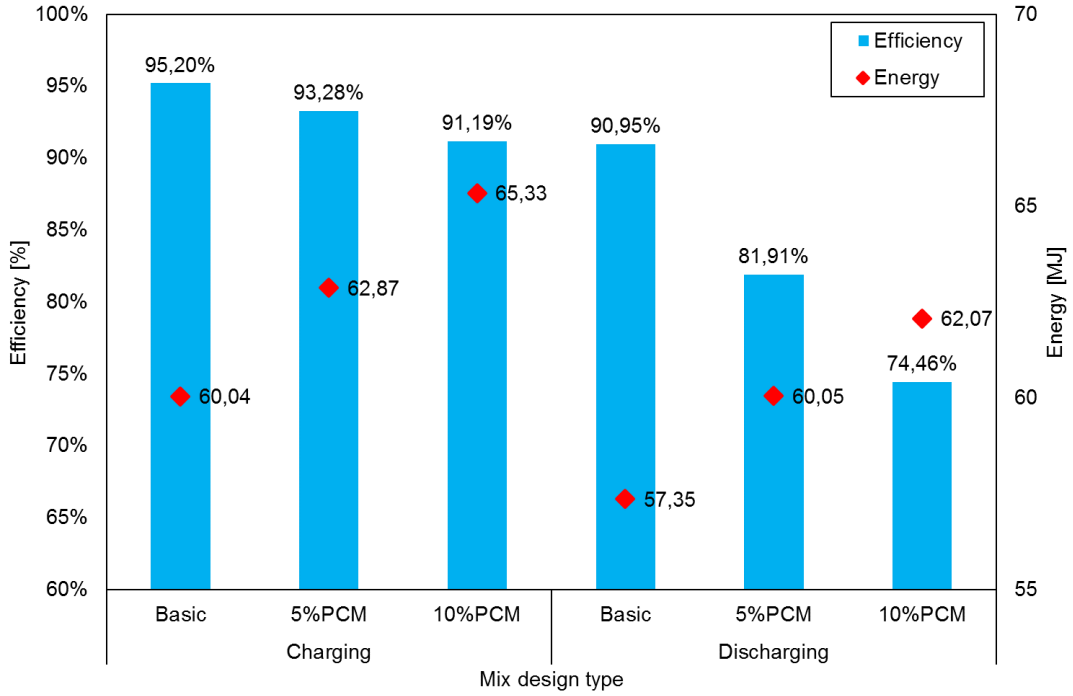

Figure 5.22: Energy and efficiency in charging and discharging stage

5.6 Conclusions

The analyses have shown how the integration of PCM in the concrete mixture can actually improve the thermal performance of the storage elements, both in heating and cooling stages. The temperature curves are less steep, due to the latent heat absorbed or released during the transition phase. The thermal energy accumulated, in heating, and released, in cooling, visibly increased with the per-

centage of integrated PCM. The potential of this technology has therefore been proven and is evident, however with the small amounts of PCM used in this study, it is not possible to fully appreciate the storage capabilities of this material.

The most suitable mixture is not uniquely definable, since several parameters could be considered and that could be prioritized, depending on the situation and the needings. The efficiency and the stored thermal energy, for example, present opposite trends, that could be more relevant in different applications. Nevertheless, also the cost should be considered as one of the main parameters since the integration of PCM also increase the initial cost of the thermal systems, that could be also not worthy over a predefined limit.

More exhaustive investigations are therefore necessary, also analyzing quantities of PCM much higher than those proposed in this stage, in order to verify how much the addition of these innovative materials can actually benefit the concrete storage elements.

6. CFD model of concrete with PCM system

6.1 Introduction

This chapter is focused on combined sensible and latent heat storage. The sensible heat storage system increases the internal energy of the storage media without a phase change and relies on its specific heat capacity and temperature difference. The latent system includes three heating/cooling processes (solid sensible, phase change, and liquid sensible) and it mainly stores energy by exploiting the phase transition of the PCMs. As before, concrete has been chosen as main sensible TES material. Its thermal properties are very important for the current study because the TES system is supposed to be integrated with a CSP plant, where the operating temperatures are normally higher than the ones at which the concrete is normally exposed. Even if the concrete TES systems have already been studied, their application is still a matter of research. In particular, the addition of PCMs in concrete storage systems needs to be further investigated.

Recently, Boquera et al. (2021) also reported that the specific heat capacity of concrete, as well as thermal conductivity, have been a great challenge so far and that the integration of PCM in the concrete mixture is considered of great interest to be further optimized and researched. Regarding this topic, Lucio-Martin et al. (2021) experimentally analyzed the evolution of thermal conductivity up to 600 °C, simulating the operation conditions of a concrete TES system in a CSP plant. The proper selection of the concrete mixture allows indeed for obtaining good resistance and stability at temperature values greater than 400 °C, as reported by Giannuzzi et al. (2017). These properties are very important for the current study because the TES system is supposed to be integrated with a CSP plant, where the operating temperatures are normally higher than the ones at which the concrete is normally exposed. Traditional practices of incorporating PCMs in construction materials include direct incorporation, immersion, semi-direct incorporation, and

microencapsulation, as reported by Berardi and Gallardo (2019).

The papers presented in the literature review chapters regarded many topics, but they did not address the integration of different PCM percentages in a concrete storage module, which is the first aim of this work. They focused on the thermal properties changes that occur while adding the PCM to the concrete matrix, also the stability, the resistance, and the other mechanical properties have been investigated. The HTF has an important role in the storage systems, so there are studies concerning the different types of HTF too. The type of integration of the PCM in the concrete mixture has been analyzed, with the result that the best solution greatly depends on the applications, the geometry, and the temperature range of the specific application. The best PCM for each condition has been studied, with a wide variety of tables that report the pros and cons of the different materials.

The PCM type strongly depends on the designed TES application, as reported by Farid et al. (2004). The main issue is that a PCM that completely fulfills all the requirements does not exist, as reported by Leite da Cunha and Barroso de Aguiar (2020). The selection of supporting materials and encapsulation techniques has a crucial effect on the use of the thermal energy released by PCM, as reported by Huang et al. (2019). As reported in the initil chapter, the PCMs can generally be classified into Organic PCM, Inorganic PCM, and Eutectics PCM, different operating temperature ranges, and melting enthalpies. For high-temperature applications, like in industrial applications, inorganic hydrates salts can be suitable because of their high latent heat storage capacity and good thermal conductivity, as reported by Rathore et al. (2020).

Many Authors developed various kinds of concrete with PCM TES systems, with different applications, both in building and industrial fields. Regarding building applications, Balapour et al. (2021) evaluated the thermal efficiency of microencapsulated PCM incorporated in cementitious composite and quantitatively identified the influential mechanical and chemical damages. Dehmous et al. (2021) developed a concrete TES by adding composite lightweight aggregates, impregnated with a low-cost biobased PCM, to a cement mortar, bentonite, sepiolite, and silica gel were used, together with two methods of impregnation. Parameshwaran et al. (2021) developed a microencapsulated biobased PCM integrated into a micro concrete composite for thermal energy storage in buildings, a sequential operation of mixing the ingredients for preparing the concrete matrix was established. Shen et al. (2021) used clastic light shale ceramsite to absorb paraffin to prepare an aggregate and PCM-concrete thermal storage blocks with different PCM weight percentages, they also presented the effects of PCM weight

percentage and the characteristics of HTF on the performance of an active thermal storage system. Srinivasaraonaik et al. (2021) tested the application of different microencapsulated PCM dosage on the cement paste specimens to elucidate its role in deciphering the thermal comfort, also effective thermo-physical parameters were investigated, and the results obtained revealed significant changes in these properties. Shi et al. (2014) studied a form-stable fiber composite concrete containing dispersed paraffin as PCM. They observed that the effective thermal conductivity of the composite concrete decreased with the increase of porosity of paraffin or basalt fiber and that it was also affected by the finite contact thermal resistance at the interface. Eddhahak-Ouni et al. (2014) investigated a Portland cement concrete modified with organic microencapsulated PCM, using experimental and homogenization approaches. They found out that the heat storage capacity of the PCM-concrete is significantly improved with the addition of the PCM and that the aged PCM-concrete exhibited similar thermal responses compared with the non-aged PCM-concrete; they concluded that this corresponds to a stabilized thermal behaviour of the modified concrete in long term.

Regarding industrial applications, just a few Authors studied the integration of PCM in concrete TES systems and they had very promising results. Suresh and Saini (2020) proposed a combined sensible-latent TES system, by incorporating the PCM spherical capsules above the concrete spheres in the same storage tank, for solar thermal energy applications. They investigated the effect of four different volume fractions of PCM, specifically 20%, 40%, 60%, and 80%, on the performance of the TES system, during charge and discharge cycles and found that the higher volume fractions of PCM have better performances. They also found that charging at higher flow rates provides faster charging and discharge at lower flow rates provides better utilization of energy for a longer duration of time in the case of solar thermal applications. Prieto et al. (2021) proposed a concrete storage tank as a molten salt container for CSP applications. Characterization of the thermal and mechanical was conducted in a pilot plant storage tank in contact with solar salts. The presence of molten salt inside the concrete changed some of the thermal and mechanical properties analyzed, obtaining an increase in the thermal conductivity as well as in the density in the concrete zones closer to the molten salt. They also found out that there is a reduction in the compression resistance in the zone closer to the molten salt crucible and density increases. This behaviour can be explained due to molten salt penetration in those zones. Pomianowski et al. (2014) investigated the specific heat capacity as a function of the temperature of concrete mixed with various amounts of PCM, they also described the experimental set-up to determine the specific heat capac-

ity of the PCM concrete material, and various methods to calculate it. Tanyildizi et al. (2022) proposed a deep learning approach to estimate the compressive strength of PCM-integrated cementitious composites based on its mixture proportions and the thermophysical properties of PCM. Extreme learning machines, autoencoders, hybrid models, and extreme gradient boosting models were developed using a large experimental dataset available from the open literature, with good results. Essid et al. (2020) developed a numerical simulation, using software ANSYS Fluent, based on experimental tests, to evaluate the energy efficiency of PCM concrete wallboards under different thermal scenarios. They used a solidification-melting model based on the enthalpy method, to solve the heat transfer problems during the solidification and melting processes. Dehdezi et al. (2013) studied the thermal, mechanical, and microstructural aspects of concrete containing different amounts of microencapsulated PCM, with also a numerical simulation, with a 1D finite-difference transient heat transport model. Yun et al. (2019) performed a thermal analysis using Finite Element Software MIDAS/GEN to evaluate the effect of applying PCM on the temperature and thermal stress of mass concrete to control the process of heat hydration.

The previous papers regarded many topics, but they did not address the integration of different PCM percentages in a concrete storage module, which is the first aim of this work. They focused on the thermal properties changes that occur while adding the PCM to the concrete matrix, also the stability, the resistance, and the other mechanical properties have been investigated. The heat transfer fluid has an important role in the storage systems, so there are studies concerning the different types of HTF too. The type of integration of the PCM in the concrete mixture has been analyzed, with the result that the best solution greatly depends on the applications, the geometry, and the temperature range of the specific application. The best PCM for each condition has been studied, with a wide variety of tables that report the pros and cons of the different materials. The impact that the different PCM percentages could have in the concrete storage systems has been introduced by some Researchers, but in a preliminary way and without focusing on the real feasibility and the performances of an operative TES system. For this reason, we developed the following analyses.

As reported, previous works showed very interesting results, but there is a need for deeper investigations of combined concrete with PCM TES systems for industrial applications. In the literature review, the Authors did not find any paper focused on the simulation of concrete with the integration of low and high percentages of PCM, for industrial applications, such as for CSP plants. The previous studies did not explore deep enough the impact of the integration of low

and high PCM percentages in a concrete storage module, hence there is the need for a study that sufficiently investigates these issues. For this reason, a new study was needed with the specific scope to investigate these applications. This work aims to fill this gap, to have a better comprehension of the thermal behaviour of concrete storage modules, integrated with PCM. Hence, different concrete mixtures were considered, with and without PCM addition, under the same operating conditions, to evaluate their performance. The numerical simulations were based on a previous experimental campaign, conducted by the Italian National Agency for New Technologies, Energy and Sustainable Economic Development (ENEA). A binary mixture of hydrated salts was used as PCMs, composed of 40% of KNO_3 and 60% of $NaNO_3$, and they were absorbed by diatomite. This PCM was used during the experimental tests that were run before the numerical simulations. This binary mixture was chosen because it has been proved to be suitable to improve the storage performances of TES systems for industrial applications, because it is stable, and the phase transition occurs between the temperature range used for CSP plants. Diatomite is a sedimentary rock, with a highly porous microstructure, that originated from the siliceous fossilized skeletons of diatoms, and it has been used to incorporate PCM in various studies , like Xu et al. (2013), Jeong et al. (2013), Wen et al. (2018), Rao et al. (2018), Cunha Costa et al. (2020), Li et al. (2020), and Yu et al. (2020). The experimental tests studied pure concrete and a mixture with a 5% weight of PCM, as reported by Miliozzi et al. (2019), with the calibrated numerical model, other analyses were developed, and other two concrete mixtures, with 20% and 40% in weight of PCM, were studied, since the 5% percentage used in the experimental test is a too low value to appreciate, evaluate and fully understand the potential and thermal behaviour of the combined system of concrete and PCM.

6.2 Experimental database

The numerical model was based on experimental tests, that investigated the effects of the concrete composition by testing two different mixtures, with and without PCM addition. For the sake of clarity, in what follows, a brief description of the concrete prototypes and the experimental procedure is given; full details can be found in Giannuzzi et al. (2017).

In Fig. 6.1 a schematic representation of the TES system is reported while in Fig. 6.2 the physical model in ANSYS Fluent environment is represented. The sample consists of an insulated cylindrical concrete element (represented in Fig.

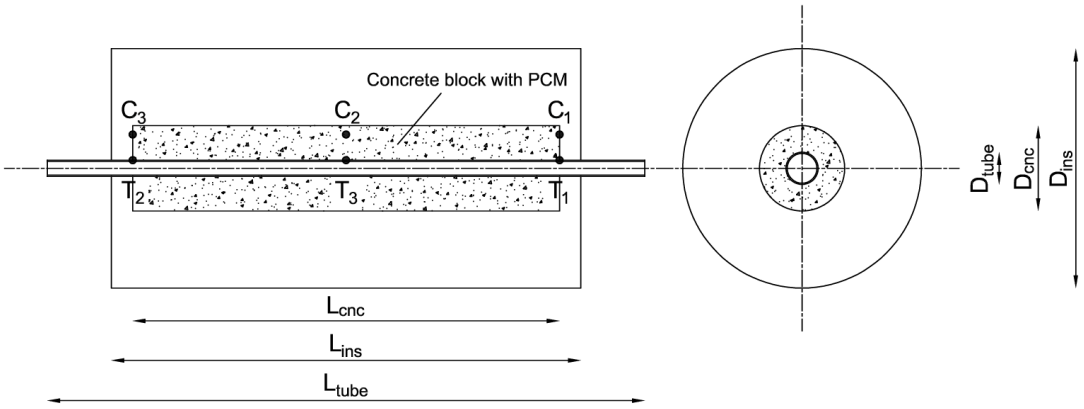

Figure 6.1: Lateral and frontal section of the experimental system

Figure 6.2: Physical model in ANSYS Fluent environment

6.3), 0.5 m long and with an external diameter of 0.1 m. The concrete block with the direct integration of PCM is reported as filled in the figure. A stainless steel pipe, 0.7 m long, passes through the centre of it and is used to heat up and cool down the TES system. Then, the whole concrete part is insulated by a 0.09 m thick Rockwool (represented in Fig. 6.4).

Before the heating tests, a degassing process was conducted, to reduce the concrete interstitial water and the related cracking risks. However, not negligible water content was still present, and it was adequately considered in the model implementation.

The temperature of the system is recorded by thermocouples, which are lo-

Figure 6.3: Cylindric concrete samples

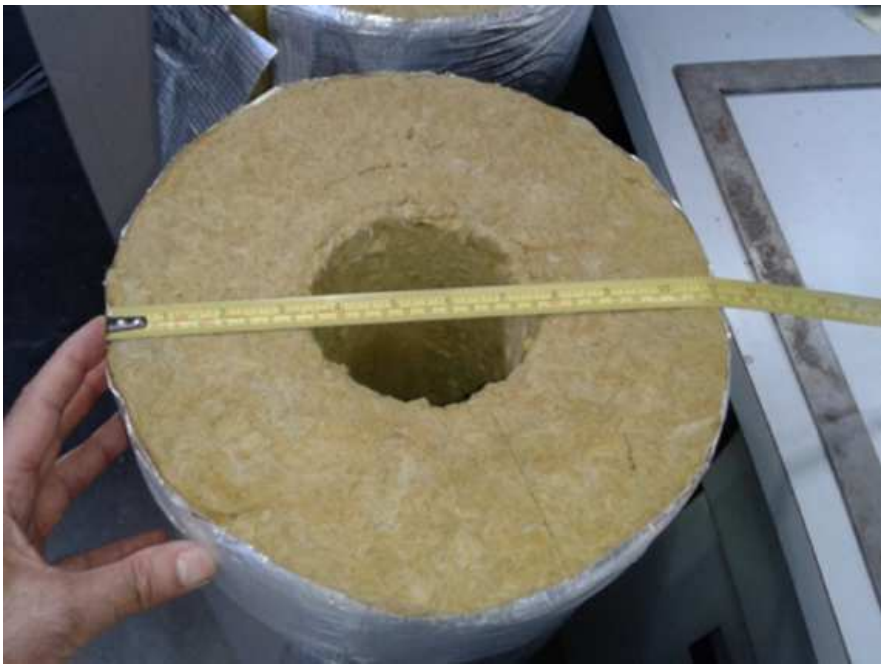

Figure 6.4: Insulating for the cylindric samples

Table 6.1: TES geometrical dimensions

TES dimensions	**Value**	**Unit of measurement**
TES length	0.50	[m]
Insulating length	0.55	[m]
Tube length	0.70	[m]
TES external diameter	0.10	[m]
Insulating external diameter	0.28	[m]
Tube external diameter	0.01905	[m]
Tube thickness	0.00165	[m]

cated at the beginning, in the middle, and at the end of the concrete block and the pipe. The tube thermocouples (T) are situated in the contact region between concrete and stainless steel. The concrete thermocouples (C) have the same axial position as the tube ones, but with a radius value of 0.03 m, so they are located inside the concrete thickness. The thermocouples scheme is also reported in Fig. 6.1. The main geometrical characteristics of the system are listed in Tab. 6.1, while the properties of the materials are reported in Tab. 6.2.

The integrated PCM, also known as "solar salts", is composed of 40% of KNO_3 and 60% of $NaNO_3$ and it was absorbed by diatomite. As reported before, diatomite is a sedimentary rock, which originated from the siliceous fossilized skeletons of diatoms. It is indicated to adsorb the PCM because of its highly porous microstructure. The PCM was added to the second concrete mixture as a 5% weight, and its thermal properties are reported in Tab. 6.3.

The concrete module is charged by Joule's effect through the stainless steel pipe. The tube was subjected to an elevated current at low tension, so the tube was kept at an almost constant temperature during the charging stage, which lasted around two hours. The heating system was based on the value recorded by the pipe's central thermocouples, set at 400 °C, so the tube did not have a uniform constant temperature along its axis. More details are reported in the following section, which also describes the procedures to reproduce those experimental conditions. The system was then cooled down for 7 minutes by insufflating compressed air through the stainless steel pipe. The velocity and temperature of the inlet air were controlled and recorded by the measuring devices. The numerical simulations were based on the tube thermocouples data and the results were compared with the concrete thermocouples' measurements.

These experimental tests were performed, as in the previous chapters, by the

Table 6.2: TES thermophysical properties

TES properties	**Value**	**Unit of measurement**
Concrete density	2398	[kg/m^3]
Concrete specific heat capacity	607	[J/(kgK)]
Concrete thermal conductivity	1.77	[W/(mK)]
Stainless steel density	8000	[kg/m^3]
Stainless steel specific heat capacity	500	[J/(kgK)]
Stainless steel thermal conductivity	17	[W/(mK)]
Rockwool density	150	[kg/m^3]
Rockwool specific heat capacity	1030	[J/(kgK)]
Rockwool l thermal conductivity	0.05	[W/(mK)]

Table 6.3: PCM "solar salts" properties

PCM properties	**Value**	**Unit of measurement**
Density	2290	[kg/m^3]
Specific heat capacity	820	[J/(kgK)]
Thermal conductivity	0.7	[W/(mK)]
Latent heat	110	[kJ/kg]
Initial melting temperature	493	[K]
Final melting temperature	517	[K]

ENEA Researchers, who had particular necessities that brought to setting up conditions that would not be feasible in a real and practical operation. For sure, in a real plant, the heating and cooling stages would have not been realized with Joule's effect for two hours, and then cooled down with compressed air for just 7 minutes. A situation like this could be useful in a preliminary research stage, but would not be representative of practical use. In a real scenario, a unique fluid would have been used for both the heating and cooling stage, like mineral oil, not fluid with low density and specific heat capacity like the air.

The experimental tests were however useful to validate and calibrate the numerical model, but then the simulations were based on different operating conditions with progressive improvements, in order to get results closer to a real operative system.

6.3 Numerical model validation

The numerical simulations were carried out with the ANSYS Fluent software. In order to reduce the computational load, a quarter of all concentric cylinders were modeled. The ambient temperature, equal to 300 K, was set as the initial temperature of the whole system. As external boundary conditions, the natural convection was imposed on all the faces that exchange heat with the surrounding ambient, except for the symmetry faces, which were set as adiabatic surfaces. An overall coefficient equal to 30 W/m^2K was set, to take into account also the radiative effects that occurred during the experiments, as done in the previous chapters. The CFD simulations are based on the $k - \varepsilon$ model and energy equations.

In order to validate the numerical model, the TES was charged by applying a temperature profile to the stainless steel pipe, according to the experimental tests. The wall T-type thermocouples recorded constant temperature values over time, but this changed along the tube axis. The central thermocouple (T3) kept the fixed value of 673 K (400 °C) and was used to control the heating system, but the lateral ones reached lower values, on average around 558 K, due to the external heat loss. To reproduce this heating thermal load, a parabolic temperature profile was imposed along the tube, to follow the thermocouples values, with the expression:

$$T = -1840 \cdot z^2 + 673 \tag{6.1}$$

with z as the axial coordinate, expressed in [m], which originated in the centre of the system. The data recorded by the three thermocouples during the experimental test were interpolated, using a parabolic curve, to have the best fit to the real measurements. The result is reported in Eq. 6.1 and it was imposed to the numerical model, as a user-defined function, to the metal tube that heats the concrete block. The thermal load was kept constant through time, as the experimental tests. In Fig. 6.5 the temperature recorded by the T3, C1, and C2 thermocouples are reported, with also an average concrete temperature.

The time step was set equal to 10 s, with a total flow time equal to 7200 s (2 hours) of the charging process and 420 s (7 minutes) of the cooling stage. These durations were selected according to the ones used during the experimental tests.

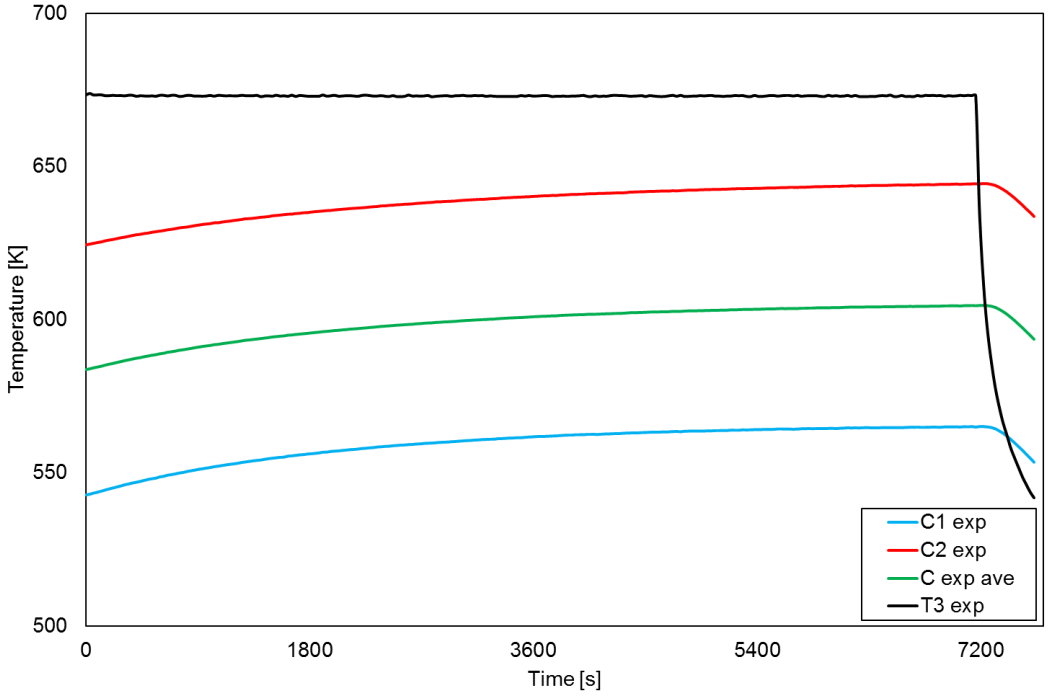

Figure 6.5: Temperature recorded by T3, C1, and C2 thermocouples. The average concrete temperature is also reported

6.3.1 PCM integration

The PCM was directly integrated into the concrete mixture, so a new homogeneous material, composed of concrete with a defined PCM percentage, was obtained. For this reason, it was not possible to divide the PCM domain from the concrete one. Hence, the PCM added concrete was modeled as a unique body with the same properties for the whole domain.

Anyhow, each thermal property was modified, according to the PCM percentage, to take into account the change made to the mixture. Each thermal property was weighted using the PCM percentage. The following expression was used:

$$c_p = (1 - f) \cdot c_{cnc} + f \cdot c_{PCM} \tag{6.2}$$

where c_p is the mean specific heat capacity and f is the PCM percentage in weight. The same model was used also for the density and thermal conductivity. Particular attention should be paid to the specific heat capacity of the PCM, which was considered as reported by Lamberg et al. (2004):

$$c_{PCM} = \begin{cases} c_{PCM}, & T < T_{im} \\ c_{PCM} + \frac{r}{T_{fm} - T_{im}}, & T_{im} \leq T \leq T_{fm} \\ c_{PCM}, & T > T_{fm} \end{cases} \tag{6.3}$$

where r is the latent heat of fusion, T is the current cell temperature, T_{im} is the initial melting temperature, and T_{fm} is the final melting temperature.

In this way, a specific heat peak occurs during the phase change, both during the heating and cooling stages.

The average specific heat capacity is also reported, during both the charging and discharging phases as a function of the PCM concentration. The charts are reported in Figs. 6.6 and 6.7, respectively. The peaks occur in the same temperature range because the PCM melts at the same temperature, but the values are very different. Three different PCM percentages are reported: 5%, 20%, and 40%, which are the ones that have been used in the simulations of the current study. The more the PCM content, the higher the peak.

Anyway, it is clear, both in the charging and discharging phase, that the ascending part of the curve is less steep than the second one, which occurs after the peak. This behaviour is typical of any PCM when it is brought to melt, during the charging stage, or to solidify, during the discharging stage.

6.3.2 Interstitial water integration

The presence of interstitial water in the concrete matrix was also considered because the degassing preliminary process did not eliminate all the water present inside the concrete matrix. Its consideration was important because a heat fraction was adsorbed by vaporizing water. A mass flow rate of 0.1175 kg/h, according to the previous simulations, was supposed to evaporate and so adsorb an energy density of about 21500 W/m^3, the latent heat of vaporization was considered equal to 2.5 MJ/kg.

6.3.3 Results of the validation

As marked points, C1 and C2 thermocouples of the experimental tests were considered and the same locations were identified in the numerical model, to compare the temperature. To simplify the analyses, the C1 thermocouple was set as a reference point also for the values of its symmetric position on the other end of the concrete block. The computed numerical values were the same for the two

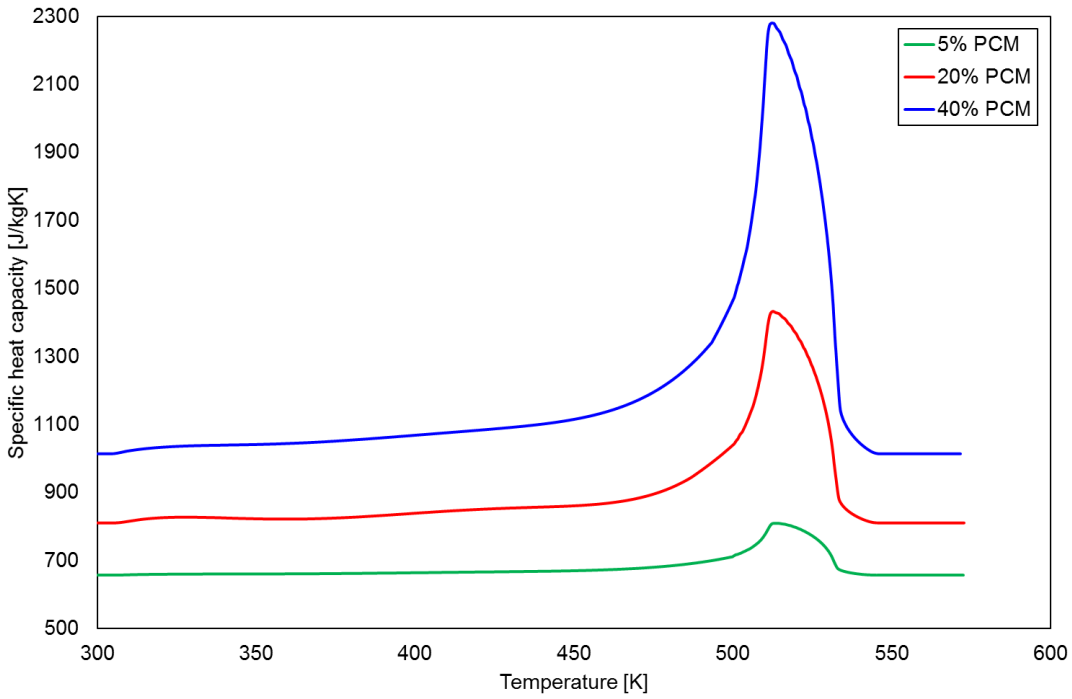

Figure 6.6: Average specific heat of the mixtures during the charging stage

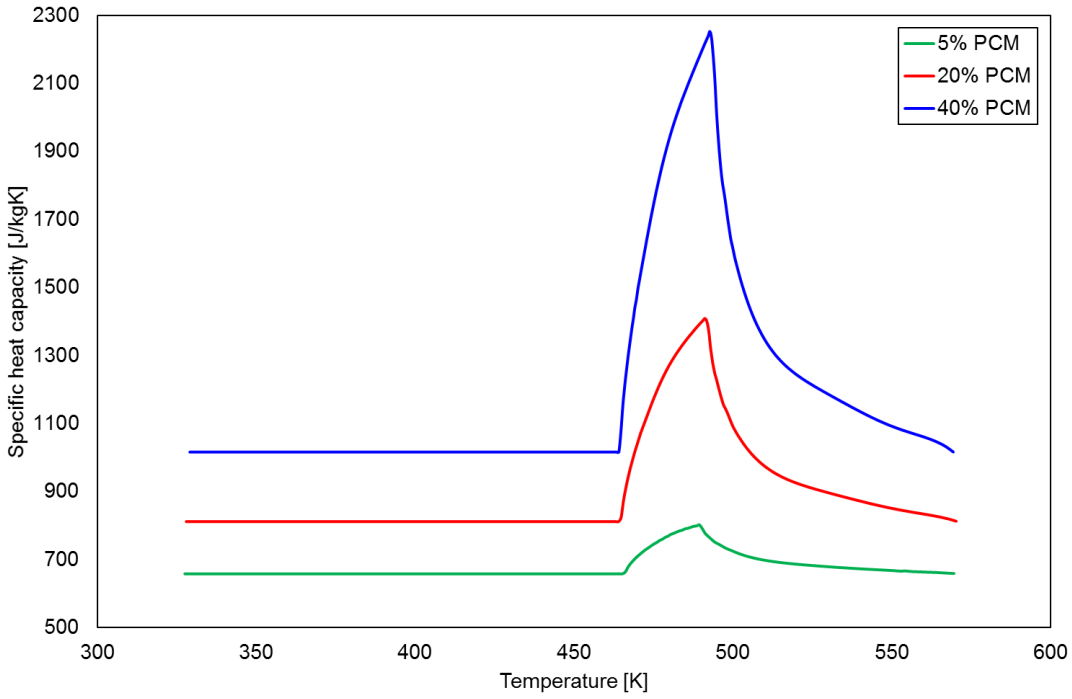

Figure 6.7: Average specific heat of the mixtures during the discharging stage

sides of the concrete block, because of the parabolic imposed temperature profile, and they perfectly coincided with the ones reported to the C1 thermocouple. The C2 thermocouples, which is the central one, is set to a higher temperature than the C1 lateral one, even in this case because of the parabolic temperature profile of the heating tube.

The initial temperature of the whole system was set at 300 K in the numerical simulation. The comparison with the experimental tests, however, is considered to start when the temperature of the points located in C1 and C2 coincided with the experimental ones. This is since the pre-heating process brought the TES to a higher and non-homogeneous temperature along the axis. Hence, it was not possible to initialize the numerical simulation with the exact conditions of the tests and an initial stage of two hours was needed to set the TES to the comparison temperature. After that, the other two hours were simulated, and the results are reported in Fig. 6.8 for the basic concrete and Fig. 6.9 for concrete with 5% of PCM.

The comparison between the experimental data and the numerical simulation showed a very good agreement with a maximum deviation of 7 K and an average deviation of 1.78 K.

These results confirmed the suitability of the developed tool in simulating the performance of this latent and sensible concrete TES. Thus, additional scenarios were simulated. The first one considered the integration of 20% and 40% PCM in weight in the concrete matrix. The same points C1 and C2 were used to compare the different temperature trends and the results are reported in Fig. 6.10.

The concrete block was set at 300 K at the beginning of the simulation and the parabolic temperature profile was imposed along the tube, for two hours, for basic concrete, and concrete with 5%, 20%, and 40% in weight of PCM. The different percentages showed very interesting results, so they were deeper investigated, also considering a comprehensive discharging stage.

However, considering the PCM percentage, 5% is too little to have a significant deviation from the pure concrete curve because they are mainly overlapped. Hence, other simulations were implemented considering higher PCM percentages. In any case, the introduction of the PCM significantly changes the thermal properties of the concrete block. In particular, the density and the specific heat capacity modify the overall thermal capacity of the storage system.

For this reason, the final asymptotic temperature is slightly higher than the one of the pure concrete mixture, as can be seen in Fig. 6.10.

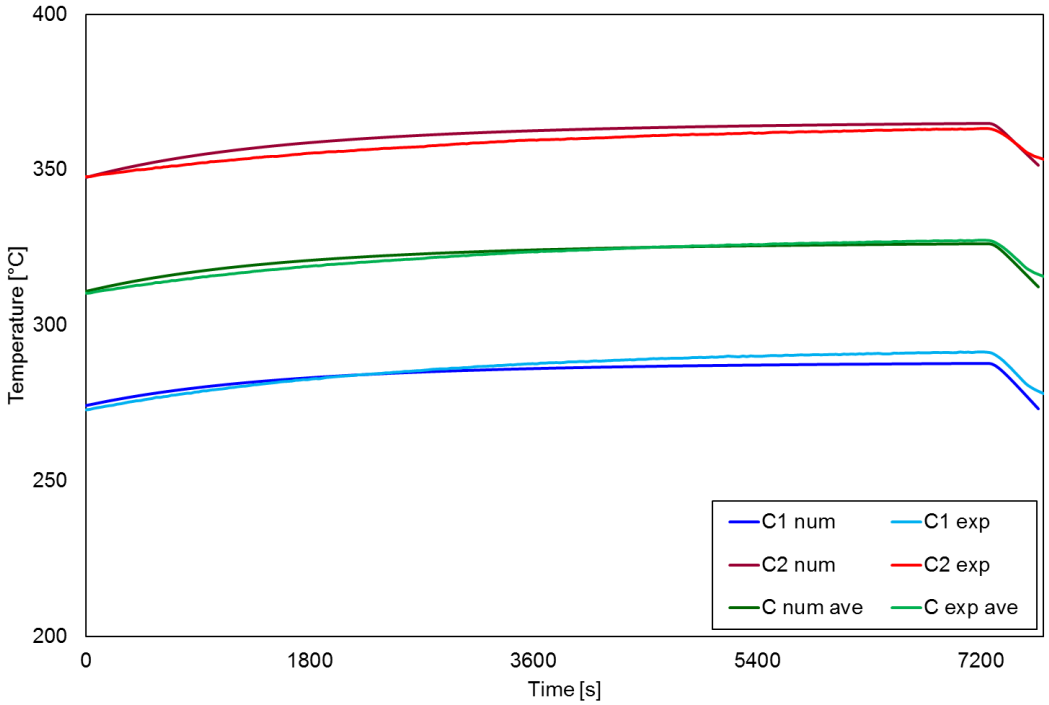

Figure 6.8: Comparison between experimental and numerical temperatures recorded by the thermocouples in pure concrete

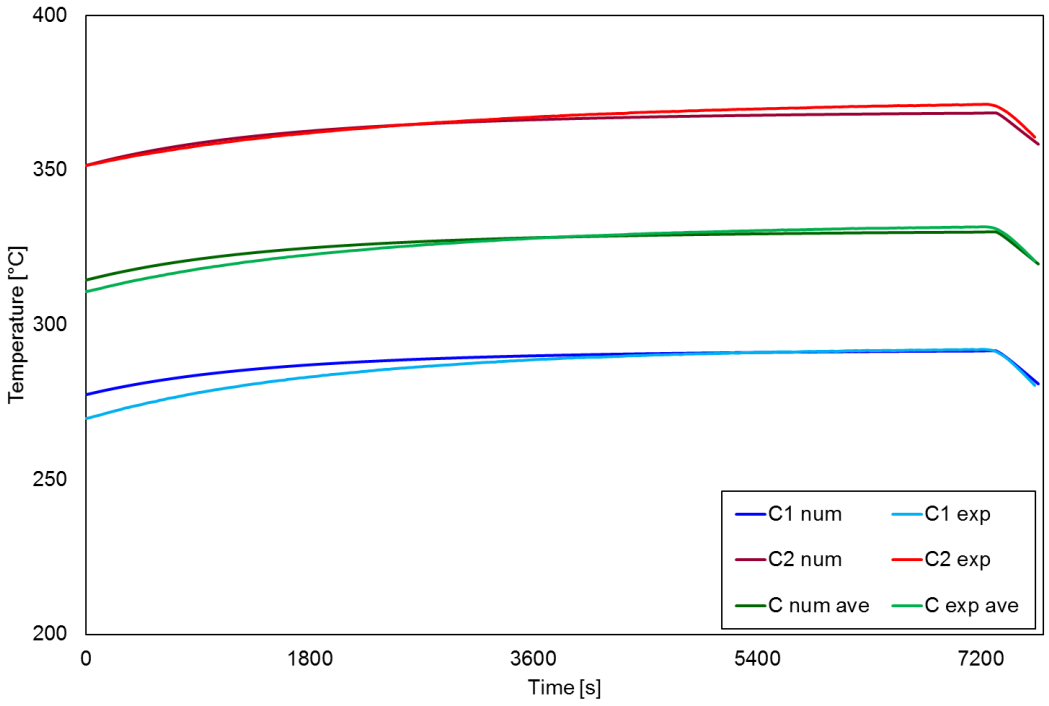

Figure 6.9: Comparison between experimental and numerical temperatures recorded by the thermocouples in concrete with 5% PCM

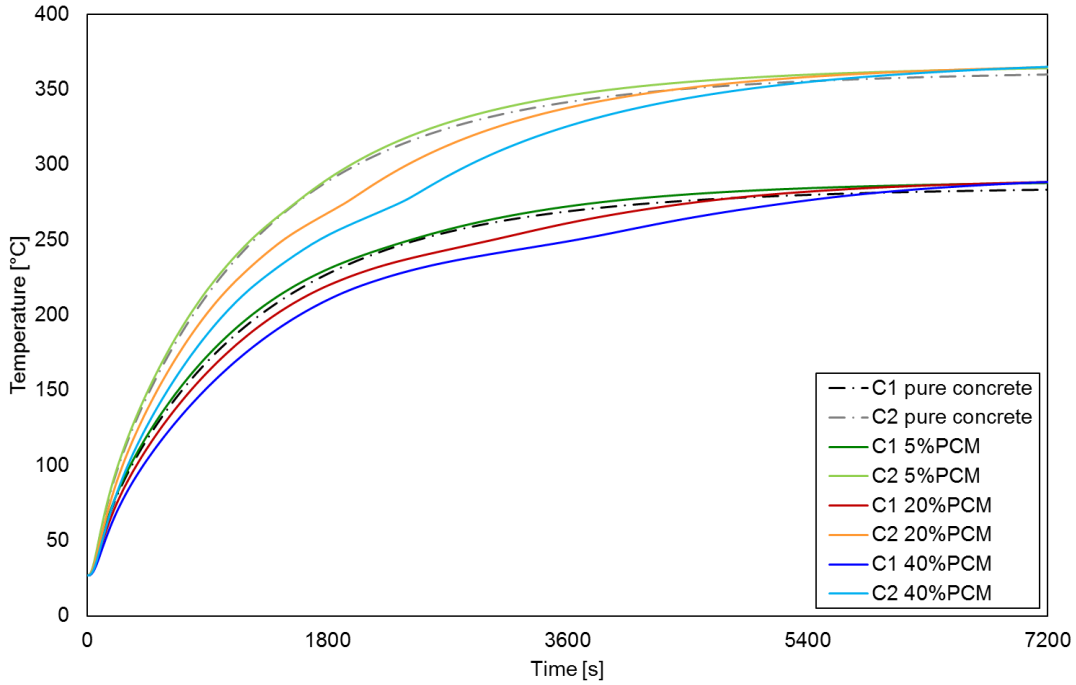

Figure 6.10: Temperature trends with different PCM amount

6.4 Effect of the PCM percentage in the concrete matrix

6.4.1 Background and mechanical properties considerations

As noted, 5% is too little to appreciate the effect of the PCM integration; for this reason, other two higher percentages were chosen to conduct the following simulations: 20% and 40%. In this way, the effects of the PCM become clearer. The curves are less steep and with some evident discontinuity points, due to the specific heat capacity definition, corresponding to the beginning and the end of the melting process in heating and the relative ones during the cooling stage, when the PCM solidifies. After that, the curves tend to the same asymptotic value.

A less steep temperature curve can reduce the risk of damaging and cracking the concrete matrix, so it represents a very interesting advantage regarding the durability of the system, stated also by Fabiani et al. (2018), and Cabeza et al. (2020). Conversely, the presence of a high percentage of PCM can reduce the compressive strength of the concrete element, as reported by Eddhahak-Ouni et al. (2014), and Cabeza et al. (2020), which is one of its most important mechanical properties. In general, a PCM content higher than 3% may be responsible for

more than 50% reduction in the original strength capability (i.e. compression and bending strength) that should properly be considered when designing structural elements (Cabeza et al. (2007), Hunger et al. (2009), Cabeza et al. (2020)). D'Alessandro et al. (2018) also reported that concretes with microencapsulated PCM exhibit a reduction in average compressive strength equal to 1.6, 33.6, and 43.1% using 1%, 3%, and 5% weight contents of fillers, respectively, while with 1, 3 and 5% microencapsulated PCM show average strength reductions of 3.5%, 17.4%, and 33.6%, respectively. Another important aspect to be considered for encapsulated PCM is the possibility of having cracks that originate from the weak points along with the contacts between the capsules and the concrete matrix. This case was investigated by D'Alessandro et al. (2018). The same phenomenon was numerically investigated, at a detailed FEM mesoscale in a non-linear regime, by Mazzucco et al. (2017), and Mazzucco et al. (2018) and the damage in the concrete matrix, related to the capsules presence, was reported.

Other colleagues, specialized in solid mechanics, have focused their research on this specific topic, as reported by Giannuzzi et al. (2017), Mazzucco et al. (2017), and Mazzucco et al. (2018). The present study is part of a bigger work, which involves researchers from different scientific areas. Regarding this paper, the aim was related to the thermal and energetic behaviour of the storage module, with various amount of PCM percentages. The structural limits need to be adequately taken into account, especially if the concrete element is meant for building applications. When the concrete elements have structural purposes, its compressive strength, which is one of its main mechanical properties, needs to be adequately designed. For this reason, the PCM content should be limited to 3% or 5%, when directly integrated into the concrete matrix. Another good option for building applications, should be the integration of the PCM in the wall as its dedicated layer, to not come into direct contact with the concrete matrix.

When the storage module has industrial application as heat storage systems, conversely, the mechanical properties are not as fundamental as in buildings. Then, the attention can be focused on the thermal performance, rather than the structural ones, and the PCM content can be higher, to better exploit the properties of the latent heat. In this specific case, the concrete module has only to support its dead load, as a structural function, without any additional stresses. Hence, a high PCM percentage would not be a limiting constriction and permits to better understand the potential of this thermal storage system.

6.4.2 Different PCM percentages

The calibrated model was then used to study the influence of the PCM percentage in the concrete matrix, with new numerical investigations. As reported, the other two PCM percentages, 20%, and 40%, were introduced and studied, to better appreciate the impact of their integration to the concrete block. All the simulations started with the concrete set at 300 K and lasted five hours, with two hours of heating stage and three hours of cooling. The charging stage is obtained by considering, even in this case, the Joule's effect, as in the experimental tests. The unique difference was the temperature profile that was applied to the stainless steel tube. The parabolic profile was useful to calibrate the model against the experimental tests, but a constant temperature along the axis was more indicated to investigate the effects of the PCM percentages considering a periodic module.

A constant temperature of 603 K was applied to the stainless steel pipe for the two hours of the heating stage. This temperature value was used to be comparable with the subsequent simulations, where the thermal oil is used as HTF, which has a maximum operative temperature. As before, for the cooling stage, compressed air was insufflated inside the pipe, with a velocity of 5 m/s at the ambient temperature of 300 K. This stage lasted three hours, to allow the complete solidification of the different PCM contents. In Fig. 6.11 the temperature profiles are reported. It can be seen that the cooling stage does not reach asymptotic values, even after three hours. In particular, the matrix with 40% PCM keeps its value very high, so it seems difficult to release the initially stored thermal energy. Hence, the stored energy should also be considered to fairly estimate the performance of the TES, as a function of the PCM amount, and the results are reported in Fig. 6.12.

The exchanged energy is calculated by considering the average specific heat capacity, which considers the PCM integration, and the difference between two consecutive mean temperatures of the concrete block, at each time step. For the generic n time step, hence, the following equation is used:

$$Q_n = m \cdot c_p \cdot (T_n - T_{n-1}) \tag{6.4}$$

Then, the total thermal energy is calculated as the sum of each contribution, as follows:

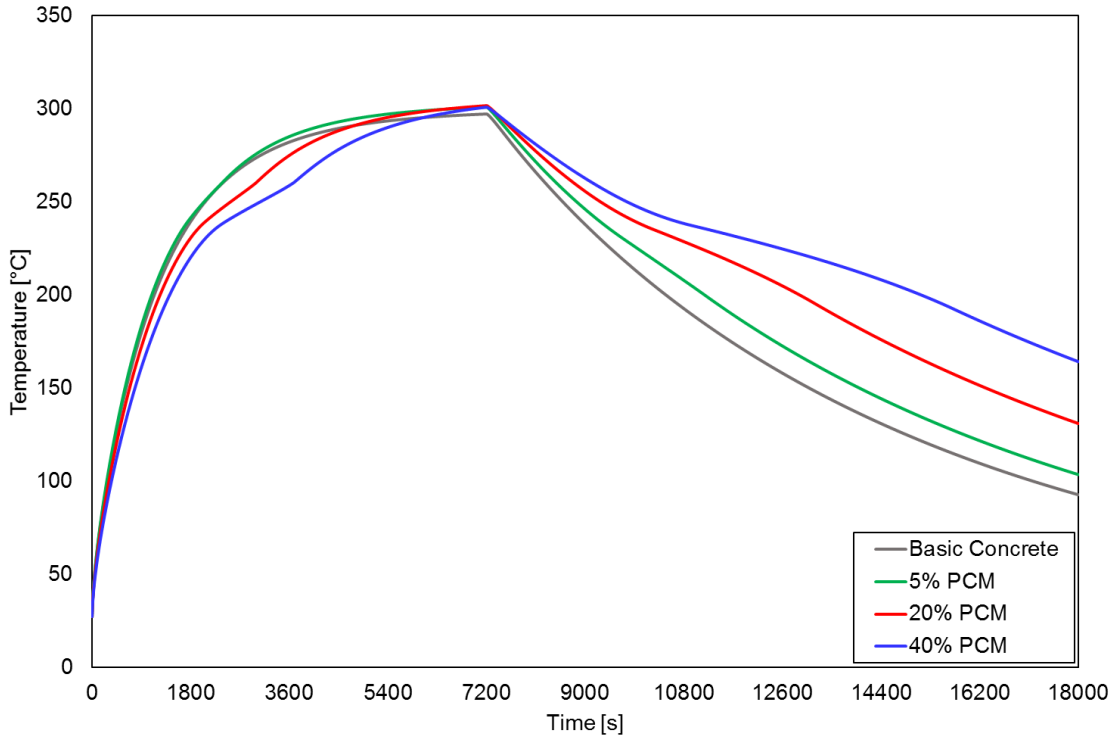

Figure 6.11: Temperature trends for heating with Joule's effect and cooling with compressed air

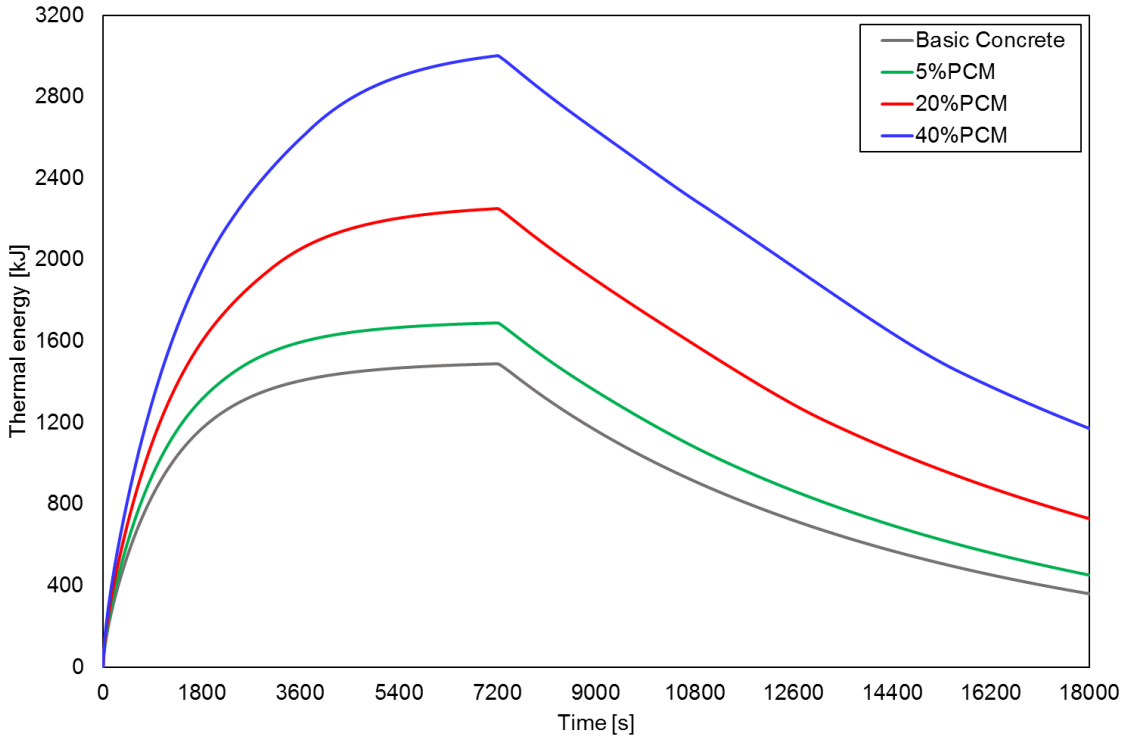

Figure 6.12: Energy trends for heating with Joule's effect and cooling with compressed air

$$Q_{tot} = \sum_{i=1}^{N} Q_i \tag{6.5}$$

The pure concrete curve reaches an asymptotic value of about 1490 kJ during the heating stage, which represents the reference for the comparisons with the PCM matrixes. When the PCM is added, the curves deviate from the reference case and the deviations can be attributed to the latent heat storage processes; the 5% one reaches thermal energy storage of 1690 kJ, the 20% one of 2250 kJ and the 40% one approached 3000 kJ, which is more than two times higher than the pure concrete one.

Regarding the cooling stage, considering 10800 s (3 hours), the pure concrete matrix can release around 1130 kJ of the 1490 kJ stored during the heating stage, the 5% one releases 1240 kJ, the 20% one releases 1520 kJ, and the 40% one releases 1830 kJ.

However, it is important to note that this cooling system is not the most adequate to adsorb the stored energy in a real scenario because it seems too slow, meaning that the heat transfer method is not efficient. Hence, this cooling mode is not the most representative of the potential of the system and it would not be useful to explore further its details.

With air as the cooling fluid, the system could have reached a steady-state, but it would have taken several hours, which is not compatible with an operating system. For this reason, another set of numerical simulations was conducted, with more conclusive results to allow for a deeper understanding of the TES system and its real working potential, by using a different fluid.

These analyses were helpful to identify the potentiality of the PCM integration because the amount of increased thermal energy was quantified, and also to set the basis to improve the system, to have a more efficient apparatus, by changing the HTF.

6.5 Simulation of a real case study

In a real scenario, the TES system would not be heated by Joule's effect and cooled by compressed air. Usually, in an operative system of a CSP plant, a heat transfer fluid is used both to charge and discharge the TES system. One of the most common HTF for CSP plants is thermal oil. In this case, Paratherm™ NF mineral oil was chosen as HTF, as already implemented in the previous chapters.

Table 6.4: Paratherm NF oil properties (temperatures in °C)

TES properties	**Best-fitting equations/Values**	**Unit of measurement**
Density	$\varrho = -0.651 \cdot t + 895.6$	[kg/m^3]
Specific heat capacity	$c = 5.284 \cdot t + 1720$	[J/(kgK)]
Thermal conductivity	$\lambda = -8 \cdot 10^{-5} \cdot t + 0.110$	[W/(mK)]
Dynamic viscosity	$\mu = (53238 \cdot t^{-2.138})/1000$	[kg/(ms)]
Max. film temperature	343	[°C]
Max. operating temperature	332	[°C]
Min. operating temperature	36	[°C]

The main thermo-physical properties of the heat transfer oil are listed in Tab. 6.4. As reported in that table, the maximum operating temperature is 605 K (332 °C).

For this reason, the thermal oil was supposed to not be heated over 603 K in the charging stage. This is the same temperature imposed as Joule's effect in the previous simulations, to have comparable conditions even with the selected HTF. The initial temperature was also set to 300 K, as the ambient temperature, like in the previous simulations. During the cooling stage, instead, a reasonable temperature of 328 K was set. The declared minimum operative temperature is 309 K (36 °C), but the dynamic viscosity at this temperature would be excessively high.

Similarly, to the validation case, the charging and discharging cycle lasted in 5 hours: two hours for the heating phase and three hours for the cooling one, respectively. The HTF inside velocity was at 3 m/s during both phases. This value is chosen to compare the results of the charging phase with the ones obtained with the Joule's effect, in terms of temperature and stored energy. Then, the same velocity is used during the cooling phase. This velocity corresponds to a mean mass flow rate of 0.40 kg/s during the charging phase and 0.50 kg/s during the discharging one. These mass flow rate values are higher than the common ones, but the focus of the simulations was to fairly compare the results of the two different scenarios, so a high oil velocity is justified by the purpose.

The air was not adequate to adsorb the stored thermal energy, due to its low density and specific heat capacity, while the thermal oil can perfectly fulfill the task. Due to the high specific heat capacity and mass flow rate, the oil temperature does not vary significantly along the 0.7 m, while the compressed air quickly warms up decreasing the heat transfer capacity along the pipe and,

thus, penalizing the discharging phase. The results of the temperature profiles are reported in Fig. 6.13 and the ones relative to the thermal energy are shown in Fig. 6.14. The results could have been expected because the improved thermal effect of PCM has been studied and documented. However, these charts are useful to quantify the difference that occurs with the temperature and the thermal energy when a specific amount of the chosen PCM is added to the concrete block object of the current study.

This is also helpful to identify a good compromise between the improvement of thermal energy due to the PCM integration and the consequent reduction of mechanical strength, concerning the desired application and the aim of the project.

During the charging phase, the effect of the PCM is evident even in this case. The integration of the PCM keeps the temperature of the concrete matrix lower than the one without PCM, due to the phase transition, bringing all the advantages previously described. With the oil as HTF, the discharging phase is significantly different from the previous ones, the temperature profiles converge and the PCM effect is noticeable. The curves are less steep and decrease more gradually. Regarding the thermal energy (Fig. 6.14), even in this case, during the charging phase, the stored heat showed an enhancement of 101% in the case of 40% PCM concentration. During the discharging phase, the full PCM potential is appreciable, due to the thermal oil. The thermal energy is efficiently released, and the profiles reach an asymptotic trend in two hours, which is a reasonable amount of time in a real situation. As expected, the enhancement decreases as the PCM concentration decreases but it remains notable and useful.

These results showed how efficient and promising this PCM addition could be to efficiently store energy. The concrete matrix can be a very suitable base to address the sensible heat storage, then the PCM addition can lead to a more performant system, with a higher capacity to store and release thermal energy.

These advantages should be considered because this solution can provide a more efficient TES system, especially when applied to industrial applications, such as for the current object of study.

This type of PCM impregnation could cause some not negligible issues. Unfortunately, important PCM leakage has been observed, as reported by Kuznik et al. (2015), also the interaction between the PCM and its porous container can deteriorate the mechanical properties of the container, because of this leakage.

For future works and investigation, the microencapsulated technology is hence suggested and should be preferred, because it showed to be one of the most reliable methods. This solution, anyway, with the appropriate arrangements can be very

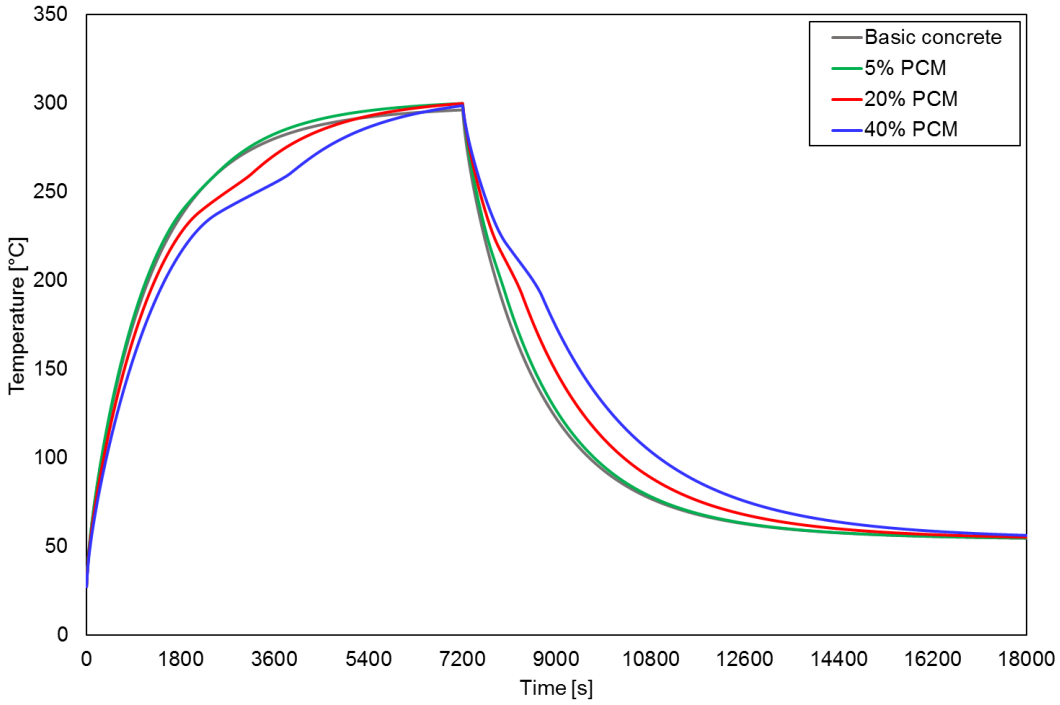

Figure 6.13: Temperature trends for the simulations with thermal oil

convenient, for many reasons: first, the materials are cheap, because the concrete does not require expensive components to be produced and the PCMs do not increase its costs. The simplicity of production should also be considered this is a mixture that can be produced all around the world and it does not require particular environmental conditions or kraft skills. Concrete, even with the PCM addition, is a stable solution that can last for decades and can be used both for civil and industrial applications, with different types of PCM, depending on the operating temperature.

Finally, the integration of the thermal oil as HTF is suitable and efficient for real operative applications and could be easily implemented in a real plant. The best PCM quantity to integrate into the concrete matrix could not be the same for every kind of system. The right amount should be selected carefully considering the improvement that these materials can bring in terms of stored and released thermal energy but also being aware of the mechanical strength reduction, to optimize the entire design of the system.

6.6 Conclusions

In this chapter, a new TES type for industrial applications, realized with a concrete matrix with the addition of PCM, was presented and investigated

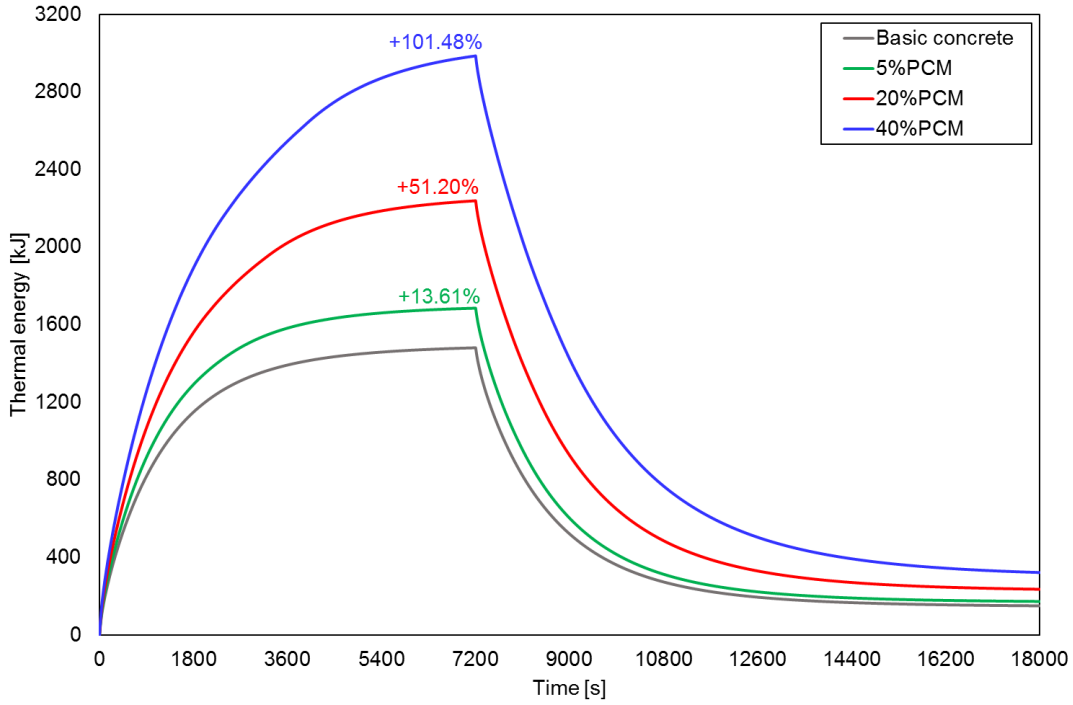

Figure 6.14: Energy trends for the simulations with thermal oil

through numerical simulations, based on a previous set of experimental tests. The numerical model was validated with a very good agreement between the simulations and the tests, the average temperature deviation is equal to 1.78 K. The experiments studied two different concrete mixtures: a reference one and a PCM added one with a 5% in weight, which was too little to have a significant deviation from the pure concrete behaviour, so different numerical analyses were conducted. The aim was to analyze in a real scenario a new TES system, designed to work in a CSP plant, so the numerical models were implemented to simulate operative conditions.

The calibrated model was used to simulate the performances of the other two PCM added concrete mixtures with a 20% and a 40% of PCM in weight. The results showed promising features, the two mixtures developed a less steep temperature increase, with advantages in terms of concrete cracking and damaging problems. The integration of high percentages of PCM in the concrete matrix could reduce its compressive strength and other mechanical properties, but it does not involve structural problems for the case study: the TES system is supposed to work as integrated into a real CSP plant, and it only has to support its dead load, without other additional stresses. For other applications, such as for buildings purposes, or when the mechanical performances of the concrete modules are particularly relevant, a low PCM percentage should be added to the block,

because it may increase the risk of mechanical failure and the degradation of the unit.

Finally, a new kind of simulation was implemented, with thermal oil as HTF, both in the heating and cooling stage, to analyze the performances of a more realistic system that could be implemented in an operative situation. With this solution, the system was able to reach an asymptotic trend both in the charging and discharging phases, in a reasonable amount of time, consistent with the needs of a real operative scenario. The stored and released thermal energy increased by 13.6%, 51.2%, and 101.5% when 5%, 20%, and 40% of PCM, respectively, was added to the concrete as compared to the reference basic TES. This important achievement demonstrates the great potential and the performance that can be achieved by adding the PCM to the sensible-only concrete TES.

7. CFD model of a building wall with PCM

7.1 Introduction

7.1.1 Overview

The building sector is one of the largest energy-consuming sectors and accounts for about 25–30% of final energy consumption on global basis, according to Rabani and Rabani (2019), and Putra et al. (2019). It is considered an equally important source of CO_2 emission (Devaux et al. 2017). Globally, this sector is the main source of energy consumption and it accounts for about 40% of the total energy usage, as reported by Vanaga et al. (2018), Poole et al. (2018), Piselli et al. (2018), Sun et al. (2018), Landi et al. (2020), and Faraj et al. (2021). IEA Solar Heating and Cooling Program findings showed that over 75% of consumed energy in single and multi-family houses is attributed to the space heating and cooling demand, as stated by Patel et al. (2018).

However, the environmental crisis is far from being over and the expectations show that the energy demand in the building sector will rise by 50% by 2050, with the space cooling demand being tripled, as reported by Souayfane et al. (2016). Hence, potential solutions to enhance energy conservation and energy storage are studied in order to try to decrease global energy consumption and mitigate the crisis of global warming (Li et al. 2019).

A policy known as 20–20–20 was established by the EU where the three numbers correspond to 20% reduction in CO_2 emissions, 20% increase in energy efficiency, and 20% increase in renewable energy share by 2020, as stated in the 20-20-20 Goals and 20-20-20 Targets. An extensive technique, regarding cooling and heating improvement by reducing the energy demand in the building sector, is the application of PCM. The potential of these materials is particularly interesting to improve the thermal performances of passive and active building systems.

If energy-efficient building materials are used to construct the building envelope then heat gains from outside air, solar radiations, and through opaque materials can be minimized (Rathore et al. (2022)).

The time to propagate heat waves from the outer environment to the inner environment is called time lag, phase lag or thermal shift, while The ability to attenuate the amplitude of the outside temperature to that of the inside is usually known as the decrement factor.The time lag, thermal amplitude, peak temperature, and decrement factor are used to evaluate indoor thermal performance quantitatively for any building when incorporated with PCM (Fathipour and Hadidi (2017), Rathore et al. (2020)).

To optimize these parameters, the thermophysical properties of the building envelope must be improved against external heat gain. Yang et al. (2021) identified thermal resistance and thermal capacitance of the building material as important parameters to be optimized for improving the energy efficiency of the building envelope.

Leccese et al. (2018) evaluated the dynamic thermal performance of the wall by measuring thermal transmittance, decrement factor, and time lag. Thermal resistance or insulation is one of the relevant technical solutions for reducing energy consumption in buildings. Various materials such as extruded and expanded polystyrene, polyurethane, mineral wool, expanded clay and expanded cork agglomerate can be used as insulating material for building envelopes. Apart from optimizing the resistance and capacitance of the building wall, optimization of the location of the insulating material and energy storage material plays an important role in improving indoor thermal performance. Jin et al. (2016) have found that the optimal location of the PCM layer is closer to the exterior surface of the wall when the PCM melting temperature, thickness of the PCM, and heat of fusion of the PCM are higher.

The optimal location and suitable temperature range varies with change in weather condition. Therefore, it is essential to conduct the regional climatic parametric analysis during building wall design concerning resistance, capacitance, and their distribution in the wall.

The novelty of the approach proposed in this chapter, which considers the applications of PCM to building walls, directly follows the evolving needings and habits of modern society. Traditional thermal comfort systems for building envelopes usually provided a series of insulating layers, applied on the outside of the external walls, with the principal aim to reduce the thermal dispersion toward the surrounding environment during the winter season, without particularly focusing on the thermal conditions of the summer season, which were considered of

fewer impacts. These materials mainly provide a thermal conductivity reduction, which acts its main role in steady state heat transfer processes, quite close to the winter temperature evolution along the day.

However, in the last years, summer temperatures are becoming more and more difficult to cope with, increasing the use of domestic HVAC systems, which also increased energy consumption. A typical summer temperature profile along an average day presents a greater excursion compared with the one that occurs in winter, moving the heat transfer process from an almost steady state system to strongly transient behaviour. In these types of cases, the dynamic physical values assume more importance than the thermal conductivity, because the main goal is to decrease the amplitude of the temperature wave through the walls and also to increase the time lag, in order to have better thermal comfort inside the building. In this scenario, the PCM can provide a significant improvement, since they act as a dynamic thermal system, due to their phase change in the operating temperature range of the building.

7.2 Conducted analyses

This chapter aims to investigate different building walls with the integration of different PCM technologies, in order to evaluate which one could be the most efficient, depending on the application. Hence, the focus will be posed on passive thermal building systems. The conducted numerical analyses regarded the implementation of a building system, with the integration of two different PCM tchnologies. A generic perimetral wall has been chosen and studied, in three different configurations, with a total thickness of 0.3 m and a height of 3 m (Fig. 7.1):

- basic concrete wall
- concrete wall with 10% micro-PCM homogeneously distributed in the mix design
- concrete wall with 2 layers of micro-PCM applied on the external side

The chosen thickness of 0.3 m is generic, but perfectly in line with the usual dimensions designed for the structural external concrete walls of a building for domestic use. Concrete has been chosen as the main structural material because in Italy it is the most used one for buildings. Also, all the previous analyses regarded concrete elements and this led to a consistent approach.

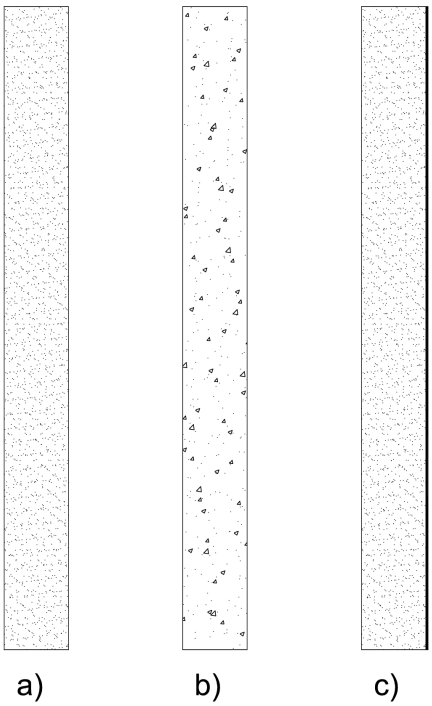

Figure 7.1: Three types of simulated walls: a) basic concrete wall; b) wall with 10% micro-PCM homogeneously distributed in the mix design; c) wall with 2 layers of micro-PCM applied on the external side

The concrete used in the previous chapters was used as it is for the basic concrete simulation of the current analyses. It was then mixed with 10% of PCM, creating a wall with a homogeneous dispersion of PCM in it. Finally, two layers of PCM were added to the basic concrete wall to create a new type of system. The three configurations were analyzed and compared to identify which one has the best performance.

The chosen PCMs have been selected according to the literature review. They are both ready for commercial use, not only for scientific purposes. Further details are reported in the dedicated sections.

7.3 Model description

The CFD model has been developed using ANSYS Fluent. The building wall is modelled as a 2D representation because, even in this form, it is representative of the thermal behaviour, because along the wall development the physical conditions are the same. With this solution, also, a more computation effort, due to a complete 3D model, is avoided, creating a simpler, but equivalently accurate representation.

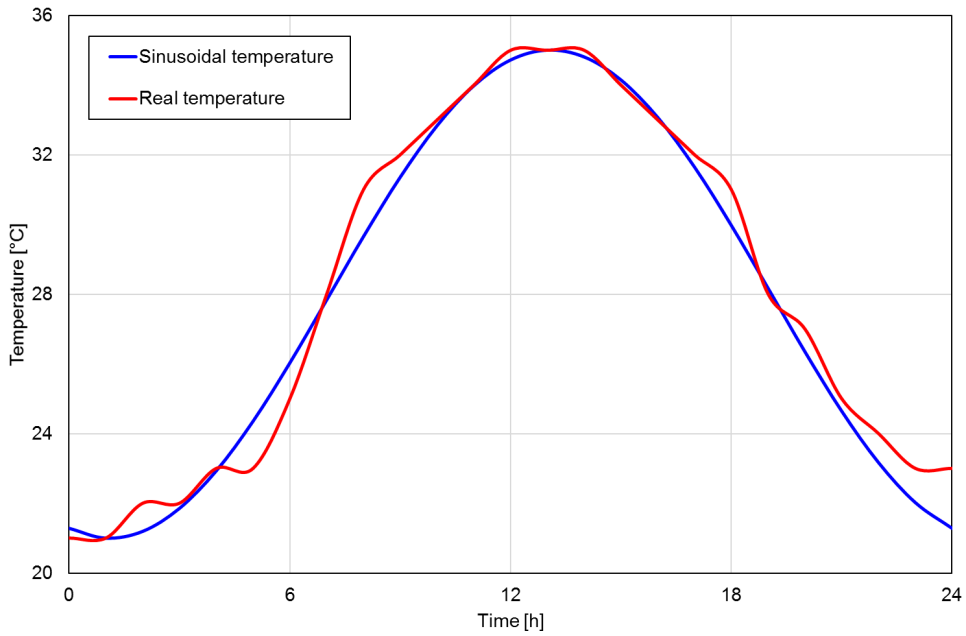

Figure 7.2: Real and sinusoidal temperatures occurred in Padua on the 5^{th} of July 2022

.

As boundary conditions, a sinusoidal temperature profile is applied to the external side of the wall. The temperature sinusoid directly follows the real profile that occurred in Padua on the 8^{th} of June 2022 and on the 5^{th} of July 2022. The real and sinusoidal temperatures of the July profile are reported in Fig. 7.2 and the UDF compiled to apply that profile in the ANSYS Fluent environment is reported in Appendix A, listing 8.1.

The June temperature profile has been chosen to have a warm thermal load, to evaluate the thermal storage capacity of the different types of walls. The July temperature profile, which is set to higher temperatures, shifted by about 5 °C, has been used to determine the performance of the different systems, subjected to a pretty hot condition. In this way, the real and full potential of the PCM integration is visible and comparable.

7.3.1 Materials

For these analyses, as written before, concrete has been used as the main material, while PCM, directly added and mixed in the mix design or applied as layers, has been integrated to improve the thermal performance of the system. The PCM, for building applications, must have a melting temperature range compatible with the ordinary temperature profile to which the structure is subjected.

More details, such as the thermal properties and the dimension, are reported

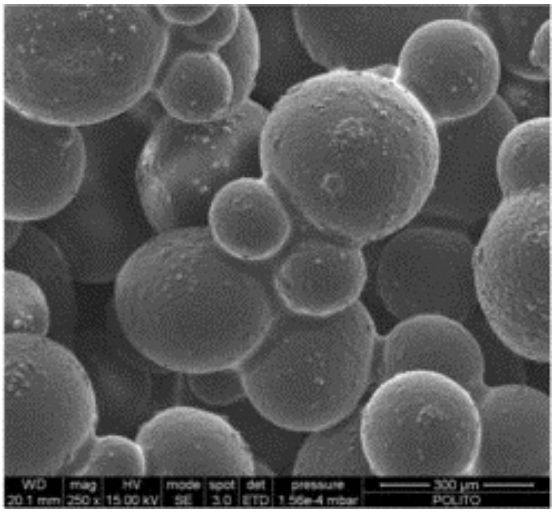

Figure 7.3: SEM analysis of some samples of PCM, by Marchi et al. (2013)

in the following paragraphs.

Concrete

The concrete physical properties have been chosen according to the ones used in the previous simulations and they are reported in Tab. 7.1.

Table 7.1: Concrete properties

Property	Unit of measurement	Value
Thermal conductivity	[W/(mK)]	1.60
Density	[kg/m^3]	2350
Specific heat capacity	[J/(kgK)]	607
Thickness	[m]	0.3

Mixed micro-PCM

For this analysis, the micro-encapsulated PCM chosen is a mixture of paraffin waxes in powder form encapsulated in poly-methyl-methacrylate (PMMA) microcapsules; its melting point is around 23 °C. This material was also used by Marchi et al. (2013), with very good results. In Fig. 7.3 are reported SEM micrographs of the mixtures. The detailed properties are listed below in Tab. 7.2.

In this case, the PCM percentage in the mix design has been set at 10%, because, for a building application, a too high percentage could be excessively restrictive of the compressive resistance of the concrete mixture.

Table 7.2: Mixed PCM properties

Property	**Unit of measurement**	**Value**
Thermal conductivity	[W/(mK)]	0.2
Density	[kg/m^3]	350
Latent heat of fusion	[kJ/(kg)]	100
Specific heat capacity	[J/(kgK)]	2100
Transition temperature range	[°C]	22-25
Particles size	[mm]	0.05-0.30

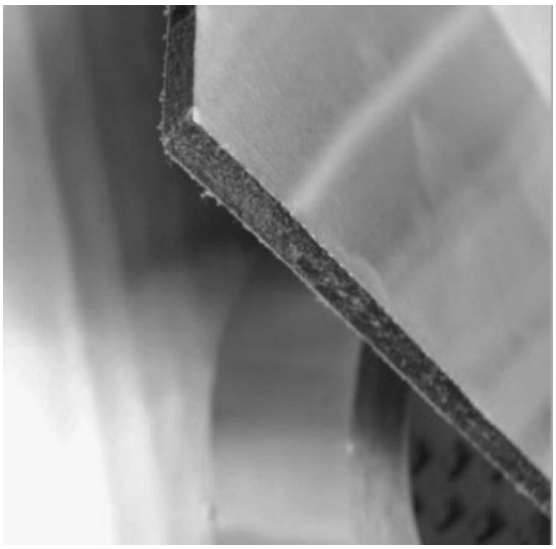

Figure 7.4: Flexible sheet of composite PCM material, by Kuznik et al. (2008)

PCM in layers

In the third configuration of the wall, two layers of PCM have been applied on the external surface of the wall. These layers are produced by the Dupont de Nemours Society and are constituted of 60% of microencapsulated paraffin within a copolymer. The final form of the composite PCM material is a flexible sheet, with an aluminium-laminated coverage, visible in Fig. 7.4. The detailed properties are listed below in Tab. 7.3.

This product has been used also by Guarino et al. (2017) and it is fully described by Kuznik and Virgone (2009), and Kuznik et al. (2008).

Two layers of this composite PCM have been added to the wall, in order to have a mass which is comparable to the one used for the mixed PCM wall. With 10% of PCM, in the second type of wall, there is a linear mass of 31.5 kg/m of PCM. If 2 layers are added to the external surface, a PCM linear mass of 28.08

Table 7.3: PCM in layers properties

Property	Unit of measurement	Value
Thermal conductivity	[W/(mK)]	0.2
Density	[kg/m^3]	900
Latent heat of fusion	[kJ/(kg)]	70
Specific heat capacity	[J/(kgK)]	2500
Transition temperature range	[°C]	18-24
Thickness	[mm]	5.26

kg/m is obtained, which is quite comparable to 31.5 kg/m. in this situation, the results of the two systems can be equivalently evaluated.

Anyway, if there are specific needs, one or more extra layers of PCM can be added, in order to obtain the desired thermal effect. The same can not be always done with direct integration, because a too high PCM percentage could reduce the compressive mechanical resistance of the structure.

7.3.2 Phase change materials integration

As done with the previous analyses, with the PCM directly integrated into the concrete mixture, a new homogeneous material, composed of concrete with a defined PCM percentage, was obtained. For this reason, it was not possible to divide the PCM domain from the concrete one. Hence, the PCM added concrete was modeled as a unique body with the same properties for the whole domain.

Anyhow, each thermal property was modified, according to the PCM percentage, to take into account the change made to the mixture. Each thermal property was weighted using the PCM percentage. The following expression was used:

$$c_p = (1 - f) \cdot c_{cnc} + f \cdot c_{PCM} \tag{7.1}$$

where c_p is the mean specific heat capacity and f is the PCM percentage in weight. The same model was used also for the density and thermal conductivity. Particular attention should be paid to the specific heat capacity of the PCM, which was considered as reported by Lamberg et al. (2004):

$$c_{PCM} = \begin{cases} c_{PCM}, & T < T_{im} \\ c_{PCM} + \frac{r}{T_{fm} - T_{im}}, & T_{im} \leq T \leq T_{fm} \\ c_{PCM}, & T > T_{fm} \end{cases} \tag{7.2}$$

where r is the latent heat of fusion, T is the current cell temperature, T_{im} is the initial melting temperature, and T_{fm} is the final melting temperature.

The Eq. 7.1 was used also for the specific heat capacity calculation in the cases with the PCM composite layers.

7.4 Standalone wall

The first set of simulations regarded the wall standalone, without the interaction of the surrounding environment. The temperature profile of the 8^{th} of June 2022 was directly applied on the external surface, without considering the convection effects. This kind of simulation was supposed to identify the storage capacity, the thermal shifting and damping, and the performances of the different kinds of the wall.

The geometry was edited using the Design Modeler tool, in ANSYS. Then, the surfaces were meshed, using a refinement corresponding to the thin PCM layers. At this stage, since the aim was to study the general thermal performances, also walls with one and three PCM layers, not just the system with the two layers. The simulation time was set as 86400 s (24 h), with a time step equal to 600 s.

In Fig. 7.5 the temperature profiles along the day are reported. On the outside, the applied boundary condition corresponds to the obtained temperature, for all the different systems. It can also be noticed that the inside temperature profile which has the highest values belongs to the basic concrete system. This massive wall still has quite good thermal properties, because the thermal shift is equal to 6.6 h and the temperature peak is lowered of about 5.53 °C.

The thermal shifting of the basic concrete wall was checked also using the procedure proposed by the UNI EN ISO 13786:2017 norm, with that calculation, the obtained value of thermal shifting is equal to 6.7 h, which almost overlapped with the 6.6 h found with the numerical model. The procedure regulated in the norm was implemented in a Matlab code, with a separate function recalling the heat transfer matrix of a homogeneous layer. The codes are reported in Appendix A, listing 7.2 and listing 7.3.

The detailed values of the thermal shifting and the temperature dumping of

Table 7.4: Results of the different types of walls

Type of Wall	Thermal shifting [h]	Temperature dumping [°C]
Basic concrete	6.6	5.53
10% micro-PCM	10.83	8.43
1 layer composite PCM	9.33	6.71
2 layers composite PCM	10.00	7.73
3 layers composite PCM	10.66	8.60

the different cases are reported in Tab. 7.4. It can be noticed that the values improved with the increasing of the PCM layers, which is an intuitive behaviour. However, looking just at these results, the most effective wall could seem the one with 10% of PCM. Nevertheless, the final values are not very different from the walls with 2 layers (which will be studied in depth in the following discussions) and three layers. Also, with a look on Fig. 7.5, during the initial stages of the simulations, the temperature on the inside is lower in the cases with 2 and three layers. Hence, more detailed analyses is needed to identify which solution is the most effective.

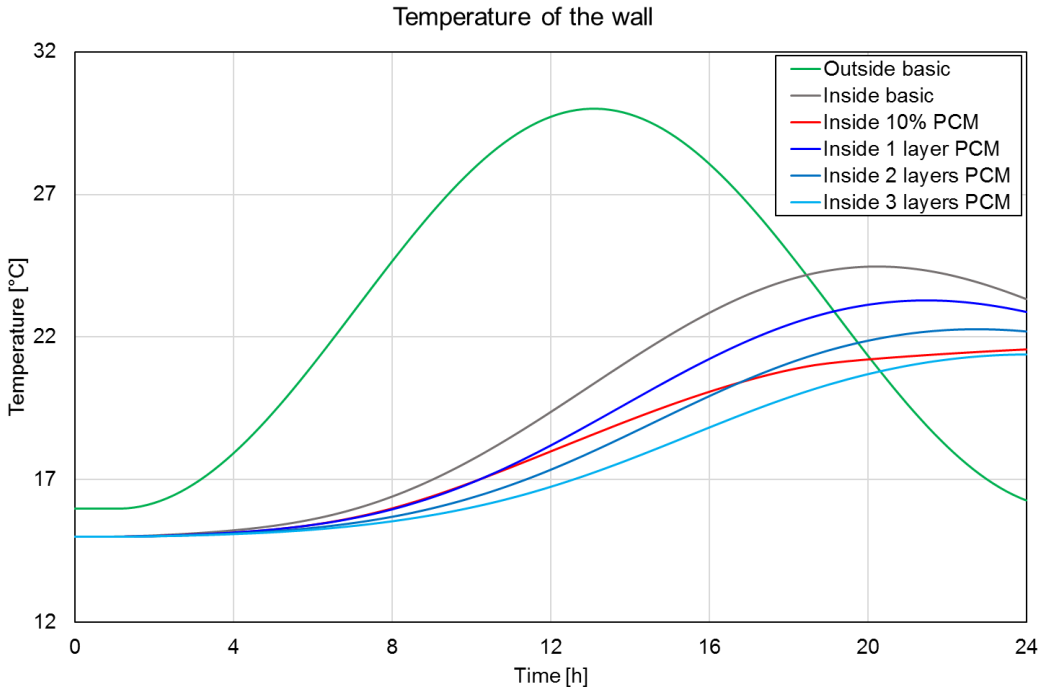

Figure 7.5: Temperature of the wall

From now on, the walls with 1 and 3 composite PCM layers will be neglected and the focus will be placed on the basic concrete, concrete with 10% mixed

PCM and 2 layers of PCM, which have almost the same PCM content. In Figs. 7.6, 7.7, and 7.8 the temperature profile along the thickness is reported for the three systems, every three hours of simulations, to check the trend during the whole day. In Fig. 7.6, with the basic concrete system, the temperature is always higher than the other two solutions with the PCM, for the whole duration of the simulation. In Fig. 7.7, with the 10% of mixed PCM, the temperature is lower, but there is a high gradient between the inside and the outside of the wall, which is not quite appreciable, especially in terms of transmitted heat flux. In Fig. 7.8, with the 2 layers of composite PCM, the whole temperature gradient almost occurs in the PCM layers, keeping low and pretty constant the temperature along the wall thickness, which lead to an optimal condition of the structure.

A specific focus can be found in Fig. 7.9, where the three temperature profiles along the thickness are reported when the external load peak occurs. The basic concrete temperature is way higher than the other two, while the system with two layers of PCM is always lower than the one with 10% of PCM and also the majority of the thermal gradient is absorbed by the PCM on the external surface. In order to have a more detailed analysis, which involves also the transmitted thermal fluxes and the convection interaction with the surrounding environment, more simulations have been realized and explained in the following section.

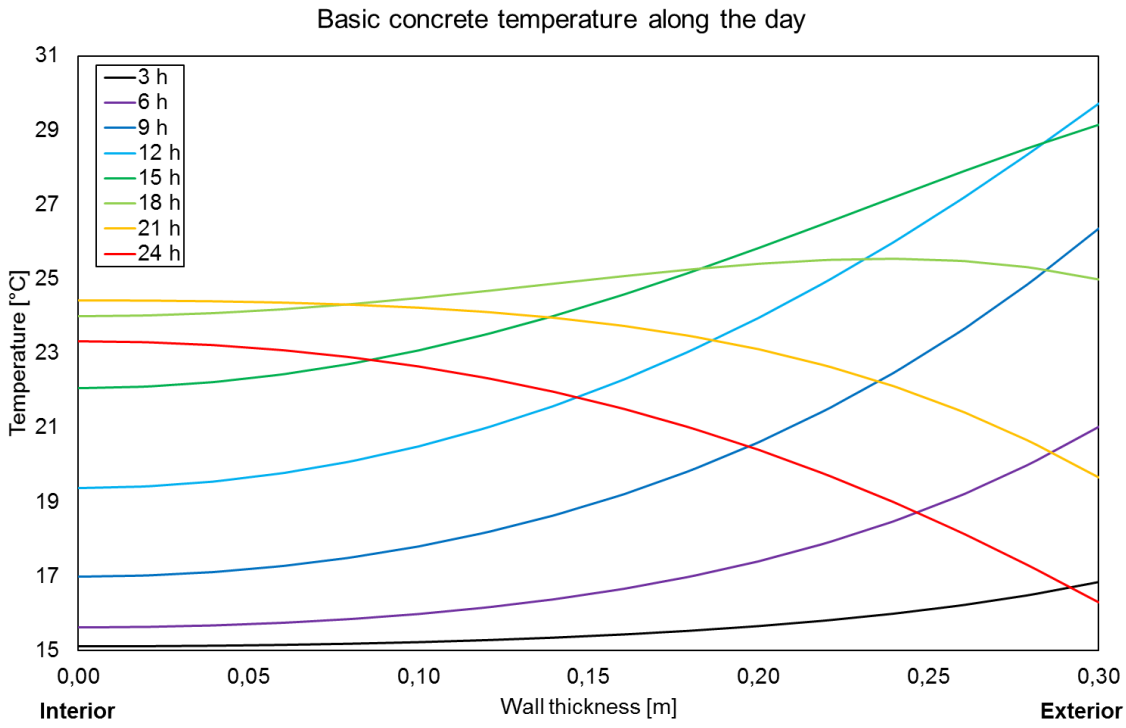

Figure 7.6: Basic concrete temperature along the day

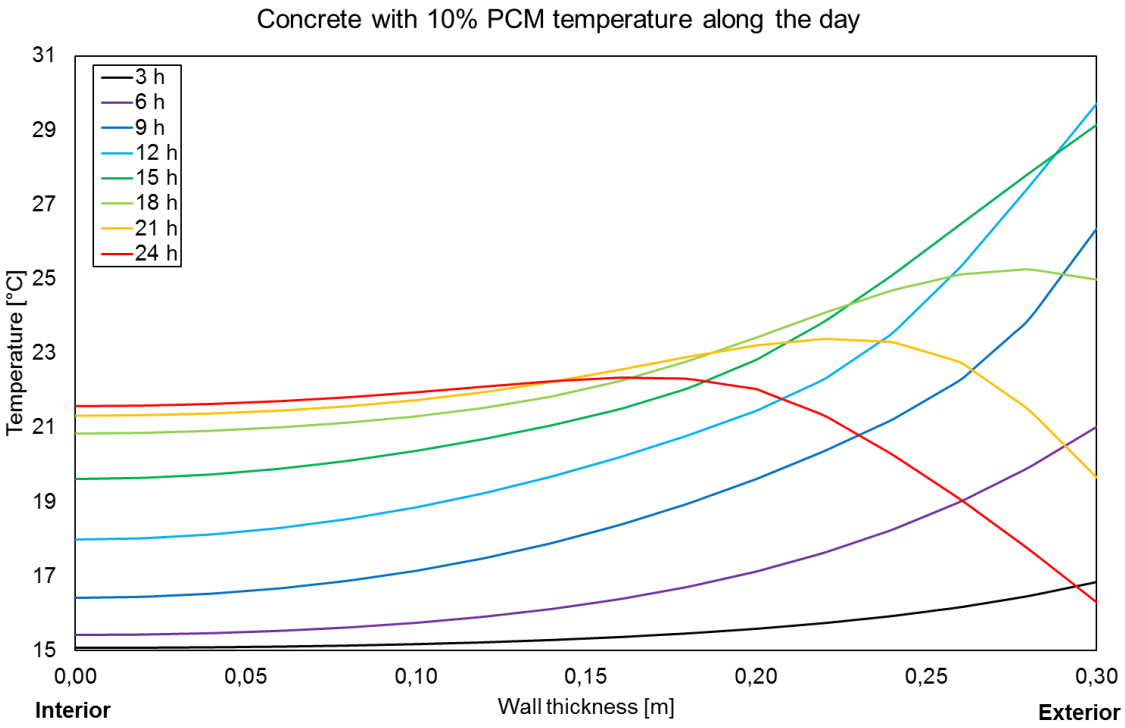

Figure 7.7: Concrete with 10% of PCM temperature along the day

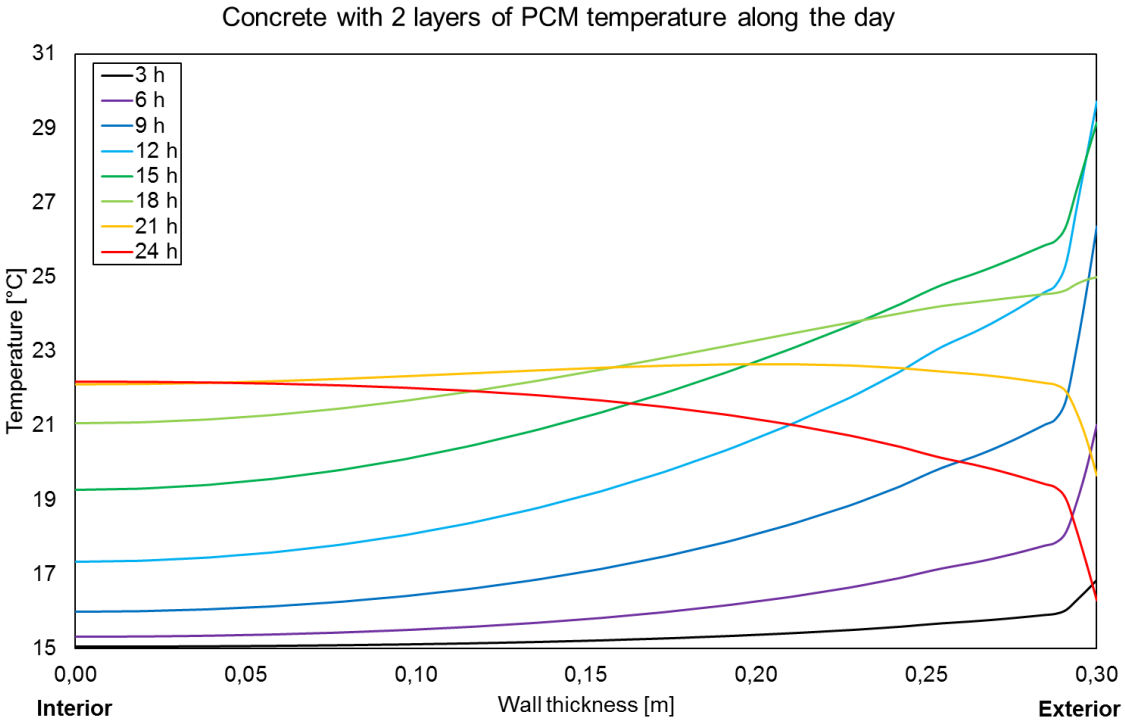

Figure 7.8: Concrete with 2 layers of PCM temperature along the day

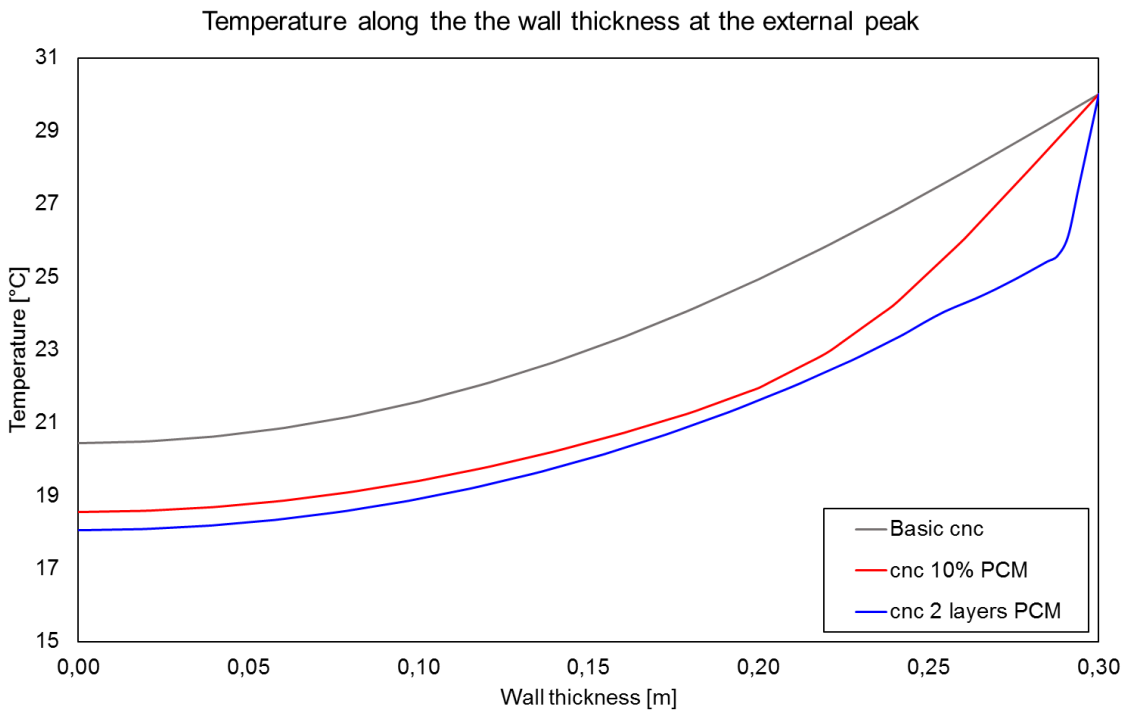

Figure 7.9: Temperature along the thickness at the external peak

7.5 Wall in the surrounding environment

This second set of simulations aimed to analyze the thermal performances and behaviour of the three previously described wall systems. The three walls were subjected to a hot thermal load, considering the one that occurred in Padua on the 5^{th} of July 2022, with a temperature range between 20 °C and 35 °C, applied on the external air. A specific focus was placed on the transmitted heat flux on the inside of the room, which gives information regarding also the thermal comfort inside the building.

The convective heat exchange has also been introduced, by imposing an external convection coefficient equal to 20 W/m^{2}K and an internal convection coefficient equal to 5 W/m^{2}K, in order to consider the convective affects that the air provides to the wall on the outside and on the inside. In these analyses, the thermal load profile has been applied to the external air cells and not directly on the external surface of the wall, obtaining also a more realistic representation. The temperature inside the room has been imposed as constant and equal to 20 °C. A schematic representation of the physical model is visible in Fig. 7.10.

The system has been considered as an indefinite plane wall, and the total wall thickness is 30 cm in each configuration, so also with the layers of PCM applied on the external side, the total dimension does not change. With these settings

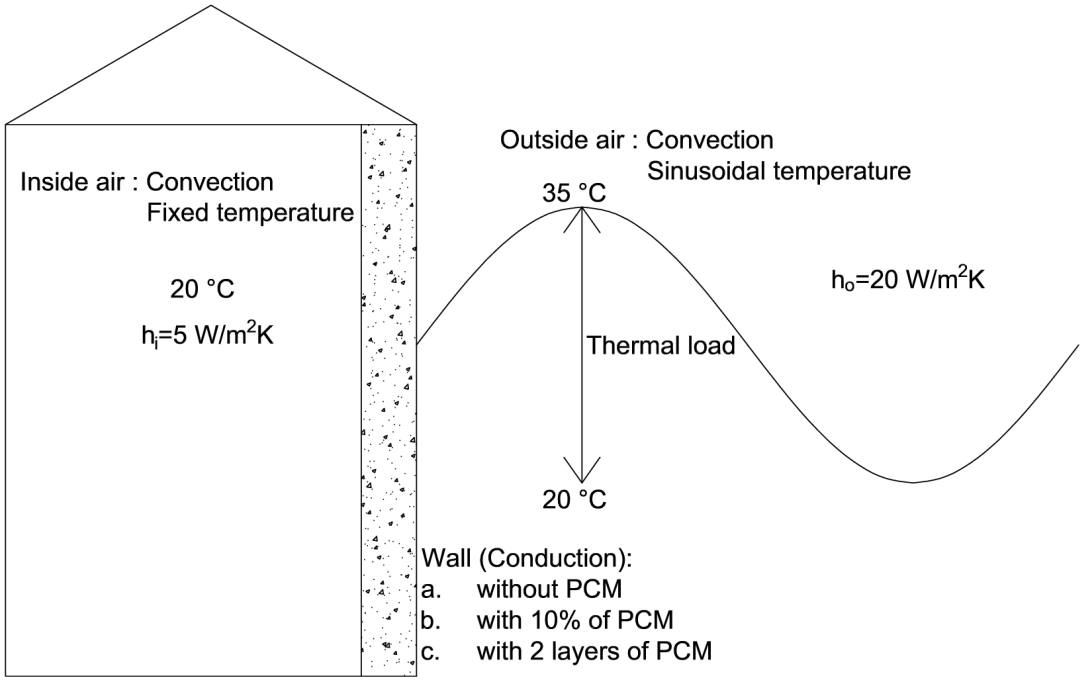

Figure 7.10: Representation of the physical model

of the boundary conditions, an initial transient period takes place. The same temperature profile has been applied to the air for days, in order to identify when the system is in full swing. It is important to analyze the data when the thermal behaviour is under regime, because it allows the determination of an average transmitted heat flux and thermal energy. During the transient stage, the data are not very useful or reliable, because they referred to a limited time frame. For each type of wall, a four-days simulation has been conducted, since after the third day it is clear that the systems are almost stabilised, or at most with a negligible drift. In particular, for the walls with basic concrete and with the two layers of PCM applied on the external side, the transient stage is practically finished after the third day. Regarding the wall with mixed PCM, however, a drift is still present during the fourth day, but it was decided to consider it under regime. This approximation has been made because it's almost a negligible drift and also for the sake of simulation time. A horizontal trend would have been reached in several days and it would have not been compatible with the simulation purposes. In Figs. 7.11 - 7.13 the temperature of the inside and outside of the walls are reported. First of all, it is clear that the system with 10% of dispersed PCM, Fig. 7.12, presents a lower temperature compared with the basic concrete one. Also, the internal temperature does not properly fluctuate, but it is almost constant during the fourth day. This proves that the integration of the 10% of PCM can effectively reduce the temperature of the building system.

A different reasoning should be proposed for the wall with the application on the external side of two layers of composite PCM. In Fig. 7.13, in fact, three curves are represented: the temperature profile at the external side of the PCM, the one between the concrete wall and the 2 layers of PCM and the internal temperature. The temperature profile that faces the external air presents a wave with high amplitude, because of the thermal properties of the layers. However, this great peak does not occur in the contact region between the PCM and the wall, since the profile is way dumped. Looking at the inside temperature profile, a fluctuation is present, but the temperature values are the lowest of all the three simulations and there is not a very high amplitude in the wave, keeping comfortable the inside of the room. From Fig. 7.14 to Fig. 7.16 the details of the temperature profiles of the last day, under full regime, are reported, to show more accurately the effect of the integration of the PCM, mixed or as layers, in the building system.

Finally, regarding the temperature profiles, in Figs. 7.17 and 7.18 the curves of the external and internal trends are represented to be compared. On the outside (Fig. 7.17), the mixed PCM keeps the temperature at its lowest value, but also the inside (Fig. 7.18) must be considered. The system with mixed PCM causes a less fluctuant curve than the wall with 2 layers of PCM. However, even if slightly more fluctuant, the temperature values are lower in the second case, which is more desirable. In order to have a deeper comprehension of the thermal behaviour of the three different building systems, the transmitted heat fluxes to the inside are calculated and compared. In Figs. 7.19, 7.20, and 7.21 the heat fluxes of the three walls are reported along the four days of simulation. In Fig. 7.22 all the heat fluxes are plotted to be easily examined in a unique chart. For all three situations, during the fourth day, as for the temperature, the heat fluxes are in full swing, with just a minor deviation in the wall with mixed PCM. Looking at the absolute values, it is clear that the lowest transmitted heat flux occurs with the system with two layers of PCM, even if the fluctuation is higher than in the case with the mixed PCM. Both solutions brought a reduction in the loss of thermal power, but the wall with the layers assures a better comfort inside the room. The transmitted heat flux, however, shows just the punctual value referred to that precise point in time. In order to have a comprehensive view of the total energy that enters the room, in Fig. 7.23 the heat of the fourth day of the simulation, at full regime, is reported. Both the solutions with the PCM integration lead to a reduction in the total transmitted energy during the day, but the system with the 2 layers of PCM overcame a 44% reduction, while the wall with 10% of mixed PCM reached just a reduction of the 32% in value.

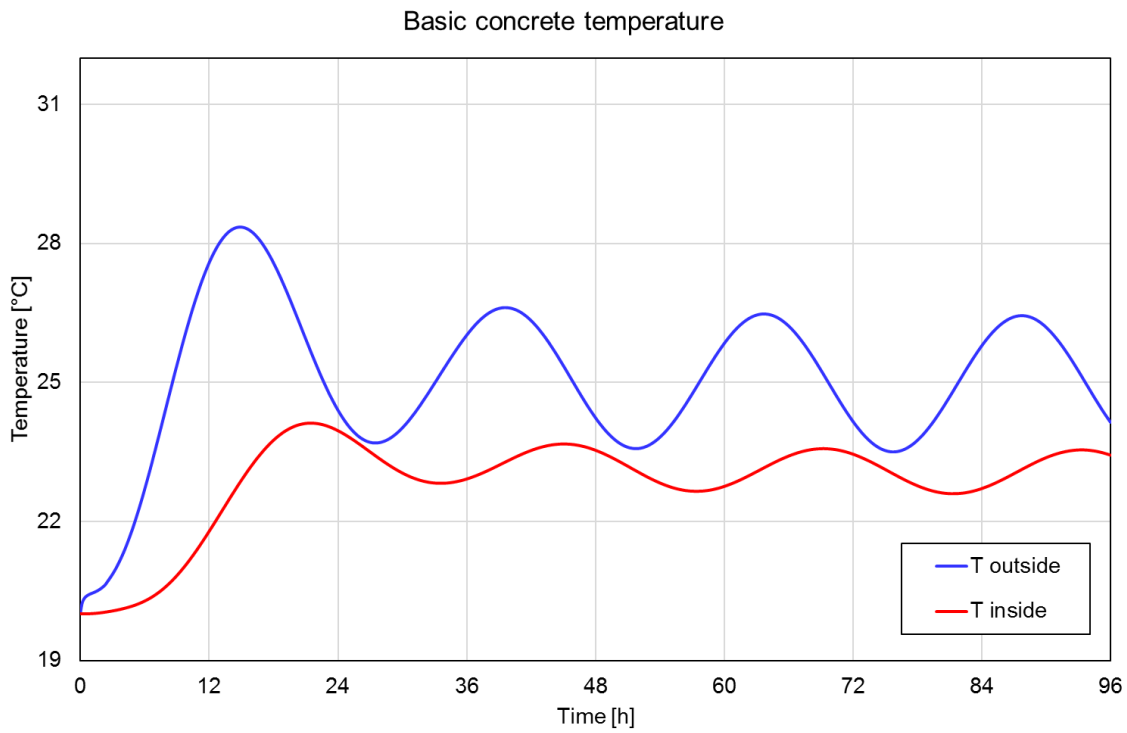

Figure 7.11: Basic concrete temperature during the 4 days of simulation, in order to identify the full swing

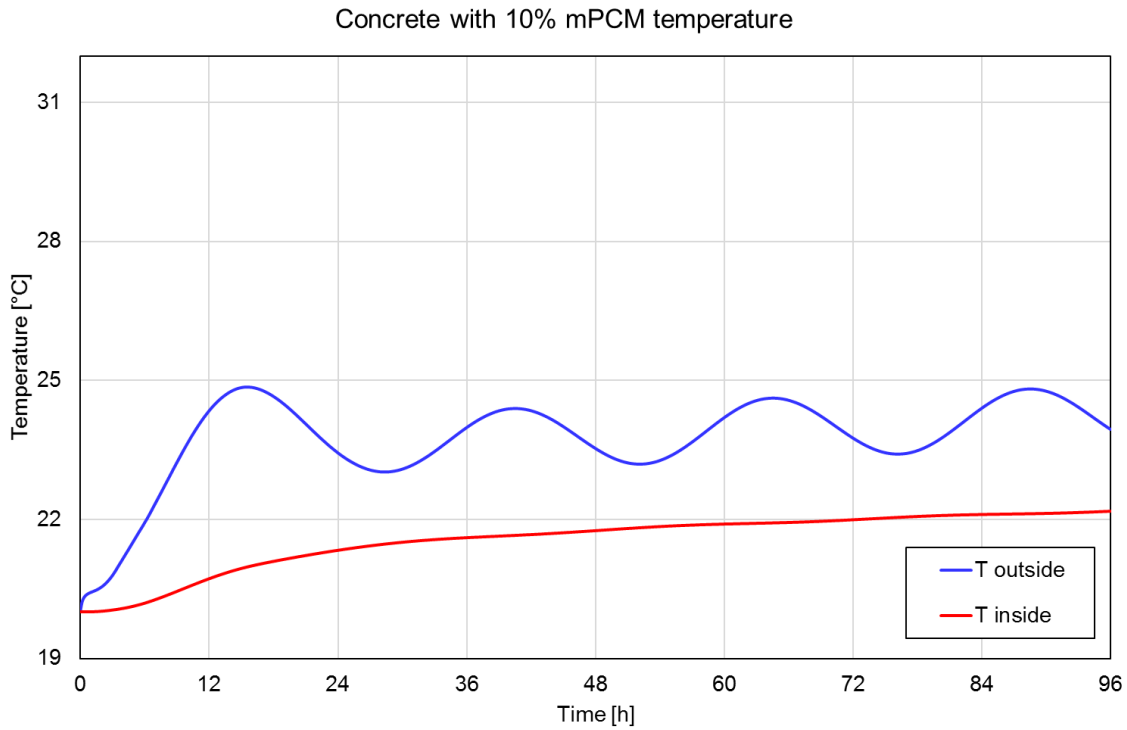

Figure 7.12: Concrete with 10% of PCM temperature during the 4 days of simulation, in order to identify the full swing

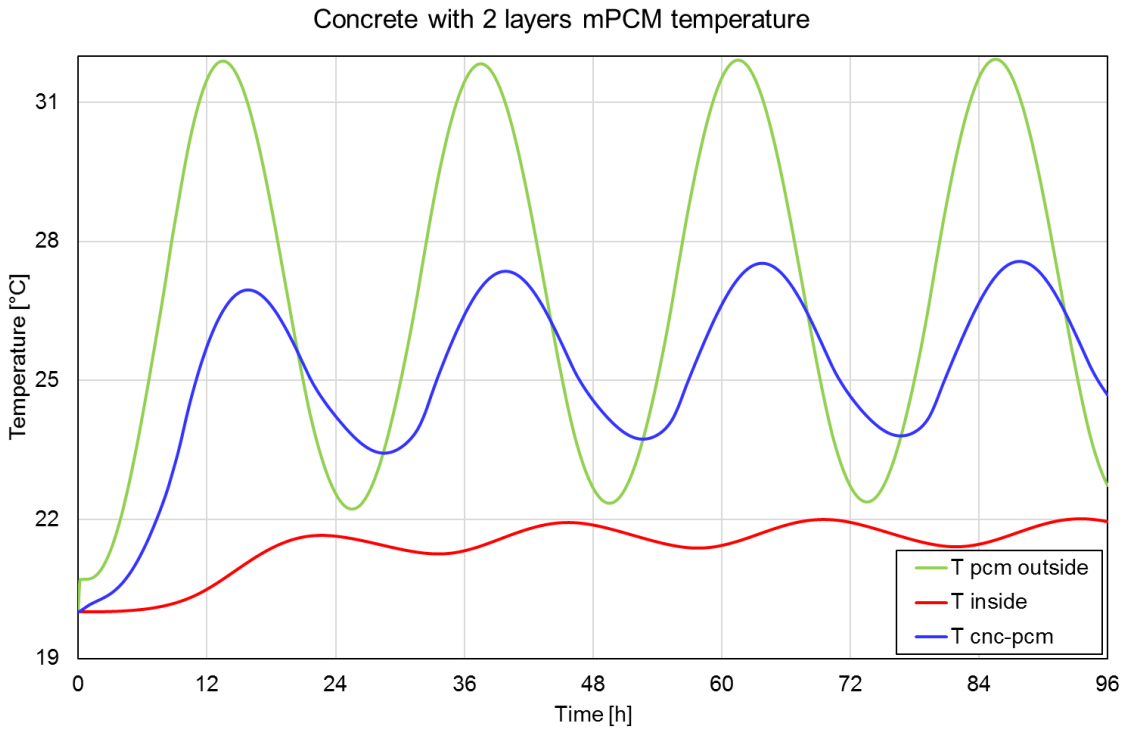

Figure 7.13: Concrete with 2 layers of PCM temperature during the 4 days of simulation, in order to identify the full swing

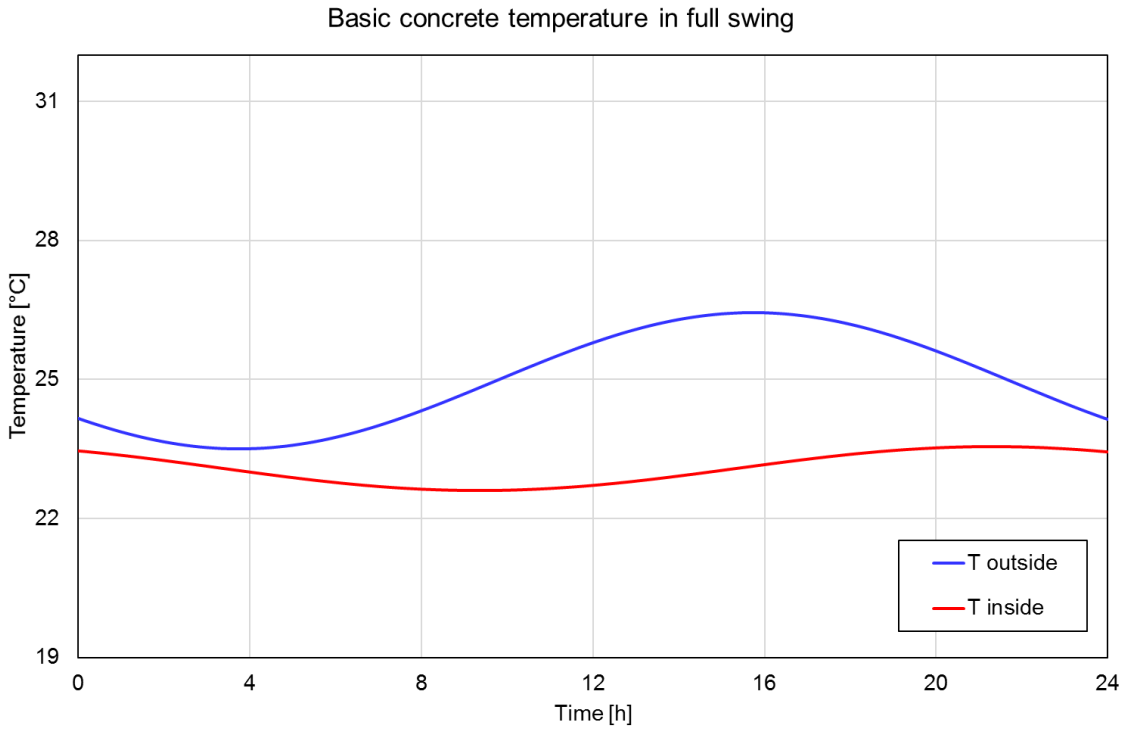

Figure 7.14: Basic concrete temperature during the fourth day of simulation, in full swing

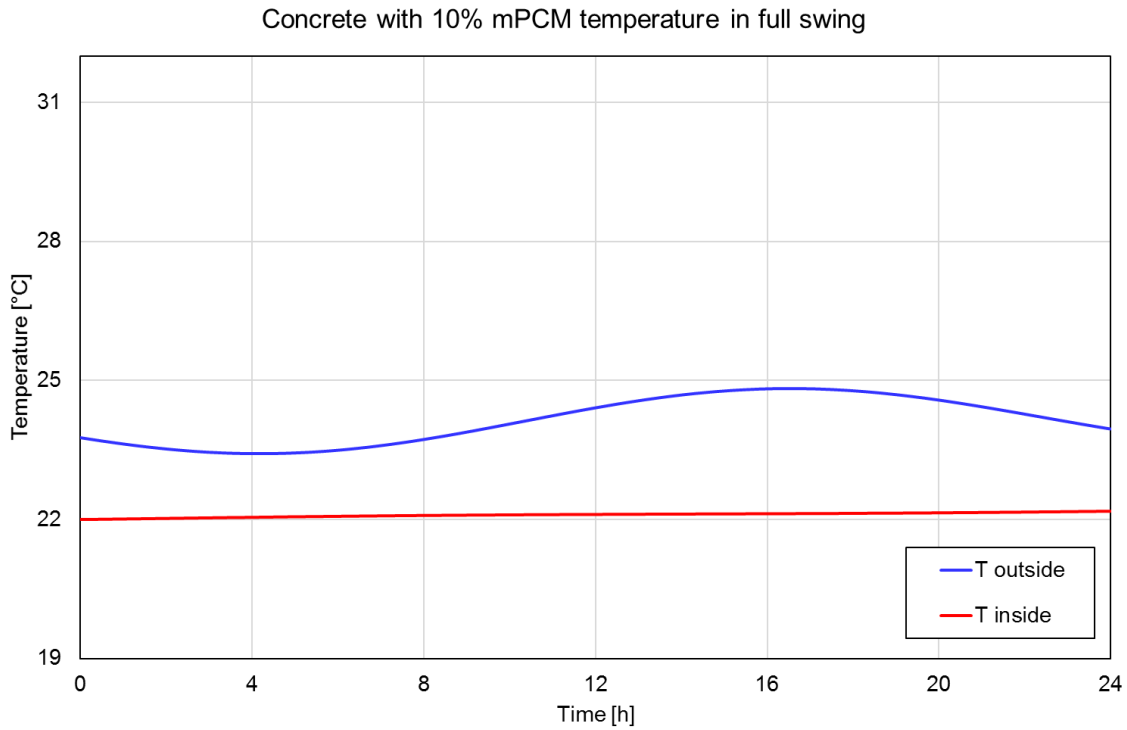

Figure 7.15: Concrete with 10% of PCM temperature during the fourth day of simulation, in full swing

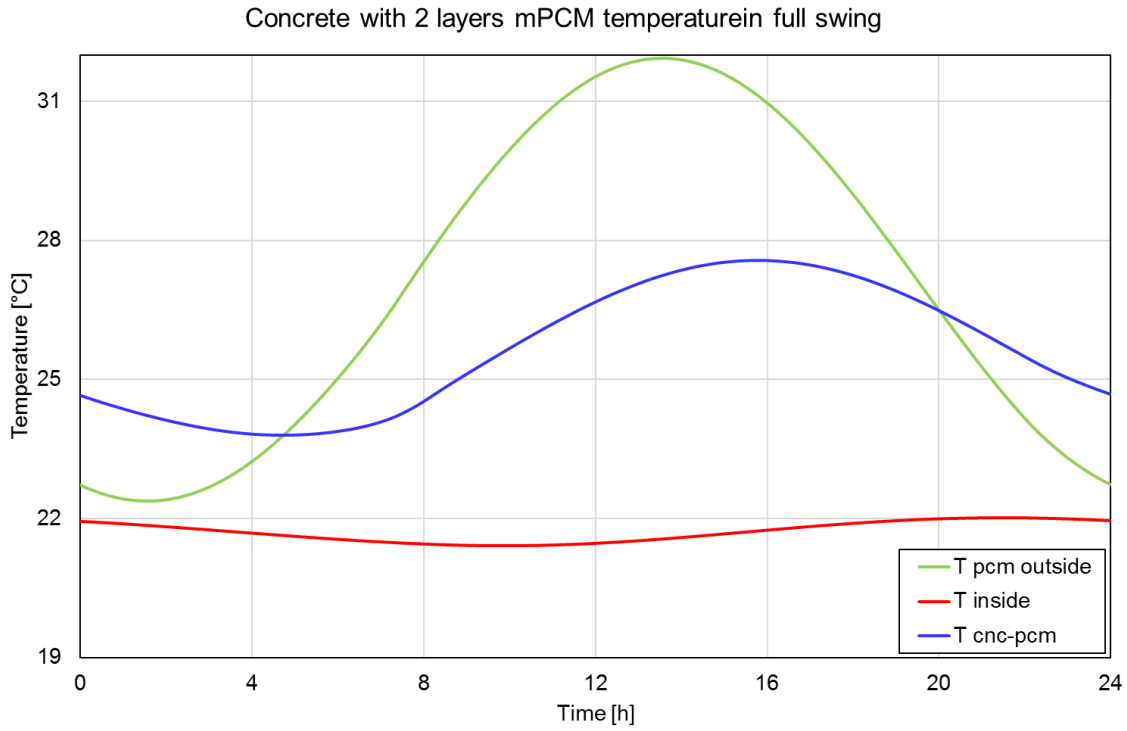

Figure 7.16: Concrete with 2 layers of PCM temperature during the fourth day of simulation, in full swing

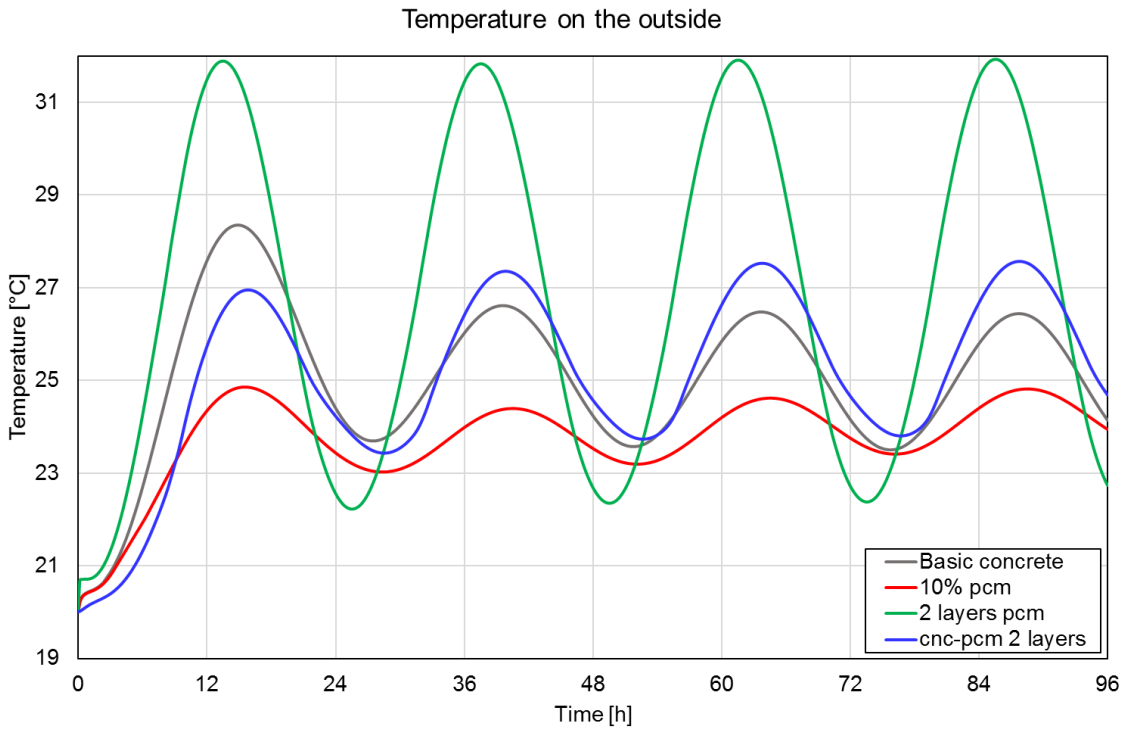

Figure 7.17: Comparison of the external temperature profiles during 4 days of simulation

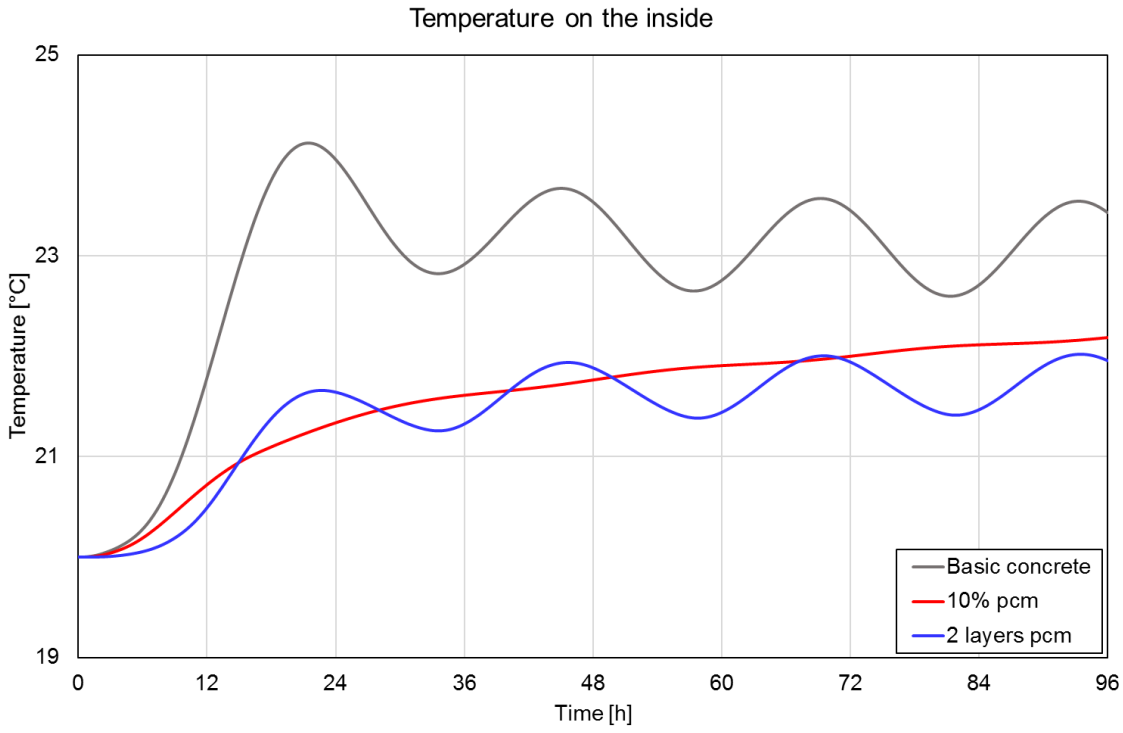

Figure 7.18: Comparison of the internal temperature profiles during 4 days of simulation

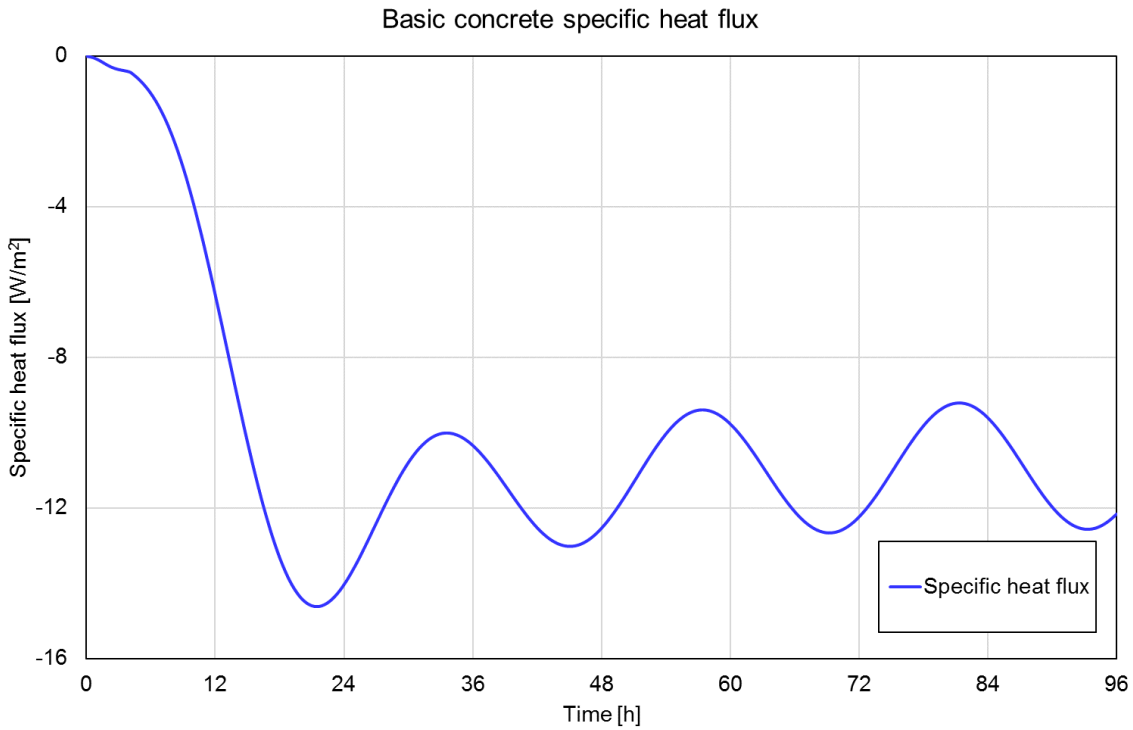

Figure 7.19: Basic concrete transmitted specific heat flux during 4 days of simulation

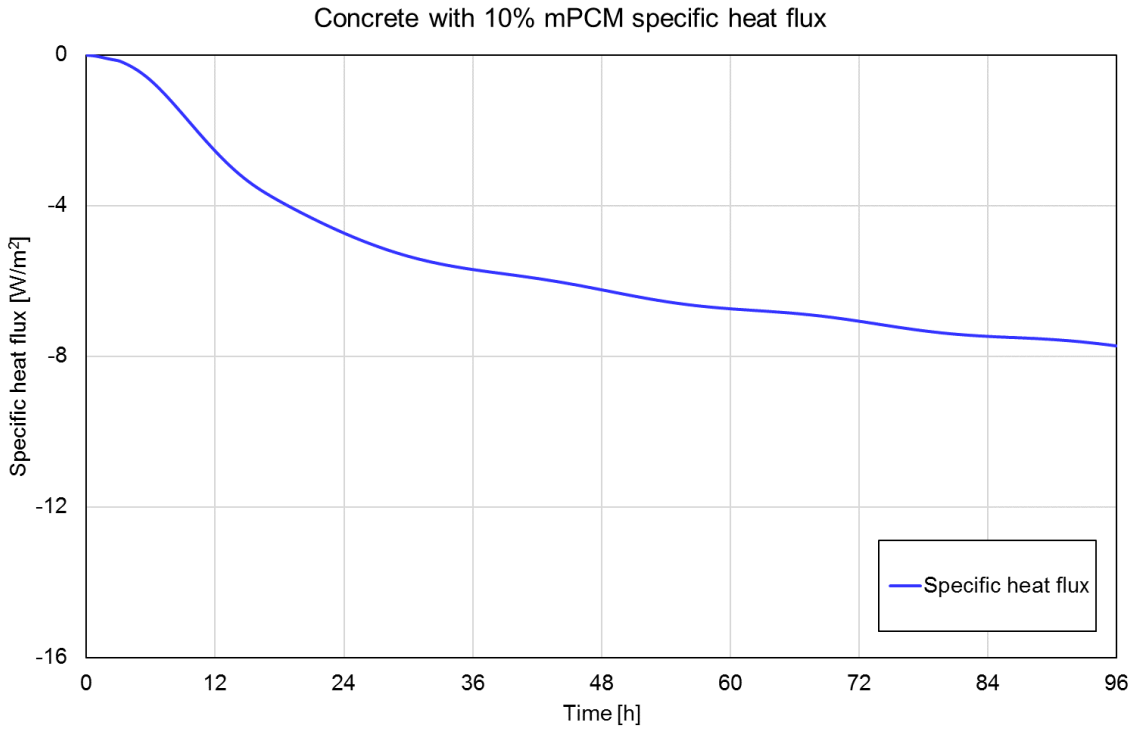

Figure 7.20: Concrete with 10% of PCM transmitted specific heat flux during 4 days of simulation

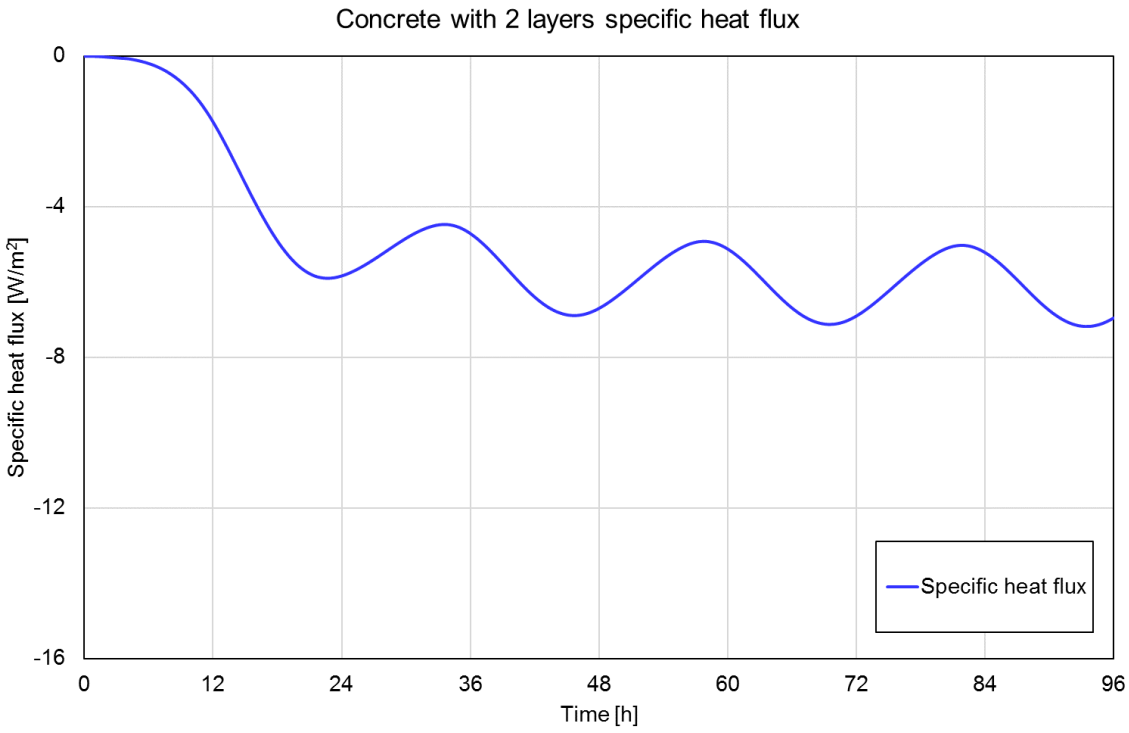

Figure 7.21: Concrete with 2 layers of PCM transmitted specific heat flux during 4 days of simulation

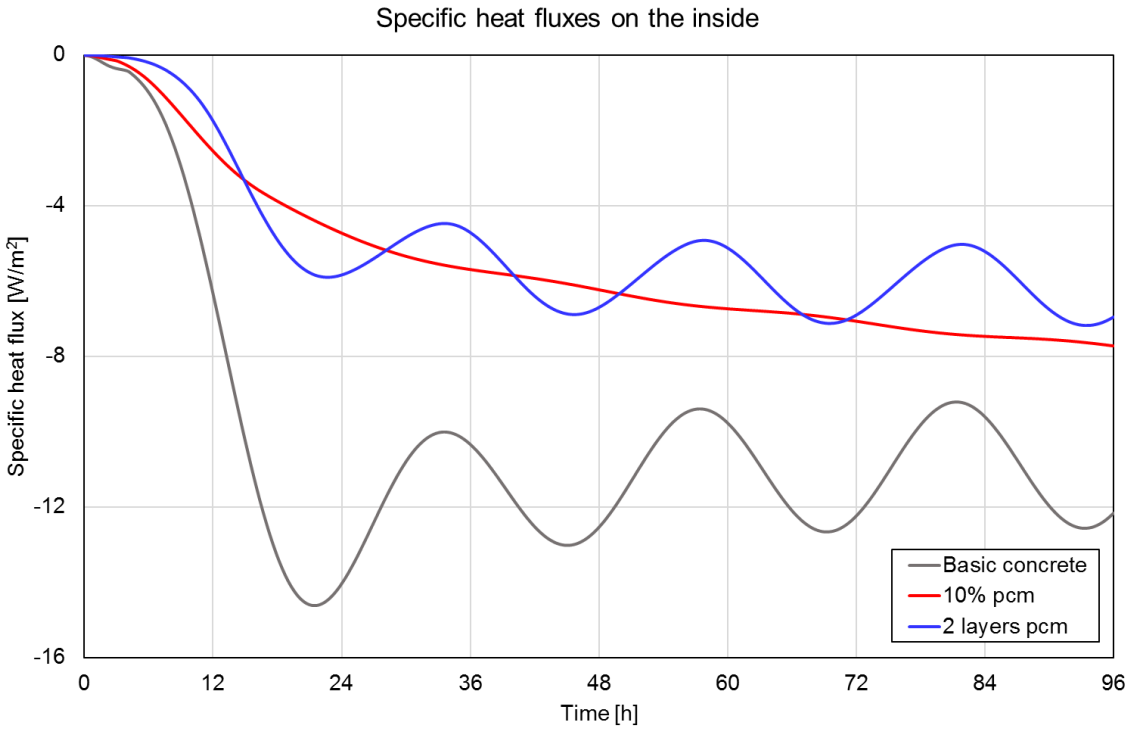

Figure 7.22: Comparison of the transmitted specific heat fluxes during 4 days of simulation

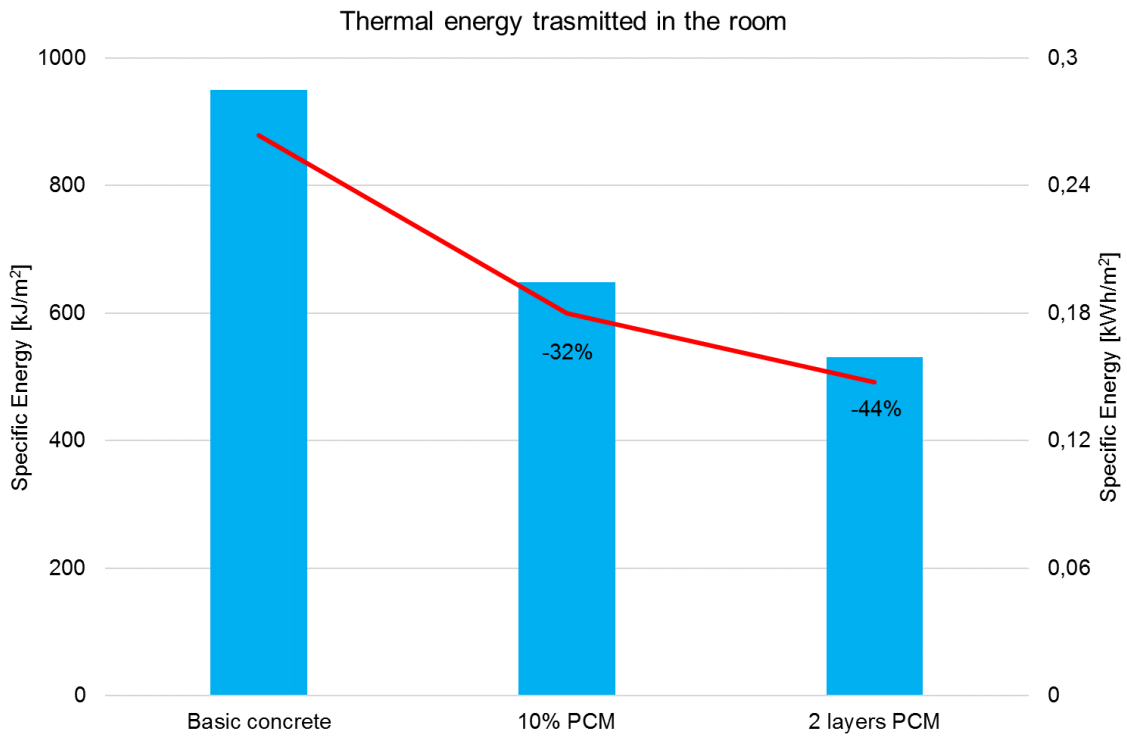

Figure 7.23: Comparison of the transmitted specific energy in the room during the fourth day of simulation, in full swing

Solar radiation was not considered because it would have been difficult to model in such a situation. I believe that even considering solar radiation, there may be differences between the various systems, without PCM and with PCM of various types, in terms of quantitative, but not qualitative, so the solution with PCM would still be more advantageous. Solar radiation involves the application of a further variable thermal heat flux incident on the walls, so it is reasonable to believe that the advantages of PCM can be further emphasized and highlighted by an additional thermal load, increasing the reduction of energy transmitted to the inside of the room, compared to the traditional concrete wall.

7.6 Conclusions

Overall, in conclusion, the best solution, in terms of temperature and energy transmitted reduction, is the wall with the integration of 2 layers of PCM. The system with the mixed PCM is however well performant and allows for a better thermal behaviour than the basic concrete wall, but its absolute improvements are less relevant than the solution with the 2 layers.

However, some further considerations must be presented. First of all, in this

chapter, the main comparison regarded the wall with the integration of 10% of PCM and another wall with 2 layers applied on the outside, because in this way the PCM amount of the systems was comparable. In a specific project, anyhow, the designer can select a different percentage of mixed PCM or a different number of applied layers, according to the needings of the systems that he is analyzing. So, with another PCM amount, the best solution could vary.

Another important consideration regards the impact that the two different technologies of integration may have on the building structure. As reported in the previous chapter, the direct integration of the PCM in the concrete matrix could compromise the compressive mechanical resistance of the concrete, which is its main property. On the other side, with the application of one or more layers on the outside, future significant changes to the building are practically impossible to be done without ruining the thermal systems (even a simple new window could be damaging). As a general recommendation, considering all the features, the suggestions could be the following: if the building to be designed does not have many floors and it is likely to have significant changes in future, then the best solution could be the direct integration of the PCM, in the chosen percentage; otherwise, if the building will have many floors or probably would not have relevant modifications, the applied layers could be the best solutions, in the selected numbers.

8. Conclusions

This thesis aimed to investigate the integration of PCM in concrete thermal energy systems, knowing that the depletion of fossil resources and climate change are increasing the need for sustainable and environmentally friendly solutions. The analyses were focused on improving thermal energy performance, reducing energy consumption, and enhancing the thermal comfort of the considered systems.

The thesis has been articulated in several steps, each one being necessary to the further, so at the end of all the chapters, the main results of the single stage were reported, to have a brief resume of the most important notes.

Thermal storage with and without PCM

As initial stage, a simplified lumped capacitance model, useful to predict the behavior of a concrete thermal storage module, was developed, validated, and proposed. The characteristics of the computing code make this model suitable for the implementation in more complex solar thermal simulation tools and software, allowing for a fair estimation of the energy storable in concrete TES as well as its transient behavior during charging and discharging processes. A unique reference concrete temperature was considered to describe the whole system; obviously it involves a few simplified assumptions, but the model computed accurate values with a computational effort drastically less than that of a more detailed model. It was compared against the data of experimental campaign on two concrete mixtures, achieving a very fine agreement. The model allows also for calculating the actual heat fluxes for a constant monitoring of the TES performance. Finally, two different thermal efficiencies were also proposed: a standard one efficiency and a new modified efficiency, in which the reference value is the true maximum achievable energy. The simulations show that the efficiency enhances with the increase of oil mass flux and time, and it achieves an asymptotic value.

The numerical analysis for large-scale modularized concrete thermal energy storage systems was conducted. The simulations were carried out by means of a

an improved version of the code presented for single concrete TES block. Different arrangements of various elements in series, parallel and mixed configurations were investigated, and their performances were compared, to determine the best configuration as a function of the imposed operating conditions. The exchanged thermal energy was assessed both during the charging and discharging phase, considering both adiabatic and diabatic external surfaces. At fixed total mass flow rate and pressure drop, the number of parallel branches was progressively increased. The number of elements in series for each branch was consequently calculated. The most performant configuration was considered as the first one which exchanges the same amount of energy as the following ones, but with fewer blocks. The oil temperature profiles were also predicted and there are relevant differences between the adiabatic and the diabatic situations. The best modules' configurations in diabatic conditions were the same for the adiabatic simulations but with different overall thermal energy, due to the heat loss to the surroundings. Moreover, in the adiabatic case, after a few hours of operation, the exchanged heat fluxes presented a maximum in the central blocks of the series, the first elements had already been fully charged, so a peak appeared in the middle. In the diabatic case, the heat loss to the surroundings had a significant role and highlighted the differences between the charging and discharging phases. Its presence was not negligible and contributed to a more aware choice of the most suitable system.

After those analyses, the PCM integration has been considered and studied. The analyses have shown how the integration of PCM in the concrete mixture can actually improve the thermal performance of the storage elements, both in heating and cooling stages. The temperature curves are less steep, due to the latent heat absorbed or released during the transition phase. The thermal energy accumulated, in heating, and released, in cooling, visibly increased with the percentage of integrated PCM. The potential of this technology has therefore been proven and is evident, however with the small amounts of PCM used in this study, it is not possible to fully appreciate the storage capabilities of this material. The results showed that the stored and released thermal energy increases with the addition of the PCM, as reported in Tab. 8.1.

The most suitable mixture is not uniquely definable, since several parameters could be considered and that could be prioritized, depending on the situation and the needings. The efficiency and the stored thermal energy, for example, present opposite trends, that could be more relevant in different applications. Nevertheless, also the cost should be considered as one of the main parameters since the integration of PCM also increase the initial cost of the thermal systems,

that could be also not worthy over a predefined limit. It is my opinion that the designer or the customer could have different preferences and necessities that should be carefully considered and evaluated in the specific case, because, as often happens, the best solution could be a good compromise of several aspects.

Table 8.1: Main results

TES type	**Energy in charging**	**Energy in disharging**
-	[MJ]	[MJ]
Basic concrete	60.04	57.35
5% PCM	62.87	60.05
10% PCM	65.33	62.07

CFD simulations of concrete module with PCM

In chapter 6 a new TES type for industrial applications, realized with a concrete matrix with the addition of PCM, was presented and investigated through numerical simulations, based on a previous set of experimental tests. The numerical model was validated with a very good agreement between the simulations and the tests. The experiments studied two different concrete mixtures: a reference one and a PCM added one with a 5% in weight, which was too little to have a significant deviation from the pure concrete behaviour, so different numerical analyses were conducted. The calibrated model was used to simulate the performances of the other two PCM added concrete mixtures with a 20% and a 40% of PCM in weight. The results showed promising features, the two mixtures developed a less steep temperature increase, with advantages in terms of concrete cracking and damaging problems. The integration of high percentages of PCM in the concrete matrix could reduce its compressive strength and other mechanical properties, but it does not involve structural problems for the case study: the TES system is supposed to work as integrated into a real CSP plant, and it only has to support its dead load. For other applications, such as for buildings purposes, or when the mechanical performances of the concrete modules are particularly relevant, a low PCM percentage should be added to the block, because it may increase the risk of mechanical failure and the degradation of the unit.

Finally, a new kind of simulation was implemented, with thermal oil as HTF, both in the heating and the cooling stage, to analyze the performances of a more realistic system that could be implemented in an operative situation. With this solution, the system was able to reach an asymptotic trend in a reasonable

amount of time, consistent with the needs of a real operative scenario. The stored and released thermal energy increased in all the mixtures and also doubled its value with the 40% of PCM. This important achievement demonstrates the great potential and the performance that can be achieved by adding the PCM to the sensible-only concrete TES.

Table 8.2: Main results

Wall type	**Thermal energy**	**Energy increase**
-	[kJ]	[%]
Basic concrete	1482	0%
5% PCM	1683	13.61%
20% PCM	2240	51.20%
40% PCM	2985	101.48%

CFD simulations of different PCM technologies for building walls

After that, the application of PCM to building systems was considered and studied, so the focus moved to different kinds of building concrete walls, considering three different elements: a basic concrete wall, used as reference, a concrete wall with the integration of 10% of PCM and a concrete wall with 2 layers of PCM on the external side. The walls have been studied both as standalone and with the interaction of the surrounding environment. As thermal load, the real temperature profile of a summer day in Padua has been used. The system with 10% of PCM presents a lower temperature compared with the basic one. Considering the wall with two layers, the temperature values are the lowest of the three. A focus was placed also on the transmitted heat flux in the room, which gives thermal comfort information. Both solutions brought a reduction in the loss of thermal power, but the wall with the two layers assured better comfort. Regarding the total transmitted energy during the day, both the solutions lead to a reduction, the system with the two layers overcame a 44% reduction, while the wall with the mixed PCM reached just 32%. The detailed results, considering the total amount of thermal energy transmitted during one day and the reduction in percentage, are reported in Tab 8.3.

Overall, I would assess that the best solution, in terms of temperature and energy transmitted reduction, is the wall with the integration of 2 layers of PCM. The system with the mixed PCM is however well performant and allows for a

better thermal behaviour than the basic concrete wall, but its absolute improvements are less relevant than the solution with the 2 layers. The main comparison regarded the wall with the integration of 10% of PCM and another wall with, because in this way the PCM amount of the systems was comparable. In a specific project the designer can select a different percentage of mixed PCM or a different number of applied layers, according to the needings of the systems that he is analyzing. So, with another PCM amount, the best solution could vary. Another important consideration regards the impact that the two different technologies of integration may have on the building structure. As reported in the previous chapter, the direct integration of the PCM in the concrete matrix could compromise the compressive mechanical resistance of the concrete, which is its main property. On the other side, with the application of one or more layers on the outside, future significant changes to the building are practically impossible to be done without ruining the thermal systems. As a general recommendation, I would suggest that if the building to be designed does not have many floors and it is likely to have significant changes in future, then the best solution could be the direct integration of the PCM, in the chosen percentage; otherwise, if the building will have many floors or probably would not have relevant modifications, the applied layers could be the best solutions, in the selected numbers.

Table 8.3: Main results

Wall type	**Transmitted energy**	**Energy reduction**
-	[kJ/m^2]	[%]
Basic concrete	949,5	0%
10% PCM	648,0	32%
2 layers of PCM	531,3	44%

I put all my effort into this work since I firmly believe that the phase change materials could proficiently help in the thermal development of building systems. The years to come will provide unknown and uncertain energetic deals, but we can act on what we can see now, and at the moment it is of extreme importance to design and adapt building with improved and advanced thermal energy and thermal comfort systems.

8.1 Future developments

The natural prosecution of the work presented in this Ph.D. thesis includes for sure the need for more experimental tests, for all the different PCM technologies since the lack of these could limit the PCM diffusion. In particular, full-scale tests on long-period simulations are needed. More exhaustive investigations were are also necessary, analyzing quantities of PCM much higher than those proposed in this thesis, in order to verify how much the addition of these innovative materials can actually benefit the concrete storage elements.

Also, new analyses regarding other building systems, elements and materials should be considered, in order to have a full understanding of the different types of effects that the integration of PCM could have: for example, ceilings, floors and roofs could also be tested, considering also wood, bricks and stones as structural materials.

The previous integration regards only the so-called "passive" systems, since the PCM are applied to structural elements: however, the PCM can be integrated also into the "active" systems, to improve the HVAC systems' performances. For example, a heat pump could be integrated with PCM storing modules and it could be powered by a photovoltaic plant; in this way, the thermal comfort would be improved, with also the thermal performance, since the storing modules would provide a more efficient heat release.

The energy production from renewable resources would hence be optimized and also the energy consumption would have been reduced. Moreover, the combination of PCM for both structural elements, energy production, and HVAC plants would be particularly interesting and provide better performances for buildings as whole energy systems.

List of publications

International Journal Papers (Q1):

- Martelletto F., Doretti L. and Mancin S. "Numerical simulation through experimental validation of latent and sensible concrete thermal energy storage system", Journal of Energy Storage (2022) 51:104567 (1 citation in Scopus)
- Doretti L., Martelletto F. and Mancin S. "Numerical analyses of concrete thermal energy storage systems: effect of the modules' arrangement", Energy Reports (2020) 6:199-214. (8 citations in Scopus)
- Doretti L., Martelletto F. and Mancin S. "A simplified analytical approach for concrete sensible thermal energy storages simulation", Journal of Energy Storage (2019) 22:68-79. (14 citations in Scopus)

International Conference Papers:

- Martelletto F., Doretti L. and Mancin S. "Numerical simulation of latent and sensible concrete thermal energy storage system", Proceedings of the Conference 13th IIR PCM international conference - PCM2021: Storing Energy can make the Difference (IIR PCM 2021), Vicenza, Italy (2021), 2081.
- Doretti L., Martelletto F. and Mancin S. "A new analytical model for concrete sensible thermal energy storages simulation", Refrigeration Science and Technology: Proceedings of the Conference 25th IIR International Congress of Refrigeration (ICR2019), Montréal, Canada (2019), 1797-1804

Bibliography

Acheampong A. O., "Economic growth, CO2 emissions and energy consumption: what causes what and where?", Energy Econ. 74 (2018), pp. 677–692

Achkari O., El Fadar A., "Latest developments on TES and CSP technologies – Energy and environmental issues, applications and research trends", Applied Thermal Engineering 167 (2020), 114806

Amirifard M., Kasaeian A., Amidpour M., "Integration of a solar pond with a latent heat storage system", Renewable Energy 125 (2018), pp. 682-693

Arora A., Sant G., Narayanan N., "Numerical simulations to quantify the influence of phase change materials (PCMs) on the early- and later-age thermal response of concrete pavements", Cement and Concrete Composites 81 (2017), pp 11-24

Asadi I., Shafigha P., Abu Hassana Z. F. B., Mahyuddina N. B., " Thermal conductivity of concrete – A review", Journal of Building Engineering 20 (2018), pp. 81–93

Athukorallage B., Dissanayaka T., Senadheera S., James D., "Performance analysis of incorporating phase change materials in asphalt concrete pavements", Construction and Building Materials 164 (2018), pp 419-432

Awad M., Muzychka Y., "Effective property models for homogeneous two-phase flows", Exp. Thermal Fluid Sci. 33 (1) (2008), pp 106-113

Bai F., Wang Z., Liye X., "Numerical simulation of flow and heat transfer process of solid media thermal energy storage unit", In: Goswami, D., Zhao, Y. (Eds.), Solar Energy and Human Settlement: Proceedings of ISES Solar World Congress 2007, vol. V. Springer; 2009, pp. 2711–2715 (Chapter 10)

Bai F., Xu C., "Performance analysis of a two-stage thermal energy storage system using concrete and steam accumulator", Appl Therm Eng 31 (2011), pp 2764-2771

Bahrar M., Djamai I., Mankibi M. El, Si Larbi A., Salvia M., "Numerical and experimental study on the use of microencapsulated phase change materials (PCMs) in textile reinforced concrete panels for energy storage", Sustainable Cities and Society 41 (2018), pp 455-468

Balapour M., Mutua A. W., Farnam Y., "Evaluating the thermal efficiency of microencapsulated phase change materials for thermal energy storage in cementitious composites" Cement and Concrete Composites 116 (2021), 103891

Bastani A., Haghighat F., Kozinski J., "Designing building envelope with PCM wallboards: Design tool development", Renewable and Sustainable Energy Reviews 31 (2014), 554-562

Bažant Z. P., Kaplan M. F., "Concrete at high temperature", Burnt Mill, Longman (1996).

Berardi U., Gallardo A. A., "Properties of concretes enhanced with phase change materials for building applications", Energy Build. 199 (2019), pp. 402-414

Bergan P. G. , Greiner C. J., "A new type of large scale thermal energy storage", Energy Procedia 58 (2014), pp. 152-159

Besagni G. , Croci L., "Experimental study of a pilot-scale fin-and-tube phase change material storage", Applied Thermal Engineering 160 (2019), 114089

Boomsma K., Poulikakos D., Zwick F., "Metal foams as compact high performance heat exchangers". Mech Mater 35 (2003), pp. 1161-1176.

Boquera L. , Castro J. R., Pisello A. L., Cabeza L. F., "Research progress and trends on the use of concrete as thermal energy storage material through bibliometric analysis", Journal of Energy Storage 38 (2021), 102562

Brousseau P., Lacroix M., "Numerical simulation of a multi-layer latent heat thermal energy storage system", Int. J. Energy Res. 22 (1) (1998), pp 1-15

Brown T., Javaid M., "The thermal conductivity of fresh concrete", Matériaux Constr 3 (6) (1970), pp. 411–416

Bruch A., Fourmigué J. F., Couturier R., "Experimental and numerical investigation of a pilot-scale thermal oil packed bed thermal storage system for CSP power plant", Solar Energy 105 (2014), pp. 116-125

Bugaje I. M., "Enhancing the thermal response of latent heat storage systems" Int J Energy Res 21 (1997), pp. 759-766

Cabeza L. F., Castell A., Barrenechea C., de Gracia A., Fernández A. I., "Materials used as PCM in thermal energy storage in buildings: A review", Renewable and Sustainable Energy Reviews 15 (2011), pp. 1675-1695

Cabeza L. F., Castellon C., Nogues M., Medrano M., Leppers R., Zubillaga O., "Use of microencapsulated PCM in concrete walls for energy savings", Energy Build 39 (2007), pp. 113-119

Cabeza L. F., Ibanez M., Solè C., Roca J., Noguès M., "Experimentation with a water tank includinga PCM module", Solar Energy Materials & Solar Cells 90 (2006), pp 1273-1282

Cabeza L. F., Navarro L., Pisello A. L., Olivieri L., Bartolomé C., Sánchez J., Álvarez S., Tenorio J. A., "Behaviour of a concrete wall containing microencapsulated PCM after a decade of its construction", Sol. Energy 200 (2020), pp. 108-113

Cao V. D., Pilehvar S., Salas-Bringas C., Szczotok A. M., Valentini L., Carmona M., Rodriguez J. F., Kjøniksen A. L., "Influence of microcapsule size and shell polarity on thermal and mechanical properties of thermoregulating geopolymer concrete for passive building applications", Energy Conversion and Management 164 (2018), pp 198-209

Cárdenas B., León N., "High temperature latent heat thermal energy storage: phase change materials, design considerations and performance enhancement techniques", Renewable and Sustainable Energy Reviews 27 (2013), pp. 724-737

Cascone Y., Capozzoli A., Perino M., "Optimisation analysis of PCM-enhanced opaque building envelope components for the energy retrofitting of office buildings

in Mediterranean climates", Applied Energy 211 (2018), 929-953

Chauhan A., Tyagi V. V., Anand S., Pandey A. K., Sari A., Al-Sulaiman F. A., "Energy Storage by PCM for Building Applications", Handbook of Energy Systems in Green Buildings, Springer (2018), pp. 995-1023

Cimmino M., "Semi-Analytical Method for g-Function Calculation of bore fields with series- and parallel-connected boreholes", Science and Technology for the Built Environment 0 (2019), pp. 1-16

Cocco D., Migliari L., Petrollese M., "A hybrid CSP–CPV system for improving the dispatchability of solar power plants", Energy Conversion and Management 114 (2016), pp. 312-323

Cruickshank C. A., Harrison S. J., "Thermal response of a series- and parallel-connected solar energy storage to multi-day charge sequences", Solar Energy 85 (2011), pp. 180-187

Cui H., Memon S. A., Liu R., "Development, mechanical properties and numerical simulation of macro encapsulated thermal energy storage concrete", Energy Build. 96 (2015), pp. 162–174

Cui H., Tang W., Qin Q., Xing F., Liao W., Wen H., "Development of structural-functional integrated energy storage concrete with innovative macro-encapsulated PCM by hollow steel ball", Appl. Energy 185 (2017), pp. 107–118

Cunha Costa J. A., Martinelli A. E., do Nascimento R. M., Monte Mendes A., "Microstructural design and thermal characterization of composite diatomite-vermiculite paraffin-based form-stable PCM for cementitious mortars", Construction and Building Materials 232 (2020), 117167

D'Alessandro A. , Pisello A. L., Fabiani C., Ubertini F., Cabeza L. F., Cotana F., "Multifunctional smart concretes with novel phase change materials: Mechanical and thermo-energy investigation", Applied Energy 212 (2018), pp. 1448–1461

Das S., Aguayo M., Rajan S. D., Sant G., Neithalath N., "Microstructure-guided numerical simulations to predict the thermal performance of a hierarchical cement-based composite material", Cement and Concrete Composites 87 (2018), pp. 20-28

de Gracia A. and Cabeza L. F., "Phase change materials and thermal energy storage for buildings", Energy and Buildings 103 (2015), pp. 414-419

De Schutter G., Taerwe L., "Specific heat and thermal diffusivity of hardening concrete", Mag. Concr. Res. 47 (172) (1995), pp. 203–208

Dehdezi P. K., Hall M. R., Dawson A. R., Casey S. P., "Thermal, mechanical and microstructural analysis of concrete containing microencapsulated phase change materials", International Journal of Pavement Engineering 14:5 (2013), pp. 449-462

Dehmous M., Franquet E., Lamrous N., "Mechanical and thermal characterizations of various thermal energy storage concretes including low-cost bio-sourced PCM", Energy & Buildings 241 (2021), 110878

Devaux P., Farid M. M., "Benefits of PCM underfloor heating with PCM wallboards for space heating in winter", Appl. Energy 191 (2017), pp. 593–602

Dickinson R. M., Cruickshank C. A., Harrison S. J., "Charge and discharge strategies for a multi-tank thermal energy storage", Applied Energy 109 (2013), pp.366-373

Dinter F., Geyer M., Tamme R., "Thermal energy storage for commercial application (TESCA), a feasibility study on economic storage systems", Berlin, Germany: Springer-Verlag; (1991)

Dittus F. W., Boelter L. M. K., "Heat transfer in automobile radiator of the tubular type", University of California at Berkley Publ. Eng., 2 1930, pp. 443-461

Du Y., Ge Y., " Multiphase Model for Predicting the Thermal Conductivity of Cement Paste and Its Applications", Materials 14 (2021), 4525

Eddhahak-Ouni A., Drissi S., Colin J., Neji J., Care S., "Experimental and multi-scale analysis of the thermal properties of Portland cement concretes embedded with microencapsulated phase change materials (PCMs)", Appl. Therm. Eng. 64 (1) (2014), pp. 32–39

Elias C. N., Stathopoulos V. N., "A comprehensive review of recent advances in materials aspects of phase change materials in thermal energy storage", Energy Procedia 161 (2019), pp. 385–394

Ellingwood B. and Lin T. D., "Flexure and Shear Behavior of Concrete Beams During Fires", J. Struct. Eng. 117 (1991), pp. 440–458

Emam M., Ahmed M., "Cooling concentrator photovoltaic systems using various configurations of phase change material heat sinks", Energy Conversion and Management 158 (2018), pp. 298-314

Essid N., Eddhahak A., Neji J., "Experimental and numerical analysis of the energy efficiency of PCM concrete wallboards under different thermal scenarios", Journal of Building Engineering 45 (2020), 103547

Fabiani C., Pisello A. L., D'Alessandro A., Ubertini F., Cabeza L. F., Cotana F., "Effect of PCM on the Hydration Process of Cement-Based Mixtures: A Novel Thermo-Mechanical Investigation", Materials 11 (2018), 871

Faheem A., Ranzi G., Fiorito F., Lei C., "A numerical study on the thermal performance of night ventilated hollow core slabs cast with micro-encapsulated PCM concrete", Energy and Buildings 127 (2016), pp. 892–906

Fallahi A., Guldentops G., Tao M., Granados-Focil S., Van Dessel S., "Review on solid-solid phase change materials for thermal energy storage: molecular structure and thermal properties", Appl. Therm. Eng. 127 (2017), pp. 1427–1441

Faraj K., Khaled M., Faraj J., Hachem F., Castelain C., "A review on phase change materials for thermal energy storage in buildings: Heating and hybrid applications", Journal of Energy Storage 33 (2021), 101913

Farid M. M., Kim Y., Kanzawa A., "Thermal performance of a heat storage module using PCMs with different melting temperatures: experimental", Journal of Solar Energy Engineering 112 (1990), pp. 125-131

Farid M. M., Khudhair A. M., Razack S. A. K., Al-Hallaj S., "A review on phase change energy storage: materials and applications", Energy Convers. Manag. 45 (2004), pp. 1597-1615

Fathipour R., Hadidi A., "Analytical solution for the study of time lag and decrement factor for building walls in climate of Iran", Energy 134 (2017), pp. 167–180

Ferone C., Colangelo F., Frattini D., Roviello G., Cioffi R., Di Maggio R.,

"Finite element method modelling of sensible heat thermal energy storage with innovative concretes and comparative analysis with literature benchmarks", Energies 7 (2014), pp. 5291-5316

Ferrari L., "I materiali a cambiamento di fase", novembre 2016, Riscaldamento Climatizzazione Idronica (RCI), pp 42-47

Figueiredo A., Lapa J., Vicente R., Cardoso C., "Mechanical and thermal characterization of concrete with incorporation of microencapsulated PCM for applications in thermally activated slabs", Constr. Build. Mater. 112 (2016), 639-647

Fukai J., Hamada Y., Morozumi Y., Miyatake O., "Improvement of thermal characteristics of latent heat thermal energy storage units using carbon-fiber brushes: experiments and modeling", Int J Heat Mass Transfer 46 (2003), pp. 4513–4525

Giannuzzi G. M., Giovannini E., Liberatore R., Mazzei D., Mele D., Crescenzi T., "Analisi sperimentale e numerica del comportamento termodinamico di sistemi di accumulo a calore sensibile in materiali cementizi", ENEA Report RdS/-PAR2014/118 2014, (in Italian, available online)

Giannuzzi G. M., Liberatore R., Mele D., Mazzucco G., Xotta G., Salomoni V. A., Majorana C. E., Di Maggio R., "Experimental campaign and numerical analyses of thermal storage concrete modules", Solar Energy 157 (2017), pp. 596–602

Gibb D., Johnson M., Romaní J., Gasia J., Cabeza L. F., Seitz A., "Process integration of thermal energy storage systems – Evaluation methodology and case studies", Applied Energy 230 (2018), pp. 750-760

Gil A., Medrano M., Martorell I., Làzaro A., Dolado P., Zalba B., Cabeza L. F., "State of the art on high temperature thermal energy storage for power generation. Part 1 - Concepts, materials and modellization", Renewable and Sustainable Energy Reviews 14 (2010), pp. 31-55

Girardi F., Giannuzzi G. M., Mazzei D., Salomoni V., Majorana C., Di Maggio R., "Recycled additions for improving the thermal conductivity of concrete in preparing energy storage systems", Construction and Building Materials 135

(2017), pp. 565-579

Girardi F., Di Maggio R., "Realizzazione e caratterizzazione di un modulo di accumulo basata su mescola sviluppata da UNITN", ENEA Report RdS/-PAR2014/119 2014, (in Italian, available online)

Gnielinki V., "On heat transfer in tubes", International Journal of Heat and Mass Transfer 63 (2013), pp. 134-140

Gobinath S., Senthilkumar G., Beemkumar N., "Comparative study of room temperature control in buildings with and without the use of PCM in walls", Energy Sources, Part A: Recovery, Utilization, and Environmental Effects 40:14 (2018), pp. 1765-1771

Grassl P., Xenos D., Nystrom U., Rempling R., Gylltoft K., "CDPM2: A damage-plasticity approach to modelling the failure of concrete", International journal of solid and structures 50 (2013), pp. 3805-3816

Guarino F., Athienitis A., Cellura M., Bastien D., "PCM thermal storage design in buildings: Experimental studies and applications to solaria in cold climates", Applied Energy 185 (2017), pp. 95-106

Gyuyong K., Euibae L., Youngsun K., Baesu K., "Hydration Heat and Autogenous Shrinkage of High-Strength Mass Concrete Containing Phase Change Material", Journal of Asian Architecture and Building Engineering 9:2 (2010), pp. 455-462

Haller M. Y., Cruickshank C. A., Streicher W., Harrison S. J., Andersen E., Furbo S., "Methods to determine stratification efficiency of thermal energy storage processes – Review and theoretical comparison", Solar Energy 83 (2009), pp.1847-1860

Hamdani H., Rizal S., Riza M., "Numerical simulation analysis on the thermal performance of a building walls incorporating Phase Change Material (PCM) for thermal management", IOP Conf. Series: Materials Science and Engineering 434 (2018), 012186

Hausen H., "Naherungsverfahren zur berechnung des warmeaustausches in regeneratoren" (1931), (in German)

Hawes D. W., Feldman D., Banu D., "Latent heat storage in building materials", Energy Build 20 (1993), pp. 77-86

Hawes D. W., "Latent heat storage in concrete", PhD Thesis, Concordia University, Montreal, Quebec, Canada (1991)

Hawlader M. N., Uddin M. S, Zhu H. J., "Encapsulated phase change materials for thermal energy storage: experiments and simulation", Int J Energy Res 26 (2002), pp. 159-171

Herrmann U., Kearney D. W., "Survey of thermal energy storage for parabolic trough power plants", Journal of Solar Energy Engineering 124(2) (2002), pp. 145-52

Hoivik N., Greiner C., Barragan J., Crespo Iniesta A., Skeie G., Bergan P., Blanco-Rodriguez P., Calvet N., "Long-term performance results of concrete-based modular thermal energy storage system", Journal of Energy Storage 24 (2019), 100735

Howlader M. K., Rashid M. H., Mallick D., Haque T., "Effects of aggregate types on thermal properties of concrete", ARPN Journal of Engineering and Applied Sciences 7 (7) (2012), pp. 900–906

Huang X., Zhu C., Lin Y., Fang G., "Thermal properties and applications of microencapsulated PCM for thermal energy storage: A review", Applied Thermal Engineering 147 (2019), pp. 841-855

Huang H., Xiao Y., Lin J., Zhou T., Liu Y., Zhao Q., "Improvement of the efficiency of solar thermal energy storage systems by cascading a PCM unit with a water tank", Journal of Cleaner Production 245 (2020), 118864

Hunger M., Entrop A. G., Mandilaras I., Brouwers H. J. H., Founti M., "The behavior of self-compacting concrete containing micro-encapsulated phase change materials" Cem Concr Compos 31 (2009), pp. 731–743

Islam M. R., Tarefder R. A., "Determining thermal properties of asphalt concrete using field data and laboratory testing", Constr. Build. Mater. 67 (2014), pp. 297–306.

Jankowiak T., Lodygowski T., "Identification of parameters of concrete dam-

age plasticity constitutive model", Foundations of civil and environmental engineering 6 (2005)

Jeong S. G., Jeon J., Cha J., Kim J., Kim S., "Preparation and evaluation of thermal enhanced silica fume by incorporating organic PCM, for application to concrete", Energy Build. 62 (2013), pp. 190–195

Jeong S. G., Jeon J., Lee J. H., Kim S., "Optimal preparation of PCM/diatomite composites for enhancing thermal properties", International Journal of Heat and Mass Transfer 62 (2013), pp. 711-717

Jian Y., Bai F., Falcoz Q., Xu C., Wang Y., Wang Z., "Thermal analysis and design of solid energy storage systems using a modified lumped capacitance method", Applied Thermal Engineering 75 (2015), pp. 213-223

Jin X., Medina M. A., Zhang X., "Numerical analysis for the optimal location of a thin PCM layer in frame walls", Appl Therm Eng 103 (2016), pp. 1057–1063

Jouhara H., Zabnienska-Gora A., Khordehgah N.,. Ahmad D, Lipinski T., "Latent thermal energy storage technologies and applications: A review", Int. J. Thermofluids. 5–6 (2020), 100039

Kalifa P., Menneteau F. D., Quenard D., "Spalling and pore pressure in HPC at high temperatures", Cement and Concrete Research 30 (2000), pp. 1915-1927

Keshavarz A., Mehrabian M. A., Abolghasemi M., Mostafavi A., "Availability (exergy) analysis in a thermal energy storage system with the phase change materials arranged in series", Proc. IMechE Vol. 225 Part A: J. Power and Energy (2010), pp. 44-52

Kheradmand M., Azenha M., de Aguiar J. L. B., Castro-Gomes J., "Experimental and numerical studies of hybrid PCM embedded in plastering mortar for enhanced thermal behaviour of buildings", Energy 94 (2016), 250-261

Kim J. S., Darkwa K., "Simulation of an integrated PCM–wallboard system", Int. J. Energy Res. 27 (2003), 215-223

Konuklu Y., Ostry M., Paksoy H. O., Charvat P., "Review on using microencapsulated phase change materials (PCM) in building applications", Energy and Buildings 106 (2015), pp. 134-155

Koschenz M., Lehmann B., "Development of a thermally activated ceiling panel with PCM for application in lightweight and retrofitted buildings", Energy and Buildings 36 (2004), 567-578

Krese G., Butala V., Stritih U., "Thermochemical seasonal solar energy storage for heating and cooling of buildings", Energy and Buildings 164 (2018), pp. 239–253

Kupfer H., Hilsdorf H. K., Rusch H., "Behavior of concrete under biaxial stresses", ACI Journal 65 (1979), pp. 656-666

Kuravi S., Trahan J., Goswami D. Y., Rahman M. M., Stefanakos E. K., "Thermal energy storage technologies and systems for concentrating solar power plants", Progress in Energy and Combustion Science 39 (2013), pp. 285-319

Kuznik F., Virgon J., Noel J., "Optimization of a phase change material wallboard for building use", Applied Thermal Engineering 28 (2008), pp. 1291-1298

Kuznik F., Virgon J., Noel J., "Experimental investigation of wallboard containing phase change material: Data for validation of numerical modeling", Energy and Buildings 41 (2009), pp. 561-570

Kuznik F., Lopez J. P. A., Baillis D., Johannes K., "Design of a PCM to air heat exchanger using dimensionless analysis: Application to electricity peak shaving in buildings", Energy and Buildings 106 (2015), pp. 65-73

Kuznik F., Johannes K., David D., "Integrating phase change materials (PCMs) in thermal energy storage systems for buildings. In: Cabeza, L.F. (Ed.)", Woodhead Publishing Series in Energy. Advances in Thermal Energy Storage Systems, 2015, pp. 325-353

Laing D., Steinmann W., Tamme R., Richter C., "Solid media thermal storage for parabolic trough power plants", Solar Energy 80 (2006), pp. 1283–1289

Laing D., Steinmann W., Fiss M., Tamme R., Brand T., Bahl C., "Solid media thermal storage development and analysis of modular storage operation concepts for parabolic trough power plants", Journal of Solar Energy Engineering – Trans ASME 130 (2008), 011006-1-5

Laing D., Lehmann D., Fiss M., Bahl C., "Test Results of Concrete Thermal

Energy Storage for Parabolic Trough Power Plants", Journal of Solar Energy Engineering 131 (2009) pp. 41007 1-6

Laing D., Bahl C., Bauer T., Fiss M., Breidenbach N., Hempel M., "High-temperature solid-media thermal energy storage for solar thermal power plants" Proceedings of the IEEE; Vol. 100, No. 2, (2012)

Laing D., Bahl C., Bauer T., Lehmann D., Steinmann W. D., "Thermal energy storage for direct steam generation", Solar Energy 85 (2011), pp. 627-633

Lamberg P., Lehtiniemi R., Henell A., "Numerical and experimental investigation of melting and freezing processes in phase change material storage", Int J Therm Sci 43 (2004), pp. 277-87

Lane G. A.; "Solar Heat Storage: Latent Heat Material - Volume I: Background and Scientific Principles" CRC Press, Florida (1983)

Landi F. F. D. A., Fabiani C., Pisello A. L., "Palm oil for seasonal thermal energy storage applications in buildings: the potential of multiple melting ranges in blends of bio-based fatty acids", J. Energy Storage 29 (2020), 101431

Lassandro P., Turi S. D., "Energy efficiency and resilience against increasing temperatures in summer: the use of PCM and cool materials in buildings", International Journal of Heat and Technology 35, Special Issue 1 (2017), pp. S307-S315

Leang E., Tittelein P., Zalewski L., Lassue S., "Numerical study of a composite Trombe solar wall integrating microencapsulated PCM", Energy Procedia 122 (2017), pp. 1009-1014

Leccese F., Salvadori G., Asdrubali F., Gori P., "Passive thermal behaviour of buildings: Performance of external multi-layered walls and influence of internal walls", Appl Energy 225 (2018), pp. 1078–1089

Lee J., Fenves G. L., " Plastic-damage model for cyclic loading of concrete structures", J. Eng. Mech. 124 (1998), pp. 892-900

Leite da Cunha S. R., Barroso de Aguiar J. L., "Phase change materials and energy efficiency of buildings: A review of knowledge", Journal of Energy Storage 27 (2020), 101083

Li P., Van Lew J., Chan C., Karaki W., Stephens J., O'Brien J. E., "Similarity and generalized analysis of efficiencies of thermal energy storage systems", Renewable Energy 39 (2012), pp. 388-402

Li P. , Xu B., Han J., Yang Y., "Verification of a model of thermal storage incorporated with an extended lumped capacitance method for various solid–fluid structural combinations", Solar Energy 105 (2014), pp. 71-81

Li C., Yu H., Song Y., Experimental investigation of thermal performance of microencapsulated PCM-containe d wallboard by two measurement modes, Energy Build. 184 (2019), pp. 34–43

Li C., Wang M., Xi B., Ma H, Chen J., "Enhanced properties of diatomite-based composite phase change materials for thermal energy storage", Renewable Energy 147 (2020) pp. 265-274.

Lindner F., "Latentwärmespeicher - Teil 1: Physikalisch-technische Grundlagen. Brennst", Wärme-Kraft 36 (1984), Nr. 7-8

Ling T. C., Poon C. S., "Use of phase change materials for thermal energy storage in concrete: An overview", Construction and Building Materials 46 (2013), pp. 55–62

Liu M., Saman W., Bruno F., "Review on storage materials and thermal performance enhancement techniques for high temperature phase change thermal storage systems", Renewable and Sustainable Energy Reviews 16 (2012), pp. 2118-2132

Lubliner J. J., Oliver S. O., Oñate E., "A plastic-damage model for concrete", International Journal of Solids and Structures 25 (1989), pp. 229-326

Lucio-Martin T., Roig-Flores M., Izquierdo M., Alonso M. C., "Thermal conductivity of concrete at high temperatures for thermal energy storage applications: Experimental analysis", Solar Energy 214 (2021), pp. 430-442

Luenberger D. G., "Linear and Nonlinear Programming", Addison–Wesley Publishing Company (1984), Reading, Mass

Macias J. D., Gutierrez-Razo R. A., Garcia-Lara H. D., Cervantes-Alvarez F., Bante-Guerra J., Ares-Muzio O., Romero-Paredes H., Leon N., Arancibia-Bulnes

C. A., Villafan-Vidales H. I., Ramos-Sanchez V., Alvarado-Gil J. J., "Thermal characterization of soda lime silicate glass-graphite composites for thermal energy storage", Journal of renewable and sustainable energy 10 (2018), 024701

Madad A., Mouhib T., Mouhsen A., "Phase Change Materials for Building Applications: A Thorough Review and New Perspectives", Buildings 8 (2018), pp. 63-79

Mahon H., O'Connor D., Friedrich D., Hughes B., "A review of thermal energy storage technologies for seasonal loops", 239 (2022), 12220

Marchi S., Pagliolico S., Sassi G., "Characterization of panels containing micro-encapsulated Phase Change Materials", Energy Conversion and Management 74 (2013), pp. 261-268

Martins M., Villalobos U., Delclos T., Armstrong P., Bergan P. G., Calvet N., "New concentrating solar power facility for testing high temperature concrete thermal energy storage", Energy Procedia 75 (2015), pp. 2144-2149

Matera N., Bevilacqua P., Arcuri N., Oliveti G., Mazzeo D., Romagnoni P., "Optimal design of PCM in internal walls for nZEB buildings", PRIN – Project of National Interest funded by Italian Ministry MIUR, 978-1-5386-5186-5, 2018 IEEE

Mazzucco G., Xotta G., V. A. Salomoni, M. Giannuzzi, C. Maiorana, "Solid thermal storage with PCM materials. Numerical investigations", Applied Thermal Engineering 124 (2017), pp. 545–559

Mazzucco G., Xotta G., Salomoni V. A., Majorana C. E., Giannuzzi G. M., Miliozzi A., "Modeling Techniques of Storage Moduleswith PCM Microcapsules: Case Study", J. Energy Eng. (2018), 144(1): 05017005

Mazzucco G., Majorana C., Salomoni V., Xotta G., "Aggregate behaviour in concrete materials under hightemperature conditions", MATEC Web of Conferences 6, 05008 (2013)

Mazzucco G., Xotta G., Majorana C. E., "Progettazione termomeccanica, realizzazione e caratterizzazione di un modulo di accumulo in materiale cementizio. Simulazioni ed analisi dei dati sperimentali", ENEA Report RdS/PAR2014/120

2014, (in Italian, available online)

Mehling H., Cabeza L., "Heat and Cold Storage with PCM", 2008, Springer

Memon S. A., Cui H., Lo T. Y., Li Q., "Development of structural–functional integrated concrete with macro-encapsulated PCM for thermal energy storage", Appl. Energy 150 (2015), pp. 245–257

Medrano M., Gil A., Martorell I., Potau X., Cabeza L. F., "State of the art on high-temperature thermal energy storage for power generation. Part 2 - Case studies", Renewable and Sustainable Energy Reviews 14 (2010), pp. 56-72

Meshgin P., Xi Y., "Multi-scale composite models for the effective thermal conductivity of PCM-concrete", Construction and Building Materials 48 (2013), pp. 371–378

Michels H., Pitz-Paal R., "Cascaded latent heat storage for parabolic trough solar power plants" Sol Energy 81 (2007), pp 829–837

Miliozzi A., Chieruzzi M., Torre L., "Experimental investigation of a cementitious heat storage medium incorporating a solar salt/diatomite composite phase change material", Applied Energy 250 (2019), pp. 1023–1035

Minkowycz W. J., Sparrow E. M., Schneider G. E., Pletcher R. H., "Handbook of Numerical Heat Transfer", Wiley, New York (1988)

Mohaine S., Feliu J., Grondin F., Karkri M., Loukili A., "Multiscale modelling for the thermal creep analysis of PCM concrete", Energy and Buildings 131 (2016), pp. 99–112

Nomura T., Okinaka N., Akiyama T., "Impregnation of porous material with phase change material for thermal energy storage", Materials Chemistry and Physics 115 (2009); pp. 846-850

Noro M., Lazzarin R. M., Busato F., "Solar cooling and heating plants: An energy and economic analysis of liquid sensible vs. phase change material (PCM) heat storage", Int. J. Refrig. 39 (2014), pp. 104–116

Opolot M., Zhao C., Liu M., Mancin S., Bruno F., Hooman K., " Influence of cascaded graphite foams on thermal performance of high temperature phase

change material storage systems", Applied Thermal Engineering 180 (2020), 11561

Osterman E., Tyagi V. V., Butala V., Rahim N. A., Stritih U., "Review of PCM based cooling technologies for buildings", Energy and Buildings 49 (2012), pp. 37-49

Othuman M. A., Wang Y., "Elevated-temperature thermal properties of lightweight foamed concrete", Constr. Build. Mater. 25 (2) (2011), pp. 705–716

Ozger O. B., Girardi F., Giannuzzi G. M., Salomoni V. A., Majorana C. E., Fambri L., Baldassino N., Di Maggio R., "Effect of nylon fibres on mechanical and thermal properties of hardened concrete for energy storage systems", Materials & Design 51 (2013), pp. 989–997

Parameshwaran R., Naresh R., Vinayaka Ram V., Srinivas P. V., "Microencapsulated bio-based phase change material-micro concrete composite for thermal energy storage", Journal of Building Engineering 39 (2021), 102247

Park J. H., Jeon J., Lee J., Wi S., Yun B. Y., Kim S., "Comparative analysis of the PCM application according to the building type as retrofit system", Building and Environment 151 (2019), 291-302

Patel J. H., Qureshi M. N., Darji P. H., "Experimental analysis of thermal energy storage by phase change material system for cooling and heating applications", Mater. Today Proc. 5 (2018), pp. 1490–1500

Pielichowska K., Pielichowski K., "Phase change materials for thermal energy storage", Progress in Materials Science 65 (2014), pp 67-123

Piselli C., Lucia V., Laura A., "How to enhance thermal energy storage effect of PCM in roofs with varying solar reflectance: experimental and numerical assessment of a new roof system for passive cooling in different climate conditions", Solar Energy 192 (2018), pp. 106-119

Pomianowski M., Heiselberg P., Zhang Y., "Review of thermal energy storage technologies based on PCM application in buildings", Energy Build. 67 (2013), pp. 56-69

Pomianowski M., Heiselberg P., Jensen R. L., Cheng R., Zhang Y., "A new experimental method to determine specific heat capacity of inhomogeneous con-

crete material with incorporated microencapsulated-PCM", Cement and Concrete Research 55 (2014), pp. 22-34

Poole M. R., Shah S. B., Boyette M. D., Stikeleather L. F., Cleveland T., "Performance of a coupled transpired solar collector — Phase change material-based thermal energy storage system", Energy Build. 161 (2018), pp. 72–79

Prieto C., Cooper P., Fernández A. I., Cabeza L. F., "Review of technology: Thermochemical energy storage for concentrated solar power plants", Renewable and Sustainable Energy Reviews 60 (2016), pp. 909–929

Prieto C., Fernàndez A. G., Pérez-Osorio D., Cabeza L. F., "Thermal and mechanical degradation assessment in refractory concrete as thermal energy storage container material in concentrated solar plants", Journal of Energy Storage 40 (2021), 102790

Putra N., Rawi S., Amin M., Kusrini E., Kosasih E. A., Mahlia T., "Preparation of beeswax/multi-walled carbon nanotubes as novel shape-stable nanocomposite phase change material for thermal energy storage", J. Energy Storage 21 (2019), pp. 32–39

Py X., Olives R., Mauran S., "Paraffin/porous graphite-matrix composite as a high and constant power thermal storage material", Int J Heat Mass Transfer 44 (2001), pp. 2727-2737

Qian T., Li J., Min X., Deng Y., Guan W., Ning L., "Diatomite: A promising natural candidate as carrier material for low, middle and high temperature phase change material", Energy Conversion and Management 98 (2015), pp. 34-45

Rabani M., Rabani M., "Heating performance enhancement of a new design trombe wall using rectangular thermal fin arrays: an experimental approach", J. Energy Storage 24 (2019), 100796

Rafi M. M. and Nadjai A., "Analytical Behaviors of Steel and CFRP Reinforced Concrete Beams in Fire", Journal of ASTM International 7 (8) (2010)

Rao V. V., Parameshwaran R., Ram V. V., "PCM-mortar based construction materials for energy efficient buildings: A review on research trends", Energy and Buildings 158 (2018), pp. 95-122

Rao Z., Zhang G., Xu T., Hong K., "Experimental study on a novel form-stable phase change materials based on diatomite for solar energy storage", Solar Energy Materials and Solar Cells 182 (2018) pp., 52-60.

Rathore P. K. S., Shukla S. K., Gupta N. K., "Potential of microencapsulated PCM for energy savings in buildings: A critical review", Sustain. Cities Soc. 53 (2020), 101884

Rathore P. K. S., Gupta N. K., Yadav D., Shukla S. K., Kaul S., "Thermal performance of the building envelope integrated with phase change material for thermal energy storage: an updated review", Sustainable Cities and Society 79 (2022), 103690

Reinhardt H. W., Blaauwendraad J., Jongedijk J., "Temperature development in concrete structures taking account of state dependent properties", Int. Conf. Concr. Early Ages (1982)

Rezaei E., Barbato M., Ortona A., Haussener S., "Design and optimization of a high-temperature latent heat storage unit", Applied Energy 261 (2020), 114330

Richardson M. J. and Woods A. W.," An analysis of phase change material as thermal mass", Proceedings of the Royal Society of London A: Mathematical, Physical and Engineering Sciences 464, The Royal Society (2008), pp. 1029-1056

Righetti G., Zilio C., Longo G. A., Hooman K., Mancin S., virgExperimental study on the effect of metal foams pore size in a phase change material based thermal energy storage tube, Applied Thermal Engineering 217 (2022), 119163

Rodat S., Bruch A., Dupassieux N., El Mourchid N., "Unique Fresnel demonstrator including ORC and thermocline direct thermal storage: operating experience", Energy Procedia 69 (2015), pp. 1667-1675

Rodríguez J. M., Sánchez D., Martínez G. S., Bennouna E. G., Ikken B., "Techno-economic assessment of thermal energy storage solutions for a 1 MWe CSP-ORC power plant" Solar Energy 140 (2016), pp. 206-218

Rosato A., Ciervo A., Ciampi G., Scorpio M., Sibilio S., "Impact of seasonal thermal energy storage design on the dynamic performance of a solar heating system serving a small-scale Italian district composed of residential and school

buildings", Journal of Energy Storage 25 (2019), 100889

Roy S., Das B., Biswas A., Debnath B. K., "Energy and Exergy Analysis of a Concrete-Based Thermal Energy Storage System", J. Inst. Eng. India Ser. C 2020

Salomoni V. A., Majorana C. E., Giannuzzi G. M., Miliozzi A., Di Maggio R., Girardi F., Mele D., Lucentini M., "Thermal storage of sensible heat using concrete modules in solar power plants", Solar Energy 103 (2014), pp. 303-315

Sarbu I., Sebarchievici C., "A comprehensive review of thermal energy storage, Sustainability", 10 (2018), 191

Sari A., Bicer A., Al-Sulaiman F. A., Karaipekli A., Tyagi V. V., "Diatomite/C-NTs/PEG composite PCMs with shape-stabilized and improved thermal conductivity: Preparation and thermal energy storage properties", Energy and Buildings 164 (2018), pp. 166-175

Šavija B., Zhang H., Schlangen E., "Influence of Microencapsulated Phase Change Material (PCM) Addition on (Micro) Mechanical Properties of Cement Paste", Materials 10 (2017), 863

Schindler A. K., Folliard K. J., "Influence of supplementary cementing materials on the heat of hydration of concrete" Adv. Cem. Concr. IX Conf. Copp. Mt. Conf. Resort Colo (2003)

Schmidt F. W., Willmott A. J., "Thermal energy storage and regeneration", McGraw-Hill, New York, NY, (1981)

Shang B., Hu J., Hu R., Cheng J., Luo X., "Modularized thermal storage unit of metal foam/paraffin composite", International Journal of Heat and Mass Transfer 125 (2018), pp. 596-603

Sharifi N. P., Freeman G. E., Sakulich A. R., "Using COMSOL modeling to investigate the efficiency of PCMs at modifying temperature changes in cementitious materials – case study", Constr. Build. Mater. 101 (2015), 965-974

Sharma A., Tyagi V., Chen C., Buddhi D., "Review on thermal energy storage with phase change materials and applications", Renewable Sustainable Energy Rev. 13 (2) (2009) pp 318-345

Shafigh P., Asadi I., Mahyuddin N. B., "Concrete as a thermal mass material for building applications - A review", Journal of Building Engineering 19 (2018), pp. 14-25

Shen Y., Liu S., Zeng C., Zhang Y., Li Y., Han X., Yang L., Yang X., "Experimental thermal study of a new PCM-concrete thermal storage block (PCM-CTSB)", Construction and Building Materials 293 (2021), 123540

Shi J., Chen Z., Shao S., Zheng J., "Experimental and numerical study on effective thermal conductivity of novel form-stable basalt fiber composite concrete with PCMs for thermal storage", Applied Thermal Engineering 66 (2014), 156-161

Shin K. Y., Kim S. B., Kim J. H., Chung M., Jung P. S., "Thermo-physical properties and transient heat transfer of concrete at elevated temperatures", Nucl. Eng. Des. 212 (1) (2002), pp. 233–241

Shukla A., Buddhi D., Sawhney R. L., "Thermal cycling test of few selected inorganic and organic phase change materials", Renew Energy 33 (2008), pp. 2606-2614

Schumann T. E. W., "Heat transfer: a liquid flowing through a porous prism", J. Franklin Inst, 208 (3) (1929), pp. 405-416

Silva T., Vicente R., Soares N., Ferreira V., "Experimental testing and numerical modelling of masonry wall solution with PCM incorporation: A passive construction solution", Energy and Buildings 49 (2012), 235-245

Simo J. C., Hughes T. J. R., "Computational Inelasticity", Springer (1998)

Soares N., Costa J. J., Gaspar A. R., Santos P., "Review of passive PCM latent heat thermal energy storage systems towards buildings' energy efficiency", Energy and Buildings 59 (2013), 82-103

Sohag K., Begum R. A., Syed Abdullah S. M., Jaafar M., "Dynamics of energy use, technological innovation, economic growth and trade openness in Malaysia", Energy 90 (2015), pp. 1497–1507

Souayfane F., Fardoun F., Biwole P. H., "Phase change materials (PCM) for cooling applications in buildings: A review", Energy and Buildings 129 (2016), pp. 396-431

Sragovich D., "Transient analysis for designing and predicting operational performance of a high temperature sensible thermal energy storage system" Solar Energy 49 (1989), pp. 7-16

Srinivas Shastri S. and Allen R. M., "Method of lines and enthalpy method for solving moving boundary problems", International Communications in Heat and Mass Transfer 25 (4) (1998), pp 531-540

Srinivasaraonaik B., Sinha S., Singh L. P., "Studies on microstructural and thermo-physico properties of microencapsulated eutectic phase change material incorporated pure cement system", Journal of Energy Storage 35 (2021), 102318

Stritih U., Butala V., "Energy saving in building with PCM cold storage", Int. J. Energy Res. 31 (2007), 1532-1544

Stritih U., Tyagi V. V., Stropnik R., Paksoy H., Haghighat F., Joybari M. M., "Integration of passive PCM technologies for net-zero energy buildings", Sustainable Cities and Society 41 (2018), 286-295

Stückle A., Laing D., Müller-Steinhagen H., "Numerical simulation and experimental analysis of a modular storage system for direct steam generation", Heat Transfer Engineering 35(9) (2014), pp. 812-821

Suárez C., Pino F. J., Guerra J., "A new simplified model for the unsteady response of concrete passive sensible TES systems", Journal of Energy Storage 27 (2020), 101042

Sun X., Medina M. A., Lee K. O., Jin X., "Laboratory assessment of residential building walls containing pipe-encapsulated phase change materials for thermal management", Energy 163 (2018), pp. 383–391

Suresh C., Saini R. P., "Experimental study on combined sensible-latent heat storage system for different volume fractions of PCM", Solar Energy 212 (2020), pp. 282-296

Tamme R., Laing D., Steinmann W. D., "Advanced thermal energy storage technology for parabolic trough", Journal of Solar Energy Engineering 126 (2004), pp. 794-800

Tanyildizi H., Marani A., Türk K., Nehdi M. L., "Hybrid deep learning model

for concrete incorporating microencapsulated phase change materials", Construction and Building Materials 319 (2022), 126146

Tu T. W., and Lee S. Y., "Analytical Solution of Heat Conduction for Hollow Cylinders with Time-Dependent Boundary Condition and Time-Dependent Heat Transfer Coefficient", Journal of Applied Mathematics (2015), article ID 203404

Tyagi V. V., Buddhi D., "PCM thermal storage in buildings: A state of art", Renewable and Sustainable Energy Reviews 11 (2007), pp. 1146-1166

Tyagi V. V., Kaushik S. C., Tyagi S. K., Akiyama T., "Development of phase change materials based micro-encapsulated technology for buildings: A review", Renewable and Sustainable Energy Reviews 15 (2011), pp. 1373-1391

Vanaga R., Blumberga A., Freimanis R., Mols T., Blumberga D., "Solar facade module for nearly zero energy building", Energy 157 (2018), pp. 1025–1034

Venegas-Reyes E., Ortega-Avila N., Rodríguez-Muñoz N. A., Nájera-Trejo M., Martín-Domínguez I. R., Ibarra-Bahena J., "Parametric Methodology to Optimize the Sizing of Solar Collector Fields in Series-Parallel Arrays", Processes 7 (2019), 294

Vigneshwaran K., Singh Sodhi G., Muthukumar P., Subbiah S., "Concrete based high temperature thermal energy storage system: Experimental and numerical studies", Energy Conversion and Management 198 (2019), 111905

Voller V., Swaminathan C., Thomas B., "Fixed grid techniques for phase change problems: a review", Int. J. Numer. Meth. Eng. 30 (4) (1990), pp 875-898

Waqas A., Din Z. U., "Phase change material (PCM) storage for free cooling of buildings - A review", Renewable and Sustainable Energy Reviews 18 (2013), pp. 607-625

Wang M., Pan N., "Predictions of effective physical properties of complex multiphase materials", Mater. Sci. Eng. R: Rep. 63 (1) (2008), pp 1-30

Wang Q., Zhao C. Y., "Parametric investigations of using a PCM curtain for energy efficient buildings", Energy and Buildings 94 (2015), pp. 33-42

Wang X., Li W., Luo Z., Wang K., Shah S. P., "A critical review on phase change materials (PCM) for sustainable and energy efficient building: Design, characteristic, performance and application", Energy & Buildings 260 (2022), 111923

Wen R., Zhang X., Huang Z., Fang M., Liu Y., Wu X., Min X., Gao W., Huang S., "Preparation and thermal properties of fatty acid/diatomite form-stable composite phase change material for thermal energy storage", Solar Energy Materials and Solar Cells 178 (2018), pp. 273-279

Wu H., Wang S., Zhu D., Ding Y., "Numerical analysis and evaluation of an open-type thermal storage system using composite sorbents", International Journal of Heat and Mass Transfer 52 (2009), pp. 5262–5265

Wu M., Li M., Xu C., He Y., Tao W., "The impact of concrete structure on the thermal performance of the dual-media thermocline thermal storage tank using concrete as the solid medium", Applied Energy 113 (2014), pp. 1363-1371

Xotta G., Mazzucco G., Salomoni V. A., Majorana C. E., Willam K. J., "Composite behavior of concrete materials under high temperatures", International Journal of Solids and Structures 64–65 (2015), pp. 86–99

Xotta G., Salomoni V. A., Majorana C. E., "Thermo-hygro mechanical meso-scale analysis of concrete as a viscoelastic-damaged material", Engineering Computations (2013), 30 (5) 17090567, pp. 728-750

Xu B., Li P. W., Chan C. L., "Extending the validity of lumped capacitance method for large Biot number in thermal storage application", Solar Energy 86 (2012), pp. 1709-1724

Xu B., Li Z., "Paraffin/diatomite composite phase change material incorporated cement-based composite for thermal energy storag", Applied Energy (2013) 105, pp. 229-237.

Yang L., Jin X., Zhang Y., Du K., "Recent development on heat transfer and various applications of phase-change materials", J Clean Prod 287 (2021), 124432

Yifen Q., Jiang N., Wei W., Zhang G., Baoliang X., "Heat transfer of heat sinking vest with phase-change material", Chin. J. Aeronaut. 24 (6) (2011), pp

720-725

Yongtai H., Lixian X., Yaohua Y., "Study on design and thermal characteristics of vacuum tube solar collector intubated with heat storage tub", International Journal of Energy Research 43(13) (2019), pp. 7409-7420

Yu H., Li C., Zhang K., Tang Y., Song Y., Wang M., "Preparation and thermophysical performance of diatomite-based composite PCM wallboard for thermal energy storage in buildings", Journal of Building Engineering 32 (2020), 101753

Yun H. D., Ahn K. L., Jang S. J., Khil B. S., Park W. S., Kim S. W., "Thermal and Mechanical Behaviors of Concrete with Incorporation of Strontium-Based Phase Change Material (PCM)", International Journal of Concrete Structures and Materials 13:18 (2019)

Zalba B., Marín J. M., Cabeza L. F., Mehling H., "Review on thermal energy storage with phase change: materials, heat transfer analysis and applications", Applied Thermal Engineering 23 (2003), pp. 251-283

Zhang D., Li Z., Zhou J., Wu K., "Development of thermal energy storage concrete", Cem. Concr. Res. 34 (6) (2004), pp. 927-934

Zhang H., Baeyens J., Cáceres G., "Concentrated solar power plants: Review and design methodology", Renewable and Sustainable Energy Reviews 22 (2013), pp. 466-481

Zhang H., Baeyens J., Cáceres G., Degrève J., Lv Y., "Thermal energy storage: Recent developments and practical aspects", Progress in Energy and Combustion Science 5353 (2016), pp. 1-40

Zhang Y. P., Lin K. P., Yang R., Di H. F., Jiang Y., "Preparation, thermal performance and application of shape stabilized PCM in energy efficient buildings" Energy Build 38 (2006), pp. 1262-1269

Zhang Z., Shi G., Wang S., Fang X., Liu X., "Thermal energy storage cement mortar containing n-octadecane/ expanded graphite composite phase change material", Renew. Energy 50 (2013), pp. 670–675

Zhou Z. W., "Analytical solution for transient heat conduction in hollow cylinders containing well-stirred fluid with uniform heat sink", International Journal

of Heat and Mass Transfer 38 (1995), pp. 2915-2919

Zhou D., Zhao C. Y., "Experimental investigations on heat transfer in phase change materials (PCMs) embedded with porous materials", Applied Thermal Engineering 31 (2011), pp. 970-977

Zhou D., Zhao C. Y., Tian Y., "Review on thermal energy storage with phase change materials (PCMs) in building applications", Applied Energy 92 (2012), pp 593-605

Zhou G. B., Zhang Y. P., Lin K. P., Xiao W., "Thermal analysis of a direct-gain room with shape-stabilized PCM plates", Renew. Energy 33 (2008), pp. 1228-1236

Appendix A: codes

Listing 8.1: UDF Temperature profile

```
#include "udf.h"

DEFINE_PROFILE(unsteady_temperature, thread, position)
{
  face_t f;
  real t = CURRENT_TIME;

  begin_f_loop(f, thread)
  {
    F_PROFILE(f, thread, position) = 301.0+7.0*sin
       (2.0*3.14/86400.0*t+25200.0);
  }
  end_f_loop(f, thread)
}
```

Listing 8.2: Script of the ISO 13786:2017 norm

```
%UNI EN ISO 13786

% Convection
Ri=0.13;
Re=0.04;

%cls
lambdacls=1.6;
rhocls=2350;
ccls=607;
tau_0=86400;
scls=0.3;

Z_cls=matriceZ(ccls,lambdacls,rhocls,tau_0,scls);

%insulating
```

```
lambdaiso=0.04;
rhoiso=30;
ciso=1400;
siso=0.1;

Z_iso=matriceZ(ciso,lambdaiso,rhoiso,tau_0,siso);

%finishing
lambdaint=1;
rhoint=1200;
cint=1500;
sint=0.005;

Z_int=matriceZ(cint,lambdaint,rhoint,tau_0,sint);

%Z matrix wall
Z_p=Z_int*Z_iso*Z_cls;
Z_p_inv=Z_cls*Z_iso*Z_int;

%Z matrix external resistances
Z_i=[1 -Ri; 0 1];
Z_e=[1 -Re; 0 1];

%Total Z matrix
Z=Z_e*Z_p*Z_i;
Z_1=inv(Z);

%Thermal shifting in hours
Delta_tau_Z_11=tau_0/(2*pi)*angle(Z(1,1))/3600;
Delta_tau_Z_12=tau_0/(2*pi)*angle(Z(1,2))/3600;
Delta_tau_Z_21=tau_0/(2*pi)*angle(Z(2,1))/3600;
Delta_tau_Z_22=tau_0/(2*pi)*angle(Z(2,2))/3600;

%Thermal shifting from T_ext to T_int
Delta_tau=tau_0/(2*pi)*angle(Z_1(1,1))/3600;

%Y Matrix admittances
Y_11=(-Z(1,1)/Z(1,2));
Y_22=(-Z(2,2)/Z(1,2));
Y_12=-1/Z(1,2);
Y_21=Y_12;

Y=[Y_11 Y_12; Y_21 Y_22];

%Admittances thermal shifting
```

```
Delta_tau_Y_11=tau_0/(2*pi)*angle(Y(1,1))/3600;
Delta_tau_Y_12=tau_0/(2*pi)*angle(Y(1,2))/3600;
Delta_tau_Y_21=tau_0/(2*pi)*angle(Y(2,1))/3600;
Delta_tau_Y_22=tau_0/(2*pi)*angle(Y(2,2))/3600;

%Stationary trasmittance
U=(0.13+scls/lambdacls+siso/lambdaiso+sint/lambdaint+0.04)
    ^(-1);

%Decrement factor
f=abs(Y(1,2))/U;

%Areal heat capacities
k1=tau_0/(2*pi)*abs((Z(1,1)-1)/Z(1,2));
k2=tau_0/(2*pi)*abs((Z(2,2)-1)/Z(1,2));
```

Listing 8.3: Function for the heat transfer matrix of the ISO 13786:2017 norm

```
%Function for the heat transfer matrix of the ISO 13786:2017
    norm
%Input: c,lambda,rho,tau_0,s
%Output: Z_p

function[Z_p]=matriceZ(c,lambda,rho,tau_0,s)

%Periodic penetration depth
delta=(lambda*tau_0/(pi*c*rho))^0.5;

%Ratio of the thickness to the penetration depth
xi=s/delta;

%Heat transfer matrix for homogeneous layer
Z_11=cosh(xi)*cos(xi)+j*sinh(xi)*sin(xi);
Z_22=Z_11;
Z_12=-delta/(2*lambda)*(sinh(xi)*cos(xi)+cosh(xi)*sin(xi)+j
    *(cosh(xi)*sin(xi)-sinh(xi)*cos(xi)));
Z_21=-lambda/delta*(sinh(xi)*cos(xi)-cosh(xi)*sin(xi)+j*(
    cosh(xi)*sin(xi)+sinh(xi)*cos(xi)));

Z_p=[Z_11 Z_12; Z_21 Z_22];
```

Ringraziamenti

Sono giunta quindi al termine anche di questo percorso. Quando ho iniziato, non mi sarei certo aspettata tutto quello che poi è successo, sia a livello personale, che globale (come il coronavirus). Se sono arrivata fin qui, è merito di molte persone, a cui vorrei dedicare qualche parola.

Ringrazio il Prof. Luca Doretti, che mi segue e mi guida da molti anni e sicuramente senza il quale ora non sarei qui. Mi sono state trasmesse non solo conoscenze scientifiche e metodologie di ricerca, ma anche supporto personale, sia nei momenti di grande gioia, sia quelli che mi hanno messa più alla prova. Grazie di tutto, veramente.

Ringrazio tutti i membri del gruppo di ricerca: il Prof. Zilio, il Prof Mancin e la Prof.ssa Righetti per essermi stati da guida in questi anni. Ringrazio anche gli altri dottorandi, con cui ho condiviso le gioie e le difficoltà affrontate: Michele, Dario e Giacomo. Siete stati un'ottima compagnia.

Ringrazio tutti i ragazzi con cui ho passato questi anni al secondo piano di Via Venezia 1: Luca, che ne inventa sempre una per stampare oggetti stravaganti; Stefano, che da buon veterano è stato sempre un punto di riferimento; Andrea, che con i suoi racconti e la sua simpatia ci riesce sempre a tenere allegri; Pierandrea, che se non ci fosse dovrebbe essere inventato, insieme alle sue disavventure. Ringrazio anche tutti coloro che hanno transitato per questi luoghi e che ora stanno camminando su altre strade, è stato un piacere condividere questi momenti con voi.

Ringrazio Cristiano, che anche se a distanza, mi è sempre stato vicino, in ogni situazione. Sono grata di averti tra i miei amici e di poter sempre contare su di te. Sono veramente poche le persone che ti fanno sentire il loro affetto, anche se non fisicamente vicine.

Ringrazio Valentina, con cui so di poter sempre parlare di tutto. Sai essere dolce e scatenata allo stesso tempo. Da quando ci siamo incontrate in collegio non ci siamo più lasciate. Grazie per tutto quello che sei sempre stata per me.

Ringrazio Sara, che ormai per tradizione vuole essere ringraziata, ma si merita

sicuramente di essere qui ricordata. Con te le risate non mancano mai, sono contenta che continuiamo a sentirci anche dopo che sono passati anni dalla nostra camera 106.

Ringrazio la mia famiglia, che mi ha sostenuta in tutto il mio percorso scolastico. Ringrazio in particolare mia mamma, per la forza che ha avuto e per l'amore che mi ha dimostrato in ogni momento della vita. Non riuscirei ad esprimere a parole tutta la mia gratitudine.

Ringrazio Mattia, che mi è sempre stato vicino, volendomi bene e affrontando con me ogni nuova sfida. Il futuro è alle porte, non resta che rimboccarsi le maniche e vivere ciò che ci aspetta. So che ne varrà la pena e che insieme riusciremo a fare tutto.